RECONSTRUCTION OF PALEO SEA ICE AND CLIMATE DYNAMICS BASED ON HIGHLY BRANCHED ISOPRENOIDS AT THE WESTERN ANTARCTIC PENINSULA

Kumulative Dissertation zur Erlangung des akademischen Grades eines Doktors der Naturwissenschaften

Dr. rer. nat.

Doctor rerum naturalium

Am Fachbereich Geowissenschaften an der Universität Bremen

Eingesendet von Maria-Elena Vorrath

Bremerhaven, 06.05.2020

Gutachter: Dr. Juliane Müller und Prof. Dr. Helge Arz

Colloquium

Reconstructions of sea ice in the Holocene: what do molecular fossils tell us?

Bremen, 28. August 2020

Versicherung an Eides Statt

Gem. § 5 Abs. 5 der Promotionsordnung vom 18.06.2018

Ich, Maria-Elena Vorrath, versichere an Eides Statt durch meine Unterschrift, dass ich die vorliegende Dissertation selbstständig und ohne fremde Hilfe angefertigt und alle Stellen, die ich wörtlich dem Sinne nach aus Veröffentlichungen entnommen habe, als solche kenntlich gemacht habe, mich auch keiner anderen als der angegebenen Literatur oder sonstiger Hilfsmittel bedient habe und die zu Prüfungszwecken beigelegte elektronische Version (PDF) der Dissertation mit der abgegebenen gedruckten Version identisch ist.

Ich versichere an Eides Statt, dass ich die vorgenannten Angaben nach bestem Wissen und Gewissen gemacht habe und dass die Angaben der Wahrheit entsprechen und ich nichts verschwiegen habe.

Die Strafbarkeit einer falschen eidesstattlichen Versicherung ist mir bekannt, namentlich die Strafandrohung gemäß § 156 StGB bis zu drei Jahren Freiheitsstrafe oder Geldstrafe bei vorsätzlicher Begehung der Tat bzw. gemäß § 161 Abs. 1 StGB bis zu einem Jahr Freiheitsstrafe oder Geldstrafe bei fahrlässiger Begehung.

Bremerhaven, 06.05.2020 _____

Maria-Elena Vorrath

"… we have to speak clearly, no matter how uncomfortable that may be.

…

Our civilization is being sacrificed for the opportunity of a very small number of people to continue making enormous amounts of money.

Our biosphere is being sacrificed so that rich people in countries like mine can live in luxury. It is the sufferings of the many which pay for the luxuries of the few.

…

You say you love your children above all else, and yet you are stealing their future in front of their very eyes.

…

We have run out of excuses and we are running out of time."

– Greta Thunberg at COP24, 12.12.2018, Katowice, Poland –

ACKNOWLEDGEMENTS

First: thank you Jule! You gave me the chance to explore past Antarctic sea ice, to visit the end of the world, Antarctica, and to graduate at AWI. Thank you for your patience, your support in all the time in highs and lows and for giving me the opportunity to investigate such a hot topic in the global climate system and at the same time let me tell the stories of biomarkers and past climate outside of AWI. I remember that for the job interview the sun was shining in Bremerhaven and Ludmilla said: this is a sign. It definitely was!

Thanks to my second supervisor Gesine Mollenhauer for inspirational conversations and challenging me to uncover the ages of one or another sediment core.

I am thankful to Ralf Tiedemann for supporting me to finish this wonderful project.

Thank you, Thomas Opel for reading and reading and reading my drafts over and over and for the enlightening discussions.

I enjoyed the work at AWI because of my colleagues from PALICE: special thanks go to Nele "PhD-comrade-in-arms" Lamping, to the wonderful lab ladies Mandy Kuck and Denise Dieckstall, to Gema Mendez-Martinez and our numerous HiWis.

Many thanks to the section of Marine Geology, from the youngsters to the oldies. I thank you all for the wonderful time, expertise and reflections about technical, scientific and personal issues, inside and outside the lab (Julia Hagemann, Nicole Syring, Michelle van der Does, Kevin Küssner, Thomas Ronge, Nicoletta Ruggieri, Walter Luttmer, Susanne Wiebe, Valea Schumacher, Rita Fröhlking, Michael Seebeck, and many more).

I am grateful to Hannes Grobe, Claudia Hanfland, Sandra Meyer and Henning Schröder for being the best colleagues, friends and teachers on our expedition in Antarctica. I also thank all the captains and crews on our expedition, without you we would have been lost… and still stuck in the ice.

I like to thank the POLMAR graduate school for the best trainings a PhD student could ever get and also the DokTeam for the warm welcome in Bremerhaven and their social events.

I truly enjoyed my time at the University of Hamburg and like to thank Niko Lahajnar and Prof. Emeis for giving me opportunities, trainings and preparing me for my PhD life.

Thank you to all the people who are never too tired to present their science in public and call for climate action. Scientists bear responsibility to society (Hannes Grobe, Thomas Ronge, Jelle Bijma, Melanie Bergmann, Franziska Pausch, Janine Schaffer, Frank Lamy and many more).

Dear co-authors, you are quite numerous and I like to give a big thank you to all for helping a small PhD student trying to make an impact in science and making this work an interdisciplinary

firework. A very special thanks goes to the Chilean researchers (Carina Lange, Lorena Rebolledo, Paola Cárdenaz and others) for your scientific dedication in turbulent political times.

I like to thank the participants of the C-side workshop at the ICP in September 2019 in Sydney for so much positive response, for new cooperations, inspirations and for new motivation for the final part of my project.

Thank you, best friends in the world, to help me keep in touch with "the other life" (kisses to Marta, Ulf, Thea, Lisa, Jakob, Katrin, Dennis and Jana, Maik, and the team from Femme Rebellion, Fusion and CCC).

The best for last: I am grateful for having the best parents in the world, Eva-Maria and Ralf Vorrath. Without your support I would never have achieved something that exceeded my wildest dreams (which was flying to the moon…but marine research in the infinite white is muuuch better).

ABSTRACT

In context of rapid environmental change, the investigation of vulnerable parts of the global climate system is the focus of recent research. The assessment of global interactions between a changing climate and Antarctic sea ice, especially at the rapidly warming Western Antarctic Peninsula (WAP), aims to improve climate and ice sheet modelling for future projections. For this, the reconstruction of past sea ice distribution provides crucial information to enhance the capability of climate models. The goal of this thesis is the evaluation of the novel organic sea ice biomarker $IPSO_{25}$ (ice proxy for the Southern Ocean with 25 carbon atoms) and its application as a new tool for past sea ice reconstructions analogously to its counterpart IP_{25} in the Arctic Ocean. This organic biomarker is a source specific organic compound from sea ice algae and associated with Antarctic spring sea ice. Information about the significance and limitations of this sea ice biomarker is still sparse and shall be revealed by using surface and downcore marine sediments. Comparisons to independent data such as biomarkers for open marine conditions, diatom assemblages, satellites data, ice core and marine sediment records improve the precise assessment of $IPSO_{25}$.

The distribution and evaluation of $IPSO_{25}$ with recent sea ice data is the topic of the first study (Part I). The multiproxy investigation of surface sediment samples from the Drake Passage and the WAP reveals a good agreement of $IPSO_{25}$ with ecological diatom data and satellite sea ice observations. The implementation of a sea ice index from combined open marine and sea ice biomarkers – $PIPSO_{25}$ – implies that this tool is promising for paleo sea ice studies. The following two investigations (Part II and III) cover the last 200 a and 17 ka BP, respectively, based on three short and one long sediment records, and highlight the regional significance of $IPSO_{25}$. Evaluation of the relation to sea salt sodium, methanesulfonic acid, numerical model output and reconstructed atmospheric circulation patterns (El Niño Southern Oscillation, Southern Annular Mode and Southern Westerly Winds) reveals that $IPSO_{25}$ and $PIPSO_{25}$ more likely indicate seasonal and dynamic sea ice changes than sea ice quantities. The development of past sea ice during the deglaciation and the Holocene at the WAP shows a significant change in sea ice seasonality in agreement with past investigations. The influence of the El Niño Southern Oscillation, the Southern Annular Mode and the Southern Westerly Winds is evident in sea ice biomarker production pattern due to high variability and the latitudinal position of westerly winds at the WAP.

This thesis provides new reference data for paleo sea ice studies and provides a first research approach in further application of $IPSO_{25}$, $PIPSO_{25}$ and paleo sea ice investigations in Antarctica and the Southern Ocean.

ZUSAMMENFASSUNG

Zur Abschätzung zukünftiger Veränderungen in Polargebieten stehen die Wechselwirkungen zwischen einzelnen Klimakomponenten im Zusammenhang mit der globalen Erwärmung im Mittelpunkt der jüngsten Forschung. Die Rekonstruktion der Meereisbedeckung in der Antarktis, und insbesondere an der sich sehr schnell erwärmenden Westantarktischen Halbinsel, zielt darauf ab, die Modelle von Klima- und Eisschildveränderungen zu verbessern. Das Ziel dieser Dissertation ist die Evaluierung und Anwendung eines neuartigen organischen Biomarkers für Meereis, $IPSO_{25}$ (**I**ce **P**roxy für den **S**üdlichen **O**zean mit **25** C-Atomen), um ihn für Meereisrekonstruktionen analog zu seinem Pendant der Arktis, dem Meereisbiomarker IP_{25}, anzuwenden. Der Ursprung des organischen Biomarkers sind Eisalgen, deren Wachstum mit Antarktischem Frühlingsmeereis assoziiert wird. Aussagen über den Informationsgehalt und mögliche Grenzen dieses Proxys sind bisher kaum vorhanden und sollen in dieser Arbeit durch die Untersuchung von marinen Sedimenten der Oberfläche und in der Tiefe offengelegt werden. Der Abgleich mit weiteren Biomarkern, mit fossilierten Diatomeen, Satelliten- und Eiskerndaten und mit vergleichbaren älteren Studien sollen die präzise Bewertung von $IPSO_{25}$ unterstützen und dessen Anwendung ermöglichen.

Die erste Studie (Part I) behandelt die räumliche Verteilung von $IPSO_{25}$ in rezenten Oberflächensedimenten und zielt auf eine Evaluierung des Biomarkers als Anzeiger für Antarktisches Meereis ab. Der Abgleich von mehreren Meereis- und Klimaanzeigern aus der Drake Passage und von der Westantarktischen Halbinsel zeigt gute Übereinstimmungen mit $IPSO_{25}$ und deutet darauf hin, dass dieser sich in den Daten von Diatomeen als auch in Satellitenaufzeichnungen wiederspiegelt. Die Anwendung eines Meereisindex in Analogie zu seinem Arktischen Pendant (eine Kombination aus Biomarkern stellvertretend für den eisfreien und eisbedeckten Ozean) als $PIPSO_{25}$ (Phytoplankton-$IPSO_{25}$) ist vielversprechend. Die folgenden zwei Paläostudien (Part II und III) über einen Zeitraum von 200 und 17.000 Jahren basieren auf drei kurzen und einem langen Sedimentkern und zeigen deutlich die regionale Aussagekraft des Biomarkers. Beim Vergleich mit Meersalz- und biologischen Aerosolen (Natrium und Methansulfonsäure), mit den Ergebnissen numerischer Modelle, mit rekonstruierten atmosphärischen Zirkulationsmustern (El Niño, die Antarktische Zirkulation und die südlichen Westwinde) und mit Meereisstudien von benachbarten Sedimentkernen zeigt sich, dass $IPSO_{25}$ und $PIPSO_{25}$ verstärkt die Saisonalität und Dynamik von Meereis statt der Meereismenge überliefern. Im Übergang von der letzten Eiszeit und während des Holozäns zeigen sich signifikante Veränderungen der Meereisbedeckung und -saisonalität, die bereits aus vorherigen Studien bekannt sind. Der Einfluss der El Niño Variabilität, der Antarktischen Zirkulation und von den südlichen

Westwinden, wirkt sich auf die Produktionsmuster des Meereisbiomarkers aus und spiegelt sich in den klimatischen Wechseln des untersuchten Zeitraumes wieder.

Diese Dissertation liefert neben einem neuen Referenzdatensatz für Paläomeereisuntersuchen auch einen Fortschritt in der Erforschung des Biomarkers $IPSO_{25}$ und dessen Meereisindex $PIPSO_{25}$ und ermöglicht so zukünftige Paläoklima- und Meereisstudien in der Antarktis und dem Südozean.

TABLE of CONTENTS

1 INTRODUCTION

1.1 WHY WE SHOULD STUDY THE ETERNAL ICE

The Swedish chemist Svante Arrhenius was the first who calculated the increase of Earth´s surface temperature caused by the greenhouse effect under rising atmospheric carbon dioxide (CO_2). In his opinion, mankind would benefit from burning fossil fuels and changing the global climate so "*we may hope to enjoy ages with more equable and better climates*" (Arrhenius, 1908). Today, facing a global warming of approximately +1.0°C above preindustrial levels and advanced environmental degradation (IPCC, 2018) we know that we push the natural system towards its limits where critical thresholds of the earth system, i.e. climate tipping points may be crossed in the coming decades leading to non-linear, fast and irreversible changes (Lenton et al., 2008). These changes could drastically diminish the ability of the earth system to support vital ecosystems that sustain human nutrition, health and livelihood, and have already become one of the biggest threats of humanity according to the World Economic Forum (2020). Yet, changes in the environment are omnipresent in everyday´s life, for example as the rise of sea level, droughts, floods, heat waves, wild fires and most prominent in the warming of polar regions (IPCC, 2019). Since the decline of Arctic sea ice, thawing of permafrost soil, atmospheric warming, and disturbance of circulation pattern in the northern hemisphere can be directly linked to anthropogenically forced global warming, changes in the Antarctic have long been overseen and not attributed to a human influence. But recent studies show: the eternal ice might be less permanent than we thought.

The urgency to study the changes in Antarctica is based on the potential of its ice sheet being the main future contributor to a global sea level rise of up to 1.0 m within the 21st century (Oppenheimer et al., 2019) leading to dramatic economic and geopolitical consequences for coastal metropoles around the globe (FitzGerald et al., 2008). Still, the observations of fast retreating Antarctic ice shelves, accelerated flow of ice sheets towards the ocean and rapid ocean warming are contradicted by an increase of sea ice extent in the Southern Ocean (Cheng et al., 2020; Meredith et al., 2019). Until now, climate models fail to reproduce observed sea ice changes in Antarctica, and their capability to project future ice sheet and sea ice development in the context of global warming is weak (Bracegirdle et al., 2019; Meredith et al., 2019). To enhance the understanding of sea ice in the global climate system and the interplay within the ice-ocean-atmosphere system, reconstructions of past climate and sea ice dynamics are an effective tool. Therefore, this study aims at the establishment and application of a novel paleo record for sea ice reconstructions in Antarctica which could improve climate models and projections in the future.

1.2 ANTARCTIC SEA ICE

Southern Ocean sea ice is highly dynamic with seasonal variations of 85% with respect to sea ice extent between seasonal minimum in March and maximum in September (Figure 1.1). Over the last 40 years, since the start of satellite observations, its extent has increased by about 70,000 km^{-2} yr^{-1} or 1.5% per decade (Eayrs et al., 2019), while the development of sea ice thickness is poorly constrained during this period (Williams et al., 2015). Due to the high inter-seasonal dynamic and the annual sea ice formation and melt, multi-year sea ice is rare and an average sea ice thickness of about 1 m is common (National Snow and Ice Data Center, NSIDC Homepage, accessed April 2020). A record low sea ice extent in 2016/17 may be due to natural variability (Schlosser et al., 2018) while the interannual variability was found to increase since satellite observations begun, especially in response to air temperatures rise (Hobbs et al., 2016; Turner et al., 2019). Many regions and seasons contribute to the total Antarctic sea ice extent and opposite trends can be observed in different sectors of the Southern Ocean (Holland, 2014). Strong positive sea ice trends in several regions and strong negative trends in other regions make it difficult to find a clear relationship of environmental drivers for sea ice growth and fate in the Southern Ocean (Stroeve et al., 2016).

The impacts of Antarctic sea ice on the environment are manifold (Figure 1.2). The white surface of sea ice and its snow cover lead to a high albedo effect where about 50% to 70% of the incoming solar radiation is reflected leading to low atmospheric temperatures, while the albedo effect of the darker sea surface reflects only about 6% of the incoming radiation (NSIDC Homepage, accessed

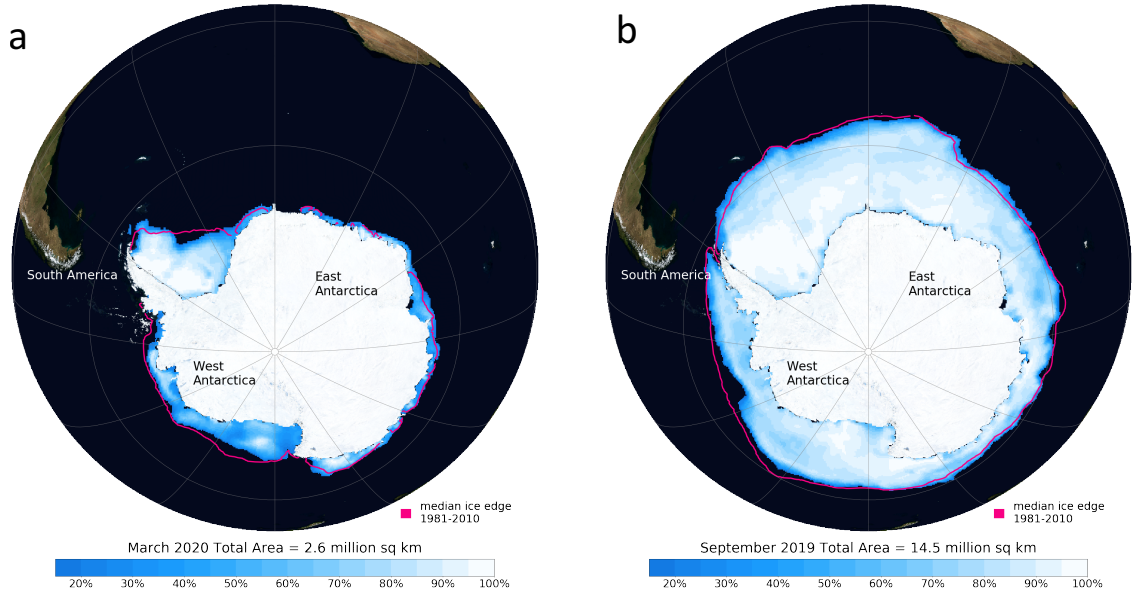

Figure 1.1 Recent Antarctic sea ice concentrations during a) the sea ice minimum in March 2020 and b) the sea ice maximum in September 2019 representative for the seasonal variability in the Southern Ocean. The pink lines present the median ice edge between 1981 and 2010 for each month. Maps are from the National Snow and Ice Data Center (NSIDC Homepage, accessed April 2020).

April 2020). Where sea ice is present the ocean surface is decoupled from the atmosphere, so the exchange of gases and heat is blocked. This causes the trap of heat in the ocean and cools down the surface air, it decreases air moisture due to diminished evaporation of the sea surface and slows down wind-induced surface mixing (Thomas, 2017). The freezing point of sea water with a salinity of 34 is at -1.86°C, which is also the point of maximum density of sea water. When sea ice forms, sea water above the freezing point starts to experience thermohaline convection, so colder water sinks down and is replaced by warmer waters at the surface, which causes a mixing and cooling of the ocean surface layer (Thomas, 2017). Sea ice growth starts from single ice crystals, often in the shape of needles or platelets, that aggregate to frazil ice (or pancake ice under wind stress) and layers of sea ice are added one after another to the bottom of sea ice. Most of inorganic dissolved ions (e.g. sea salt) are excluded from the ice crystal lattice, so brine solution drains in the underlying sea water (Petrich and Eicken, 2016) and only small amounts of sea water remain trapped in a labyrinth of channels. As a result, cold, salty, and dense water masses form and act as a barrier for warm ocean currents to enter the shelf area at the continental margin of Antarctica. This prevents basal melting of the ice shelves with implications for the ice sheet stability especially in West Antarctica (Cook et al., 2016; Hellmer et al., 2012). Further, the dense water contributes to the formation of Antarctic Bottom Water and is an important driver of the global thermohaline circulation (Nicholls et al., 2009). Not only sea ice formation but also the melting of sea ice releases

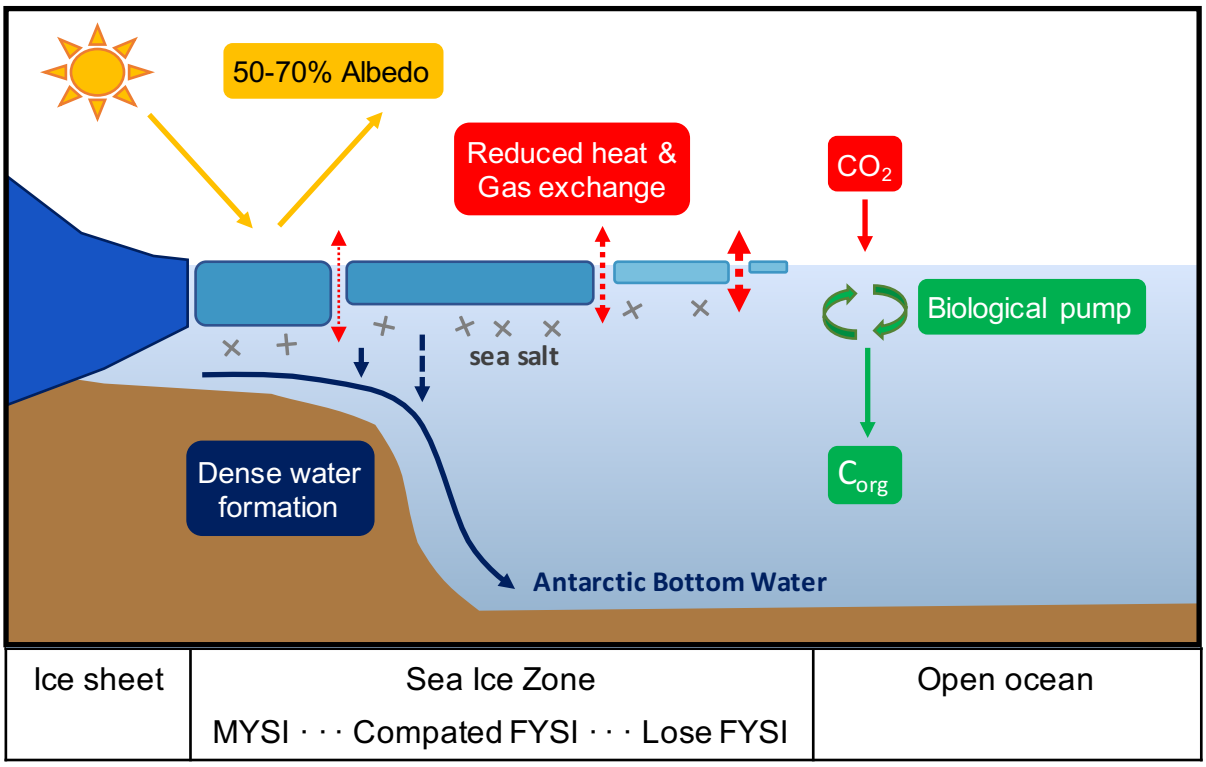

Figure 1.2 Scheme of the impacts of sea ice in the Southern Ocean and Antarctica. Only a small part is multi-year sea ice (MYSI) while the majority is first-year sea ice which can be compacted (sea ice concentrations above 40%) or lose (sea ice concentrations below 40%). Figure after Crosta (2009).

less dense, fresher water and support ocean stratification during spring and summer (Arrigo et al., 1997; Klinck, 1998). The formation of leads by break-up of floating ice can be initiated by divergence or shear stress and is an important gateway for latent heat and moist exchange (Marcq and Weiss, 2012). The fate of sea ice via melting in spring and summer is mainly driven by ocean heat transfer and takes place along margins and at the sea ice bottom (Thomas, 2017).

At the sea ice bottom a dense network of brine filled channels and pores build a unique habitat for marine species and influence the chemical composition of biogenic matter formed under these conditions (Thomas and Dieckmann, 2002). In case of high primary production, the brine composition shifts to a remarkable reduction of total inorganic carbon, depletion of CO_2, higher pH values and higher oxygen concentrations (Thomas and Dieckmann, 2002). Photosynthesis in the semi-enclosed channels lead to the consumption of ^{12}C stable isotopes and an enrichment of ^{13}C stable isotopes (Sinninghe Damsté et al., 2007) expressed in heavy $\delta^{13}C$ isotope signatures of up to -8‰ for sea-ice derived organic matter (Arrigo et al., 2003; Gibson et al., 1999).

Photosynthesis and marine primary production are depleted under sea ice because of the lack of ocean mixing, depletion of nutrients and reduced light penetration, especially with snow cover (Arrigo, 2014). Nevertheless, sea ice provides a habitat for settling and hiding for many microorganisms and metazoans (Garrison, 1991), large vertebrates (Ainley and DeMaster, 1990) and sea ice algae (Arrigo, 2014). Sea ice algae are responsible for the typical brown colour at the bottom of sea ice floes and their growth sustains the rich marine sea ice community (Lizotte, 2001). Although their microbial mass is generally low due to the depletion of nutrients in the brine channels (Arrigo and Thomas, 2004), carbon fixation is enhanced with the presence of sea ice due to higher primary production (Schofield et al., 2018). The thickness and snow cover of sea ice is crucial for algae growth, responding with initial growth to the onset of irradiance in early spring (Hancke et al., 2018). At the same time wind-induced upwelling occurs at the sea ice edges (Alexander and Niebauer, 1981) and melting sea ice releases nutrients and fuels algae growth in both, sea ice and ice-free waters (Vernet et al., 2008). For this reason, high sea-ice related primary production occurs mainly at the sea ice edge where it is a crucial factor for enhanced fixation of CO_2 from the atmosphere and transformation into organic carbon (C_{org}) that is transported to the ocean floor via sinking particles (Berger and Wefer, 1990; DeLaRocha and Passow, 2007; Wefer et al., 1988)(Figure 1.2). This so-called biological carbon pump drives the long-term sequestration of CO_2 in the Southern Ocean and is an important mechanism affecting atmospheric CO_2 concentrations (Falkowski et al., 1998). The primary production within sea ice is restricted due to its physical properties and contributes only a small fraction to the production of the Southern

Ocean. Still, it is estimated that the marginal ice zone and continental shelf make up 12% of the total annual production (Arrigo et al., 1998).

Within sea ice, the most habitable and biologically productive zone is the bottom within the lowest 5 cm to 10 cm due to connection to seawater nutrients and mild temperatures (compared to the upper sea ice)(Arrigo, 2014). The microbial community in sea ice consists of archaea, bacteria and eukaryota, the latter most prominent through single-celled microalgae which form the base of the marine food web in this area (Arrigo and Thomas, 2004). The most common microalgae are sea ice diatoms with 30 to 170 different species. Because sea ice deforms during aging and requires robust diatom frustules it is mainly inhabited by small pennate sea ice diatoms like *Fragilariopsis curta* (Arrigo and Thomas, 2004; Hamm et al., 2003), but also large species such as *Amphiprora*, *Pinnularia* and *Pleurosigma* are common (Riaux-Gobin et al., 2003; Smetacek et al., 1992). The growth of sea ice algae is also responsible for the production of dimethylsulphide which is the main source of marine derived sulphates in Antarctica and acts as a cloud nuclei changing the radiation budget due to cloud formation (Arrigo and Thomas, 2004; Trevena and Jones, 2006). Due to sea ice melt in spring and summer, sea ice algae are released and small amounts are deposited on the ocean floor via downward particle flux.

Since the start of satellite observations of Antarctic sea ice in 1979 changes in its distribution and seasonality have been recorded (Hobbs et al., 2016). For example, sea ice concentrations in austral summer show an increase of up to 20% across East Antarctica (here March 2020, Figure 1.3a), while there is a decline of sea ice concentrations of 20% in West Antarctica leading to large sea-ice

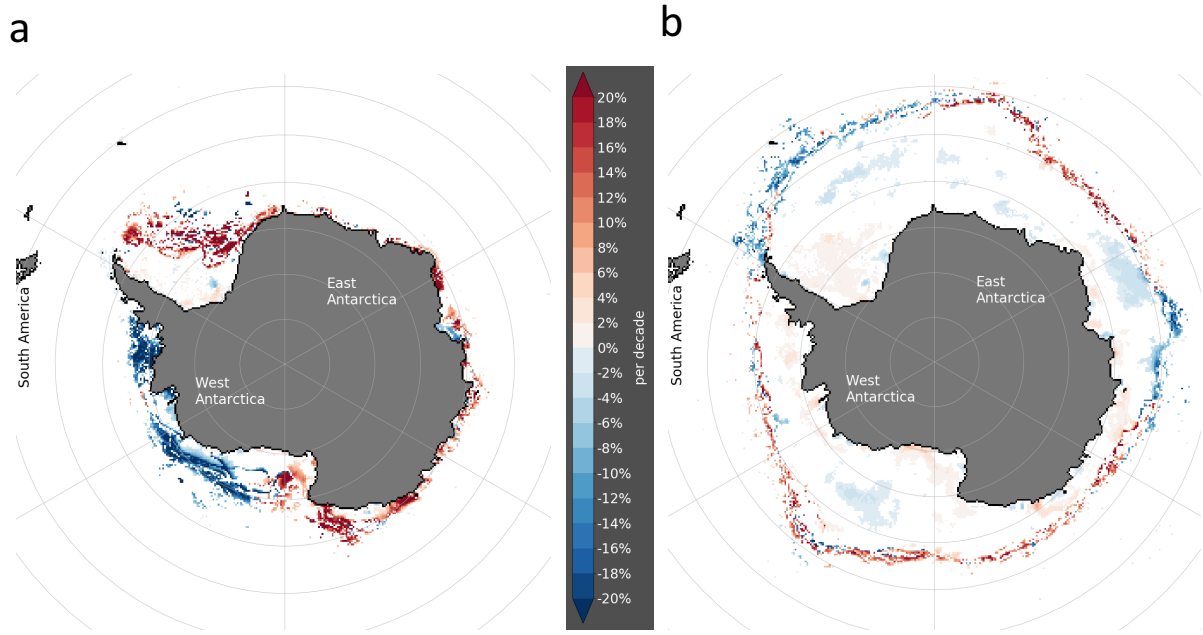

Figure 1.3 Maps of sea ice concentration trends for a) March 2020 and b) September 2019 where blue areas stand for a decrease and red areas for an increase of sea ice. Maps are from the National Snow and Ice Data Center (https://nsidc.org, accessed April 2020).

free areas during summer and shorter sea ice seasons (Parkinson, 2002). In winter, the differences are smaller (here September 2019, Figure 1.3b). These different trends affect the physical and ecological properties that interact with sea ice and sea ice formation. Since the flow of the West Antarctic Ice Sheet accelerated and melting rates increased over the last decades (Meredith et al., 2019), it has been suggested that the ocean is the main driver of ice sheet retreat and that basal melting of the ice shelves due to warm water intrusion of the deep ocean is connected to the loss of sea ice in West Antarctica (e.g. Hellmer et al., 2013; Hillenbrand et al., 2017). Higher temperatures and in particular the thinning of sea ice lead to a possible intensification of algae growth with increased grazing and nutrient cycling (Melnikov, 2009). A general loss of sea ice is suggested to reduce its related algae communities and the decrease of krill which is crucial for the marine food web of higher trophic levels (Flores et al., 2012; Nicol et al., 2008).

1.3 SEA ICE RECONSTRUCTION

Sea ice reconstructions in Antarctica

In the course of global warming, projections of Arctic sea ice point to a significant decline and potentially sea ice free summers within the next decades, while projections of future Antarctic sea ice show a wide range of trends and uncertainties and confidence levels of model outputs are still very low (Meredith et al., 2019). As the direct observation of sea ice is limited to the satellite era, climate-archive based reconstructions of past sea ice target the questions of drivers and implications within the global climate system during different climate periods and transitions (De Vernal et al., 2013). To understand the past boundary conditions for sea ice variability is a key to translate these findings to modern day interaction of ocean, atmosphere and ice. It is still unclear how different kinds of forcing from atmosphere, ocean heat flux or thermal isolation affect long-term sea ice variability (Armand et al., 2016). Without this knowledge modelling of past and future climate interactions in response of sea ice is strongly limited. Further, the global impact of Antarctic sea ice variability is still unclear, nor, how Antarctic sea ice will change under global warming.

Antarctic past sea ice estimations from ice cores are based on their chemical and isotopic composition, revealing differences in e.g. temperature driven fractionation of stable isotopes, the precipitation of sea salt and marine aerosols and snow accumulation (Thomas et al., 2019). Sea salt aerosols origin from sea spray by breaking waves and are often used in the form of sea salt sodium ($ssNa^+$) fluxes (e.g. EPICA Community Members et al., 2004; WAIS Divide Project Members et al., 2015). The longest records from the 800,000 year ice core from EPICA Dome C shows a response of sea salt fluxes in relation to the last eight glacial cycles and is referred to Southern Ocean sea ice extent (Wolff et al., 2006). Other, shorter records, resolve regional sea ice dynamics in relation to climate modulations much better, e.g. the EPICA Dronning Maud Land ice core that

is related to Weddell Sea ice (Rahaman et al., 2016) or the WAIS Divide ice core that represents sea ice in the Ross and Amundsen Sea (WAIS Divide Project Members et al., 2013). Currently, the longest sea ice record based on the organic aerosol methanesulfonic acid (MSA) is an ice core dating back to 1702 (Thomas and Abram, 2016). MSA is an oxidation product of dimethylsulfide originating from diatoms and is referred to the break-up of sea ice in spring and related to high algae production. Stable isotopes ($\delta^{18}O$ and δD) depend on temperature, evaporation and precipitation and are more likely to represent climate conditions (Jouzel et al., 1987). Nevertheless, the deuterium excess ($d = \delta D - 8 * \delta^{18}O$) was related to sea ice area in addition to MSA and sea salt aerosols (Sinclair et al., 2014). Snow accumulation may reflect increased air moisture and evaporation from open ocean surfaces and correlates negatively with sea ice extent e.g. at the Antarctic Peninsula (Porter et al., 2016; Thomas and Bracegirdle, 2015). Sea ice reconstructions from ice cores depend on knowledge of past wind patterns and meteorological conditions that control the catchment area of the ice core. Records must always considered to display regional changes and not absolute sea ice cover. Also, regional difference in the interpretation of ice core records may occur. For example, MSA is suggested to be an indicator for summer sea ice mainly in the ocean of West Antarctica (Criscitiello et al., 2013; Rhodes et al., 2009; Sinclair et al., 2014), while it is representative for winter sea ice in East Antarctica (Foster et al., 2006) and the Southern Indian Ocean (Xiao et al., 2015a).

Marine sediments contain information of paleo sea ice in form of fossilised diatoms, sedimentological composition, and biogeochemical records. The most commonly used proxies are diatoms and their ecological community composition that allows estimations about primary production, environmental conditions and the qualitative estimation of past seasonal sea ice extent (Crosta, 2009). In a statistical examination the quantities of different diatom species are applied to estimate the probability of winter sea ice (Esper and Gersonde, 2014a) and summer sea surface temperatures (Esper and Gersonde, 2014b). Fossilised diatom frustules are found all around Antarctica which make them very useful for inter-comparison studies and allow sea ice reconstructions for the whole Southern Ocean (Gersonde et al., 2005). Nevertheless, during the process of sinking, deposition and fossilisation frustules from sea ice algae are affected by dissolution of biogenic opal (Burckle and Cooke, 1983; Esper and Gersonde, 2014b; Leventer, 1998; Ragueneau et al., 2000) leaving a gap in the scope of their interpretation.

The sedimentological approach for sea ice reconstructions is mainly based on the presence of drop stones, ice rafted debris (IRD) and lithogenic particles transported from icebergs or with free-floating ice which broke up from fast ice after incorporating sediment loads from the coast (Rothwell and Croudace, 2015, and references therein). Also, the composition of stable carbon

isotopes ($\delta^{13}C$) of calcium carbonate (from foraminifera, corals and shells) allows conclusions on the presence of sea ice. This is based on the fact that sea ice derived organic matter has significant higher $\delta^{13}C$ isotope signatures due to the limited gas exchange within the brine channels (Gibson et al., 1999; Sinninghe Damsté et al., 2007; Tortell et al., 2013).

Biomarker-based sea ice reconstructions: the novel sea ice proxy $IPSO_{25}$

A comprehensive approach for past sea ice reconstructions provide the use of biomarkers: biosynthesized, chemically persistent molecules, produced by species living under certain environmental conditions, that leave a characteristic biogeochemical signature in marine sediments (Eglinton and Eglinton, 2008; Volkman, 2006). First described by Nichols et al. (1988), an unique source-specific lipid, a highly branched isoprenoid alkene (HBI) with 25 carbon atoms, is used as a biomarker and a proxy for the presence of sea ice. In Antarctica the diunsaturated HBI (also expressed as $C_{25:2}$) remains from Antarctic sea-ice associated (sympagic) algae and was first assessed by Massé et al. (2011) as a possible proxy for past sea ice conditions (Figure 1.4). The expression $IPSO_{25}$, ice proxy for the Southern Ocean, was introduced for the HBI diene (Belt et al., 2016) in analogy to the Arctic sea ice proxy IP_{25} (Belt et al., 2007). The sea ice origin of $IPSO_{25}$ is identified by its heavy isotopic composition characteristic of sea ice derived organic matter, showing common $\delta^{13}C$ signatures between -5.7‰ and -8.5‰ in sea ice and -18‰ in sediments (Massé et al., 2011). $IPSO_{25}$ is referred to the diatom species *Berkeleya adeliensis* (Belt et al., 2016), a species found commonly widespread in Antarctic sea ice but rare in fossil assemblages. Although *B. adeliensis* is not highly abundant in present sea ice diatom communities, it is yet the only identified $IPSO_{25}$ producer (Belt et al., 2016) and the present distribution of this diatom species in near-coastal land fast sea and platelet ice (Riaux-Gobin and Poulin, 2004) corresponds to their sedimentary abundance (a summary of both *B. adeliensis* and $IPSO_{25}$ occurring in the same region can be found

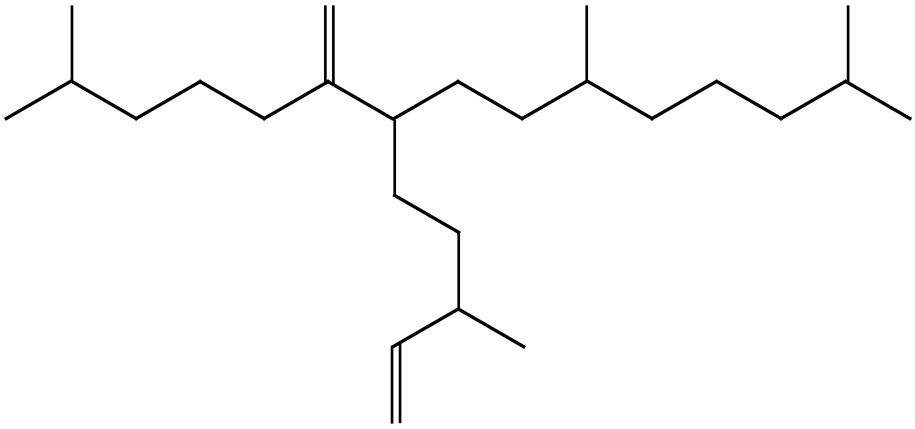

Figure 1.4 The chemical structure of $IPSO_{25}$ (systematic name 2,10,14-Trimethyl-6-enyl-7-(3-methylpent-1-enyl)pentadecene) with two double bonds at C_{7-8} and C_{23-24} (after Belt et al., 2000; Johns et al., 1999).

in Belt et al., 2016). As the growth of sea ice diatoms is mainly restricted to sunlight availability, growth starts with the end of the polar night and the onset of spring. With sea ice melt in late spring and summer, sea ice diatoms are released and transported to the ocean floor and deposited via downward particle flux (Kim et al., 2005). Therefore, $IPSO_{25}$ is supposed to possibly indicate spring sea ice distribution but due to the small number of studies, it is suggested to rather be a qualitative indicator for e.g. sea ice extent or seasonality (Belt, 2019). During sinking in the water column, $IPSO_{25}$ is supposed to be affected by photo-degradation, induced by visible light in the upper water column (Rontani et al., 2011) but so far this effect was not found to be significant. Although it is likely that $IPSO_{25}$ is affected by partial autoxidative and bacterial degradation in surface sediments (Rontani et al., 2019a) and within the sediment (Rontani et al., 2014), it is known to sustain up to 60,000 years in marine sediments (Collins et al., 2013).

So far, $IPSO_{25}$ has been studied in Antarctic sea ice, diatoms, the water column and marine sediments for identification, distribution and degradation of the biomarker and further in a small number of sea ice reconstruction studies (see Table 1.1). Past sea ice reconstructions were mainly conducted at the Antarctic Peninsula, in the Scotia Sea and in the Ross Sea in the west, and in the Pacific and Indian sector in East Antarctica. Except for one study that covers 60,000 years (Collins et al., 2013), the majority of sea ice reconstructions covers for the last 11,000 years or shorter time periods. The interpretation of sea ice cover and seasons is examined by the concentration or anomaly of $IPSO_{25}$ in the sediment cores. Biomarkers such as the triunsaturated HBI ($C_{25:3}$ or HBI triene) produced by e.g. *Rhizosolenia* and *Pleurosigma* diatom species (Belt et al., 2000, 2017) are commonly used as an indicator for open marine conditions like the marginal sea ice zone (Collins et al., 2013) or permanently open ocean zone (Massé et al., 2011; Smik et al., 2016a). Both, $IPSO_{25}$ and HBI triene, are either used in direct comparison or as a ratio. With this procedure the presence of sea ice as well as estimations of seasonal characteristics and amplitudes could be determined in combination with other proxy data (e.g. specific diatom assemblages). The comparison of concentration pattern of $IPSO_{25}$ and the open ocean biomarker can be interpreted as indicators for seasonal variability (Collins et al., 2013). The ratio of $IPSO_{25}$ and open marine biomarker points out the dominance of either sea ice or ice-free environmental conditions (e.g. Barbara et al., 2016; Etourneau et al., 2013). It has been discussed that downcore records of both sea ice and open marine biomarkers may show patterns that correlate positively or negatively to teach other, depending on different environmental conditions (Müller et al., 2011; Navarro-Rodriguez et al., 2013; Xiao et al., 2013). Biomarker production is not linearly related to sea ice: sea ice edges with thin, translucent ice or high sea ice dynamics with sufficient nutrient supply allow producers of both IP_{25} and phytoplankton biomarker to bloom, while their concentrations under extensive sea

ice conditions is lower. Therefore, similar patterns of sea ice and open marine biomarkers are seen as a marker of rapid seasonal changes, whereas opposite patterns represent changing positions of sea ice margins (Belt, 2018).

Table 1.1 Overview of past studies on $IPSO_{25}$ regarding the sample material and study focus.

Sample material	Study focus	References
Sea Ice	- Identification - Distribution	Belt et al., 2016 Johns et al., 1999 Massé et al., 2011 Nichols et al., 1993, 1988, 1989 Smik et al., 2016a
Water column	- Identification - Distribution - Degradation	Cripps and Clarke, 1998 Rontani et al., 2019b Schmidt et al., 2018
Diatoms	- Identification - Distribution - Laboratory cultures	Belt et al., 2017 Johns et al., 1999 Massé et al., 2011 Smik et al., 2016a
Surface sediments	- Identification - Distribution	Belt et al., 2016 Johns et al., 1999 Massé et al., 2011 Rontani et al., 2019a Smik, 2016
Short sediment cores	- Distribution - Analytical methods - Degradation	Belt and Cabedo-Sanz, 2015 Cabedo-Sanz et al., 2016 Massé et al., 2011 Rontani et al., 2018a, 2018b Sinninghe Damsté et al., 2007 Venkatesan, 1988
Long sediment cores	- **Sea ice reconstructions** - Reconstruction of ice shelf and climatic development	Barbara et al., 2010, 2013, 2016 Campagne et al., 2015, 2016 Collins et al., 2013 Denis et al., 2010 Etourneau et al., 2013 Matsumoto et al., 1992

1.4 THE WESTERN ANTARCTIC PENINSULA

The Antarctic Peninsula (AP) is the northernmost spur of the Antarctic continent and approximately 1000 km away from South America. The opening of the Drake Passage through sea floor spreading initialized the transition to the modern configuration of the Antarctic continent by the separation of South America and the Antarctic Peninsula. The opening of the Southern Ocean

gateways began in the Eocene, 50 Ma, continued with the spreading of the West Scotia Ridge (water depth >2000 m) and finally established in the Miocene around 20 Ma (Livermore et al., 2005). Today, the geology of the AP is dominated by volcanic and magmatic formations from the Mesozoic and Cenozoic with the South Shetland Islands as an (mostly inactive) volcanic island arc and the Bransfield Strait as a backarc basin (Figure 1.5 left)(Barker et al., 2003; Haase et al., 2012). On both sides of the AP the continental shelf is between 200 km and 300 km wide. The Bransfield Basin is located between the AP and the South Shetland Islands, next to the steep continental slope, and sedimentation in the Bransfield Basin is frequently disturbed by sediment discharge from the continental margin and turbidites with various volcanic, magmatic and glacial debris (Barker et al., 2003; Haase et al., 2012). The opening of deeper ocean gateways in the Drake Passage between 34 Ma and 30 Ma correlates with $\delta^{18}O$ Southern Ocean isotope records (Scher and Martin, 2006). The establishment of the Antarctic Circumpolar Current (ACC) (Figure 1.5 right) led to the thermal isolation of the Antarctic continent, promoted southern hemisphere glaciation and the formation of the Antarctic Ice Sheet (Kennett, 1977). The abrupt cooling at the Eocene-Oligocene boundary is supposed to be related to a higher Southern Ocean upwelling and turnover that led to enhanced carbon sequestration in the ocean and a decrease in atmospheric CO_2 (Pearson and Palmer, 2000; Scher and Martin, 2006). Several tectonic events such as the opening of the deep-sea passage between Australia and Indonesia were connected to the progressing glaciation of Antarctica and ice sheet formation in the Miocene (approximately between 14 Ma and 11 Ma) and the global

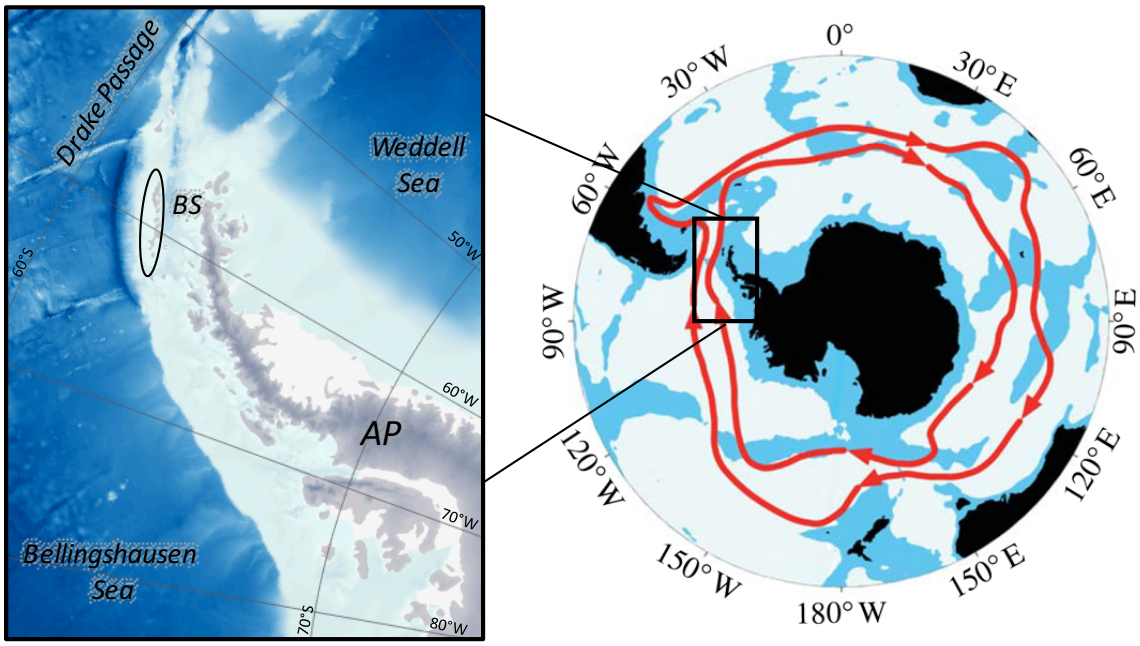

Figure 1.5 Left: bathymetric features at the Antarctic Peninsula (AP) between the Bellingshausen Sea and the Weddell Sea. The Bransfield Strait (BS) is located between the Antarctic mainland the South Shetland Islands (black elipse). Map done with QGIS 3.0 (2018), bathymetry taken from GEBCO_14 (2015). Right: the modern configuration of the Antarctic Circumpolar Current (ACC) (red arrows) in the Southern Ocean (Thompson, 2008).

cooling after 5 Ma with significant Antarctic ice sheet extension (Kennett, 1977). Since the onset of the Cenozoic glaciation the extent of the Antarctic ice sheet is controlled by the oscillating global glacial-interglacial cycles, driven by orbital forcing (DeConto et al., 2008). With the end of the Last Glacial Maximum (LGM, about 20 ka ago, Clark et al., 2009) the Antarctic Peninsula ice sheet (APIS) retreated significantly from 18 ka to 10 ka nearly to its present configuration (Bentley et al., 2014).

Diatom-based studies by Gersonde et al. (2005) suggest a latitudinal northward migration of winter sea ice extent by 3° to 4° degree in the Drake Passage during the last glacial period, but due to a lack of sufficient data of siliceous microfossils these results are quite uncertain. Further, the dissolution of siliceous microfossils and absence of microfossil records under perennial sea ice limits the ability of diatom studies for summer sea ice reconstructions. Applications of coupled climate models revealed a huge disagreement to climate proxies and poorly reproduced seasonal sea ice cycles during the LGM and recent times. For example, the northward boundary of LGM winter sea ice was estimated near the Antarctic mainland (63° S) or near South America (55° S) by different models, respectively (Roche et al., 2012).

The ice sheet retreat after the LGM is often investigated through glacial sediment records (e.g. Heroy and Anderson, 2007) and shows a rapid warming that is interrupted by a cold excursion, called the Antarctic Cold Reversal from 14.7 ka to 13.0 ka BP (e.g. Mulvaney et al., 2012; Pedro et al., 2016). The development of Holocene climate and sea ice at the western and eastern AP was examined in numerous studies from marine and lake sediments (several summaries in Allen et al., 2010; Ingólfsson et al., 2003; Minzoni et al., 2015; Taylor and Sjunneskog, 2002). The Antarctic Peninsula Climate Synthesis by Minzoni et al. (2015) (Figure 1.6 left) summarizes the major findings from terrestrial and marine records and displayed the warm Holocene Climatic Optimum clearly at all study sites. Holocene sea ice reconstructions reveal certain differences in timing and intensity of sea ice cover between the west and east side of the AP (Figure 1.6 right) but also on smaller local scales. The Western Antarctic Peninsula (WAP) experienced higher ocean temperatures and reduced sea ice conditions during the deglacial and Early Holocene, while conditions were opposite at the Eastern Antarctic Peninsula (EAP). The Middle Holocene Climatic Optimum led to high seasonal amplitudes with moderate and/or increasing sea ice cover on both sides, while the Late Holocene is clearly colder and favourable for extended sea ice cover in the whole region (Allen et al., 2010; Barbara et al., 2016; Etourneau et al., 2013; Heroy et al., 2008; Minzoni et al., 2015; Shevenell et al., 2011; Taylor and Sjunneskog, 2002).

The Southern Westerly Winds (SWWs) form a wind belt around the Antarctic continent. When the winds are strong, the core of the wind belt contracts, shifts southward and enhanced upwelling of

deep warm waters brings heat to the WAP shelf (Lamy et al., 2010; Pike et al., 2013). In case of weak SWWs this mechanism is reduced. Due to a strong coupling of atmosphere and ocean, large-scale atmospheric circulation pattern, such as the Southern Annular Mode (SAM) and the El Niño Southern Oscillation (ENSO) seem to influence not just ocean temperature but also sea ice distribution and seasonality (Liu et al., 2004; Stammerjohn et al., 2008a). At the WAP, a high variability of ENSO is suggested to contribute to an amplification of seasonal contrasts and fast changing interannual sea ice cover (Etourneau et al., 2013) which is similar to EAP sea ice and climate variability but not fully constrained yet (Barbara et al., 2016). Further, the state of SAM describes the north-southward movement of the westerly wind belt and causes different sea ice

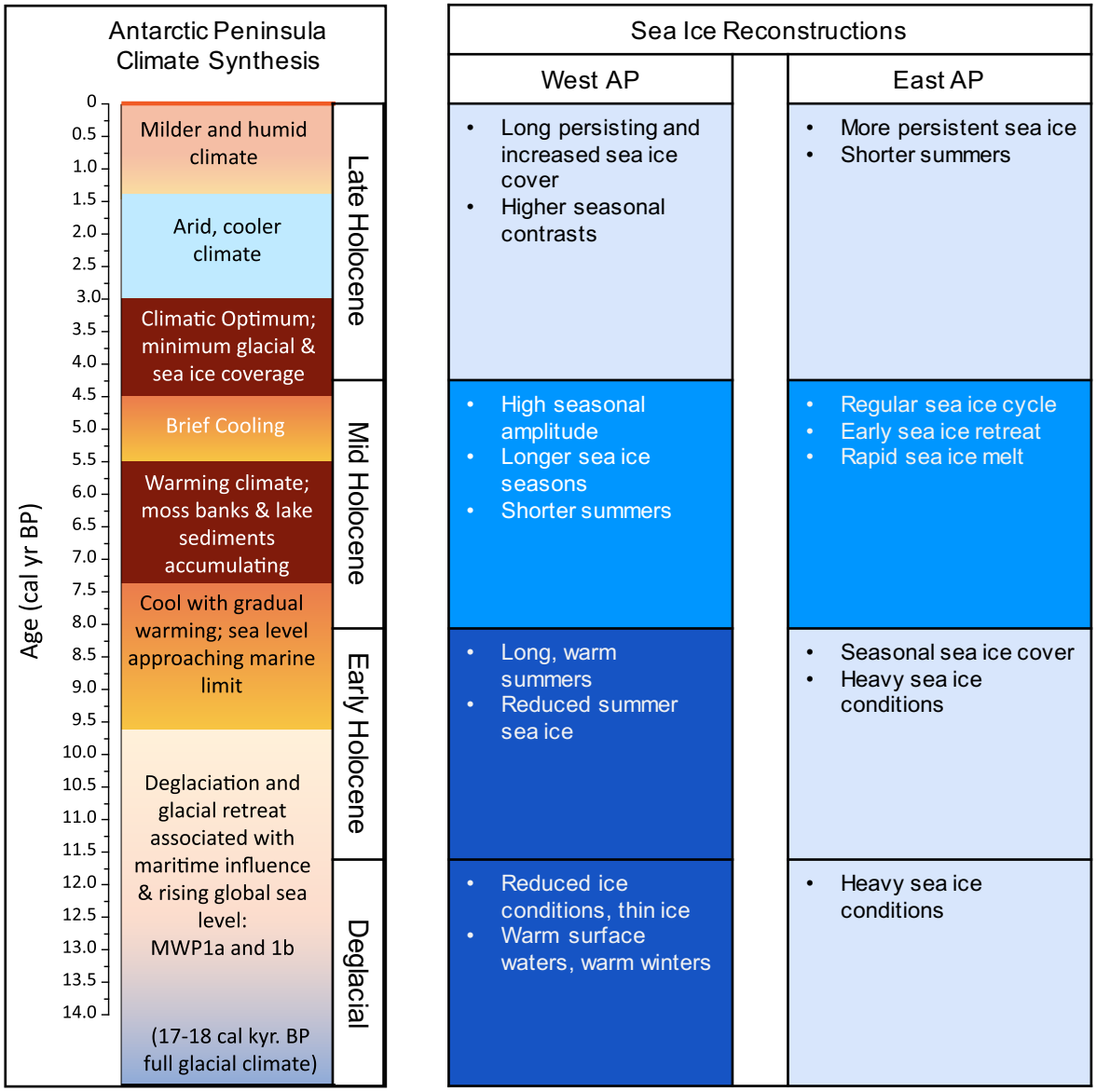

Figure 1.6 Left: the Antarctic Peninsula Climate Synthesis by Minzoni et al. (2015) (after Ingólfsson et al., 2003) summarizes the climatic history derived from marine and lake sediments since the end of the Last Glacial Maximum. Right: a broad summary of sea ice reconstructions at the west AP (Allen et al., 2010; Etourneau et al., 2013; Heroy et al., 2008; Shevenell et al., 2011; Taylor and Sjunneskog, 2002) and the east AP (Barbara et al., 2016; Minzoni et al., 2015), the background colours refer to dark blue = open waters and low sea ice concentrations, light blue = higher sea ice concentrations.

trends in the Pacific and Atlantic sector of the Southern Ocean and drives the upwelling of warm upper circumpolar deep waters (Stammerjohn et al., 2008b; Yuan, 2004). Because of the sparse high-resolution sea ice reconstructions at both sides of the AP, the exact interplay of atmospheric circulation patterns with sea ice cover is only constrained for the era of satellite observations. For the WAP, a tendency to cold and ice-rich ocean was found during an El Niño event simultaneous to a negative state of SAM. In contrast, warm, ice-reduced conditions were evident when La Niña events occurred together with a positive SAM (Stammerjohn et al., 2008b).

Today, the AP is a region extremely exposed to modern global warming (Vaughan et al., 2003) with distinct differences between the warmer western and colder eastern side (Siegert et al., 2019). Further, heavy retreat of West Antarctic Peninsula glaciers (Cook et al., 2005), the disappearance of almost all perennial sea ice (Stammerjohn et al., 2008a), near-surface ocean temperature rise of +1° C (Meredith and King, 2005) and the decline of e.g. Adélie penguin populations (Ducklow et al., 2007) are observed. Therefore, a detailed assessment of past sea ice development is helpful for the determination of future implications of global climate and the ice sheet at the AP and West Antarctica.

2 OBJECTIVES OF THIS THESIS

The primary goal of this thesis is the assessment of the organic biomarker $IPSO_{25}$ for paleo sea ice and climate reconstructions in Antarctica. The specific objectives are the evaluation of $IPSO_{25}$ itself and the assessment of its application as a new biomarker-based sea ice index according to the concept of PIP_{25} in the Arctic. Since $IPSO_{25}$ is only applied in a few numbers of sea ice studies and its specific characteristics were not studied yet, relevant basic information about this proxy is still missing. For example, there is only one study on how $IPSO_{25}$ water samples correspond to the sea ice extent in East Antarctica (Smik et al., 2016a) and none for West Antarctica. A number of studies were done to reveal the significance of $IPSO_{25}$ in comparison with qualitative sea ice reconstructions from diatom assemblages (Barbara et al., 2010, 2013, 2016; Campagne et al., 2015, 2016; Collins et al., 2013; Denis et al., 2010; Etourneau et al., 2013) but a comparison to sea ice cover quantifications from diatom assemblages via a transfer function (Esper and Gersonde, 2014a) are still missing. Further, the promising concept of a PIP_{25} analogue was not tested against sea ice data. To close these knowledge gaps **Part I** of the thesis consists an **evaluation of $IPSO_{25}$**. A number of marine surface sediment samples will be related to satellite observations of recent sea ice cover and diatom assemblages. This pilot study aims to provide robust evidence of $IPSO_{25}$ as a spring sea ice marker and to identify possible limitations and significance at the WAP. Further, the approach of the sea ice index PIP_{25} from the Arctic will be applied for the first time as the novel "$PIPSO_{25}$ index" for the Southern Ocean and tested with different phytoplankton biomarkers.

More open questions concern the regional coverage and the significance of $IPSO_{25}$ and $PIPSO_{25}$ for studies of past sea ice and environmental conditions. It is also not clear how changes in sea ice, sea ice seasonality and the influence of ENSO and SAM affect $IPSO_{25}$ based sea-ice reconstructions on decadal scales. To address these issues, **Part II** is a multiple short-core study designed for the **reconstruction of spring sea ice cover over the last 200 years** and shall provide information about the suitability and applicability of $IPSO_{25}$ and $PIPSO_{25}$. The study on three short sediment cores at the WAP is supposed to reveal the regional coverage of sea ice records. This study benefits from the access to high-resolution sea ice and climate data from satellite observations, marine sediments and ice cores as well as the application of numerical modelled data for comparison.

Sea ice reconstructions on longer, i.e. centennial to multi-millennial, time scales are needed for validation of modelling studies and, in particular, to reveal the interactions of sea ice with changing climate conditions as well as in relation to atmospheric or oceanic circulation patterns on regional and global scales. Hence, **Part III** of this thesis will aim for the application of $IPSO_{25}$ and $PIPSO_{25}$ in a **multi-proxy intercomparison sea ice reconstruction over the last 17,000 years**. This allows the application of sea ice proxies for time periods with fundamental climate changes, i.e.

during the deglaciation and the Holocene. The response of sea ice to long- and short-term climate changes will be assessed and compared with regional paleo data. The dynamics in sea ice and climate conditions shall reveal the impact of ENSO and the SWWs on sea ice cover, biomarker production and oceanographic configurations.

The WAP as study region was chosen mainly for two reasons. First, this region is strongly affected by recent global warming and therefore a key site for the detailed reconstruction of paleo sea ice and climate conditions for future projections. Second, numerous studies with multiple different climate proxies were already examined at the WAP that allow the assessment of climate and sea ice indicators from several sources.

3 MATERIAL AND METHODS

3.1 CONCEPTUALIZATION OF BIOMARKER STUDY

The study is designed as a step by step approximation to the significance of $IPSO_{25}$ in Antarctic sediments from recent sea ice conditions, over the period of 200 years and finally to millennial scales. Since the reconstruction of sea ice is the main focus of this thesis the analytical description includes the detailed examination of HBIs and sterols necessary for the application of $IPSO_{25}$ and the phytoplankton-$IPSO_{25}$ index ($PIPSO_{25}$, chapter 3.2), all other analytical steps are described briefly (chapter 3.3) and documented more precisely in the individual studies. For analyses, 26 surface sediment samples (multicores and boxcores) were taken from different ocean regimes, additionally three short cores and one 10 m piston core were analysed downcore. The samples were retrieved during the cruise PS97 of RV *Polarstern* (expedition report Lamy, 2016) in 2016. Multicores and boxcores were sampled aboard and stored frozen in glass vials, the piston corer was stored at 4° C and sampled at the Alfred Wegener Institute (AWI) in Bremerhaven. The study includes numerous laboratory analyses (Table 3.1) and the use of additional data of satellite sea ice observations, numerical modelling of sea ice and ocean temperature and ice core and sediment data of paleo sea ice, climate, SWWs, ENSO and SAM for comparison (chapter 3.4).

Table 3.1 Overview of the laboratory analytics for this study.

Type	Parameter	Laboratory
Organic bulk parameters	Carbon, nitrogen, total organic carbon (TOC), biogenic opal	AWI Bremerhaven Universidad de Concepción
Highly branched isoprenoids	$IPSO_{25}$, HBI Z-triene, HBI E-triene	AWI Bremerhaven
Phytosterols	Brassicasterol, dinosterol, campesterol, ß-sitosterol, desmosterol	AWI Bremerhaven
Glycerol dialkyl glycerol tetraethers	GDGTs, OH-GDGTs, crenarchaeol	AWI Bremerhaven
Diatom fossils	Ecological groups Transfer function for winter sea ice and summer sea surface temperature	Universidad de Concepción Colgate University, New York AWI Bremerhaven
Stable carbon isotopes	$\delta^{13}C$ of TOC $\delta^{13}C$ of $IPSO_{25}$	University of Hamburg Universidad de Concepción Washington State University GFZ Potsdam, MARUM
Radiocarbon dating	^{14}C, acid-insoluble organic carbon	AWI Bremerhaven
Pb dating	^{210}Pb excess	AWI Bremerhaven Instituto Antártico Chileno, Punta Arenas Université de Montpellier
Sediment composition	XRF-scan, magnetic susceptibility, ice rafted debris	AWI Bremerhaven

3.2 AN ADVANCED CONCEPT OF SEA ICE BIOMARKER INTERPRETATION

One difficulty in the interpretation of sea ice biomarkers is their absence that can refer to a permanentely open ocean or an ocean permanentely covered by thick sea ice (Müller et al., 2011) or a floating ice shelf canopy covering the ocean surface which does not allow diatom growth at the bottom of the ice shelf due to light limitation. An advanced concept beyond the simple ratio of biomarkers for sea ice reconstruction and a semi-quantitative estimation of sea ice cover was established in the Arctic by Müller et al. (2011). It is applied to the sea ice biomarker IP_{25}, (ice proxy with 25 carbon atoms, Belt et al., 2007) which is the northern hemisphere counterpart of $IPSO_{25}$. Sea ice is not just a habitat for sympagic diatom species but also promotes diatom blooms at the sea ice edge through nutrient release and water column stratification in late spring and summer (Arrigo et al., 1997; Vernet et al., 2008). Therefore, an index based on the relative contribution of both environmental biomarkers helps to avoid the over- or underestimation of single indicators and refines the differentiation between various states of sea ice cover, dynamics and characteristics depending on the surrounding conditions. For the Arctic, the index is calculated with the sea ice biomarker (IP_{25}) and open marine phytoplankton markers (either phytosterols or HBI trienes), constituted as the phytoplankton-IP_{25} index (PIP_{25}) (Müller et al., 2011) and provides a detailed assessment of sea ice conditions with a range of the index between 0 and 1. Figure 3.1 illustrates the gradation of environmental conditions from open ocean towards permanent sea-ice cover.

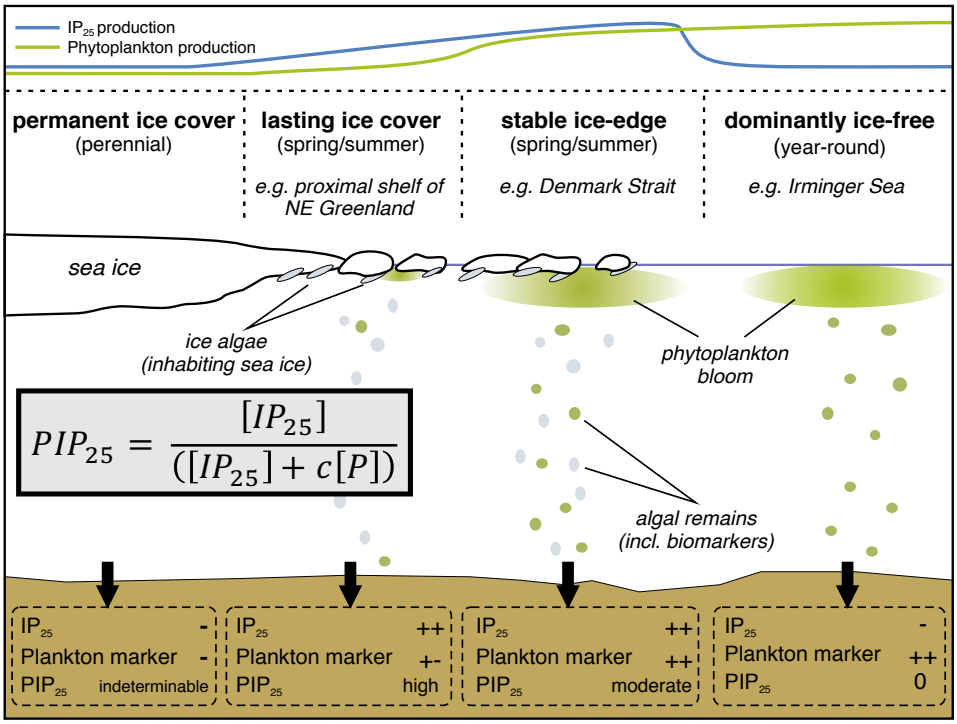

Figure 3.1 The illustrated conception of the phytoplankton-ice proxy approach PIP_{25} and its equation (grey box) for Arctic sea ice reconstructions after Müller et al. (2011). Square brackets represent biomarker concentrations, the balance factor c (c = mean IP_{25}/mean phytoplankton) equalizes concentration differences between sea ice and phytoplankton biomarkers.

Due to the absence (or low concentrations) of IP_{25}, zero to low PIP_{25} values indicate dominantly ice-free ocean conditions, while rising values point to the presence of a stable sea-ice edge and long-lasting sea-ice cover in spring and summer. The value 1 marks a sea ice cover that suppresses phytoplankton growth but still allows photosynthesis of sea ice diatoms. When both biomarkers are absent and the sea ice index is not calculable and refelcts perennial, thick sea ice without any diatom growth (Müller et al., 2011). Calibration studies in the Arctic have revealed a positive correlation of the PIP_{25} approach to modern spring sea ice distributions (Kolling et al., 2017; Müller et al., 2011; Navarro-Rodriguez et al., 2013; Xiao et al., 2015b), most successful with PIP_{25} indicators based on HBI trienes (Köseoğlu et al., 2018).

3.3 LABORATORY STUDY ON $IPSO_{25}$ AND PHYTOPLANKTON MARKERS

For the analysis of $IPSO_{25}$ and phytoplankton markers the methodological approach of biomarker lipid extraction, identification and quantification is based on the analytical protocol to perform HBI and sterol-based sea ice reconstructions in the Arctic (Belt et al., 2013, 2014; Stein et al., 2012). Besides $IPSO_{25}$, the E- and Z-isomeres of HBI trienes, ((9E)-2,6,10,14-tetramethyl-7-(3-methylpent-4-enyliden)pentadeca-9-ene) and (9Z)-2,6,10,14-tetramethyl-7-(3-methylpent-4-enyliden)pentadeca-9-ene), brassicasterol (24-methylcholesta-5,22E-dien-3β-ol), dinosterol (4α,23,24-trimethyl-5α-cholest-22E-en-3β-ol), β-sitosterol (24-ethylcholest-5-en-3β-ol), campesterol (24-methylcholest-5-en-3β-ol) and desmosterol (cholesta-5,24-dien-3β-ol) were examined (Belt et al., 2017; Volkman, 1986; Xiao et al., 2013). To account for different laboratory facilities the method was modified to fit the laboratory standard at the AWI Bremerhaven including analyses of HBI trienes and sterols.

Sediment samples were freeze-dried and homogenised before extraction. Between 3 g and 5 g of sediment was taken and internal standards 7-hexylnonadecane (7-HND for HBIs, 0.076 μg per sample), 5α-androstan-3β-ol (for sterols, 0.78 μg per sample) and C_{46} (for GDGTs, 0.78 μg per sample) were added for quantification and quality control of the extraction procedure. The sediment was treated three times with 6 ml dichloromethane:methanol (CH_2Cl_2:MeOH, *v*/*v* 2:1) in a 15 min ultrasonification and the solvent was decanted after centrifugation (2500 rpm, 1 min). The separation of the apolar hydrocarbons was done via column chromatography with silica gel (SiO_2) acting as the stationary phase. The different biomarker lipids were eluted as following: first, 5 ml hexane (HBI fraction), second, 8 ml ethylacetate:hexane (sterol fraction, *v*/*v* 20:80), and third, 5 ml CH_2Cl_2:MeOH (GDGT fraction, *v*/*v* 1:1). The separation of sterol and GDGT fraction was modified during the project: for the second study sterols and GDGTs were eluted together (with 5 ml CH_2Cl_2:MeOH) and this extract was purified and filtrated for GDGT measurement and later

silylated (with 200 µl BSTFA under 60° C for 2h, Belt et al., 2013; Brault and Simoneit, 1988; Fahl and Stein, 2012) for sterol measurement. In the third study, again, sterols and GDGTs were eluted together and split into half for individual examination and measurement of each biomarker fraction.

HBIs and sterols were analyzed via gas chromatography mass spectrometry (GC-MS) with an Agilent 7890B gas chromatograph (30m DB 1MS column, 0.25mm diameter, 0.250 µm film thickness, carrier gas helium) coupled to an Agilent 5977B mass spectrometer (MSD, 70 eV constant ionization potential, ion source temperature 230 ° C). The individual oven temperature program for HBIs was 60° C for 3 min, a temperature increase to 325° C within 23 min and holding of the temperature for 16 min. For sterols the initial temperature (60° C) was hold for 2 min, then increased to 150° C within 6 min, and further increased to 325° C within 57 min. The identification of individual biomarkers is based on the comparison of measured and published mass spectra from HBIs (Belt, 2018; Belt et al., 2000). Published mass spectra from sterols (Belt et al., 2007; Boon et al., 1979; Brown and Belt, 2016; Volkman, 1986) were also compared in a reference compound run within the analytical sequence. The molecular ions were m/z 348 for $IPSO_{25}$, m/z 346 for HBI trienes and fragment ion m/z 266 for 7-HND. For sterols, the molecular ions were m/z 470 for brassicasterol, m/z 500 for dinosterol, m/z 486 for β-sitosterol, m/z 472 for campesterol and m/z 456 for desmosterol. The quantification was done via integration of peak areas from the selected ion monitoring (SIM) mode allowing the detection of low concentrations (Figure 3.2). Concentrations of biomarkers were calculated in relation to the internal standard 7-HND which is assumed to be affected equally under the extraction and analytical process as the biomarkers:

$$Biomarker\ [\mu g/g\ sed] = \left(\frac{Std\ \mu l * Std\ \mu g/\mu l}{Peak\ Std * Peak\ Biomarker}\right)/g\ sed \qquad (1)$$

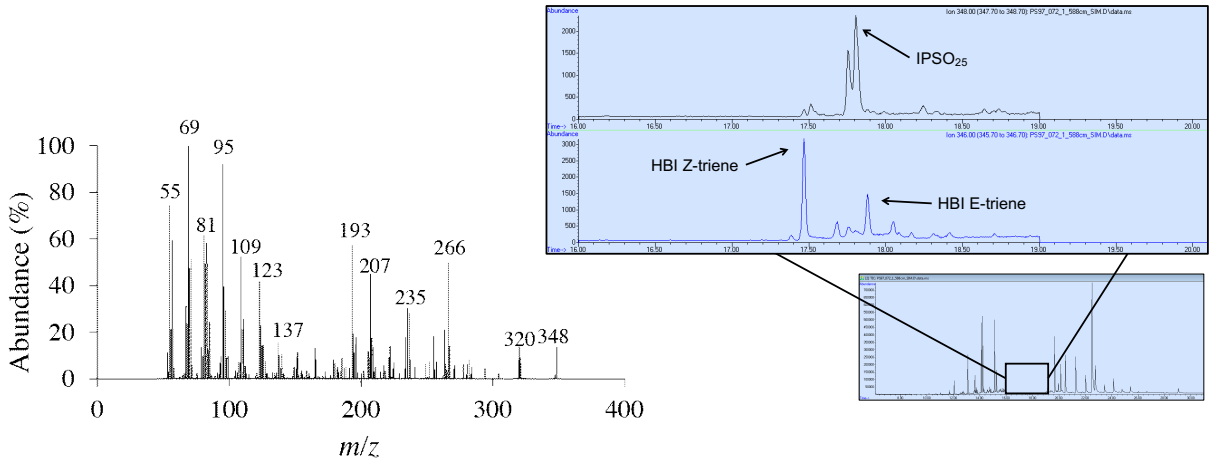

Figure 3.2 On the left: the characteristic mass spectrum of the diunsaturated HBI alkene $C_{25:2}$, expressed as $IPSO_{25}$ (from Belt and Cabedo-Sanz, 2015). Right: Chromatograms of $IPSO_{25}$ and HBI Z- and E-trienes. Peak areas were integrated manually.

The concentrations were corrected via multiplication with the specific response factor determined by running an external standard sediment with known HBI concentrations from the Lancaster Sound, Canada (PS72/287-2). The manual quantification also acted as a visual quality control on e.g. for the occurrence of HBI C_{25} sulfides from potential sulfurization of $IPSO_{25}$ (Sinninghe Damsté et al., 2007). The calculation of $PISPO_{25}$ is based on the original equation from IP_{25} (Figure 3.1). For a better distinction of different phytoplankton sources in the sea ice index the respective letter of the biomarker is part of the expression as P_ZIPSO_{25} (based on HBI Z-triene), P_EIPSO_{25} (based on HBI E-triene), P_BIPSO_{25} (based on brassicasterol), and P_DIPSO_{25} based on dinosterol.

3.4 ADDITIONAL LABORATORY ANALYSES

This chapter contains a brief overview of additional laboratory analyses that are described in the individual studies in detail including all technical data.

The analyses of sediment bulk content of carbon (C) and nitrogen (N) was done with a CNS analyser (Elementar Vario EL III). The content of total organic carbon (TOC) was determined with a carbon-sulphur determinator (CS-2000, ELTRA) on acidified samples (500 µl hydrochloric acid) (details in paper 2 and 3). Biogenic opal was determined following the alkaline extraction procedure (Mortlock and Froelich, 1989; modified after Müller and Schneider, 1993) and measured via molybdate-blue spectrometry at the University of Concepción (Cárdenas et al., 2019).

Stable carbon isotopes of organic $\delta^{13}C$ were examined from acidified samples (three times 100 µl 1 N HCl) via an elemental analyser coupled with an IsoPrime isotope ratio mass spectrometer (details in Cárdenas et al., 2019 and paper 3). The examination of compound specific stable carbon isotopes $\delta^{13}C$ on $IPSO_{25}$ was done with GC-irm-MS (ThermoFisher Scientifi GC) coupled with an isotope ratio mass spectrometer (Finnigan MAT 252) at the MARUM and GFZ Potsdam (details in paper 1 and 3). All $\delta^{13}C$ (in ‰) relied on the Vienna PeeDee Belemnite (VPDB).

GDGTs (lipid extraction, see chapter 3.3) were analysed after filtration (polytetrafluoroethylene filters) with high performance liquid chromatography (Agilent 1200 HPLC system) connected with a single quadrupole mass spectrometer (Agilent 6120 MSD) and via an atmospheric pressure chemical ionization (APCI) interface. Results were used to calculate ocean temperatures based on TEXL86 (Kim et al., 2010), RI-OH' (Lü et al., 2015) and an index for terrestrial organic matter (Hopmans et al., 2004)(details paper 2 and 3).

Diatom fossils were washed with hydrogen peroxide and hydrochloric acid, microscope slides were prepared after Gersonde and Zielinski (Gersonde and Zielinski, 2000) and diatom valves were counted (Schrader and Gersonde, 1978). Diatom ecological groups were defined (Buffen et al., 2007; Campagne et al., 2016; Heroy et al., 2008) and marine diatom transfer function was applied

for winter sea ice (Esper and Gersonde, 2014a) and summer sea surface temperature (Esper and Gersonde, 2014b)(details paper 1, 2 and 3).

^{14}C radiocarbon dating was done on calcite samples with the mini carbon dating system (MICADAS) after Wacker et al. (2010) and on acid-insoluble organic carbon following Heroy et al. (2008) at AWI. Surface sediment samples were calibrated based on MARINE13 (Reimer et al., 2013), for downcore sediment samples the reservoir age was corrected based on reservoir age simulations (Butzin et al., 2017) and calibration was done based on and SHCal13 (downcore sediment samples, Hogg et al., 2013) with Calib 7.1 (http://calib.org/, Stuiver et al., 2018). For downcore records the relative fraction of marine and terrestrial organic matter was estimated from a two end-member mixing model (Thornton and McManus, 1994) based on stable carbon isotope endmembers from marine plankton and terrestrial mosses and peat. Since input of reworked, older organic carbon led to an overestimation of ^{14}C ages, radiocarbon dates of the long sediment core PS97/072-1 were matched to independent chronologies of the West Antarctic Ice Sheet Divide ice core (WAIS Divide Project Members et al., 2015). Interpolation of ages based on the Bayesian age model HummingBird (https://hummingage.awi.de/)(details paper 3).

The geochronology for the short sediment cores (PS97/056-1, PS97/068-2 and PS97/072-2) was derived from $^{210}Pb_{xs}$ activities by alpha spectrometry (Flynn, 1968) and ages based on $^{210}Pb_{xs}$ inventories according the Constant Rate of Supply Model (CRS, Appleby and Oldfield, 1978). On samples analyzed at the Université de Montpellier an age model was applied using the software R (R Core Team, 2017) and the package clam (Blaauw, 2010). On ages from AWI a Monte-Carlo approximation was applied (Sanchez-Cabeza et al., 2014)(details paper 2).

The sediment composition was examined via core description (sediment core PS97/072-1) and smear slides (short cores). Additionally, the magnetic susceptibility for the long core was conducted on the whole round core sections (GEOTEK multi-sensor core logger) aboard and profiling X-ray fluorescence (AVAATECH core-scanner) was done at AWI.

3.5 ADDITIONAL DATA SETS

Paper 2 includes monthly environmental data (ocean and atmospheric temperature, sea ice cover and thickness) from the numerical model AWI-ESM2 consisting of the atmospheric model ECHAM6 (Stevens et al., 2013) and the finite element sea ice-ocean model (FESOM2, Danilov et al., 2017) coupled to a climate model (Sidorenko et al., 2019)(details paper 2).

For papers 1 and 2 monthly mean satellite sea ice concentrations were derived from passive microwave satellite data from the National Snow and Ice Data Center (NSIDC, Cavalieri et al.,

1996) and the mean spring sea ice data (September to November) was taken for evaluation of $IPSO_{25}$ and $PIPSO_{25}$.

For large-scale atmospheric modes the paleo ENSO index (Li et al., 2013) and modelled SAM data (Abram et al., 2014) was used for the short time scale (paper 2). For the Holocene, a sand record from El Junco was considered for ENSO variability (Conroy et al., 2008) and the clay/silt ratio from a sediment core from the Chilean fjord were used for paleo SWWs strength (Lamy et al., 2010)(paper 3).

Information from short ice core records were retrieved from stable isotope data (δD, James Ross Island, Abram et al., 2013; $\delta^{18}O$, Bruce Plateau, Goodwin et al., 2016) and methansulfonic acid (MSA, Dyer Plateau, Abram et al., 2010)(paper 2). Stable isotope data from long cores were used in paper 3 (WAIS Divide Project Members et al., 2013). Holocene sea salt sodium flux data were taken from the EPICA Dronning Maud Land ice core (EPICA Community Members et al., 2004) and the WAIS Divide ice core (δD, Mulvaney et al., 2012; $\delta^{18}O$, WAIS Divide Project Members et al., 2015)(paper 3).

4 AUTHOR´S CONTRIBUTION

The sediment cores and boxcorers used in all three studies were taken and mainly sampled by Juliane Müller and members of the Marine Geology section of AWI during the *Polarstern* cruise PS97 in the year 2016. Juliane Müller also supervised the PhD project and all studies throughout the time and contributed to the manuscripts and interpretations. For all manuscripts I arranged the data, did calibration and calculations of indices and correlations, wrote the drafts and created the figures. In every study, all co-authors were part of the interpretation, discussion and review process.

Part I (Chapter 5): For first study I performed the preparation of sediment samples, the measurement of total organic carbon as well as the lipid extraction of HBIs and sterols and prepared the microscopy slides for the diatom analyses. Measurements of stable carbon isotopes of $IPSO_{25}$, the ^{14}C radiocarbon dating, the retrieval of satellite sea ice data and the analysis of diatoms assemblages were done in cooperation with different sections at AWI and MARUM, Bremen.

Part II (Chapter 6): For second study I sampled the trigger core PS97/072-1 and performed the lipid extraction of HBIs, sterols and GDGTs on two of three cores in the laboratory. The third core was analysed by Denise Diekstall from PALICE, AWI. In cooperation with the Instituto Antártico Chileno in Punta Arenas, Chile, and different sections at AWI the ^{210}Pb dating, the modelling study, retrieval of satellite sea ice data, analysis of GDGTs, and the complete diatom analyses and transfer function were done.

Part III (Chapter 7): For the third study I performed the lipid extraction on the sediment core, measured stable carbon isotopes on TOC and employed an age model for the sediment core. Further analyses of stable carbon isotopes on TOC and $IPSO_{25}$, biogenic opal, diatom assemblages and their transfer functions, GDGTs and radiocarbon dating were done at AWI and in cooperation with the University of Hamburg, Universidad de Concepción, Chile, Colgate University and Washington State University, USA, and GFZ Potsdam.

5 PART I: HIGHLY BRANCHED ISOPRENOIDS FOR SOUTHERN OCEAN SEA ICE RECONSTRUCTIONS: A PILOT STUDY FROM THE WESTERN ANTARCTIC PENINSULA

Maria-Elena Vorrath[1], Juliane Müller[1,2,3], Oliver Esper[1], Gesine Mollenhauer[1,2], Christian Haas[1], Enno Schefuß[2], Kirsten Fahl[1]

[1]Alfred Wegener Institute, Helmholtz Centre for Polar and Marine Research, Bremerhaven, Germany

[2]MARUM – Center for Marine Environmental Sciences, University of Bremen, Germany

[3]Department of Geosciences, University of Bremen, Germany

Published in *Biogeosciences* in August, 2019. DOI: 10.5194/bg-16-2961-2019

Abstract

Organic geochemical and micropaleontological analyses of surface sediments collected in the southern Drake Passage and the Bransfield Strait, Antarctic Peninsula, enable a proxy-based reconstruction of recent sea ice conditions in this climate sensitive area. We study the distribution of the sea ice biomarker $IPSO_{25}$, and biomarkers of open marine environments such as more unsaturated highly branched isoprenoid alkenes and phytosterols. Comparison of the sedimentary distribution of these biomarker lipids with sea ice data obtained from satellite observations and diatom-based sea ice estimates provide for an evaluation of the suitability of these biomarkers to reflect recent sea surface conditions. The distribution of $IPSO_{25}$ supports earlier suggestions that the source diatom seems to be common in near-coastal environments characterized by an annually recurring sea ice cover, while the distribution of the other biomarkers is highly variable. Offsets between sea ice estimates deduced from the abundance of biomarkers and satellite-based sea ice data are attributed to the different time intervals recorded within the sediments and the instrumental records from the study area, which experienced rapid environmental changes during the past 100 years. To distinguish areas characterized by permanently ice-free conditions, seasonal sea ice cover and extended sea ice cover, we apply the concept of the PIP_{25} index from the Arctic Ocean on our data and introduce the term $PIPSO_{25}$ as a potential sea ice proxy. While the trends in $PIPSO_{25}$ are generally consistent with satellite sea ice data and winter sea ice concentrations in the study area estimated by diatom transfer functions, more studies on the environmental

significance of $IPSO_{25}$ as a Southern Ocean sea ice proxy are needed before this biomarker can be applied for semi-quantitative sea ice reconstructions.

5.1 INTRODUCTION

In the last century, the Western Antarctic Peninsula (WAP) has undergone a rapid warming of the atmosphere of 3.7 ± 1° C, which exceeds several times the average global warming (Pachauri et al., 2014; Vaughan et al., 2003). Simultaneously, a reduction in sea ice coverage (Parkinson and Cavalieri, 2012), a shortening of the sea ice season (Parkinson, 2002) and a decreasing sea ice extent of ~4-10 % per decade (Liu et al., 2004) are recorded in the adjacent Bellingshausen Sea. The loss of seasonal sea ice and increased melt water fluxes impact the formation of deep and intermediate waters, the ocean-atmosphere-exchange of gases and heat, the primary production and higher trophic levels (Arrigo et al., 1997; Mendes et al., 2013; Morrison et al., 2015; Orsi et al., 2002; Rintoul, 2007). Since the start of satellite-based sea ice observations, however, a slight increase in total Antarctic sea ice extent has been documented, which contrasts the significant decrease of sea ice in Western Antarctica, especially around the WAP (Hobbs et al., 2016).

For an improved understanding of the oceanic and atmospheric feedback mechanisms associated with the observed changes in sea ice coverage, reconstructions of past sea ice conditions in climate sensitive areas such as the WAP are of increasing importance. A common approach for sea ice reconstructions in the Southern Ocean is based on the investigation of sea ice associated diatom assemblages preserved in marine sediments (Bárcena et al., 1998; Gersonde and Zielinski, 2000; Heroy et al., 2008; Leventer, 1998; Minzoni et al., 2015). By means of transfer functions, this approach can provide quantitative estimates of a paleo sea ice coverage (Crosta et al., 1998; Esper and Gersonde, 2014a). The application of diatoms for paleoenvironmental studies, however, can be limited by the selective dissolution of biogenic opal frustules (Burckle and Cooke, 1983; Esper and Gersonde, 2014b) in the photic zone (Ragueneau et al., 2000) and in surface sediments (Leventer, 1998). As an alternative or additional approach to diatom studies, Massé et al. (2011) proposed the use of a specific biomarker lipid – a diunsaturated highly branched isoprenoid alkene (HBI $C_{25:2}$, Figure 5.1a) – for Southern Ocean sea ice reconstructions. The HBI diene was first described by Nichols et al. (1988) from sea ice diatoms. ^{13}C isotopic analyses of the HBI diene suggest a sea ice origin for this molecule (Sinninghe Damsté et al., 2007; Massé et al., 2011) and this is further corroborated by the identification of the sea ice diatom *Berkeleya adeliensis* as a producer of this HBI diene (Belt et al., 2016). *Berkeleya adeliensis* is associated with Antarctic landfast ice and the underlying so-called platelet ice (Riaux-Gobin and Poulin, 2004). In a survey of surface sediments collected from proximal sites around Antarctica, Belt et al. (2016) note a widespread sedimentary occurrence of the HBI diene and – by analogy with the Arctic HBI monoene termed

IP_{25} (Belt et al., 2007) – proposed the term $IPSO_{25}$ (Ice Proxy for the Southern Ocean with 25 carbon atoms) as a new name for this biomarker.

In previous studies, an HBI triene (HBI $C_{25:3}$; Figure 5.1b-c) found in polar and sub-polar phytoplankton samples (Massé et al., 2011) has been considered alongside $IPSO_{25}$ and the ratio of $IPSO_{25}$ to this HBI triene hence has been interpreted as a measure for the relative contribution of organic matter derived from sea ice algae versus open water phytoplankton (Massé et al., 2011; Collins et al., 2013; Etourneau et al., 2013; Barbara et al., 2013, 2016).

Collins et al. (2013) further suggested that the HBI triene might reflect phytoplankton productivity in marginal ice zones (MIZ) and, based on the observation of elevated HBI triene concentrations in East Antarctic MIZ surface waters, this has been strengthened by Smik et al. (2016a). Known source organisms of HBI trienes (Figure 5.1 shows molecular structures of both the E- and Z-isomer) are, for example, *Rhizosolenia* and *Pleurosigma* diatom species (Belt et al., 2000, 2017). In the subpolar North Atlantic, the HBI Z-triene has been used to further modify the so-called PIP_{25} index (Smik et al., 2016b) - an approach for semi-quantitative sea ice estimates. Initially, PIP_{25} was based on the employment of phytoplankton-derived sterols, such as brassicasterol (24-

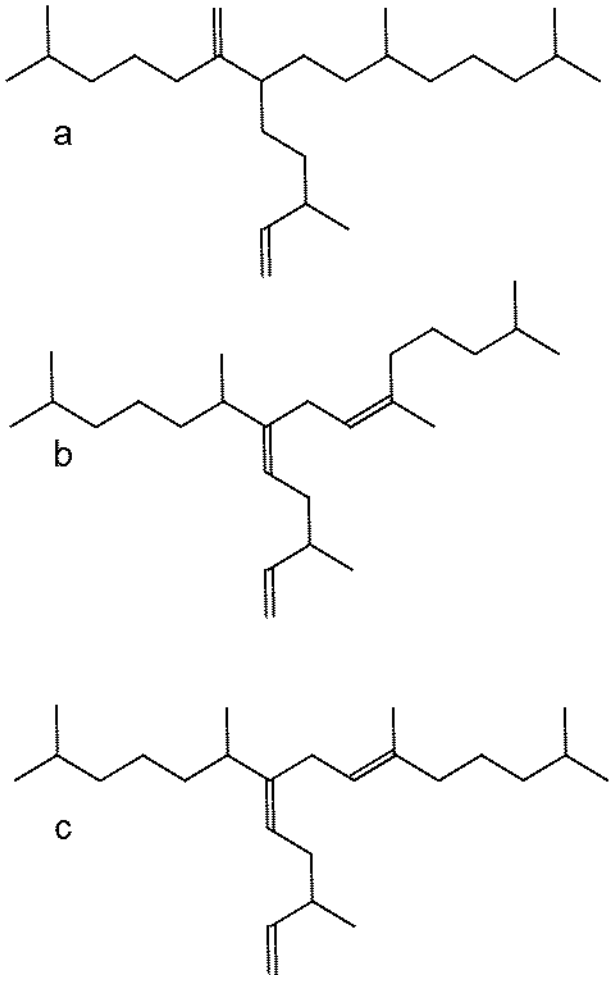

Figure 5.1 The molecular structures of a) $IPSO_{25}$, b) the HBI Z-triene, and c) the HBI E-triene.

methylcholesta-5,22E-dien-3β-ol) and dinosterol (4α,23,24-trimethyl-5α-cholest-22E-en-3β-ol) (Kanazawa et al., 1971; Volkman, 2003), to serve as open-water counterparts, while IP_{25} reflects the occurrence of a former sea ice cover (Belt et al., 2007; Müller et al., 2009, 2011). Consideration of these different types of biomarkers helps to discriminate between ice-free and permanently ice-covered ocean conditions, both resulting in a lack of IP_{25} and $IPSO_{25}$, respectively (for further details see Belt, 2018; Belt and Müller, 2013). Uncertainties in the source-specificity of brassicasterol (Volkman, 1986) and its identification in Arctic sea ice samples, however, require caution when pairing this sterol with a sea ice biomarker lipid for Arctic sea ice reconstructions (Belt et al., 2013). In this context, we note that Belt et al. (2018) reported that brassicasterol is not evident in the $IPSO_{25}$ producing sea ice diatom *Berkeleya adeliensis*. While the applicability of HBIs (and sterols) to reconstruct past sea ice conditions has been thoroughly investigated in the Arctic Ocean (Belt, 2018; Stein et al., 2012; Xiao et al., 2015b), only two studies document the distribution of HBIs in Southern Ocean surface sediments (Belt et al., 2016; Massé et al., 2011). The circum-Antarctic data set published by Belt et al. (2016), however, does neither report HBI triene nor sterol abundances. Significantly more studies so far focused on the use of $IPSO_{25}$ and the HBI Z-triene for paleo sea ice reconstructions and these records are commonly compared to micropaleontologial diatom analyses (e.g., Barbara et al., 2013; Collins et al., 2013; Denis et al., 2010).

Here, we provide a first overview of the distribution of $IPSO_{25}$, HBI trienes, brassicasterol and dinosterol in surface sediments from the permanently ice-free ocean in the Drake Passage towards the seasonal sea ice inhabited area of the Bransfield Strait at the northern WAP. Sea ice estimates based on biomarkers are compared to sea ice concentrations derived from diatom transfer functions and satellite-derived data on the recent sea ice conditions in the study area. We further introduce and discuss the so-called $PIPSO_{25}$ index (phytoplankton-$IPSO_{25}$ index), which, following the PIP_{25} approach in the Arctic Ocean (Müller et al., 2011), may serve as a further indicator of past Southern Ocean sea ice cover.

5.2 OCEANOGRAPHIC SETTING

The study area includes the southern Drake Passage and the Bransfield Strait located between the South Shetland Islands and the northern tip of the WAP (Figure 5.2a and b). The oceanographic setting in the Drake Passage is dominated by the Antarctic Circumpolar Current (ACC) and several oceanic fronts showing large geostrophic water mass flows and subduction and upwelling of water masses (Orsi et al., 1995). The Antarctic Polar Front (APF) divides relatively warm subantarctic waters from the cold and salty Antarctic waters, while the southern Antarctic Circumpolar Current Front (SACCF) often associates with the maximum sea ice extent (Kim and Orsi, 2014). The

current system in the Bransfield Strait is relatively complex and the mixture of water masses is not yet well understood (Moffat and Meredith, 2018; Sangrà et al., 2011). A branch of the ACC enters the Bransfield Strait in the west as the Bransfield Current, carrying transitional waters under the influence of the Bellingshausen Sea (Transitional Bellingshausen Sea Water, TBW). The TBW is characterized by a well-stratified, fresh and warm water mass with summer sea surface temperatures (SST) above 0° C. Below the shallow TBW, a narrow tongue of circumpolar deep water (CDW) flows along the slope of the South Shetland Islands (Sangrà et al., 2011). In the eastern part, transitional water from the Weddell Sea (Transitional Weddell Sea Water, TWW) enters the Bransfield Strait through the Antarctic Sound and from the Antarctic Peninsula (AP). This water mass corresponds to the Antarctic Coastal Current (Collares et al., 2018; Thompson et al., 2009). The TWW is significantly colder (summer SST < 0° C) and saltier due to extended sea ice formation in the Weddell Sea Gyre. The two water masses are separated at the sea surface by the Peninsula Front characterized by a TBW anticyclonic eddy system (Sangrà et al., 2011). While the TWW occupies the deep water column of the Bransfield Strait (Sangrà et al., 2011), it joins the surface TBW in the southwestern Bransfield Strait (Collares et al., 2018).

Due to high concentrations of dissolved iron on the shelf (Klunder et al., 2014), the area around the WAP is characterized by a high primary production with high vertical export fluxes during early

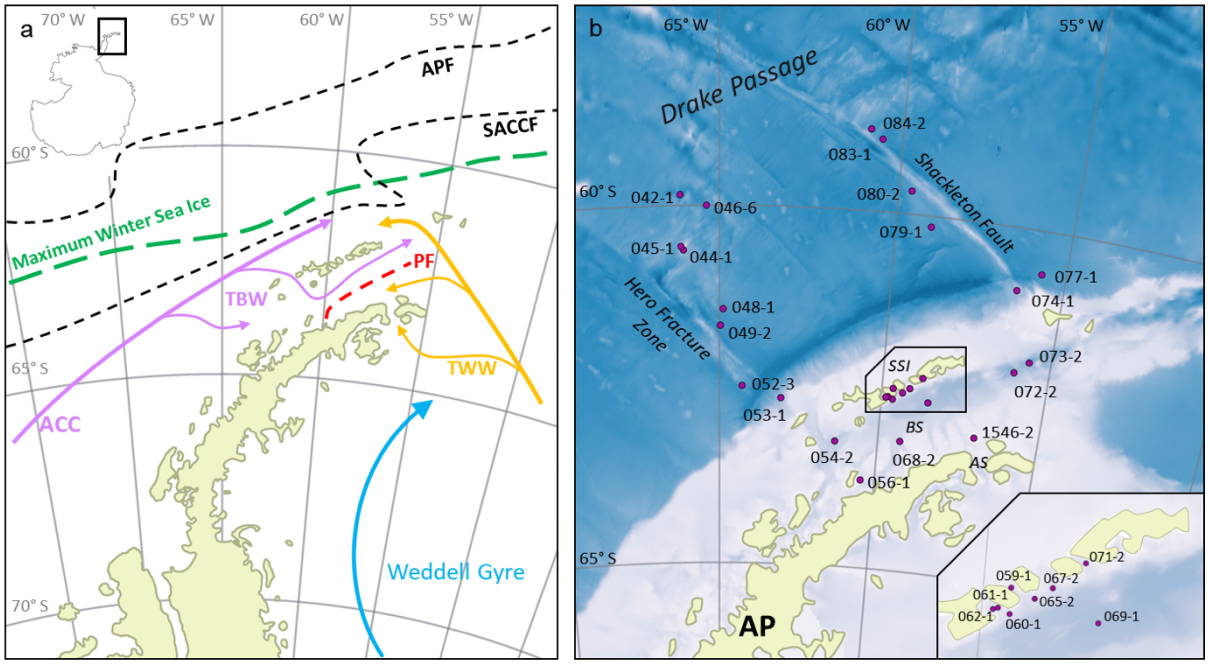

Figure 5.2 a) Oceanographic setting of the study area (modified after Hofmann et al., 1996; Sangrà et al., 2011) with ACC = Antarctic Circumpolar Current, TBW = Transitional Bellingshausen Water, TWW = Transitional Weddell Water, APF = Antarctic Polar Front, SACCF = Southern Antarctic Circumpolar Front, and PF = Peninsula Front, and the maximum winter sea ice extent (after Cárdenas et al., 2018). b) The bathymetric map of the study area with locations of all stations; AP = Antarctic Peninsula, AS = Antarctic Sound, BS = Bransfield Strait, and SSI = South Shetland Islands. A detailed station map at the South Shetland Islands is integrated.
The overview maps were done with QGIS 3.0 from 2018 and the bathymetry was taken from GEBCO_14 from 2015.

summer associated with the formation of fast sinking mineral aggregates and fecal pellets (Kim et al., 2004; Wefer et al., 1988). The Peninsula Front divides the Bransfield Strait into two biogeographic regimes of high chlorophyll and diatom abundance in the TBW and low chlorophyll values and a pre-dominance of nanoplankton in the TWW (Gonçalves-Araujo et al., 2015), which is also reflected in the geochemistry of surface sediments (Cárdenas et al., 2019).

5.3 MATERIALS AND METHODS

5.3.1 SEDIMENT SAMPLES AND RADIOCARBON DATING

In total, 26 surface sediment samples obtained by multicorers and boxcorers during the RV *Polarstern* cruise PS97 (Lamy, 2016) were analyzed (Figure 5.2, Table Appendix 1). All samples were stored frozen and in glass vials. The composition of the sediments ranges from foraminiferal mud in the Drake Passage to diatomaceous mud with varying amounts of ice rafted debris in the Bransfield Strait (Lamy, 2016).

^{14}C radiocarbon dating of two samples from the PS97 cruise and one from the *Polarstern* cruise ANT-VI/2 (Fütterer, 1988) was conducted using the mini carbon dating system (MICADAS) at the Alfred Wegener Institute (AWI) in Bremerhaven, Germany, following the method of Wacker et al. (2010). The ^{14}C ages were calibrated to calendar years before present (cal BP) using the Calib 7.1 software (Stuiver et al., 2018) with an estimated reservoir age of 1178 years, derived from the six closest reference points listed in the Marine Reservoir Correction Database (www.calib.org).

5.3.2 ORGANIC GEOCHEMICAL ANALYSES

For biomarker analyses, sediments were freeze-dried and homogenized using an agate mortar. After freeze-drying, samples were stored frozen to avoid degradation. The extraction, purification and quantification of HBIs and sterols follow the analytical protocol applied by the international community of researchers performing HBI and sterol-based sea ice reconstructions (Belt et al., 2013, 2014; Stein et al., 2012). Prior to extraction, internal standards 7-hexylnonadecane (7-HND) and 5α-androstan-3β-ol were added to the sediments. For the ultrasonic extraction (15 min), a mixture of CH_2Cl_2:MeOH (v/v 2:1; 6 ml) was added to the sediment. After centrifugation (2500 rpm for 1 min), the organic solvent layer was decanted. The ultrasonic extraction step was repeated twice. From the combined total organic extract, apolar hydrocarbons were separated via open column chromatography (SiO_2) using hexane (5 ml). Sterols were eluted with ethylacetate:hexane (v/v 20:80; 8 ml). HBIs were analyzed using an Agilent 7890B gas chromatography (30 m DB 1MS column, 0.25 mm diameter, 0.250 μm film thickness, oven temperature 60° C for 3 min, increase to 325° C within 23 min, holding 325° C for 16 min) coupled to an Agilent 5977B mass spectrometer (MSD, 70 eV constant ionization potential, ion source temperature 230° C). Sterols

were first silylated (200 µl BSTFA; 60° C; 2 hours; Belt et al., 2013; Brault and Simoneit, 1988; Fahl and Stein, 2012) and then analyzed on the same instrument using a different oven temperature program (60° C for 2 min, increase to 150° C within 6 min, increase to 325° C within 56 min 40 sec). As recommended by Belt (2018), the identification of $IPSO_{25}$ and HBI trienes is based on comparison of their mass spectra with published mass spectra (Belt, 2018; Belt et al., 2000; see Figure Appendix 2). Regarding the potential sulfurization of $IPSO_{25}$, we examined the GC-MS chromatogram and mass spectra of each sample for the occurrence of the HBI C_{25} sulfide (Sinninghe Damsté et al., 2007). The C_{25} HBI thiane was absent from all samples. For the quantification, manually integrated peak areas of the molecular ions of the HBIs in relation to the fragment ion m/z 266 of 7-HND were used. Instrumental response factors are determined by means of an external standard sediment from the Lancaster Sound, Canada. The HBI concentrations in this sediment are known and a set of calibration series was applied to determine the different response factors of the HBI molecular ions (m/z 346; m/z 348) and the fragment ion of 7-HND (m/z 266) (Figure Appendix 3; Belt, 2018; Fahl and Stein, 2012). The identification of sterols was based on comparison of their retention times and mass spectra with those of reference compounds run on the same instrument. Comparison of peak areas of individual analytes and the internal standard was used for sterol quantification. The error determined by duplicate GC-MS measurements was below 0.7 %. The detection limit for HBIs and sterols was 0.5 ng/g sediment. Absolute concentrations of HBIs and sterols were normalized to total organic carbon content (for TOC data see Cárdenas et al., 2018).

The herein presented phytoplankton-$IPSO_{25}$ index ($PIPSO_{25}$) is calculated using the same formula as for the PIP_{25} index following Müller et al. (2011):

$$PIPSO_{25} = \frac{IPSO_{25}}{IPSO_{25} + (c \times phytoplankton\ marker)} \quad (1)$$

The balance factor c (c = mean $IPSO_{25}$ / mean phytoplankton biomarker) is applied to account for the high offsets in the magnitude of $IPSO_{25}$ and sterol concentrations (see Belt and Müller, 2013; Müller et al., 2011; Smik et al., 2016b for details and a discussion of the c-factor). Since the concentrations of $IPSO_{25}$ and both HBI trienes are in the same range, the c-factor has been set to 1 (following Smik et al., 2016b). For the calculation of the sterol-based $PIPSO_{25}$ index using brassicasterol and dinosterol the applied c-factor is 0.0048 and 0.0137, respectively.

Stable carbon isotope composition of $IPSO_{25}$, requiring a minimum of 50 ng carbon, was successfully determined on five samples using GC-irm-MS. The ThermoFisher Scientific Trace GC was equipped with a 30 m Restek Rxi-5 ms column (0.25 mm diameter, 0.25 µm film thickness) and coupled to a Finnigan MAT 252 isotope ratio mass spectrometer via a modified GC/C interface. Combustion of compounds was done under continuous flow in ceramic tubes filled with

Ni wires at 1000° C under an oxygen trickle flow. The same GC program as for the HBI identification was used. The calibration was done by comparison to a CO_2 monitoring gas. The values of $\delta^{13}C$ are expressed in per mill (‰) against Vienna PeeDee Belemnite (VPDB) and the mean standard deviation was <0.9 ‰. An external standard mixture was measured every six runs, achieving a long-term mean standard deviation of 0.2 ‰ and an average accuracy of <0.1 ‰. Stable isotopic composition of neither HBI trienes nor sterols could be determined due to coeluting compounds.

5.3.3 DIATOMS

Details of the standard technique of diatom sample preparation were developed in the micropaleontological laboratory at the Alfred Wegener Institute (AWI) in Bremerhaven, Germany. The preparation included a treatment of the sediment samples with hydrogen peroxide and concentrated hydrochloric acid to remove organic and calcareous remains. After washing the samples several times with purified water, the water was removed and the diatoms were embedded on permanent mounts for counting (see detailed description by Gersonde and Zielinski, 2000). The respective diatom counting was carried out according to Schrader and Gersonde (1978). On average, 400 to 600 diatom valves were counted in each slide using a Zeiss Axioplan 2 at x1000 magnification. In general preservation state of the diatom assemblages was moderate to good in the Bransfield Strait and decreased towards the Drake Passage where it is moderate to poor.

Diatoms were identified to species or species group level and if possible to forma or variety level. The taxonomy follows primarily Hasle and Syvertsen (1996), Zielinski and Gersonde (1997), and Armand and Zielinski (2001). Following Zielinski and Gersonde (1997) and Zielinski et al. (1998) we combined some taxa to groups:

The *Thalassionema nitzschioides* group combines *T. nitzschioides* var. *lanceolata* and *T. nitzschioides* var. *capitulata*, two varieties with gradual transition of features between them and no significantly different ecological response. The species *Fragilariopsis curta* and *Fragilariopsis cylindrus* were combined as *F. curta* group taking into account their similar relationship to sea ice and temperature (Armand et al., 2005; Zielinski and Gersonde, 1997). Furthermore, the *Thalassiosira gracilis* group comprises *T. gracilis* var. *gracilis* and *T. gracilis* var. *expecta* because the characteristic patterns in these varieties are often transitional, which hampers distinct identification.

Although the two varieties *Eucampia antarctica* var. *recta* and *E. antarctica* var. *antarctica* display different biogeographical distribution (Fryxell and Prasad, 1990), they were combined to the *E. antarctica* group. This group was not included in the transfer function (TF) as it shows no relationship to either sea ice or temperature variation (Esper and Gersonde, 2014a, b). Besides the *E. antarctica* group, we also discarded diatoms assembled as *Chaetoceros* spp. group from the TF-

based re-constructions, following Zielinski et al. (1998) and Esper and Gersonde (2014a). This group combines mainly resting spores of a diatom genus with a ubiquitous distribution pattern that cannot be identified to species level due to the lack of morphological features during light microscopic inspection. Therefore, different ecological demands of individual taxa cannot be distinguished.

For estimating winter sea ice (WSI) concentrations we applied the marine diatom TF MAT-D274/28/4an, comprising 274 reference samples from surface sediments in the western Indian, the Atlantic and the Pacific sectors of the Southern Ocean, with 28 diatom taxa and taxa groups, and an average of 4 analogs (Esper and Gersonde, 2014a). The WSI estimates refer to September sea-ice concentrations averaged over a time period from 1981 to 2010 at each surface sediment site (National Oceanic and Atmospheric Administration, NOAA; Reynolds et al., 2002, 2007). The reference data set is suitable for our approach as it uses a 1° by 1° grid, representing a higher resolution than previously used and results in a root mean squared error of prediction (RMSEP) of 5.52 % (Esper and Gersonde, 2014a). We defined 15 % concentration as threshold for maximum sea-ice expansion following the approach of Zwally et al. (2002) for the presence or absence of sea ice, and 40 % concentration representing the average sea-ice edge (Gersonde et al., 2005; Gloersen et al., 1993). MAT calculations were carried out with the statistical computing software R (R Core Team, 2017) using the additional packages Vegan (Oksanen et al., 2012) and Analogue (Simpson and Oksanen, 2012). Further enhancement of the sea-ice reconstruction was obtained by consideration of the abundance pattern of the diatom sea-ice indicators allowing for qualitative estimate of sea-ice occurrence, as proposed by Gersonde and Zielinski (Gersonde and Zielinski, 2000).

5.3.4 SEA ICE DATA

The mean monthly satellite sea ice concentration was derived from Nimbus-7 SMMR and DMSP SSM/I-SSMIS passive microwave data and downloaded from the National Snow and Ice Data Center (NSIDC; Cavalieri et al., 1996). The sea ice concentration is expressed to range from 0 to 100 %, with concentrations below 15 % suggesting the minor occurrence of sea ice. Accordingly, the sea ice extent is defined as the ocean area with a sea ice cover of at least 15 %.

An interval from 1980 to 2015 was used to generate an average sea ice distribution for each season; spring (SON), summer (DJF), autumn (MAM) and winter (JJA) (Table Appendix 4) and the data is considered to reflect the modern mean state of sea ice coverage around the WAP. The high standard deviation in the seasonal sea ice concentrations (up to 26 % in winter; Table Appendix 4) in the vicinity of the WAP is attributed to the distinct intra- and interannual variability in sea ice coverage. In this regard, Kim et al. (2005) already related interannual changes in particle flux to

annual changes in sea ice cover in the Bransfield Strait. We here suggest that by considering mean sea ice concentrations determined for an observational period of 35 years, reflects a good estimate of average sea ice conditions and facilitates the comparison with sedimentary archives.

5.4 RESULTS AND DISCUSSION

In the following we present and discuss the sedimentary concentrations of $IPSO_{25}$, HBI trienes and phytosterols regarding their spatial distribution patterns in relation to the environmental conditions and oceanographic features in the study area. We especially focus on the applicability of these biomarkers for reconstructing sea ice conditions and integrate information derived from satellite observations and diatom-based sea ice estimations. We further discuss the possible approach of a sea ice index $PIPSO_{25}$ by analogy with the Arctic sea ice index PIP_{25} (Müller et al., 2011).

5.4.1 BIOMARKER DISTRIBUTION IN SURFACE SEDIMENTS

Distribution of $IPSO_{25}$

The sea ice biomarker $IPSO_{25}$ was detected in 14 samples, with concentrations ranging between 0.37 and 17.81 μg g^{-1} TOC (Table Appendix 1). The distribution of $IPSO_{25}$ in the study area shows a clear northwest-southeast gradient (Figure 5.3a) with concentrations increasing from the continental slope and around the South Shetland Islands towards the continental shelf. Maximum $IPSO_{25}$ concentrations are observed at stations under TWW influence with distinctly cold summer SSTs in the Bransfield Strait. According to Belt et al. (2016), deposition of $IPSO_{25}$ is highest in areas covered by landfast sea ice and platelet ice during early spring and summer. Platelet ice is formed under supercooling ocean conditions in the vicinity of ice-shelves and subsequently may be incorporated into drifting sea ice (Gough et al., 2012; Hoppmann et al., 2015). We note that, for example, core sites PS97/068, PS97/069, PS97/072, and PS97/073 in the central and eastern Bransfield Strait are located too distal to be covered by fast ice and suggest that peak $IPSO_{25}$ concentrations at these sites may refer to the frequent drift and melt of sea ice exported from the Weddell Sea into the Bransfield Strait. The vertical export of biogenic material from sea ice towards the seafloor may be accelerated significantly by the formation of organic-mineral aggregates, fecal pellets or by (cryogenic) gypsum ballasting, which promotes a rapid burial and sedimentation of organic matter in polar settings (De La Rocha and Passow, 2007; Wefer et al., 1988; Wollenburg et al., 2018). A recent study from Schmidt et al. (2018) shows that the occurrence of $IPSO_{25}$ in suspended matter and pelagic grazers (krill) is closely linked to the position of the sea ice edge. Lateral subsurface advection of organic matter (including biomarkers) through the TWW, however,

may also contribute to elevated $IPSO_{25}$ concentrations at these sites. $IPSO_{25}$ was not detected in sediments from the permanently ice-free areas in the Drake Passage.

The $\delta^{13}C$ values of $IPSO_{25}$ are between -10.3 ‰ and -14.7 ‰ which is the commonly observed range for $IPSO_{25}$ in surface sediments, sea ice derived organic matter, and in Antarctic krill stomachs (Belt et al., 2016; Massé et al., 2011; Schmidt et al., 2018). These values contrast the low $\delta^{13}C$ values of marine phytoplankton lipids in Antarctic sediments (-38 ‰ to -41 ‰ after Massé et al., 2011) and support the sea ice origin of $IPSO_{25}$ in the study area.

Distribution of HBI trienes

The HBI Z-triene was present in all 26 samples (0.33-26.86 μg g^{-1} TOC) and the HBI E-triene was found in 24 samples (0.15-13.87 μg g^{-1} TOC) (Table Appendix 1). Highest concentrations of both HBI trienes are found in the eastern Drake Passage and along the continental slope, where $IPSO_{25}$ is absent, while their concentrations in the Bransfield Strait are generally low (Figure 5.3b and c) suggesting unfavorable environmental conditions for their source diatoms (e.g., cooler SSTs, sea ice cover, grazing pressure). Contrary to the finding of elevated HBI Z-triene concentrations in surface waters along an ice-edge (Smik et al., 2016a) and earlier suggestions that this biomarker may be used as a proxy for MIZ conditions (Belt et al., 2015; Collins et al., 2013; Schmidt et al., 2018), we observe highest concentrations of the HBI Z- and E-triene at the permanently ice-free northernmost stations PS97/083 and PS97/084 in the eastern Drake Passage. These core sites are located in close vicinity to the Antarctic Polar Front (Figure 5.2) and we assume that the productivity of HBI triene source diatoms may benefit from mixing and upwelling of warm and cold water masses in this area (Moore and Abbott, 2002). Sediments

collected south of the Antarctic Polar Front and along the Hero Fracture Zone in the western Drake Passage (Figure 5.2) contain moderate and very low concentrations of HBI trienes, respectively. The Hero Fracture Zone is mainly barren of fine-grained sediments and dominated by sands (Lamy, 2016), which may point to intensive winnowing by ocean currents impacting the deposition and burial of organic matter. Moderate concentrations of HBI trienes at the continental slope along the WAP (PS97/053, PS97/074, PS97/077) and in the Bransfield Strait likely refer to primary production associated with the retreating sea ice margin during spring and summer. This indicates seasonally ice-free waters in high production coastal areas influenced by upwelling (Gonçalves-Araujo et al., 2015) and feeding of the local food web (Schmidt et al., 2018). The similarity in the distribution of the HBI Z- and the E-triene in our surface sediments – the latter of which so far is not often considered for Southern Ocean paleoenvironmental studies – supports the assumption of a common diatom source for these HBIs (Belt et al., 2000, 2017).

We consider that degradation of biomarker lipids may affect their distribution within surface sediments. While laboratory studies on HBIs in solution point to a low reactivity of $IPSO_{25}$ towards auto- and photooxidative degradation (Rontani et al., 2014, 2011), a more recent investigation into Antarctic surface sediments shows that $IPSO_{25}$ may potentially be affected by partial autoxidative and bacterial degradation but oxidation products are found in only minor proportions (Rontani et al., 2019a). Since HBI trienes exhibit a generally higher sensitivity to degradation than the C_{25} HBI diene (Rontani et al., 2014, 2019b) - and this is supported by a recent observation of increasing $IPSO_{25}$/HBI triene ratios with increasing water depths in a polynya system off Eastern Antarctica (Rontani et al., 2019b) – their lower concentrations in the Bransfield Strait have to be considered

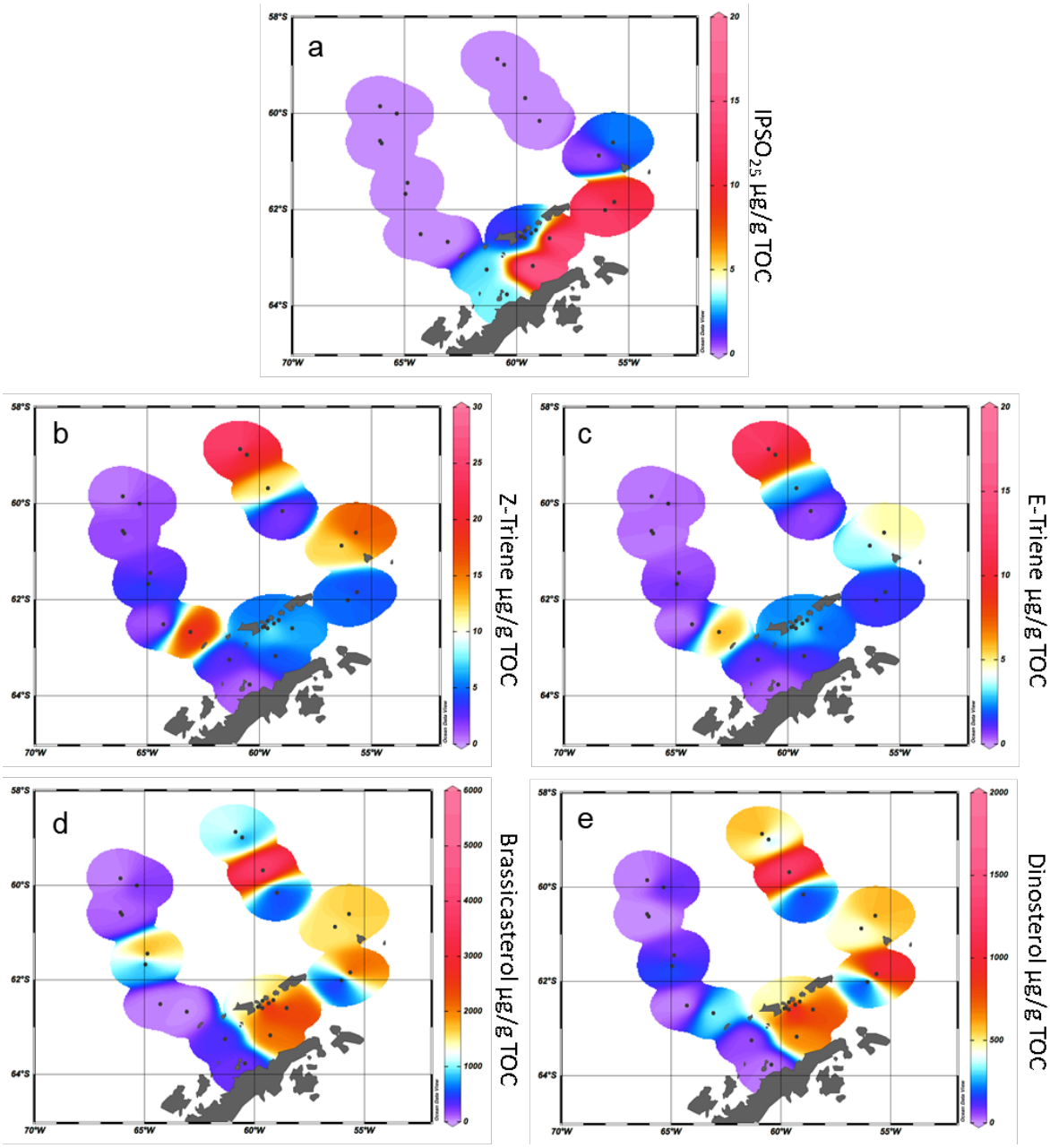

Figure 5.3 Distribution of a) $IPSO_{25}$, b) HBI Z-triene, c) HBI E-triene, d) brassicasterol, and e) dinosterol concentrations normalized to TOC. All distribution plots were made with Ocean Data View 4.7.10 (2017).

with care. Vice versa, regarding maximum HBI triene concentrations and the absence of $IPSO_{25}$ in Drake Passage sediments, we conclude that the absence of the latter in these samples can be linked to the lack of sea ice (and not to the degradation of $IPSO_{25}$ as HBI trienes would have been removed first).

Distribution of sterols

Brassicasterol is present in all samples with concentrations ranging from 3.39 to 5017.44 μg g^{-1} TOC, while dinosterol was detected in 22 samples (0.0002-1983.75 μg g^{-1} TOC). It is noticeable that the concentrations of sterols exceed the concentrations of $IPSO_{25}$ and HBI trienes by more than two orders of magnitude. We observe higher concentrations of brassicasterol and dinosterol in the eastern part of the Drake Passage supporting an open marine source for these sterols. Surprisingly, elevated concentrations of brassicasterol are also found at stations PS97/048-1 and 049-2 in the Hero Fracture Zone, which may argue against a winnowing signal leading to lower accumulation of organic matter. We can only speculate if transport and deposition of reworked sediment containing brassicasterol via iceberg rafting could explain these higher values. In contrast to the observation made for HBI trienes, high sterol concentrations are found in the eastern and central Bransfield Strait (Figure 5.3d and e). Previously, elevated concentrations of steroidal components including brassicasterol and dinosterol in sediment cores from the Bransfield Strait have been interpreted to reflect a high productivity and significant inputs from diatoms and dinoflagellates (Brault and Simoneit, 1988). In a more recent overview, also Cárdenas et al. (2018) report peak concentrations of pigments, sterols and total organic carbon in the Bransfield Strait, which they relate to large seasonal phytoplankton blooms and higher accumulation rates. Dinosterol and, in particular, brassicasterol are known to have different source organisms including diatoms, dinoflagellates, cryptophytes, prymnesiophycean algae and cyanobacteria (Volkman, 1986) and we assume that this diversity accounts for the higher concentration of these lipids in Bransfield Strait sediments, while concentrations of HBI trienes, mainly derived from diatoms, are significantly lower. Regarding the potential input of brassicasterol from cryptophytes (Gladu et al., 1990; Goad et al., 1983), changes in the dominance of this phytoplankton group over diatoms have been reported for our study area and have been associated with a shallowing of the mixed layer and lower salinity due to intensified glacial ice-melting along the WAP (Mendes et al., 2013).

Similar to the observations made for HBIs, selective degradation may also affect the concentration of phytosterols within surface sediments. With respect to the preservation potential of terrigenous and marine derived sterols, Rontani et al. (2012) note an only weak effect of biotic and abiotic degradation of brassicasterol in Arctic Ocean shelf sediments – if this is also true for Southern Ocean shelf areas needs to be determined. In general, further investigations into degradation

processes affecting both HBIs and phytosterols within (the same) sediment samples would address an important knowledge gap regarding in-situ biochemical modifications of the biomarker signal.

5.4.2 COMPARISON OF SATELLITE-DERIVED MODERN SEA ICE CONDITIONS AND BIOMARKER DATA

The spring and winter sea ice concentrations are shown in Figure 5.4a and b. Winter sea ice is estimated to not extend north of 61° S (Figure 5.4b) and varies between 1 % and 50 % in the study area, while sea ice is reduced to less than 20 % in spring (Figure 5.4a, Table Appendix 4). Sea ice concentrations of up to 50 % are common in winter between the South Shetland Islands and north of the Antarctic Sound where the influence of TWW is highest. Permanent sea ice cover is uncommon in the Bransfield Strait and around the WAP and this area is mainly characterized by a high sea ice seasonality, drift ice from the Weddell Sea (Collares et al., 2018) and a seasonally fluctuating sea ice margin.

Comparisons of $IPSO_{25}$ and winter sea ice concentrations derived from satellite data reveal a positive correlation (r^2 = 0.53). The strongest relationship is observed in the eastern Bransfield Strait where the influence of TWW is high. Correlations with spring sea ice (r^2 = 0.27) and other seasons are weak. As photosynthesis is not possible and a release of sea ice diatoms from melting sea ice is highly reduced during the Antarctic winter, the observation of a stronger correlation between recent winter sea ice concentrations and $IPSO_{25}$ is unexpected. We hence suggest that this offset may be related to the fact that the sediment samples integrate a longer time interval than is covered by satellite observations. Radiocarbon dating of selected samples that contain calcareous material reveals an age of 100 years BP in the vicinity of the South Shetland Islands (station PS97/059-2) and 142 years BP at the Antarctic Sound (station PS1546-2, Table 5.1). A significantly older age was determined for a sample of *N. pachyderma* from station PS97/044-1 (4830 years BP) which likely denotes the winnowing and/or very low sedimentation rates in the Drake Passage. Bioturbation effects and uncertainties in reservoir ages potentially mask the ages of the near-coastal

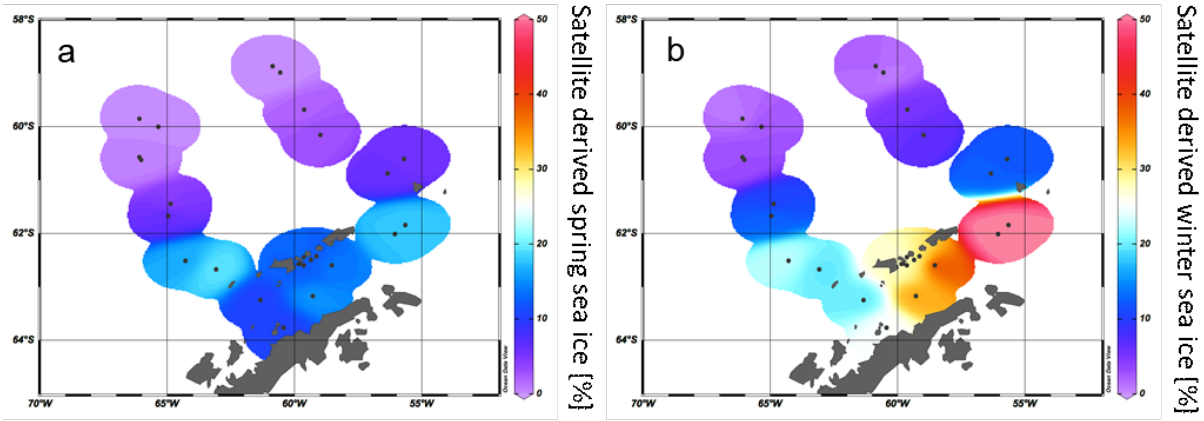

Figure 5.4 The satellite derived mean sea ice concentrations at each sampling station for a) spring and b) winter.

samples. Nevertheless, since also other published ages of surface sediments within the Bransfield Strait (Barbara et al., 2013; Barnard et al., 2014; Etourneau et al., 2013; Heroy et al., 2008) are in the range of 0-270 years, we consider that our surface samples likely reflect the paleoenvironmental conditions that prevailed during the last two centuries (and not just the last 35 years covered by satellite observations). In the context of the rapid warming during the last century (Vaughan et al., 2003) and the decrease of sea ice at the WAP (King, 2014; King and Harangozo, 1998), we suggest that the biomarker data of the surface sediments relate to a spring sea ice cover, which must have been enhanced compared to the recent (past 35 years) spring sea ice recorded via remote sensing. Presumably, the average spring sea ice conditions over the past 200 years might have been similar to the modern (past 35 years) winter conditions, which would explain the stronger correlation between $IPSO_{25}$ and winter sea ice concentrations. The absence of $IPSO_{25}$ at stations PS97/052 and PS97/053, off the continental slope, is in conflict with the satellite data depicting an average winter sea ice cover of 23 %. Earlier documentations that the $IPSO_{25}$ producing sea ice diatom *Berkeleya adeliensis* favors land-fast ice communities in East Antarctica and platelet ice occurring mainly in near-coastal areas (Belt et al., 2016; Riaux-Gobin and Poulin, 2004) could explain this mismatch between biomarker and satellite data, which further strengthens the hypothesis that the application of $IPSO_{25}$ seems to be confined to continental shelf or near-coastal and meltwater affected environments (Belt, 2018; Belt et al., 2016). Alternatively, strong ocean currents (i.e. the ACC) could have impacted the deposition of $IPSO_{25}$ in this region.

Although the distribution pattern of HBI trienes reveals generally higher concentrations in ice-free environments, we note only very weak negative correlations with satellite sea ice data ($r^2 < 0.1$). This may relate to the strong spatial variability in HBI triene concentrations within the Drake Passage and the different time periods represented by the satellite and sediment data. Similar to the HBI trienes, also the sterols do not show any significant relationship to the satellite sea ice concentrations. High abundances of brassicasterol and dinosterol are observed in both ice free as well as in seasonally ice-covered regions, which points to a broad environmental adaptation of the source organisms. We hence consider that other environmental parameters than sea ice (e.g.,

Table 5.1 Details of the radiocarbon dates and calibrated ages.

Sample Name	AWI-No.	Material	$F^{14}C \pm$ error	Conventional ^{14}C age [a]	Calibrated age (ca [a]
PS97/044-1	1657.1.1	N. pachyderma	0.5076	5447 ± 111	4830
PS97/059-2	1434.1.1	calcareous	0.8507	1299 ± 49	100
PS1546-2	1602.1.1	Moll.-Echinod	0.8456	1347 ± 64	142

nutrient availability, water temperature and/or grazing pressure) exert a major control on the productivity of HBI triene and sterol producers in the study area.

5.4.3 COMPARISON OF BIOMARKER DISTRIBUTIONS AND DIATOM-BASED SEA ICE ESTIMATES

The diatoms preserved in sediments from the study area (Table Appendix 5) can be associated with open ocean and sea ice conditions (Figure 5.5a-d). North of the South Shetland Islands, the strong influence of the ACC is reflected in the high abundance of open ocean diatom species such as *Fragilariopsis kerguelensis* and *Thalassiosira lentiginosa* (Esper et al., 2010). The two diatom species *Fragilariopsis curta* and *Fragilariopsis cylindrus* – known to not produce HBIs (Belt et al., 2016; Damsté

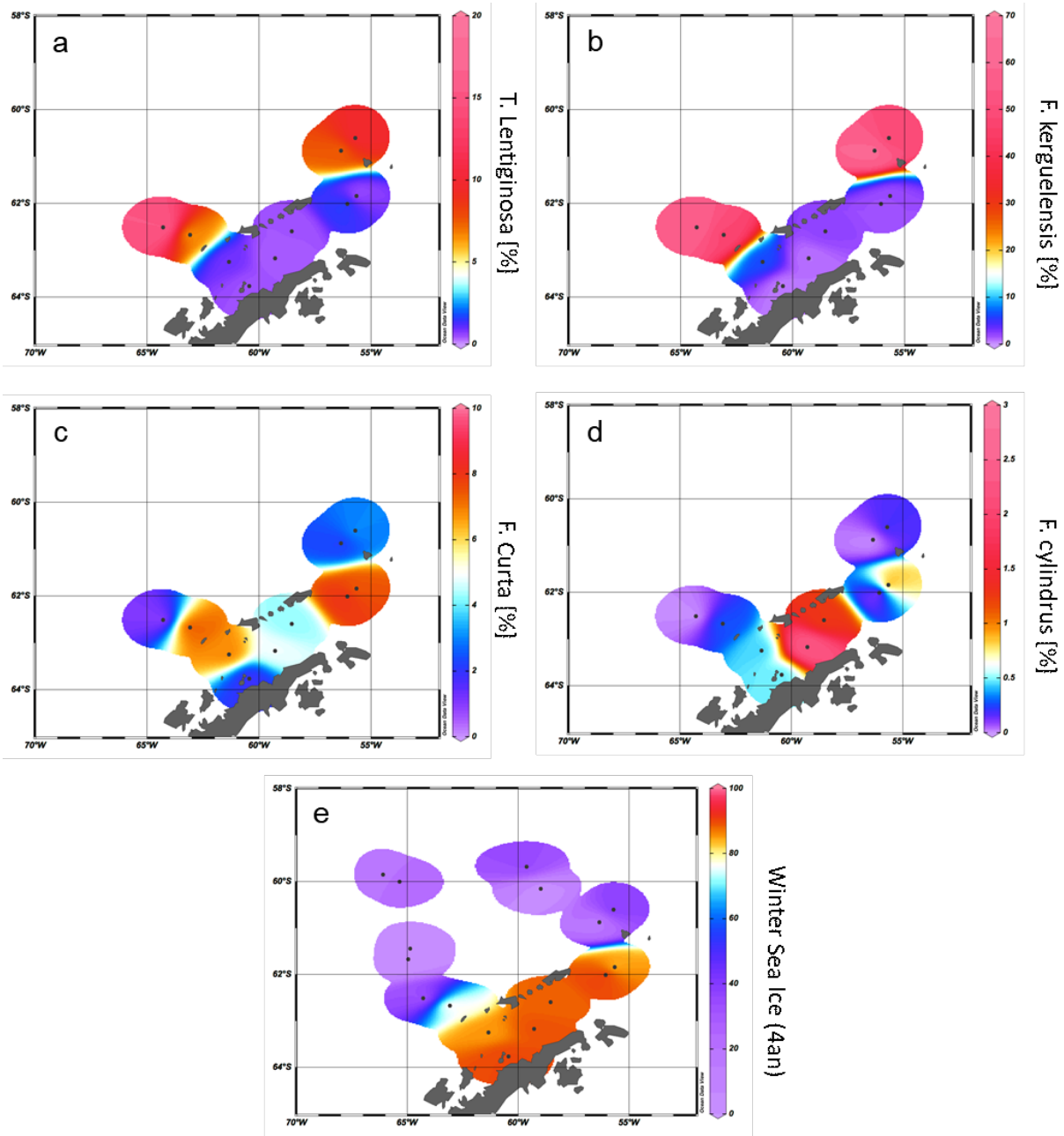

Figure 5.5 Distribution of the diatoms a) T. lentiginosa, b) F. kerguelensis, c) F. curta, and d) F. cylindrus in the study area (percentage per sample). The winter sea ice concentrations from the application of transfer function of Esper and Gersonde (2014a) are shown in e).

et al., 2004) - mark the vicinity to sea ice (Buffen et al., 2007; Pike et al., 2008) and indicate fast and melting ice, a stable sea ice margin and stratification due to melting processes and the occurrence of seasonal sea ice. These observations are in accordance with previous diatom studies revealing a dominance of *Fragilariopsis kerguelensis* in the permanently open-ocean zone in the Drake Passage and an assemblage shift to more cold water adapted and sea ice-associated species in the seasonal sea ice zone of the Bransfield Strait (Cárdenas et al., 2019).

The high abundance of these sea ice diatoms in our samples is in good agreement with high and moderate $IPSO_{25}$ concentrations in the Bransfield Strait and around the South Shetland Islands, respectively. The only HBI source diatom identified is the HBI Z-triene producing *Rhizosolenia hebetata* (Belt et al., 2017), which is present in four samples in relatively small amounts which do not show a relation to the measured HBI Z-triene concentrations (Tables Appendix 1 and 5). The source diatom of $IPSO_{25}$ *Berkeleya adeliensis* was not observed (or preserved) in the samples, and we suggest that additional, hitherto unknown, producers for $IPSO_{25}$ as well as for the HBI trienes may exist.

We applied the transfer function of Esper and Gersonde (2014a) with four analogs (4an, Table Appendix 5) to our samples to estimate winter sea ice concentrations (WSI; Figure 5.5e). The diatom approach shows a clear trend of high winter sea ice concentrations in the range of 78-91 % in the Bransfield Strait and low sea ice concentrations (between 6-39 %) north of the continental slope. The fact that diatom data propose sea ice in the Drake Passage may result from the high ages of surface sediments but also from drift, resuspension and sedimentation of diatom remains. Because of the absence of $IPSO_{25}$ in the Drake Passage the correlation of its concentrations with WSI is only weak ($r^2 = 0.29$).

5.4.4 TESTING A SEMI-QUANTITATIVE SEA ICE APPROACH FOR THE SOUTHERN OCEAN: $PIPSO_{25}$

Following the PIP_{25}-approach applied in the Arctic Ocean (Müller et al., 2011; Belt and Müller, 2013; Xiao et al., 2015), we used $IPSO_{25}$, HBI triene and sterol data to calculate the $PIPSO_{25}$ index. The main concept of combining the sea ice proxy with an indicator of an ice-free ocean environment (i.e. a phytoplankton biomarker; Müller et al., 2011), aims at a more detailed assessment of the sea ice conditions. By reducing the light penetration through the ice, a thick and perennial sea ice cover limits the productivity of bottom sea ice algae (Hancke et al., 2018) , which results in the absence of both sea ice and pelagic phytoplankton biomarker lipids in the underlying sediments. Vice versa, sediments from permanently ice-free ocean areas only lack the sea ice biomarker but contain variable concentrations of phytoplankton biomarkers (Müller et al., 2011). The co-occurrence of both biomarkers in a sediment sample suggests seasonal sea ice coverage promoting algal production indicative of sea ice as well as open ocean environments (Müller et al.,

2011). Consideration of a phytoplankton biomarker alongside the sea ice proxy hence helps to avoid an underestimation of the past sea ice cover deduced from the absence of the sea ice proxy, which, in fact, may also be due to a permanent sea ice cover (Belt, 2018, 2019; Belt and Müller, 2013). Depending on the biomarker reflecting pelagic (open ocean) conditions, we here define P_ZIPSO_{25} (using the HBI Z-triene), P_EIPSO_{25} (using the HBI E-triene), P_BIPSO_{25} (using brassicasterol), and P_DIPSO_{25} (using dinosterol).

The $PIPSO_{25}$ values are 0 in the Drake Passage and increase to intermediate values at the South Shetland Islands and the continental slope and reach highest values in the Bransfield Strait (Figure 5.6a-d). Minimum $PIPSO_{25}$ values are supposed to refer to a predominantly ice-free oceanic environment in the Drake Passage, while moderate $PIPSO_{25}$ values mark the transition towards a marginal sea ice coverage at the continental slope and around the South Shetland Islands. Elevated $PIPSO_{25}$ values in samples from the northeastern Bransfield Strait suggest an increased sea ice cover (probably sustained through the drift of sea ice originating in the Weddell Sea). This pattern reflects the oceanographic conditions of a permanently ice-free ocean north of the South Shetland Islands and a seasonal sea ice zone at the WAP influenced by the Weddell Sea as described by Cárdenas et al. (2018). Both HBI triene-based $PIPSO_{25}$ indices show constantly high values at the coast of the WAP of >0.7 (P_ZIPSO_{25}) and >0.8 (P_EIPSO_{25}), respectively, and in the southern

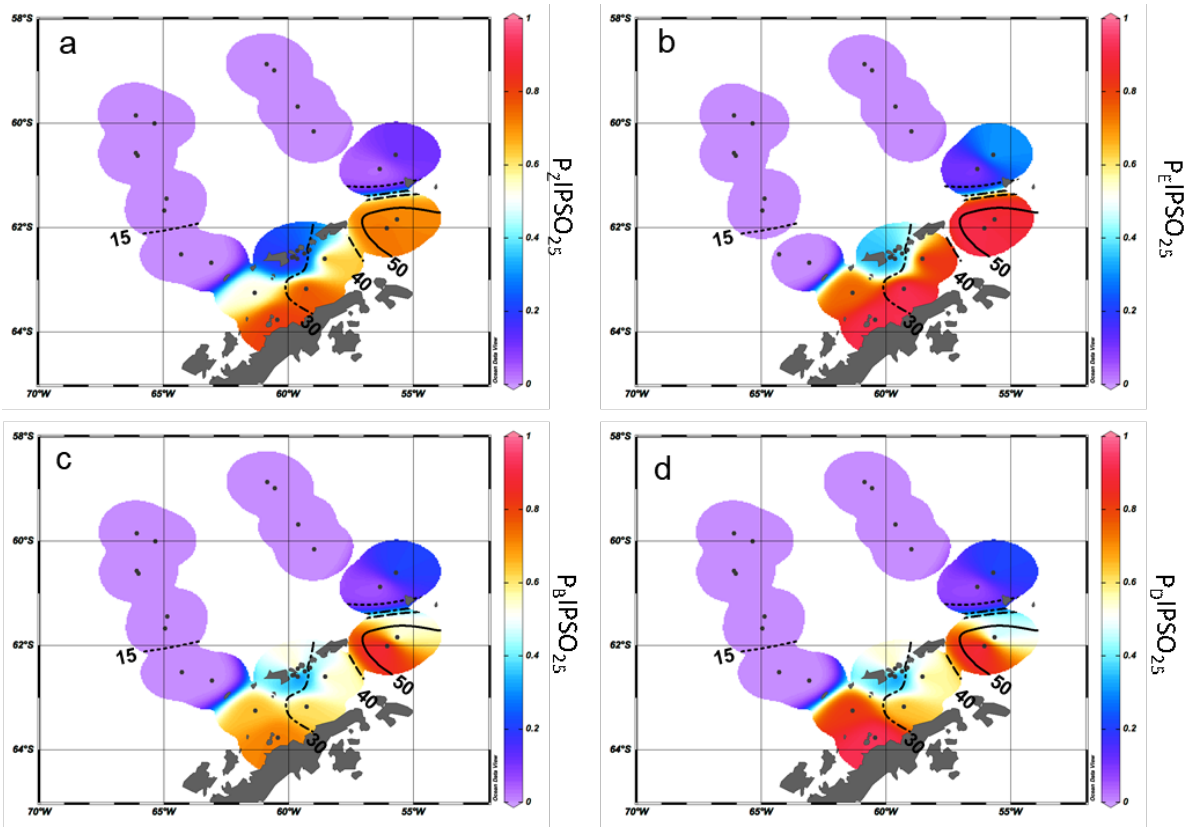

Figure 5.6 Distribution of a) P_ZIPSO_{25}, b) P_EIPSO_{25} , c) P_BIPSO_{25}, and d) P_DIPSO_{25} values in the study area. The extent of 15 %, 30 %, 40 % and 50 % satellite sea ice concentrations during winter is added as contour lines (see also Figure 3.4b).

Bransfield Strait paralleling the southwest-northeast oriented Peninsula Front described by Sangrà et al. (2011). This front is reported to act as a barrier for phytoplankton communities (Gonçalves-Araujo et al., 2015) and is associated with the encounter between TWW carrying Weddell Sea sea ice through the Antarctic Sound and the TBW. The high $PIPSO_{25}$ values suggesting an extended sea ice cover west of the Peninsula Front (station PS97/054 and PS97/056) result from minimum concentrations of pelagic biomarkers and moderate concentrations of $IPSO_{25}$. $PIPSO_{25}$ values based on the HBI E-triene are about 0.2 higher compared to P_ZIPSO_{25}, due to the generally lower concentrations of the HBI E-triene (Table Appendix 1).

The sterol-based $PIPSO_{25}$ values display a generally similar pattern as P_ZIPSO_{25} and P_EIPSO_{25}, respectively, and we note a high comparability between the P_EIPSO_{25} and P_BIPSO_{25} values (r^2 = 0.73). Some differences, however, are observed in the southwestern part of the Bransfield Strait (station PS97/056) where P_BIPSO_{25} indicates a lower sea ice cover and in the central Bransfield Strait (stations PS97/068 and PS97/069) where P_BIPSO_{25} and P_DIPSO_{25} point to only MIZ conditions. Regarding the modern sea ice conditions, the HBI triene-based $PIPSO_{25}$ indices hence seem to reflect the oceanographic conditions within the Bransfield Strait more satisfactorily. It has to be noted that the brassicasterol- or dinosterol-based $PIPSO_{25}$ index links environmental information derived from biomarker lipids belonging to different compound classes (i.e. HBIs and sterols), which have fundamentally different chemical properties. This requires special attention as, for example, selective degradation of one of the compounds may affect the sedimentary concentration of the respective lipids (Rontani et al., 2018b). Previous studies linking HBI and sterol-based sea ice reconstructions with satellite-derived or, with respect to downcore paleo studies, paleoclimatic data, however, demonstrate that the climatic/environmental conditions controlling the production of HBIs and sterols seem to exceed the influence of a potential preferential degradation of these biomarkers within the sediments (e.g., Berben et al., 2014; Cabedo-Sanz et al., 2013; Müller et al., 2009, 2012; Müller and Stein, 2014; Stein et al., 2017; Xiao et al., 2015). A comparison of PIP_{25} records determined using brassicasterol and the HBI Z-triene for three sediment cores from the Arctic realm covering the past up to 14.000 years BP (Belt et al., 2015) reveals very similar trends for both versions of the PIP_{25} index in each core, which may point to, at least, a similar degree of degradation of HBI trienes and sterols through time. More such studies are needed to evaluate the preservation potential of HBIs and sterols in Southern Ocean sediments, especially for down core paleo studies.

Since brassicasterol and dinosterol are highly abundant in both seasonally ice-covered Bransfield Strait sediments as well as in permanently ice-free Drake Passage sediments, their use as an indicator of fully open-marine conditions in the study area is questionable. Elevated concentrations

of both sterols in the Bransfield Strait could either point to an additional input of these lipids from melting sea ice (Belt et al., 2013) or a better adaptation of some of their source organisms to cooler and/or ice-affected ocean environments. Production and accumulation of these lipids in (late) summer (i.e. after the sea ice season) has to be considered as well. This observation highlights the need for a better understanding of the source organisms and the mechanisms involved in the synthesis of these sterols. Similarly, more research is needed on the production of $IPSO_{25}$ in Southern Ocean sea ice environments. The source diatom *Berkeleya adeliensis* seems to be restricted to a very unique ice environment. Previous studies documenting the lack of $IPSO_{25}$ in distal though winter sea ice covered areas (e.g., Belt et al., 2016) emphasize this limitation and it has been suggested that $IPSO_{25}$ may be more indicative of the type of sea ice rather than sea ice extent (Belt, 2019), which needs to be considered when targeting at more quantitative sea ice reconstructions using this biomarker.

Comparison of $PIPSO_{25}$ with satellite sea ice data and diatom sea ice estimations

In the northeastern part of the study area, the HBI triene based $PIPSO_{25}$ indices align well with winter sea ice concentrations and depict the gradient from the marginally ice-covered southern Drake Passage towards the intensively ice-covered Weddell Sea. This is visualized with contour lines from the observed sea ice extent of 15 %, 30 %, 40 % and 50 % winter sea ice compared to the $PIPSO_{25}$ values in Figure 5.6a-d. In the southwestern part of the Bransfield Strait, all $PIPSO_{25}$ indices suggest a higher sea ice cover than it is reflected in the satellite data. This may be explained by the transport (and melt) of drift ice through the TWW, joining the TBW at the southwestern Peninsula Front and/or a higher sea ice cover in this area prior to the remote sensing observational period (and prior to the recent WAP warming).

Correlations of $PIPSO_{25}$ values with satellite-derived sea ice concentrations (for spring, summer, autumn and winter) contrast earlier observations made for the PIP_{25} index in the Arctic Ocean, where the closest linear relationship is found mainly with the spring sea ice coverage (i.e. the blooming season of sea ice algae; Müller et al., 2011; Xiao et al., 2015). We observe a remarkably low correlation between $PIPSO_{25}$ values and spring sea ice concentrations of less than 20 % with a coefficient of determination $r^2 = 0.37$ for P_ZIPSO_{25}, $r^2 = 0.50$ for P_EIPSO_{25} (Figure 5.7a), $r^2 = 0.31$ for P_BIPSO_{25}, and $r^2 = 0.34$ for P_DIPSO_{25} (Figure 5.7b). The highest correlation is observed between winter sea ice concentrations and P_EIPSO_{25} ($r^2 = 0.72$), and P_ZIPSO_{25} ($r^2 = 0.65$, Figure 5.7c) with a weaker correlation for the sterol-based $PIPSO_{25}$ values (P_BIPSO_{25}: $r^2 = 0.52$; P_DIPSO_{25}: $r^2 = 0.44$, Figure 5.7d). As discussed above, we attribute this seemingly conflicting result of a better agreement between biomarker data and winter (instead of spring) sea ice conditions to the offset in the time intervals reflected in satellite and sediment data. For the application of the $PIPSO_{25}$

approach, more aspects concerning the physical environmental conditions controlling the formation of platelet ice, which, at least at this state of research, is regarded as a main source of $IPSO_{25}$ (Belt et al., 2016) need to be considered. The formation and accumulation of platelet ice in supercooled waters below landfast sea ice or underneath an ice-shelf (e.g., Gough et al., 2012; Hoppmann et al., 2015) seem to limit the spatial occurrence of $IPSO_{25}$ and hence the applicability of $PIPSO_{25}$ to coastal environments. However, transport of supercooled waters away from the coast may lead to platelet ice formation (and colonization of *Berkeleya adeliensis*) in more distal areas (Hoppmann et al., 2015) and also the drift of sea ice (including the underlying platelet ice) may impact the distribution of $IPSO_{25}$ in Southern Ocean sediments and these processes require further investigations. Even though $PIPSO_{25}$ values show a stronger relationship to satellite sea ice concentrations than $IPSO_{25}$ concentrations more insight into the production and sedimentation of the involved biomarker lipids is needed to develop such a semi-quantitative approach.

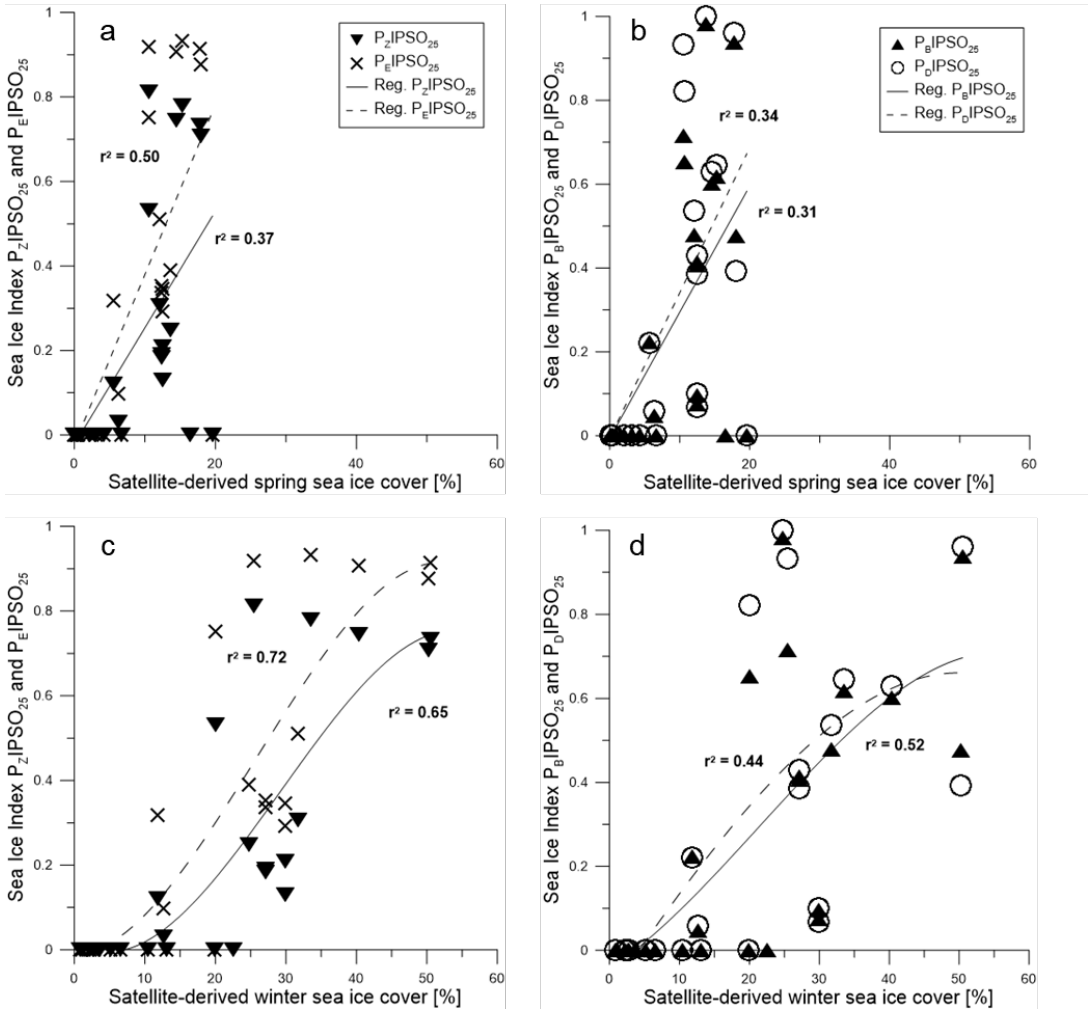

Figure 5.7 Scatter plots of satellite spring sea ice concentrations and a) P_ZIPSO_{25} (triangles, solid regression line) and P_EIPSO_{25} (crosses, dashed regression line) and b) P_BIPSO_{25} (triangles, solid regression line) and P_DIPSO_{25} (circles, dashed regression line). Scatter plots of satellite winter sea ice concentrations with c) P_ZIPSO_{25} (triangles, solid regression line) and P_EIPSO_{25} (crosses, dashed regression line) and d) P_BIPSO_{25} (black triangles, solid regression line) and P_DIPSO_{25} (circles, dashed regression line). All scatter plots were done with Grapher™ 13.

With regard to the spatially and temporally variable sea ice extent, Esper and Gersonde (2014a) studied the response of diatom species to changes in environmental conditions and their response to the non-linear behavior of sea ice dynamics (Zwally et al., 2002). In contrast to ice free areas or areas of permanent sea ice cover, areas characterized by the transition from consolidated to unconsolidated sea ice show rapid changes in satellite derived sea ice concentrations (ranging from 90 % to 15 %) and exhibit a large variability in species composition. To reflect this curve in sea ice we hence chose a cubic polynomial regression (polynomial of third degree) to determine the relation between $PIPSO_{25}$ values and satellite data depicting sea ice concentrations of more than 20 %. A slightly sigmoid-shaped regression line of winter sea ice concentrations and $PIPSO_{25}$ values depicts the non-linearity of sea ice cover in different sea ice regimes.

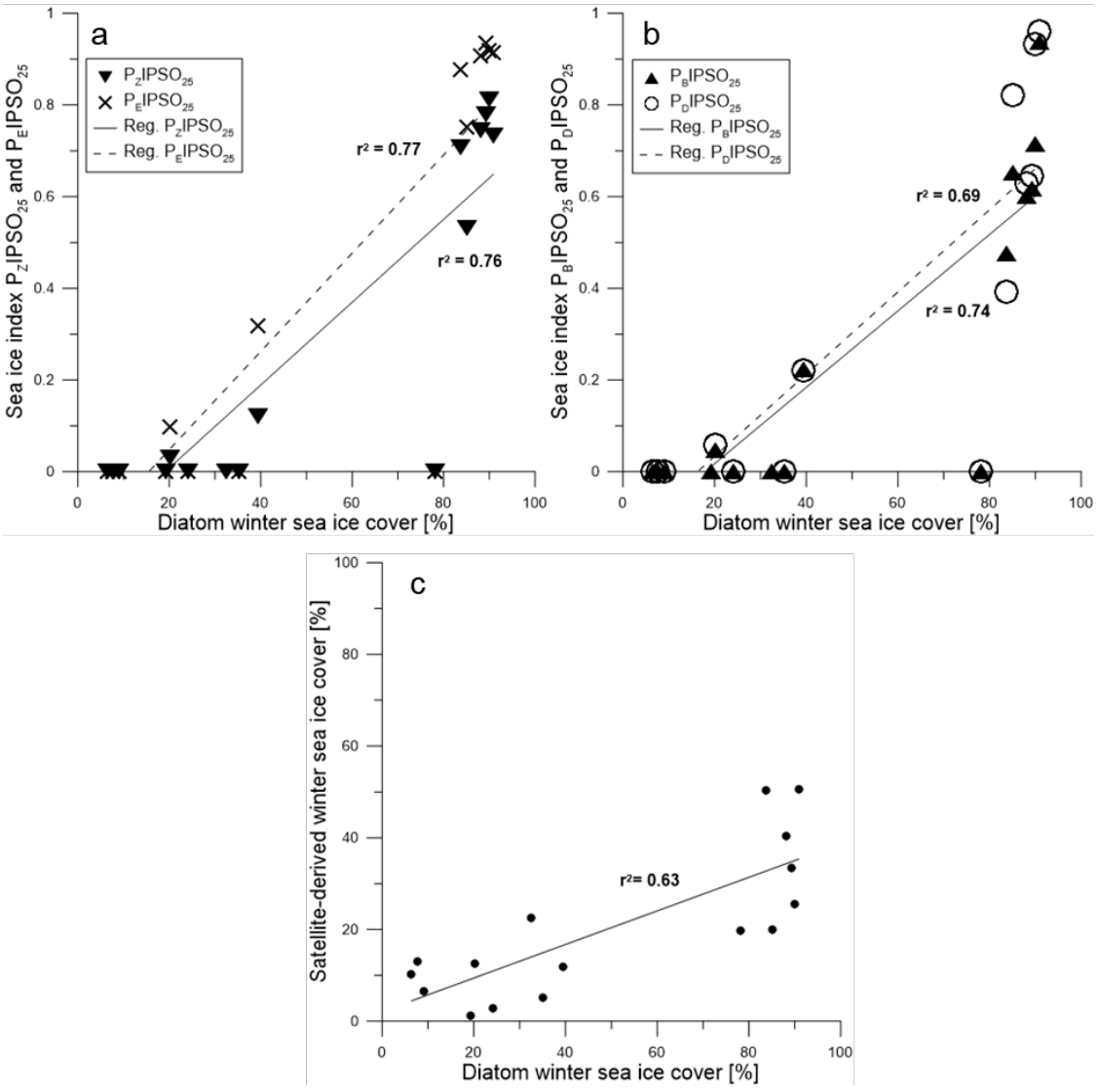

Figure 5.8 Scatter plots of a) P_ZIPSO_{25} (triangles, solid regression line) and P_EIPSO_{25} (crosses, dashed regression line) and b) P_BIPSO_{25} (triangles, solid regression line) and P_DIPSO_{25} (circles, dashed regression line) against diatom derived winter sea ice concentrations. c) Scatter plot of diatom transfer function winter sea ice concentrations and satellite winter sea ice concentrations.

A positive correlation is found between WSI concentrations derived from diatoms and the $PIPSO_{25}$ indices based on HBI trienes (P_ZIPSO_{25} with $r^2 = 0.76$; P_EIPSO_{25} with $r^2 = 0.77$, Figure 5.8a). The correlations of sterol-based $PIPSO_{25}$ values with WSI are slightly lower but in the same range (P_BIPSO_{25} with $r^2 = 0.74$; P_DIPSO_{25} with $r^2 = 0.69$, Figure 5.8b). A slightly weaker correlation is noted for diatom- and satellite-based winter sea ice concentrations ($r^2 = 0.63$; Figure 5.8c). Overall, the diatom approach indicates higher sea ice concentrations than the satellite data with an offset of up to 65 %. This may be due to different sources of satellite reference data used for the transfer function or also due to the fact that the sediment samples integrate a longer time period with a higher sea ice cover than the satellite data (see discussion in chapter 5.4.2). Regarding future sea ice reconstructions based on $IPSO_{25}$ and other biomarkers, we note that the simultaneous study of diatom assemblages provides valuable information on the sea surface conditions and may help to avoid misleading interpretation of the biomarker data (Belt, 2019). Vice versa, while diatom-based transfer functions mainly refer to winter sea ice concentrations, the $IPSO_{25}$ (and $PIPSO_{25}$) signal holds critical information on coastal spring/summer sea ice conditions, which are often crucial for ice-shelf (melting) processes. Pairing the micropaleontological and the biomarker approach hence provides for a more comprehensive reconstruction of Southern Ocean sea ice conditions.

5.5 CONCLUSIONS

The distribution of the sea ice biomarker $IPSO_{25}$, related HBI trienes and phytosterols as well as diatoms in a suite of surface sediments from the southern Drake Passage and the WAP reflects recent sea surface water characteristics reasonably well. While highest HBI triene concentrations are observed in the permanently open ocean zone of the Drake Passage, they are significantly reduced in the seasonally ice-covered Bransfield Strait. This pattern is reversed for the sea ice proxy $IPSO_{25}$ and in accordance with previous surface sediment analyses revealing a preferential occurrence of this biomarker in near-coastal environments. The distribution of phytosterols points to a broader environmental significance of brassicasterol and dinosterol in terms of ocean temperature and sea ice tolerance, and/or nutrient availability. Following the PIP_{25} approach established for Arctic Ocean sea ice reconstructions, the herein proposed sea ice index $PIPSO_{25}$ indicates seasonal sea ice cover along the coast of the WAP and in the Bransfield Strait, whereas mainly ice-free conditions prevail in the Drake Passage. In general, this pattern is consistent with satellite-derived sea ice data and diatom-based sea ice estimates and we note that the $PIPSO_{25}$ index seems a potential approach towards semi-quantitative sea ice reconstructions in the Southern Ocean. The recent rapid warming in the study area, however, affects the comparability of proxy and satellite data. The fact that the surface sediments integrate a significantly longer time interval than the remote sensing data thwarts attempts to calibrate $PIPSO_{25}$ values against observed sea ice

concentrations. Additional data from other circum-Antarctic coastal (and distal) environments and investigations into potential calibration methods are needed to further develop this approach. Importantly, more information is needed on the mechanisms of $IPSO_{25}$ and HBI triene synthesis, transport and preservation within sediments. Despite a generally good agreement between $PIPSO_{25}$-, diatom- and satellite-based sea ice distributions, we note that the basically different sea ice patterns and sea ice varieties in the Southern Ocean and accordingly different mechanisms controlling the $IPSO_{25}$ signal need to be considered carefully, when adapting a (not yet fully validated) semi-quantitative approach initially developed for the Arctic Ocean.

DATA AVAILABILITY

All data can be found in this paper and will be available at the open access repository www.pangaea.de (https://doi.pangaea.de/10.1594/PANGAEA.897165).

AUTHOR CONTRIBUTIONS

The study was conceived by MV and JM. Data collections and experimental investigations were done by MV together with OE (diatoms), GM (radiocarbon dating), CH (satellite data), and ES (isotope data). MV wrote the manuscript and did the visualizations. KF provided technical support. JM supervised the study. All authors contributed to the interpretation and discussion of the results and the conclusion of this study.

ACKNOWLEDGEMENT

We thank the captain, crew and chief scientist Frank Lamy of RV Polarstern cruise PS97, and the following supporters: Mandy Kiel and Denise Diekstall (technicians), Lester Lembke-Jene (biology, dating), Liz Bonk and Hendrik Grotheer (from MICADAS), Max Mues (sample preparation), Nicoletta Ruggieri (lab support), Walter Luttmer (lab support). Simon Belt is acknowledged for providing the 7-HND internal standard for HBI quantification. We also acknowledge the two anonymous reviewers and the editor for their constructive and detailed comments. Financial support was provided through the Helmholtz Research grant VH-NG-1101.

6 PART II: SEA ICE DYNAMICS AT THE WESTERN ANTARCTIC PENINSULA DURING THE INDUSTRIAL ERA: A MULTI-PROXY INTERCOMPARISON STUDY

Maria-Elena Vorrath[1], Juliane Müller[1,2,3], Lorena Rebolledo[4,5], Paola Cárdenas[4], Xiaoxu Shi[1], Oliver Esper[1], Thomas Opel[1], Walter Geibert[1], Praxedes Muñoz Parra[6], Carina B. Lange[4,7,8], Gerrit Lohmann[1], Gesine Mollenhauer[1,2]

[1]Alfred Wegener Institute, Helmholtz Centre for Polar and Marine Research, Bremerhaven, Germany

[2]MARUM – Center for Marine Environmental Sciences, University of Bremen, Germany

[3]Department of Geosciences, University of Bremen, Germany

[4]Centro de Investigación Dinámica de Ecosistemas Marinos de Altas Latitudes (IDEAL), Universidad Austral de Chile, Valdivia, Chile

[5]Instítuto Antártico Chileno (INACH), Punta Arenas, Chile

[6]Facultad de Ciencias del Mar, Universidad Católica del Norte, Antofagasta, Chile

[7]Centro Oceanográfico COPAS Sur-Austral, Universidad de Concepción, Chile

[8]Departamento de Oceanografía, Universidad de Concepción, Chile

Submitted in *Climate of the Past*, 4th May 2020.

Abstract

In the last decades, changing climate conditions have had a severe impact on sea ice at the Western Antarctic Peninsula (WAP), an area rapidly transforming under global warming. To study the development of spring sea ice and environmental conditions in the pre-satellite era we investigated three short marine sediment cores for their biomarker inventory with particular focus on the sea ice proxy $IPSO_{25}$ and micropaleontological proxies. The core sites in the Bransfield Strait are located in shelf to deep basin areas characterized by a complex oceanographic frontal system, coastal influence and sensitivity to large-scale atmospheric circulation patterns. We analyzed geochemical bulk parameters, biomarkers (highly branched isoprenoids, glycerol dialkyl glycerol tetraethers, sterols), and diatom abundances and diversity over the past 200 years (^{210}Pb dating), and compared them to observational data, sedimentary and ice core climate archives as well as

results from numerical models. Based on biomarkers we could identify four different stratigraphic units with (1) stable conditions and moderate sea ice cover before 1860, (2) low to moderate sea ice cover between 1860 and 1930, (3) high seasonal variability and changes in sea ice regimes from 1930 to 1990 and (4) a shift to increasing sea ice cover despite anthropogenic warming since 1990. Although $IPSO_{25}$ concentrations correspond quite well with satellite sea ice observations for the past 40 years, we note discrepancies between the biomarker-based sea ice estimates and the long-term model output for the past 200 years, ice core records and reconstructed atmospheric circulation patterns such as El Niño Southern Oscillation (ENSO) and Southern Annular Mode (SAM). We propose that the sea ice biomarker proxies $IPSO_{25}$ and $PIPSO_{25}$ are not linearly related to sea ice cover and, additionally, each core site reflects specific, local environmental conditions. High $IPSO_{25}$ and $PIPSO_{25}$ values may not be directly interpreted as referring to high spring sea ice cover because variable sea ice conditions and enhanced nutrient supply may affect the production of both the sea-ice associated and phytoplankton-derived (open marine, pelagic) biomarker lipids. For a more meaningful interpretation we recommend to carefully consider individually biomarker records to distinguish between cold, sea ice favoring and warm, sea ice diminishing environmental conditions.

6.1 INTRODUCTION

Observations of global mean surface temperatures show a warming since the industrialization of approximately 1.0±0.2°C (IPCC, 2018) above the 1850-1900 baseline. An acceleration of this trend due to anthropogenic forcing has been projected (IPCC, 2019). The ocean, and especially the Southern Ocean, takes up the majority of the atmospheric heat, and warming has already been observed at all depths (IPCC, 2019). Antarctica´s hot spot of warming is the Western Antarctic Peninsula (WAP) (Jones et al., 2016) with atmospheric temperature increases of 3.7±1.6°C per century (Vaughan et al., 2003) and a slight cooling from 2000 to 2010 (Turner et al., 2019). A warming of up to 1°C of subsurface water is evident in different water masses around the WAP (Cook et al., 2016). On land, glaciers and ice shelves on both sides of the Antarctic Peninsula (AP) retreat rapidly (Cook et al., 2016; Rignot et al., 2019), pointing towards a potential collapse of the WAP ice shelves. In the ocean, the loss of sea ice cover is significant (Parkinson and Cavalieri, 2012). Shortened sea ice seasons (Parkinson, 2002) and a reduction of sea ice extent accelerating from 4 % up to 10 % per decade (Liu et al., 2004) have been observed via satellite since 1979. A recent compilation shows that the slight increase in sea ice around the entire Antarctic continent since 1979 seems to be interrupted since 2014 (Parkinson, 2019). However, the region of the WAP, the Bellingshausen Sea and Amundsen Sea show contrasting sea ice trends and high sea ice variability in 2014 and afterwards (Hobbs et al., 2016). The changes in sea ice cover are not only

related to warm water intrusion and higher sea surface temperatures (SSTs) at the WAP (Martinson and McKee, 2012; Meredith and King, 2005), but also to large-scale modes of atmospheric circulation such as the Southern Annular Mode (SAM) (e.g. Barbara et al., 2013) and the El Niño Southern Oscillation (ENSO) (e.g. Liu et al., 2004), or a combination of both (Etourneau et al., 2013; Stammerjohn et al., 2008b, 2008a).

Sea ice is an important factor that shapes and influences the Southern Ocean. Melting sea ice releases nutrients and leads to enhanced primary production and ocean stratification during spring and summer (Arrigo et al., 1997; Vernet et al., 2008). Interestingly, a higher number of sea ice days is associated with to an increased photosynthetic efficiency and enhanced carbon fixation rates due to enhanced nutrient delivery stimulating primary production (Schofield et al., 2018) but also thinning of sea ice affects marine productivity positively (Hancke et al., 2018). Release of dense brine during sea ice formation influences the thermohaline circulation by feeding of deep and intermediate waters (Nicholls et al., 2009) but also induce upwelling at sea ice edges (Alexander and Niebauer, 1981). Sea ice cover also regulates the ocean-atmosphere exchange of heat and gases as well as regional precipitation and albedo (Allison et al., 1982; Butterworth and Miller, 2016; Turner et al., 2017) and is a potential source of the radiative-relevant volatile dimethylsulphide (Trevena and Jones, 2006) – a precursor of methanesulphonic acid (MSA) (Abram et al., 2010). Sea ice changes at the WAP may lead to the destabilization and/or collapse of local ice shelves due to warm water intrusions and basal melting (Cook et al., 2016; Etourneau et al., 2019; Hellmer et al., 2012) promoting an accelerated ice-sheet flow towards the ocean (Huss and Farinotti, 2014). Sea ice decline in this region may thus also indirectly impact global sea level rise.

Atmospheric circulation patterns such as ENSO and SAM have been suggested to influence the distribution of SST and sea ice at the WAP (Ding et al., 2012; Stammerjohn et al., 2008b, 2008a). Etourneau et al. (2013) concluded from the occurrence of higher sea ice cover together with higher SSTs that a rising number of ENSO events would increase the seasonal amplitude of warmer summers and colder winters in the region. SAM is the leading mode in the Southern Hemisphere (Jones et al., 2016) and has significant impacts on temperatures at the northeast AP (Clem et al., 2016). Stammerjohn et al. (2008b) link ENSO and SAM related teleconnections to opposite sea ice trends in the Pacific and Atlantic sector of the Southern Ocean on decadal scales during the satellite era. The high-latitude responses and ice-atmosphere anomalies are strongest when a positive ENSO occurs "in-phase" with a negative SAM (+ENSO/-SAM) and the subtropical jet over the Pacific Ocean is strengthening whereas the polar frontal jet and the westerlies are weaker. In this state, a positive sea level pressure establishes a high-pressure cell in the Pacific Southern Ocean and warmer, moister conditions with less sea ice establish there. Meanwhile, the Weddell Sea and

the WAP experience a cooling with an advance of sea ice. During the opposite state (-ENSO/+SAM) a stronger polar frontal jet establishes a low-pressure cell in the Bellingshausen Sea. In this case, increased, south-ward migrated westerlies transport heat towards the WAP and the Weddell Sea and sea ice cover is reduced under high atmospheric and sea surface temperatures (Marshall et al., 2006; Stammerjohn et al., 2008b; Yuan, 2004). Clem et al. (2016) describe that the combined effect of in-phase ENSO and SAM is strongest in spring.

For modelling past and future Antarctic climate, its ice sheet stability, the thermohaline circulation or the impacts of sea ice loss for ecosystems, data of past sea ice cover are crucial but barely available (Bracegirdle et al., 2015, 2019). For the WAP, insights into climate and sea-ice dynamics during the industrial era are available from ice cores (stable isotopes and marine aerosols) but information from high resolution marine sediments and in particular sedimentary, geochemical or diatom-based sea ice proxies remain sparse (Thomas et al., 2019). Sinking marine particles carry environmental information from the sea surface to the ocean floor and, when buried in the sediments, the environmental history including sea ice can be deduced from these marine climate archives. For sea ice reconstructions, the use of sea ice-associated diatom species and biogeochemical parameters are common (Crosta et al., 1998; Esper and Gersonde, 2014a; Gersonde and Zielinski, 2000). Since diatom frustules may be affected by the dissolution of biogenic opal in the photic zone (Ragueneau et al., 2000), on the ocean floor (Leventer, 1998) and in the sediments (Burckle and Cooke, 1983; Esper and Gersonde, 2014b), an increasing attention is directed to their molecular remains, i.e. specific biomarker lipids, as promising tools for past sea ice reconstructions (Massé et al., 2011). A specific diunsaturated highly branched isoprenoid alkene (HBI diene, $C_{25:2}$) has been proposed as potential tool for past spring sea ice reconstructions in the Southern Ocean (Massé et al., 2011). It is produced by sea ice diatoms (Nichols et al., 1988) and its sea ice origin is evident from the high $\delta^{13}C$ isotopic signature of the molecule (Massé et al., 2011; Sinninghe Damsté et al., 2007; Vorrath et al., 2019). The sea ice diatom *Berkeleya adeliensis* which is found in Antarctic landfast ice and platelet ice (Riaux-Gobin and Poulin, 2004) was identified as a producer of the HBI diene (Belt et al., 2016). HBI diene is present in surface and downcore sediments around Antarctica and can be used as $IPSO_{25}$ (**I**ce **P**roxy for the **S**outhern **O**cean with **25** carbon atoms) in analogy to the Arctic IP_{25} (Belt et al., 2016; Lamping et al., 2020; Massé et al., 2011; Vorrath et al., 2019). To differentiate among an extended spring sea ice cover, the occurrence of a stable sea ice margin and/or an open marine environment, $IPSO_{25}$ is combined with phytoplankton-derived biomarker from lipids such as HBI trienes and/or sterols, which are assumed to refer to open water conditions (Belt and Müller, 2013; Volkman, 1986). Analogous to the PIP_{25} index (P stands for open marine phytoplankton marker) for semi-quantitative sea ice estimations in the Arctic (Müller et al., 2011), the recently proposed $PIPSO_{25}$ approach (Vorrath et

al., 2019) allows for a differentiation between several sea ice conditions of a permanently open ocean, a sea ice marginal zone and a permanent sea ice cover (Müller et al., 2011).

Here, we provide the first $IPSO_{25}$-based high-resolution assessment of the spring sea ice development at the WAP during the industrial era and examine the response of sea ice to changes in atmospheric and oceanic oscillation patterns. To achieve this, we conducted a multiproxy study on three short sediment cores from different depths and oceanic regimes within the Bransfield Strait. In addition to $IPSO_{25}$, we analyzed HBI trienes, sterols and glycerol dialkyl glycerol tetraethers (GDGTs) for subsurface ocean temperature (SOT) reconstruction as well as diatom assemblages for estimating winter sea ice concentrations (WSI) and summer sea surface temperatures (SSST) by means of transfer functions. We furthermore consider sea ice and temperature data from an atmosphere-sea ice-ocean numerical model (AWI-ESM2), historical surface air temperatures from local meteorological stations, ice core records (stable isotopes $\delta^{18}O$ and δD, MSA), and paleo records of atmospheric circulation patterns such as ENSO and SAM.

6.2 Material and Methods

6.2.1 Study Area

The study area is the Bransfield Strait at the northern tip of the WAP (Figure 6.1a and b). The region includes the shallow shelf of the WAP as well as the Bransfield Basin with depths exceeding 2000 m at its deepest parts. The Bransfield Basin is located between the South Shetland Islands (SSI) to the northwest and the AP to the southeast. The shallow ocean has been shaped by ice sheet dynamics during the last glaciation (Canals and Amblas, 2016b; Ingólfsson et al., 2003) and several troughs discharge sediment load from the AP into the basin (Canals et al., 2016; Canals and Amblas, 2016a). The oceanographic setting in this area is complex and yet not fully constrained (Moffat and Meredith, 2018; Sangrà et al., 2011) because water masses enter the basin from the west and east (Figure 6.1b). From the east, relatively cold (< 0°C) and salty Weddell Sea Water (WSW) flows at the surface alongshore the Antarctic mainland as a coastal current but also fills the Bransfield Basin completely below 150 m. It is also observed on the northern slope of the SSI at 200-600 m depth and around Elephant Island as a result of wind driven modulation (Meijers et al., 2016). The main source from the west is the Bellingshausen Sea Water (BSW), a branch of the Antarctic Circumpolar Current (ACC). This well-stratified, fresh and warm surface water flows along the slope of the SSI and forms the Peninsula Front with the WSW in the central Bransfield Strait, trending southwest-northeast parallel to the Antarctic mainland (Sangrà et al., 2011). Additionally, Circumpolar Deep Water (CDW) enters from the southwest as a subsurface current, forming the Bransfield Front to the BSW at 200m to 550m depth along the SSI slope (Sangrà et al., 2017). Both BSW and CDW are observed to turn and flow back at the northern side of the SSI

(Sangrà et al., 2011). The mixing and transformation of the three water masses in the Bransfield Strait is yet not well understood but a study of iceberg drifts from Collares et al. (2018) showed that water from the Weddell Sea join waters from the Bellingshausen Sea in the vicinity of Trinity Island (Figure 6.1b). It has been suggested that eddies between the Peninsula Front and the Bransfield Front are a key mechanism for water exchange and/or upwelling (Sangrà et al., 2011; Zhou et al., 2002) and meltwater discharge from the adjacent glaciers has to be considered (Meredith et al., 2018). In the southwest, south of the Bransfield Strait, a narrow, fast flowing Antarctic Peninsula Coastal Current (APCC) is present, enriched in glacial freshwater and characterized by downwelling (Moffat and Meredith, 2018).

Primary productivity at the WAP is mainly controlled by eddies and fronts (Gonçalves-Araujo et al., 2015), due to upwelling (Sangrà et al., 2011), sea ice dynamics (Vernet et al., 2008) and iron distribution (Klunder et al., 2014). High productivity regimes and high chlorophyll concentrations are found north of the Peninsula Front along the SSI under the influence of the BSW, while the area influenced by the WSW is characterized by lower production of nanoplankton (Gonçalves-Araujo et al., 2015). Upwelling, iron fertilization and sea-ice retreat lead to high interannual variability in the production patterns and a strong onshore-offshore gradient is evident. In consequence high production is related to coastal areas, shallow mixed layers and higher stratification owing to sea ice melting (Sanchez et al., 2019; Vernet et al., 2008). High production is also reflected in high vertical export of sinking particles (e.g. Wefer et al., 1988; Kim et al., 2004) and in the biogeochemical distribution of surface sediments, dominated by high concentrations of

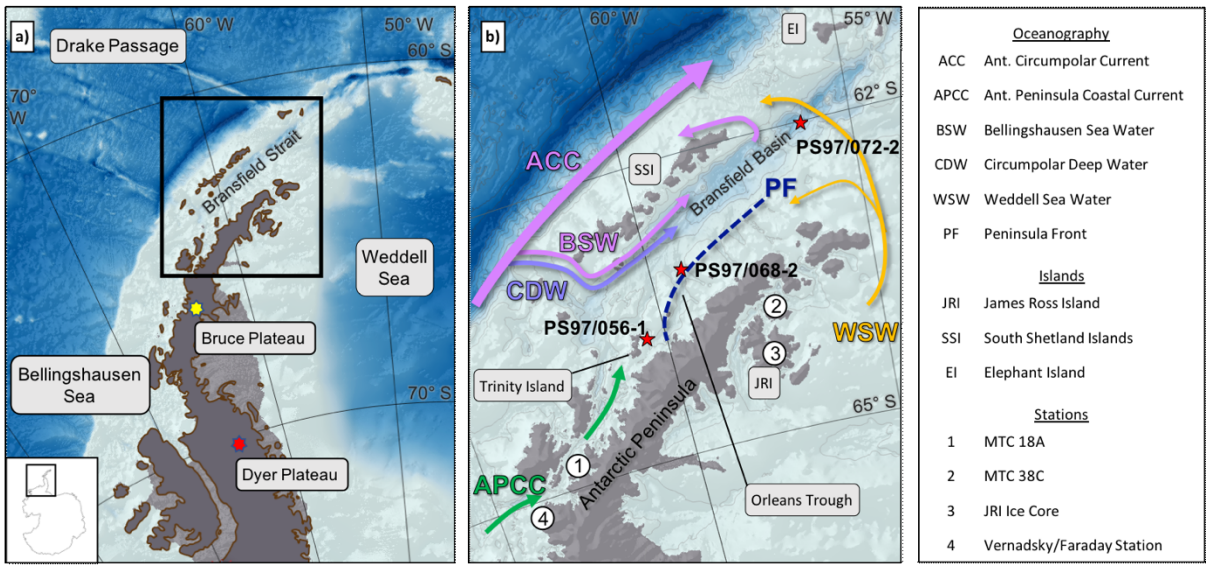

Figure 6.1 a) Overview map of the Antarctic Peninsula with the position of the Dyer Plateau (Abram et al., 2010), Bruce Plateau (Goodwin et al., 2016) and bathymetric features in the Bellingshausen Sea, the Weddell Sea and the Drake Passage. b) Oceanographic setting in the study area (modified after Hofmann et al., 1996; Moffat and Meredith, 2018; Sangrà et al., 2011), sediment and ice core locations and geographic locations mentioned in the text. Maps were generated with QGIS 3.0 (2018) and the bathymetry was taken from GEBCO_14 from 2015.

TOC, pigments, sterols and diatoms but low calcium carbonate (Cárdenas et al., 2019). Organic matter is mainly of marine origin as supported by low values of C/N and the stable carbon isotope composition (Cárdenas et al., 2019) whereas the AP is an important source of terrestrial silt and clay input (Wu et al., 2019).

6.2.2 SAMPLING AND AGE MODEL

The cores were collected in 2016 during the RV *Polarstern* cruise PS97 (ANT-XXXI/3) using multicorers at stations PS97/056-1 (63°45.42'S, 60°26.51'W, 633 m water depth) east of Trinity Island, PS97/068-2 (63°10.05'S, 59°18.12'W, 794 m water depth) in the Orleans Trough, and PS97/072-2 (62°00.39'S, 56°03.88'W, 1992 m water depth) in the East Bransfield Basin (Figure 6.1b). Smear slides were examined and microscopic description of the surface sediments was done onboard (Lamy, 2016). Immediately after recovery of the sediments were sectioned in 1 cm slices and samples designated for biomarker analyses were stored frozen in glass vials, while separate samples for micropaleontological investigation were stored at 4° C in plastic bags. A second suite of samples from a trigger core from station PS97/072-1 was used for total organic carbon (TOC) and diatom analyses (diatom samples from core PS97/072-2 were not available).

Geochronology for the sediment cores from sites PS97/056-1 and PS97/072-2 was established using $^{210}Pb_{xs}$ activities quantified by alpha spectrometry of its daughter ^{210}Po in secular equilibrium with ^{210}Pb and using ^{209}Po as a yield tracer (Flynn, 1968). The activities were corrected to the time of plating considering the ^{210}Po decay (half life: 138 days). $^{210}Pb_{xs}$ (unsupported) activities were determined as the difference between ^{210}Pb and ^{226}Ra activities measured by gamma spectrometry in some intervals of the sediment core. Alpha and gamma counting were performed at the Laboratoire Géosciences of the Université de Montpellier (France). The ages were based on $^{210}Pb_{xs}$ inventories according the Constant Rate of Supply Model (CRS, Appleby and Oldfield, 1978). Standard deviations (SD) were estimated propagating the counting uncertainties (Bevington et al., 1993). Since the dating on core PS97/056-1 and PS97/072-2 was done on selected samples the age model was established using the software R (R Core Team, 2017) and the package clam (Blaauw, 2010, version 2.3.2, calibration curve Marine13.14C). Trigger core PS97/072-1 was correlated to the age model of core PS97/072-2 based on TOC data.

$^{210}Pb_{xs}$ for core PS97/068-2 was measured at the Alfred Wegener Institute (AWI, Germany) on dried and ground bulk sediment samples in sealed gas-tight petri dishes, using a HPGe gamma spectrometer with planar geometry. ^{210}Pb was measured at 46 keV, ^{226}Ra for the excess correction in each depth interval via its indirect decay products at 295, 352 and 609 keV. Analytical errors were calculated considering error propagation. For core PS97/068-2 the calculation of CRS ages and the Monte-Carlo approximation of age uncertainties was based on Sanchez-Cabeza et al.

(2014), modified to accommodate the variable sample sizes and fractions for different depths. Due to residual inventory of $^{210}Pb_{xs}$ below the available samples in cores PS97/056-1 and PS97/072-2, the CRS model had increasing uncertainties below ~130 years (Figure Appendix 6). We therefore extrapolated ages before 1880 based on the average respective sedimentation rates for the oldest 3 cm.

6.2.3 ORGANIC GEOCHEMICAL ANALYSES

Organic geochemical analyses were done on freeze-dried and homogenized sediments. Bulk content of carbon (C) and nitrogen (N) were determined with a CNS analyzer (Elementar Vario EL III, standard error < 2%), whereas the analysis of TOC content was done on 0.1 g acidified (500 µl hydrochloric acid) sediment using a carbon-sulphur determinator (CS-2000, ELTRA, standard error < 0.6 %). The C/N ratio was calculated as TOC/total nitrogen.

The extraction procedure of HBIs follows the analytical protocol of the international community conducting HBI-based sea ice reconstructions (Belt et al., 2013, 2014; Stein et al., 2012). For the quantification of biomarkers the internal standards 7-hexylnonadecane (7-HND), 5α-androstan-3β-ol and C_{46} were added to the sediments. Sediment samples of 5 g were extracted ultrasonically three times using 6 ml of CH_2Cl_2:MeOH (v/v 2:1, 15 min) followed by centrifugation (2500 rpm, 1 min) and decantation of the total organic solvent extract. The different biomarkers were separated via open column chromatography with silica gel used as a stationary phase. First, the apolar fraction containing HBIs was separated with 5 ml hexane, while the second polar fraction containing GDGTs and sterols was eluted with 5 ml CH_2Cl_2:MeOH (v/v 1:1). The polar fraction (GDGT and sterols) was dried using nitrogen, re-dissolved in 120 µl hexane:isopropanol (v/v 99:1) and filtered through a polytetrafluoroethylene filter (0.45 µm in diameter). After measuring GDGTs, the polar fraction was silylated (200 µl BSTFA; 60° C; 2 hours) and used for sterol analysis.

The HBIs and sterols were analyzed by GC-MS with an Agilent 7890B gas chromatograph equipped with a 30 m DB 1 MS column (0.25 mm diameter, 0.250 µm film thickness) and coupled to an Agilent 5977B mass spectrometer (MSD, 70 eV constant ionization potential, ion source temperature 230° C). Apolar and polar lipid fractions were analyzed using different temperature programs. For HBIs, the temperature was held at 60° C for 3 min, ramped to 325° C over 23 min, and was held at this level for 16min. Sterol analysis started at a temperature of 60° C for 2 min, followed by a temperature increase to 150° C over 6 min, and to 325° C within 57 min. HBIs were identified via comparison of mass spectra of the measured compounds and published mass spectra (Belt et al., 2000). Quantification of HBIs was based on manual peak integration. Instrumental response factors of molecular ions of HBI diene (m/z 348) und trienes (m/z 346) were determined by means of calibration measurements using a sample with known concentrations of HBIs.

Identification of sterols was based on comparison of their retention times and mass spectra with those of reference compounds analyzed on the same instrument. The mean relative error of duplicates was < 5% for HBIs and < 1% for sterols (desmosterol had exceptional high relative errors of up to 14%), the detection limit was determined at 0.5 ng/g sediment. Co-elution of other compounds hampered identification and quantification of sterols in several samples (PS97/056-1; 0-13cm and PS97/072-2; 0-16cm).

GDGTs were analyzed using high performance liquid chromatography (HPLC, Agilent 1200 series HPLC system) coupled to a single quadrupole mass spectrometer (MS, Agilent 6120 MSD) via an atmospheric pressure chemical ionization (APCI) interface. Individual GDGTs were separated at 30° C on a Prevail Cyano column (150 mm x 2.1 mm, 3 µm). Each sample was injected (20 µl) and passed a 5 min isocratic elution with mobile phase A (hexane/2-propanol/chloroform; 98:1:1) at a flow rate of 0.2 ml/min. The mobile phase B (hexane/2-propanol/chloroform; 89:10:1) increased linearly to 10% within 20 min and after this to 100% within 10 min. After 7 min the column was cleaned with a backflush (5 min, flow 0.6 ml/min) and re-equilibrated with solvent A (10 min, flow 0.2 ml/min). The APCI had the following conditions: nebulizer pressure 50 psi, vaporizer temperature 350°C, N_2 drying gas temperature 350°C, flow 5 l/min, capillary voltage 4 kV, and corona current 5 µA. GDGT detection was done by selective ion monitoring (SIM) of $(M+H)^+$ ions (dwell time 76ms). The molecular ions m/z of GDGTs-I (m/z 1300), GDGTs-II (m/z 1298), GDGTs-III (m/z 1296), and Crenarchaeol (m/z 1292) as well as of the branched GDGTs-Ia (m/z 1022), GDGTs-IIa (m/z 1036), GDGTs-IIIa (m/z 1050) and hydroxylated GDGTs OH-GDGT-0 (m/z 1318), OH-GDGT-1 (m/z 1316), and OH-GDGT-2 (m/z 1314) were quantified in relation to the internal standard C_{46} (m/z 744). The hydroxylated GDGTs quantified in the scans of their related GDGTs (see Fietz et al., 2013). The standard deviation was 0.01 units of TEX^L_{86}.

We follow Kalanetra et al. (2009), proposing that GDGT-derived temperatures represent near-surface waters which is underlined by studies from Kim et al. (2012) and Park et al. (2019) and consider our results to reflect subsurface ocean temperatures (SOT). For calculation of TEX^L_{86} (Kim et al., 2010) only GDGTs with the m/z 1296 (GDGT-3), m/z 1298 (GDGT-2), m/z 1300 (GDGT-1) were considered:

$$TEX^L_{86} = \log\left(\frac{[GDGT-2]}{[GDGT-1]+[GDGT-2]+[GDGT-3]}\right) \quad (1)$$

and calibrated it with $SOT^{TEX} = 67.5 \times TEX^L_{86} + 46.9$ (Kim et al., 2010). (2)

The calculation based on OH-GDGT was done after Lü et al. (2015)

$$RI-OH' = \frac{[OH-GDGT-1]+2\times[OH-GDGT-2]}{[OH-GDGT-0]+[OH-GDGT-1]+[OH-GDGT-2]} \quad (3)$$

and calibrated with SOT^{OH} = (RI-OH' - 0.1) / 0.0382. (4)

To determine the influence of terrestrial organic matter the BIT index was calculated following Hopmanns et al. (2004) as

$$BIT = \frac{[GDGT-Ia]+[GDGT-IIa]+[GDGT-IIIa]}{[Crenarchaeol]+[GDGT-Ia]+[GDGT-IIa]+[GDGT-IIIa]}. \quad (5)$$

The phytoplankton-$IPSO_{25}$ index ($PIPSO_{25}$) was calculated following Vorrath et al. (2019) with

$$PIPSO_{25} = \frac{IPSO_{25}}{IPSO_{25}+(c \times phytoplankton\ marker)} \quad (6)$$

using sterols and HBI trienes as phytoplankton marker (Vorrath et al., 2019). The balance factor c (c = mean $IPSO_{25}$ / mean phytoplankton biomarker) is used to account for concentration offsets between $IPSO_{25}$ and phytoplankton biomarkers (Belt and Müller, 2013; Müller et al., 2011; Smik et al., 2016b; Vorrath et al., 2019). Since the concentrations of HBI trienes are within the same range as the sea ice proxy we set the c-factor to 1 (Smik et al., 2016b) and c-factors for sterols were calculated individually for every core site (Table Appendix 7). To distinguish the different indices based on their phytoplankton marker we use the terms P_ZIPSO_{25} for an index based on Z-trienes, P_EIPSO_{25} based on E-trienes, P_BIPSO_{25} based on bassicasterol, and P_DIPSO_{25} based on dinosterol.

6.2.4 DIATOM ANALYSIS AND TRANSFER FUNCTION

Diatom analyses were done on cores PS97/056-1, PS97/068-2 and the trigger core from the core site of PS97/072-1 (correlated with PS97/072-2 via TOC content). About 300 mg of freeze-dried sediments were treated after the method described by Cárdenas et al. (2018) to prepare slides for microscopy analysis. Two permanent slides per sample were prepared and observed with a Carl Zeiss Axio Lab.1 microscope with phase contrast at 1000× magnification at the Instituto Antártico Chileno in Punta Arenas. Diatoms were identified and counted on transects on microslides until reaching at least 400 valves on each slide, following counting procedures of Schrader and Gersonde (1978). Diatom identification was done to species or species group level following the taxonomy described by Armand and Zielinski (2001), Taylor et al. (2001), Crosta et al. (2004), Buffen et al. (2007), Cefarelli et al. (2010), Esper et al. (2010), Allen (2014), and Campagne et al. (2016). The Hyalochaete of the genus *Chaetoceros* were identified as vegetative cells and/or resting spores.

We applied the marine diatom transfer function TF MAT-D274/28/4an to estimate winter sea ice (WSI) concentrations. It comprises 274 reference samples with 28 diatom taxa and/or taxonomic groups and an average of 4 analogues from surface sediments in the Atlantic, Pacific, and western Indian sectors of the Southern Ocean(Esper and Gersonde, 2014a). Winter sea ice (WSI) estimates reflect September sea-ice concentrations averaged over the period from 1981-2010 (National Oceanic and Atmospheric Administrations, NOAA; Reynolds et al., 2002, 2007) in a 1 by 1 grid. We follow the approach of Zwally et al. (2002) and define a sea ice concentration of 15% as the threshold for presence or absence of sea ice and 40% as the representative average of sea-ice edge

(Gersonde et al., 2005; Gloersen et al., 1993). For summer sea surface temperature (SSST), we used the transfer function TF IKM336/29/3q from 336 reference samples (Pacific, Atlantic and Indian Southern Ocean) with 29 diatom taxa and three factors (Esper and Gersonde, 2014b). For calculations of MAT and IKM the software R (R Core Team, 2017) was used with the packages Vegan (Oksanen et al., 2012) and Analogue (Simpson and Oksanen, 2012).

6.2.5 MODELLED DATA

We used data from numerical modelling to compare and evaluate our biogeochemical analyses. The AWI-ESM2 is a state-of-the-art coupled climate model developed at AWI (Sidorenko et al., 2019). The model consists of the atmospheric model ECHAM6 (Stevens et al., 2013) and the finite element sea ice-ocean model (FESOM2) (Danilov et al., 2017). The model also includes a Land-Surface Model (JSBACH) with dynamical vegetation (Raddatz et al., 2007).

The atmosphere grid in the high-resolution experiment is T63 (about 1.9 degree) with 47 vertical levels. A multi-resolution approach is employed in the ocean module. In detail, the high-resolution experiment applies up to 20 km horizontal resolution over the Arctic region and 150 km for the far field ocean (Figure Appendix 8). Moreover, the tropical belt has a refined resolution of 30-50 km in this configuration. There are 46 uneven vertical depths in the ocean component. The model has been validated under modern climate condition (Sidorenko et al., 2019). Previous versions of the model have been applied for the Holocene (Shi et al., 2020; Shi and Lohmann, 2016).

We run the climate model from the Mid-Holocene as a starting point (*midHolocene* simulation), and performed a transient simulation from the Mid-Holocene to the pre-industrial (*past6k* simulation) along the recipe as described in Otto-Bliesner et al. (2017). The transient orbital parameters are calculated according to Berger (1978). Moreover, as the change of topography from mid-Holocene to present is minor, we use constant topography under pre-industrial conditions for the entire transient period. In our modeling strategy, we follow Lorenz and Lohmann (2004) and use the climate condition from the pre-industrial state as spinup and initial state for the transient simulation covering the period 1850-2017 CE. Greenhouse gases concentrations are taken from the ice core records (Köhler et al., 2017) and from Meinshausen et al. (2011).

6.2.6 ADDITIONAL DATA SETS

Regional monthly satellite sea ice concentrations were derived from Nimbus-7 SMMR and DMSP SSM/I-SSMIS passive microwave data from the National Snow and Ice Data Center (NSIDC, grid cell size 25x25 km, Cavalieri et al., 1996) and mean winter (JJA) and spring (SON) sea ice concentrations were used in this study.

For the large-scale atmospheric modes we used the paleo ENSO index from Li et al. (2013) and the modelled SAM data from Abram et al. (2014). After Stammerjohn et al. (2008b), years with

positive ENSO and negative SAM indices cause higher sea ice cover at the WAP and years with a negative ENSO and positive SAM lead to warmer seasons with reduced sea ice cover.

We used ice core stable isotope data representing relative air temperature at James Ross Island (δD, Abram et al., 2013) and at Bruce Plateau ($\delta^{18}O$, Goodwin et al., 2016). We compared the marine sea ice proxies (biomarkers, diatoms) with MSA data from coastal West Antarctic Dyer Plateau ice core (Abram et al., 2010).

6.3 RESULTS

6.3.1 AGE MODEL AND CORE DESCRIPTION

The ^{210}Pb signals indicated continuously increasing ages with depth in all sediment cores (Figure 6.2). All sediment cores roughly cover the last 240 years (including the extrapolated time) with resolution between 2 and 12 years per centimeter and sedimentation rates from 0.1 to 0.5 cm/a (Tables Appendix 9-11). Core PS97/056-1 located east of Trinity Island is characterized by silt-bearing diatomaceous clay (Lamy, 2016) and covers the timespan from 1830 to 2006 CE with sedimentation rates increasing from 0.1 to 0.4 cm/a over time. Core PS97/068-2 from Orleans Trough consists mainly of diatom-bearing silty clay (Lamy, 2016) and spans from 1780 to 2007 CE with sedimentation rates from 0.1 to 0.5 cm/a. Sediment core PS97/072-2 from the East Bransfield Basin is the deepest record characterized as silt-bearing diatomaceous clay (Lamy, 2016) with increasing sedimentation rates (from 0.1 to 0.4 cm/a) covering the time from 1823 to 2000 CE. The TOC contents of all cores ranged between 0.7 and 1.1 wt%. Low C/N ratios (< 8.6) and BIT values (< 0.02) point to a marine origin of the organic matter (Tables

Appendix 9-11).

6.3.2 BIOMARKER LIPIDS

A summary of biomarker results that will be discussed in detail is visualized in Figure 6.3 (results of HBI E-trienes, sterols and their related sea ice indices can be found in Figure Appendix 12, all data in Tables Appendix 9-11). All biomarker records show an overall increasing trend towards the present with a few exceptional peaks along the record. $IPSO_{25}$ is abundant at all core sites with values ranging from 0.2 μg g^{-1} TOC up to 6.4 μg g^{-1} TOC. All three cores display similar patterns with low values before 1850 CE followed by moderate concentrations until 1970 CE and maxima in the 2000s (Figure 6.3). Concentrations of HBI trienes are much lower than $IPSO_{25}$ concentrations with values below 1.4 μg g^{-1} TOC for Z-trienes (Figure 6.3) and below 0.7 μg g^{-1} TOC for E-trienes (Figure Appendix 12). The exception is core PS97/072-2 from of the East Bransfield Basin where both HBI trienes reach up to 3.7 μg g^{-1} TOC and 1.6 μg g^{-1} TOC, respectively, in the second half of the 19th century. The concentrations of brassicasterol (10.2–241.3

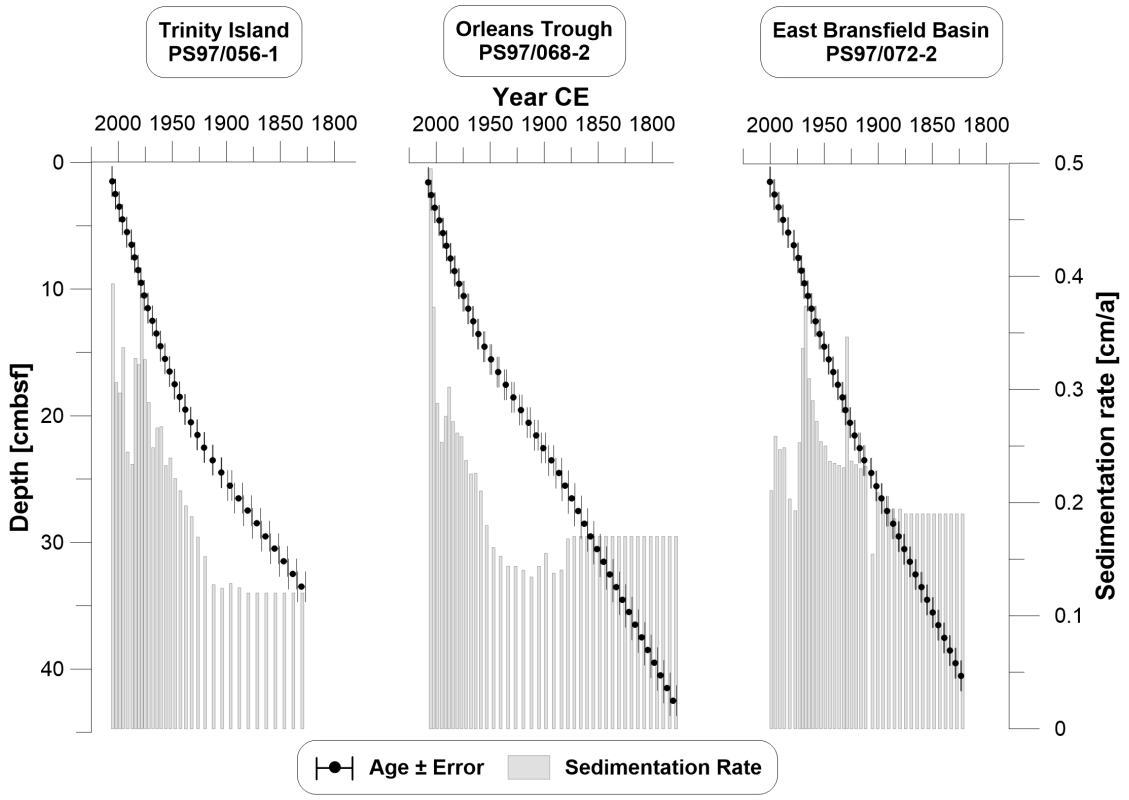

Figure 6.2 Age-depth models with error bars of all three core sites. The sedimentation rate is displayed in grey bars. Ages were extrapolated prior to 1880 CE for all cores based on their average respective sedimentation rate for the oldest 3 cm. All plots were done with Grapher™ 13.

μg g^{-1} TOC) and dinosterol (5.0–145.2 μg g^{-1} TOC) are two to three magnitudes higher than the HBIs; markedly lower concentrations characterize the Orleans Trough (PS97/068-2) (Figure Appendix 12). The $PIPSO_{25}$ indices calculated with Z- and E-trienes run parallel to $PIPSO_{25}$ based on brassicasterol and dinosterol and show increasing trends with time. In general, HBI triene-based $PIPSO_{25}$ have higher values (P_ZIPSO_{25} from 0.32 to 0.91; P_EIPSO_{25} from 0.25 to 0.95) than $PIPSO_{25}$ based on sterols (P_BIPSO_{25} from 0.15 to 0.70; P_DIPSO_{25} from 0.11 to 0.75). The $PIPSO_{25}$ indices suggest an increasing spring sea ice cover over time (Figure 6.3, Figure Appendix 12). This is most prominent at the East Bransfield Basin (PS97/072-2) where lowest sea ice cover is indicated around 1870 CE and increase towards the present is indicated. Indications of short-term low spring sea ice cover are found for the 1960s and 1970s at the near-coastal core sites (PS97/056-1 and PS97/068-2) but do not change the overall trend.

Temperatures based on GDGTs show a wide range of values. At Trinity Island (PS97/056-1) and the East Bransfield Basin (PS97/072-2), SOT^{TEX} range from -3.87°C to 2.34°C (Figure 6.3) whereas temperatures are always above zero from 0.73° C to 3.62° C at the Orleans Trough (PS97/068-2). Distinct cold events occur in the 1860s at the East Bransfield Basin (PS97/072-2) and as a longer cool period from 1940 to 1970 CE at the coastal core sites but general trends are hard to distinguish.

In contrast, SOT^{OH} displays a decreasing temperature trend at all core sites with a narrow range of -2.58 °C to -0.99° C reversed by rapid warming since the 1990s (Figure 6.3).

6.3.3 DIATOM ASSEMBLAGES

Winter sea ice estimations derived from diatom assemblages point to a high variability (74% to 92% WSI at PS97/056-1, 64% to 92% at PS97/068-2, 68% to 90% at PS97/072-1) with a minimum around 1840 and 1880 CE and a slight increment toward 1990s (Figure 6.3, Tables Appendix 9, 10 and 13). This variability coinciding with the high abundances of sea ice diatom species *Fragilariopsis curta* that show a high contribution at cores PS97/056-1 and 068-2 (Tables Appendix 9-10). In addition, WSI records reveal similar features compared to $IPSO_{25}$ and $PIPSO_{25}$, which points to a relationship of winter and spring sea ice estimates based on different approaches. The SSST from diatom assemblages have a small amplitude in all cores (-0.9 to 0.5°C at PS97/056-1, -1.1 to 0.2°C at 068-2 and -0.8 to 0.1°C at 072-1) and show a similar pattern to SOT^{TEX} at the sites PS97/068-2 and 072-1 (Figure 6.3, Tables Appendix 9, 10 and 13).

6.3.4 MODELLED DATA

We use model data as derived from the AWI-ESM2 which include spring sea ice concentration (mSSIC), spring sea ice thickness (mSSIT), subsurface ocean temperature (mSOT, mean temperature from 30-100 m below sea surface), and surface air temperature (mSAT) (Table Appendix 14). Based on 10-year means, we detect negative trends for the last 200 years in both mSSIC (decrease by 30% to 50%) and mSSIT (decrease from 0.5 m down to 0.1 m). At the same time, positive trends for mSOT and mSAT at all core sites show temperatures rising by 0.3°C to 0.6°C. Further, a time series of the latitudinal shift of the sea ice edge at the WAP (between 50°W and 70°W) which shows a southward shift of 1.5° from 61.9°S to 63.4°S in the 20th century (Table Appendix 14).

6.4 DISCUSSION

6.4.1 SPATIAL AND TEMPORAL DISTRIBUTION OF PALEOENVIRONMENTAL BIOMARKERS

The core site at Trinity Island (PS97/056-1) is dominated by the APCC and receives freshwater input from the Peninsula with influence of BSW from the ACC (Moffat and Meredith, 2018). We suggest that sea ice proxies originate from free floating or land fast sea ice in this region since the core site is only 8 km away from Trinity Island. Coastal upwelling of macro- and micronutrients, especially iron, and a stratified water column fuel open marine primary production (Sanchez et al., 2019; Vernet et al., 2008) and may explain highest concentrations of sterols at this core site. $IPSO_{25}$, HBI Z-triene, P_ZIPSO_{25} and WSI records exhibit similar trends and fluctuations over time (Figure 6.3). A direct relation between reconstructed sea ice conditions and temperature (SSST, SOT^{TEX}

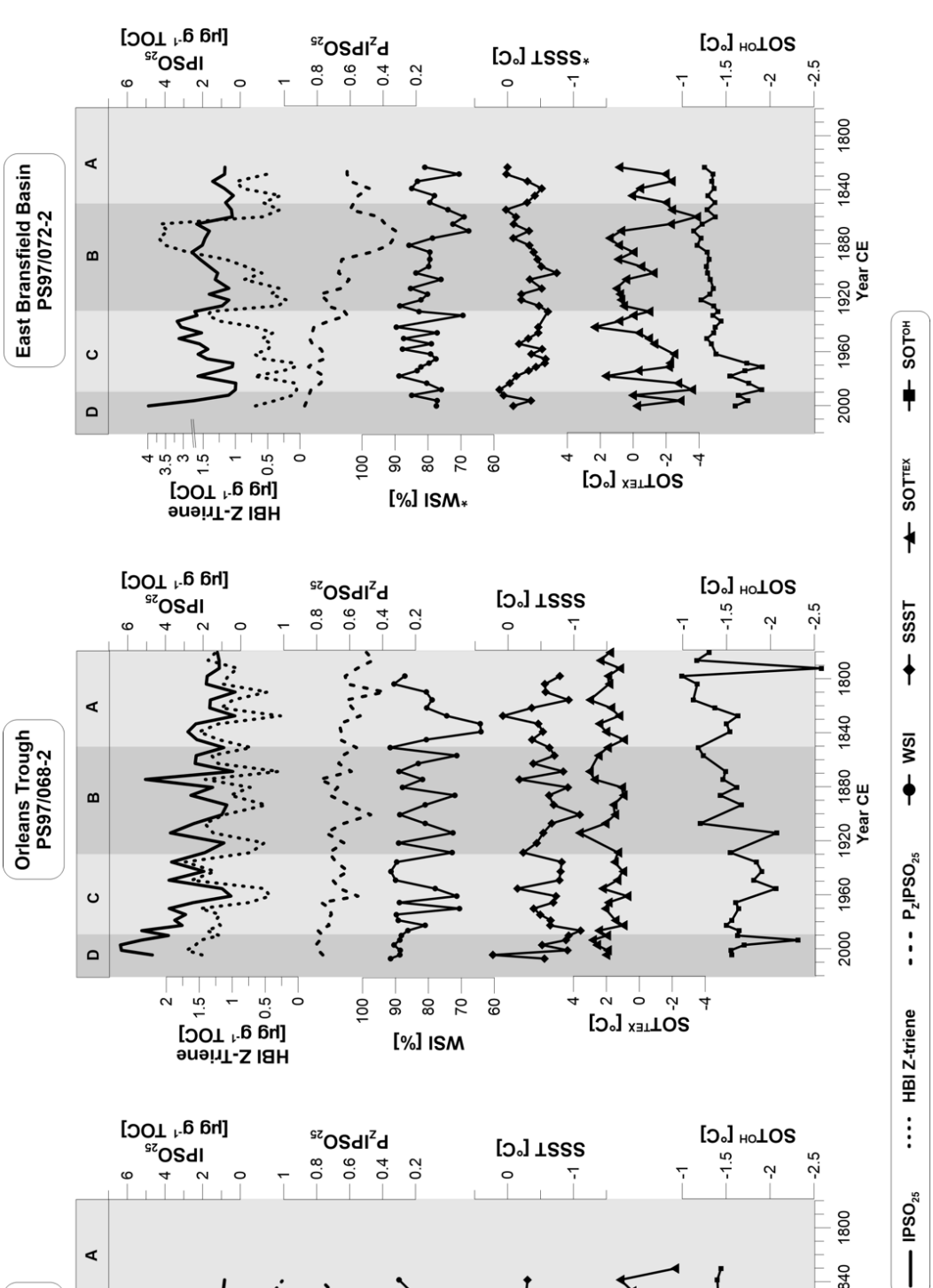

Figure 6.3 Biomarker composition of the three sediment cores showing concentrations of (from top to bottom) $IPSO_{25}$ and HBI Z-trienes, the sea ice index P_ZIPSO_{25}, diatom-derived winter sea ice (WSI) concentrations and temperatures of summer sea surface temperatures (SSST), subsurface ocean temperature derived from TEX'_{86} (SOT^{TEX}), and OH-GDGTs (SOT^{OH}). Data marked with * are from the trigger core PS97/072-1. Vertical grey bars denote the stratigraphic units A to D.

and SOT^{OH}) is not evident. However, slightly higher temperatures deduced from SOT^{OH} and diatom data seem to coincide with lower $IPSO_{25}$ concentrations, lower $PIPSO_{25}$ values and reduced WSI in the 19th century, while variable but higher temperatures in the 20th century are accompanied by higher $IPSO_{25}$ and WSI concentrations at site PS97/056-1 (Figure 6.3). The remarkably low SOT^{TEX} in the year 2006 CE might be a result of cold meltwater injections due to enhanced glacier melting (e.g. Pastra Glacier on Trinity Island). A general weak cooling trend is present in SSST and SOT^{OH} from 1920 CE to the 1990s.

The data obtained from the sediment core in the Orleans Trough (PS97/068-2) suggest that the core site is affected by the Peninsula Front where water masses from both salty and cold WSW and fresh and warm BSW meet. The water here is characterized by enhanced mixing within a narrow eddy zone and deepening of the mixed layer (Sangrà et al., 2011). High concentrations of biomarkers point towards a strengthening of primary productivity associated with BSW (Gonçalves-Araujo et al., 2015) in a less stratified and mixed water column (Vernet et al., 2008). The patterns of $IPSO_{25}$, HBI Z-triene as well as P_ZIPSO_{25} and WSI have a good visual correspondence. They indicate higher phytoplankton productivity and higher sea ice cover towards present time. Also, SSST corresponds quite well with SOT^{OH} at PS97/056-1 and with SOT^{TEX} at PS97/072-2 (Figure 6.3). The SOT^{TEX} is remarkably high (above 0° C) throughout the studied period contrasting modern ocean temperatures of the upper 400 m at the WAP below -0.5°C (Cook et al., 2016). Compared to SOT^{TEX}, SOT^{OH} temperatures are closer to modern ocean temperatures in this area (Cook et al., 2016) within a narrow range. As this core site is in the middle of BSW and WSW influenced, no clear dominance from one or the other regime is evident and we suggest that GDGT-derived temperatures are affected by influences of both BWS and WSW.

The core site in the East Bransfield Basin (PS97/072-2) is further away from the coast (145 km) compared to the other two core sites. Marine productivity is expected to be lower due to the presence of WSW (Gonçalves-Araujo et al., 2015) but relatively high concentrations of $IPSO_{25}$ and HBI Z-triene may be related to fertilization through iron input (Sanchez et al., 2019). A remarkable maximum in HBI Z-triene concentrations in the late 19th century have resulted from drastic changes in the local oceanographic settings and productivity patterns. As indicated by SOT^{TEX}, this period is marked by a rapid shift from cold to warm water temperatures, pointing to a possible dominance of warmer BSW. A corresponding retreat of sea ice cover and likely ice-free summers, as reflected by P_ZIPSO_{25} and WSI values, could have promoted the productivity of open marine or coastal phytoplankton communities, e.g. *Rhizosolenia* and *Pleurosigma*, synthesizing the HBI Z-triene (Belt et al., 2000, 2017).

Despite the different oceanographic settings, all cores sites exhibit increasing trends in $IPSO_{25}$ and HBI Z-triene concentrations as well as rising P_ZIPSO_{25} values and WSI towards the present reflecting an overall advance of sea ice cover. At the same time, SOT^{TEX} and SOT^{OH} tend to decrease until the 1990s and rise since the 1990s, which we interpret as a delayed ocean warming compared to other parts of the global ocean (Cook et al., 2016). The overall trend in our records is a rise of both open marine and sea ice biomarkers and an ocean cooling (mainly indicated by SOT^{OH}). A clear stratigraphy is hard to distinguish but four units could be roughly divided by sea ice and temperature biomarker records:

Unit A:Moderate sea ice cover before 1850 CE. In the period before 1850 CE, the WAP experienced low productivity of sea ice algae as well as ice-edge or open marine algae (low $IPSO_{25}$ and HBI triene values). Diatom and biomarker sea ice indices reveal decreasing winter sea ice and moderate spring sea ice cover with low variability in seasonal sea ice changes. The fluctuating water temperatures display no clear trend except for a weak cooling at the East Bransfield Basin, which may have resulted from an enhanced WSW inflow into the Bransfield Strait.

Unit B: Moderate winter sea ice cover and ice-free summers from 1850 to 1930 CE. In this period, changes in the oceanographic pattern may have led to a dominance of BSW in the East Bransfield Basin (PS97/072-2) and a weakened WSW inflow causing sea ice retreat and ocean warming. During this time, seasonal shifts from winter sea ice to ice-free summers occurred faster and promoted enhanced open marine biomarker production (Gonçalves-Araujo et al., 2015) fueled by high nutrient release through melting (Vernet et al., 2008). Sea ice cover remained at a moderate level near the coast (core sites PS97/056-1 and 068-2), as suggested by Barbara et al. (2013) who interpreted near-coastal diatom assemblages and HBIs at both sides of the AP to reflect long persisting sea ice cover in spring (Figure Appendix 15). They furthermore postulated that enhanced productivity occurs due to a stratified water column and nutrient injections by meltwater and autumn storm activity in the southern Bransfield Strait. Despite this, we see high fluctuations of winter sea ice (up to 20% WSI between two data points). Furthermore, high (low) winter sea ice cover as indicated by WSI at PS97/068-2 and 072-2 occurs contrary to low (high) spring sea ice reflected by P_ZIPSO_{25} pointing to fast seasonal changes.

Unit C: Higher variability and increasing sea ice cover from 1930 to 1990 CE. In contrast to Unit B, all biomarkers indicate an increasing sea ice cover in Unit C. It is characterized by a general ocean cooling (except for SSST in the East Bransfield Basin), which may suggest a delayed onset of anthropogenic warming in Antarctic waters (Abram et al., 2016; Cook et al., 2016)

and the atmosphere (Abram et al., 2013). High fluctuations in $IPSO_{25}$ and HBI Z-triene concentrations indicate conditions favorable for both sea ice and phytoplankton productivity potentially resulting from a higher seasonal variability characterized by high winter sea ice cover and ice-free summers. High winter sea ice cover now coincides with high spring sea ice coverat all core sites. WSI and $IPSO_{25}$ indicate enhanced coastal winter and spring sea ice cover in the 1940s and 1950s and low sea ice cover in the 1960s and 1970s in correspondence with other paleo records (e.g. Abram et al., 2010; Hobbs et al., 2016). A distinct increase in $IPSO_{25}$ and HBI Z-triene concentrations since 1930 CE was also reported by Barbara et al. (2013) on both sides of the AP (Figure Appendix 15). We suggest that higher production of $IPSO_{25}$ and sterols could be related to pulses of cold water and nutrients due to glacier retreat (Cook et al., 2016; Kunz et al., 2012). The increasing sea ice cover at all core sites contrasts a reconstructed sea ice decrease from satellite and ice cores since the 1950s for the Bellingshausen Sea (Abram et al., 2010; Hobbs et al., 2016). This contradicting long-term sea ice growth is also evident in the study by Barbara et al. (2013) who first observed a shortening of the sea ice season but an advance thereafter due to a stable, sea ice favoring environment under mild conditions after 1950 CE.

Unit D: Warm reversal and sea ice peak from 1990 to 2006 CE. The last unit is marked by the trend reversal to a warm subsurface ocean (Cook et al., 2016), present at all core locations in the Bransfield Strait. Sea ice cover tends to increase towards maximum values and seems to reflect recent observations of sea ice cover rebounds in the Bellingshausen Sea and the WAP after 2005 CE (Hobbs et al., 2016; Schofield et al., 2018). Since the last unit is very short, the interpretation of warm ocean temperature together with a high sea ice cover is rather tentative.

We note that for the interpretation of biomarker-based sea ice reconstructions the potential degradation of biomarkers affecting their downcore concentration profile needs to be taken into consideration. We observe that the upper part of the sediment cores contains higher concentrations of $IPSO_{25}$, HBI trienes and sterols compared to the underlying older sediments. A similar pattern in $IPSO_{25}$ and HBI triene concentrations is also reported by Barbara et al. (2013). Their biomarker concentrations from the western AP equal the concentrations in the Bransfield Strait but do not show such high values near the sediment surface, as in our data, are not present. Auto- and photooxidative degradation of $IPSO_{25}$ and HBI trienes was already studied in laboratory experiments (Rontani et al., 2014, 2011) and autoxidative and bacterial degradation was also found in the oxic layers of surface sediments (Rontani et al., 2019a). According to these results, a faster

degradation of HBI trienes (because of their higher number of double bonds) in the upper centimeters of the herein studied sediment cores would lead to higher $PIPSO_{25}$ values with progressive degradation. Sterols might also undergo degradation (Rontani et al., 2012) but studies from Antarctic sediments are still missing. As we observe remarkably high HBI triene concentrations in core PS97/072-2 in the late 20th century and lower concentrations towards present (Figure 6.3, Figure Appendix 12), we suggest that degradation does not have major impacts on biomarker concentrations presented in this study.

6.4.2 COMPARISON OF PROXY-DERIVED AND MODELLED SEA ICE ESTIMATES WITH SATELLITE SEA ICE OBSERVATIONS

We compared $IPSO_{25}$ concentrations, P_ZIPSO_{25} values, and diatom-based WSI estimates with satellite data and with mSSIC to evaluate their accuracy in reflecting spring and winter sea ice cover variability at the core sites over the past 40 years (Figure 6.4, Table Appendix 18). Satellite-derived spring sea ice concentrations (satSSIC) show general similarities to fluctuations observed in the $IPSO_{25}$ record indicating lower sea ice cover in the 1980s, a peak in the mid 1990s and a drop in sea ice cover in the early 2000s, except for the coastal remote core site (PS97/072-2) where sea ice concentrations rise towards present (Figure 6.4). At the near-coastal core sites (PS97/056-1 and 068-2), these dynamics are well reflected in $IPSO_{25}$ and $PIPSO_{25}$, in particular for site PS97/056-1, where a good correspondence is observed between biomarker and satellite data (Figure 6.4). However, we cannot exclude aliasing effects due to a lower temporal resolution of the sediment cores (Pisias and Mix, 1988). Maximum sea ice concentrations observed in 1996 CE, are well reflected by elevated $IPSO_{25}$ concentrations but the drop afterwards is not that clearly reflected. Diatom-based WSI compared to satellite-derived winter sea ice concentrations (satWSIC) show that these two data sets are in moderate agreement at the near-coastal core sites (PS97/056-1 and PS97/068-2) and winter sea ice coverage seems to be less dynamic at the Peninsula Frontal mixing zone (PS97/068-2). We note that the modelled spring sea ice cover is mostly opposite to satellite data, in particular during the 1990s and 2000s. While modelled and satellite derived data have similar grid sizes (model: 30x30 km, satellite: 25x25 km) we suppose that global models such as AWI-ESM2 cannot resolve the AP sub-aerial and marine topography and have difficulties in capturing local to regional near coastal sea-ice dynamics in the study region. Another reason is related to internal variability and missing feedbacks which makes a direct comparison of short time series difficult. However, both modelled and satellite data show a decreasing trend in spring sea ice cover (about 10%) and a slightly rising trend in winter sea ice cover over the recorded period (about 7%), while sea-ice proxies suggest an increasing trend of spring sea ice. For winters sea ice, core sites PS97/056-1 and PS97/072-2 display a decreasing trend, whereas PS97/068-1 clearly point to

Figure 6.4 Concentrations of (from top to bottom) $IPSO_{25}$, P_ZIPSO_{25}, WSI compared to modelled spring sea ice concentrations (mSSIC) and satellite derived winter and spring sea ice concentrations (satWSIC and satSSIC, 5 year running mean) from the National Snow and Ice Data Center (NSIDC, Cavalieri et al., 1996) for all three core sites. Data marked with * are from the trigger core PS97/072-1. Vertical grey bars denote the stratigraphic units C and D.

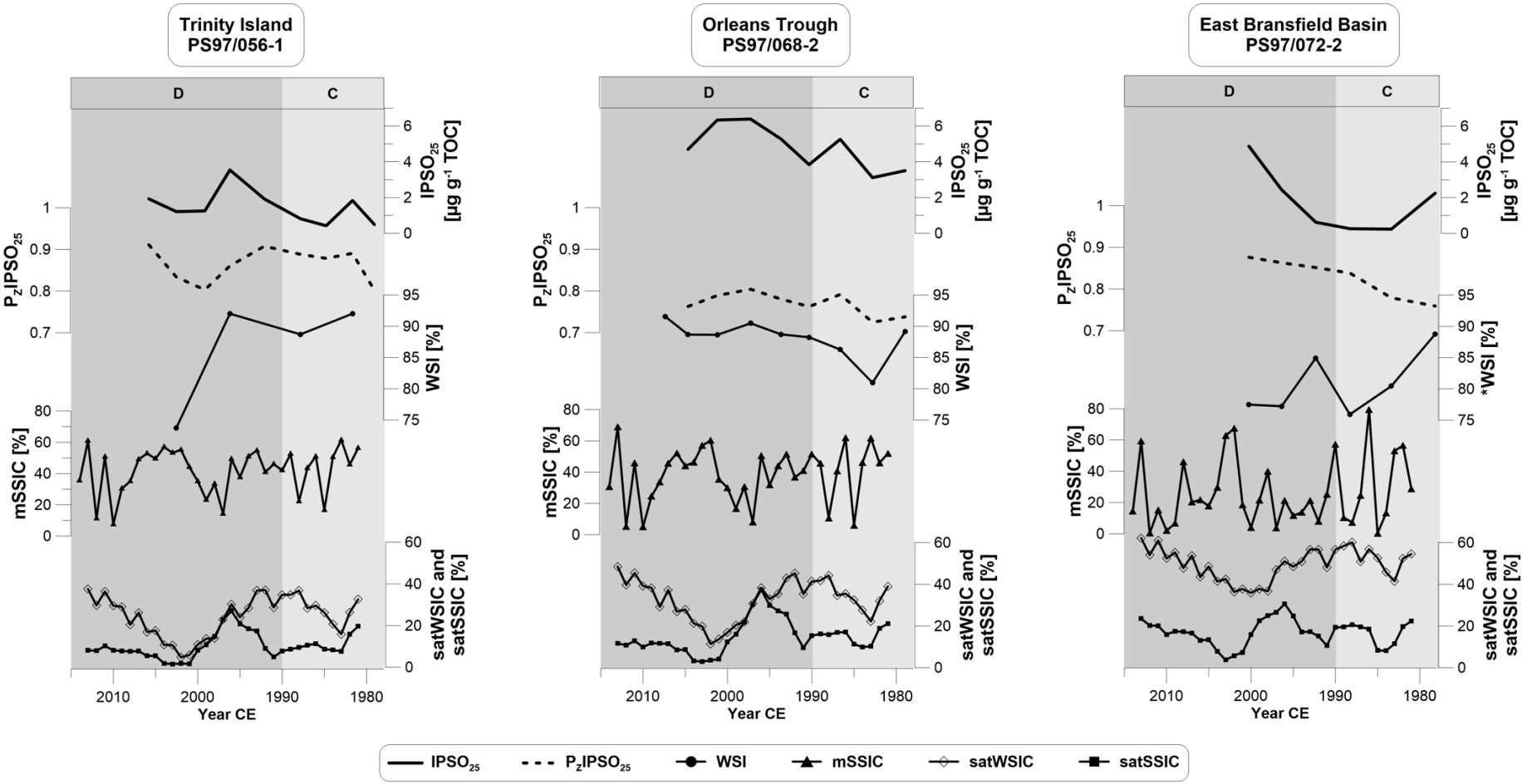

an increase of winter sea ice.

For the offshore core site at the East Bransfield Basin (PS97/072-2), $IPSO_{25}$ and $PIPSO_{25}$ correspond better with satSSIC than with mSSIC sea ice data (Figure 6.4). Between 1985 and 1995 CE, both $PIPSO_{25}$ indices suggest a similar increase in spring sea ice as the satellite observations. Sea ice estimates from WSI seem to be more related to satSSIC than to satWSIC. Also, WSI estimates are remarkably lower than at the other core sites, although satellite winter sea ice cover is the highest of all. Regarding the oceanographic setting, we consider that also drift ice originating in the Weddell Sea may have affected the deposition of $IPSO_{25}$ at this core site. Input of allochthonous material from the shelf is also possible, which might impact the fidelity of the proxy records.

Based on the overall accordance with satellite data, we conclude that the biomarker and diatom-based sea ice estimations are related to regional dynamics of sea ice cover, as far as we can assess it from the low resolution of the sediment cores. Since HBI Z-trienes and sterol concentration profiles are similar to $IPSO_{25}$ concentrations (Figure 6.3, Figure Appendix 12) we suggest that sea ice dynamics also promote growth of open marine phytoplankton species due to nutrient release or nutrient upwelling (Sanchez et al., 2019; Vernet et al., 2008). As the record of satellite observations is short, it is not clear if decadal or centennial sea ice trends can be directly derived from our biomarker records. Hence, we use modelled and ice core data for further insights over the full sediment records.

6.4.3 COMPARISON OF SEA ICE PROXY RECORDS WITH MODELLED AND ICE CORE DATA COVERING THE PRE-SATELLITE ERA

By comparing $IPSO_{25}$, P_ZIPSO_{25}-based sea ice estimates and WSI with modelled spring sea ice data, we note opposite long-term sea ice trends reflected in the proxy records and the modelled data for the past 240 years (Figure 6.5). Modelled spring sea ice concentration and thickness show a clear decreasing trend at all core sites with a loss of sea ice cover between 15% and 20%. Modelled sea ice cover fluctuates strongly at the East Bransfield Basin (PS97/072-2) while the coastal core sites run almost parallel. Although the modelled spring sea ice does not agree with satellite data on local to regional scale (Figure 6.4) it does reflect the satellite observations of the large-scale general trend of sea ice decline and warming in the Bellingshausen Sea and at the WAP (Parkinson and Cavalieri, 2012; Vaughan et al., 2003).

The increasing concentrations of $IPSO_{25}$ as well as the rise of both parallel running P_ZIPSO_{25} values and diatom-derived WSI concentrations recorded in all three sediment cores suggest a long-term sea ice advance. On the other hand, the rise in the concentrations of the HBI Z-triene and sterols also rise (Figure Appendix 12), which indicates more open marine and/or stable ice edge conditions

promoting phytoplankton productivity. We suppose that a thinning of the ice and a hence higher light penetration permitting photosynthesis at the ice-water interface (Hancke et al., 2018) could have triggered the productivity of $IPSO_{25}$ source diatoms. In addition, increased melting of sea

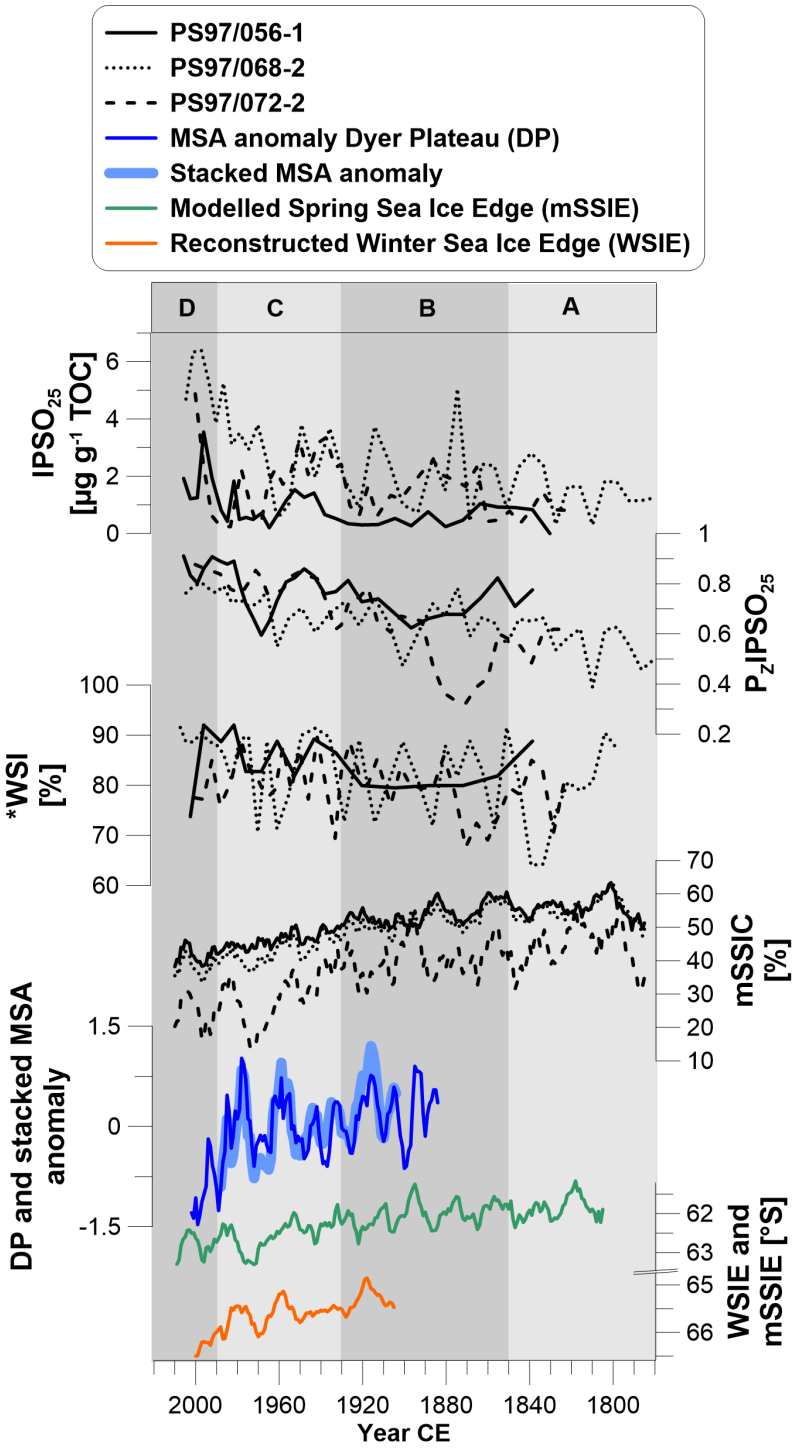

Figure 6.5 The biomarker (from top to bottom) $IPSO_{25}$, sea ice index P_ZIPSO_{25}, and winter sea ice concentration (WSI) from diatom assemblages compared to modelled spring sea ice cover (mSSIC, 10 year running mean), MSA anomaly from Dyer Plateau and stacked MSA covering the Bellingshausen Sea sector (5 year running mean, Abram et al., 2010), modelled spring sea ice edge latitude (mSSIE, 10 year running mean) and econstructed winter sea ice edge latitude from MSA (WSIE, 10 year running mean, Abram et al., 2010). Data marked with * are from the trigger core PS97/072-1. Vertical grey bars denote the stratigraphic units A to D.

could have contributed to a higher deposition of sea ice diatoms and $IPSO_{25}$. Thinner ice and accelerated melting during spring may have resulted in a largely ice-free sea surface during summer promoting phytoplankton (biomarker) productivity. The declining mSSIC and mSSIT (Figure Appendix 17) support this interpretation. Increasing concentrations of both $IPSO_{25}$ and phytoplankton-derived biomarker lipids accordingly may reflect more pronounced ice-edge conditions and/or a distinct seasonality in spring and summer conditions at the WAP through the past 200 years.

For the WAP, we generally expect influences of meltwater inputs from glacial melting (Meredith et al., 2018), additional nutrient input from the APCC and intense mixing at the Peninsula Front. As the distribution of $IPSO_{25}$ is sensitive to local oceanographic conditions (Smik et al., 2016a), biomarker-based sea ice studies require an interpretation that takes the specific environmental characteristics of the region into account. Obviously, high fluctuation in sea ice cover, sea ice thickness and water temperature stimulate phytoplankton growth rather than stable conditions with very high and long lasting or low ice covers and/or ice-free sea surface (e.g. Xiao et al., 2013). We hence propose to compare the individual concentration records of $IPSO_{25}$ and phytoplankton biomarkers rather than using the $IPSO_{25}$ (and $PIPSO_{25}$) record alone to deduce sea ice conditions.

We further consider records of MSA, an organic aerosol, which is associated with marine biological activity during sea ice breakup and is used as a proxy for paleo marine productivity and seasonal sea ice reconstructions in ice cores. Influenced by timing, duration and spatial extent of sea ice breakup MSA concentrations are linked with winter sea ice extent in some regions and summer productivity within the sea ice zone in other regions of Antarctica (Thomas et al., 2019 and references therein). Here we use records of MSA from the Dyer Plateau on the AP as well as a stacked MSA record based on three regional ice cores including Dyer Palteau (Abram et al., 2010) that reflect winter sea ice dynamics in the Bellingshausen Sea. Both records display an overall decreasing trend in MSA concentrations since 1900 CE indicating less sea ice (Figure 6.5). The pattern shows some agreement with the mSSIC from the East Bransfield Basin (PS97/072-2) but is opposite to our biomarker records and sea ice indices for all three core sites. This is likely due to the fact that our sediment records reflect local to regional changes strongly influenced by the AP as a geographic barrier and the complex oceanography within the Bransfield Strait from interaction of BSW and WSW. As both the Dyer Plateau and the stacked MSA records are dominated by large-scale winter sea ice cover variability in the Bellingshausen Sea (centered between 70° and 100°W) (Abram et al., 2010), we suggest that the regional sea ice variability within the Bransfield Strait covered by our sediment cores is not well reflected in the ice core records.

Additionally, we took the latitudinal movement of the spring sea ice edge from modelled data (mSSIE, Figure 6.5) into account, which displays a southward shift down to 63.5°S reflecting sea ice retreat and proposes the occasional absence of spring sea ice at all core sites since the 1970s. The spatial shift of the sea ice edge must be treated with caution because the model does not account for regional impacts, coastal and peninsula interactions and seasonal input of drift ice from the Weddell Sea. The MSA-based winter sea ice edge (WSIE, Figure 6.5) (Abram et al., 2010) displays the same decreasing trend in the Bellingshausen Sea but is located 3° to the south of the modelled ice edge (from 65° to 66°S). The fact that our core sites are located north of this projected WSIE shift is another argument why the ice core MSA cannot be considered to reflect sea ice conditions in our study area, which, according to the ice core data would have been free of sea ice during the entire 20th century.

6.4.4 COMPARISON OF MARINE TEMPERATURE PROXY RECORDS WITH MODEL AND ICE CORE DATA

Comparison of GDGT-based temperatures with modelled subsurface ocean temperature mSOT reveals a general disagreement over the 20th century (Figure 6.6). Only at the Orleans Trough (PS97/068-2) we assume SOT^{TEX} to reflect atmospheric temperatures due to an enhanced water mixing at the Peninsula Front since the mean temperature of +1.9° C is remarkably higher compared to the other core sites with -0.1° C at PS97/056-1 and -0.6° C at PS97/072-2. During the 19th century, SOT^{TEX}-based cold (around 1850s and 1900 CE) and warm events (from 1860 to 1880 CE, and around 1910 CE), respectively, agree better with mSOT at all core sites than in the 20th century. SOT^{OH} does not correspond to mSOT except since the 1990s when both data sets reflect the modern warming. SSST from diatoms show a short cool period around 1900 CE similar to SOT^{TEX} and modelled data. In general, biomarker derived temperatures point to a slight cooling trend over the last 200 years at the WAP which is contradicted by the mSOT data.

Interestingly, highly variable but continuously increasing mSOT (and mSAT) match with the observed trends in atmospheric warming derived from stable isotope ice core data (Figure 6.6). The records of $\delta^{18}O$ records at Bruce Plateau (Goodwin et al., 2016) and δD records from *James Ross Island* (Abram et al., 2013) display the large-scale air temperature evolution in the sector of the Bellingshausen Sea and the Antarctic Peninsula region, and show the same upward trend as air temperatures from several meteorological stations at the WAP (Stastna, 2010). However, we note that ice cores represent a large regional scale and meteorological station records are influenced by e.g. altitude, morphology and local wind patterns, while GDGT-based derived ocean temperatures picture a local to regional marine record controlled by BSW and WSW. We also note that the ocean is decoupled from the atmosphere during periods with sea ice cover and a heating of the ocean by

the atmosphere is diminished. Further, sea ice melting in spring enhances the stratification of the upper water column and restricts heat exchange between the subsurface ocean and atmosphere.

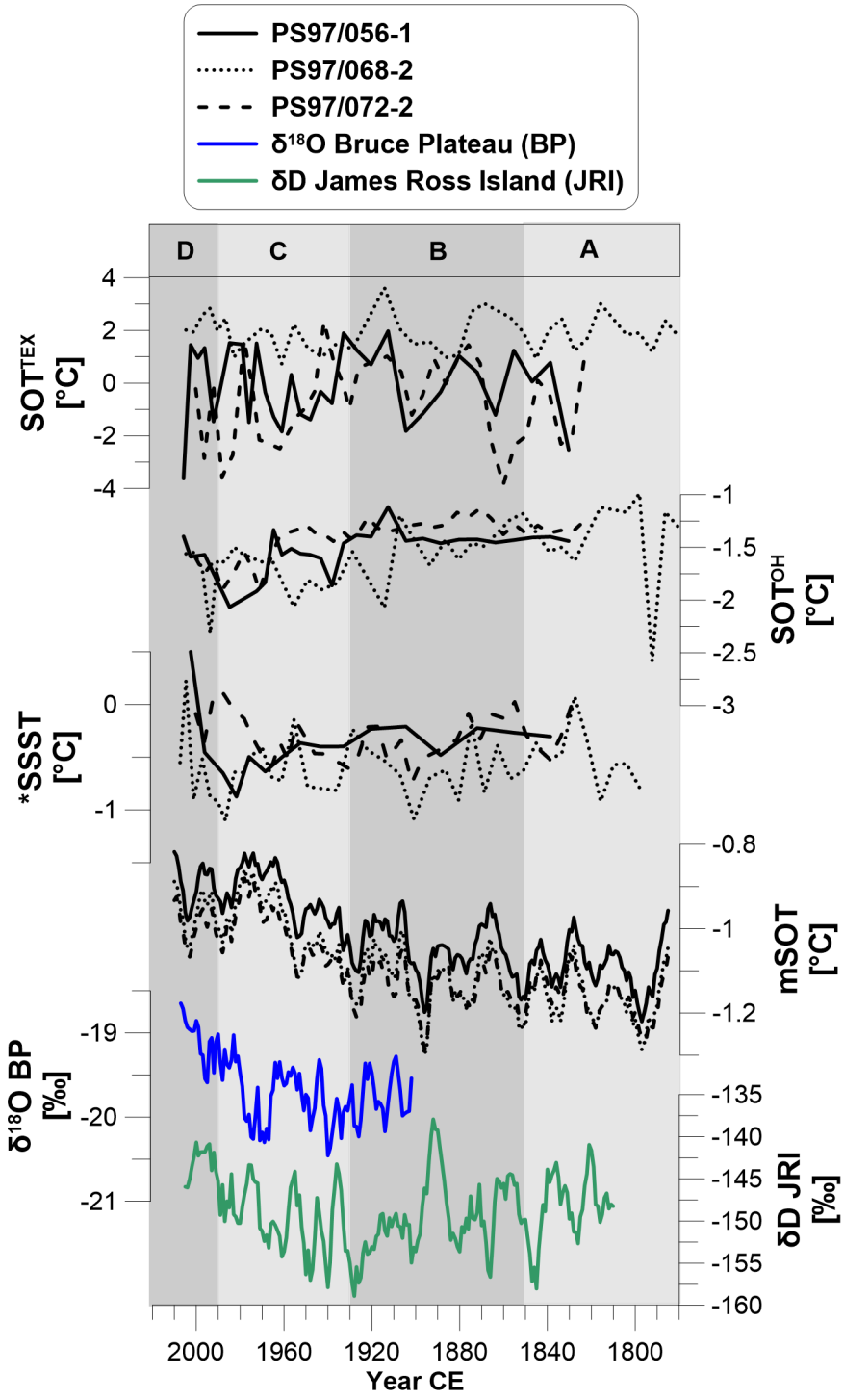

Figure 6.6 Biomarker derived subsurface ocean temperatures based on TEX^{L}_{86} (SOT^{TEX}), and hydroxylated GDGTs (SOT^{OH}), and summer sea surface temperatures (SSST) derived from diatom assemblages compared to modelled subsurface ocean temperature (mSOT), stable isotope ice core records from the Bruce Plateau (BP, $\delta^{18}O$, 5 year running mean; Goodwin et al., 2016) and from James Ross Island (JRI, δD, 5 year running mean; Abram et al., 2013). Data marked with * are from the trigger core PS97/072-1. Vertical grey bars denote the stratigraphic units A to D.

6.4.5 SEA ICE EVOLUTION AND LARGE-SCALE ATMOSPHERIC CIRCULATION PATTERNS

Since atmospheric circulation affects the heat and sea ice distribution at the WAP especially during spring time (Clem et al., 2016), we expect patterns of ENSO and/or SAM to leave a footprint in our spring sea ice $IPSO_{25}$ record. Several studies suggest an enhanced influence of ENSO and SAM on Antarctic temperatures with increasing greenhouse gas concentrations, so their relation to sea ice is a crucial factor for sea ice and climate predictions (Rahaman et al., 2019; Stammerjohn et al., 2008b). For example, the atmosphere-ocean-sea ice interactions impact the WAP strongly through increased northerly winds during an in-phase -ENSO/+SAM mode. They lead to a strong, positive feedback of atmospheric warming amplification due to shorter sea ice seasons, thinner sea ice cover with more leads and an enhanced heat flux from the ocean (Stammerjohn et al., 2008a).

We compared $IPSO_{25}$ from all core sites with a tree-ring based ENSO reconstruction (Li et al., 2013) and SAM data from proxy records including the full mid-latitude to polar domain of the Drake Passage (Abram et al., 2014) (Figure 6.7). Both, ENSO and SAM, have oscillating positive and negative periods and SAM shows a slight decrease until 1860 CE. Since 1930 CE, SAM, and since 1960 CE, ENSO, increase again and reach maximum positive states in the 2000s. When comparing biomarker and circulation patterns, SAM matches best with elevated HBI concentrations, especially at the coastal core sites, relating a higher accumulation of $IPSO_{25}$ with a +SAM. During a +SAM, stronger westerlies lead to a southward shift of the low-pressure cell over the Bellingshausen Sea and the strengthening of the polar frontal jet (Marshall et al., 2006). The blocking effect of the AP is diminished because air masses pass over the northern AP from west to east (Marshall et al., 2006). This results in a remarkable impact on rising summer air temperatures on the eastern AP leeside due to a "Föhn" effect (Klemp and Lilly, 1975). In contrast, the temperature effects on the western AP are very small and not even detectable at e.g. the southwest Vernadsky/Faraday Station (Marshall et al., 2006). Nevertheless, our records suggest that a +SAM is positively related to the production of $IPSO_{25}$ and HBI Z-triene at the WAP, especially since the mid 20th century.

The pattern of ENSO is related negatively with biomarker concentrations in the 19th century (especially at core site PS97/072-2) and more positively in the 20th century. The recent shift to a positive ENSO is accompanied by increased $IPSO_{25}$ concentrations. After Yuan (2004) a +ENSO causes sea ice advance under cold conditions in the Weddell Sea and the WAP, and warm, moist conditions in the Southern Pacific Ocean. However, due to observations of recently rising atmospheric temperature (Stastna, 2010), ocean temperature (Cook et al., 2016) and declining sea ice cover, a +ENSO seems to be more likely related to warm and sea ice reduced conditions at the WAP in the studied period. Nevertheless, we observe that the $IPSO_{25}$ production at the coastal

core sites (PS97/056-1 and 068-1) correspond to ENSO since the 1980s. While neither SAM nor ENSO alone seem to exert a consistent control on $IPSO_{25}$ and phytoplankton production at the WAP, +ENSO together with +SAM seem to be linked to higher $IPSO_{25}$ concentrations especially in the 20th century, which agrees with previous suggestions regarding the impact of atmospheric circulation pattern on sea ice conditions (Barbara et al., 2013; Etourneau et al., 2013).

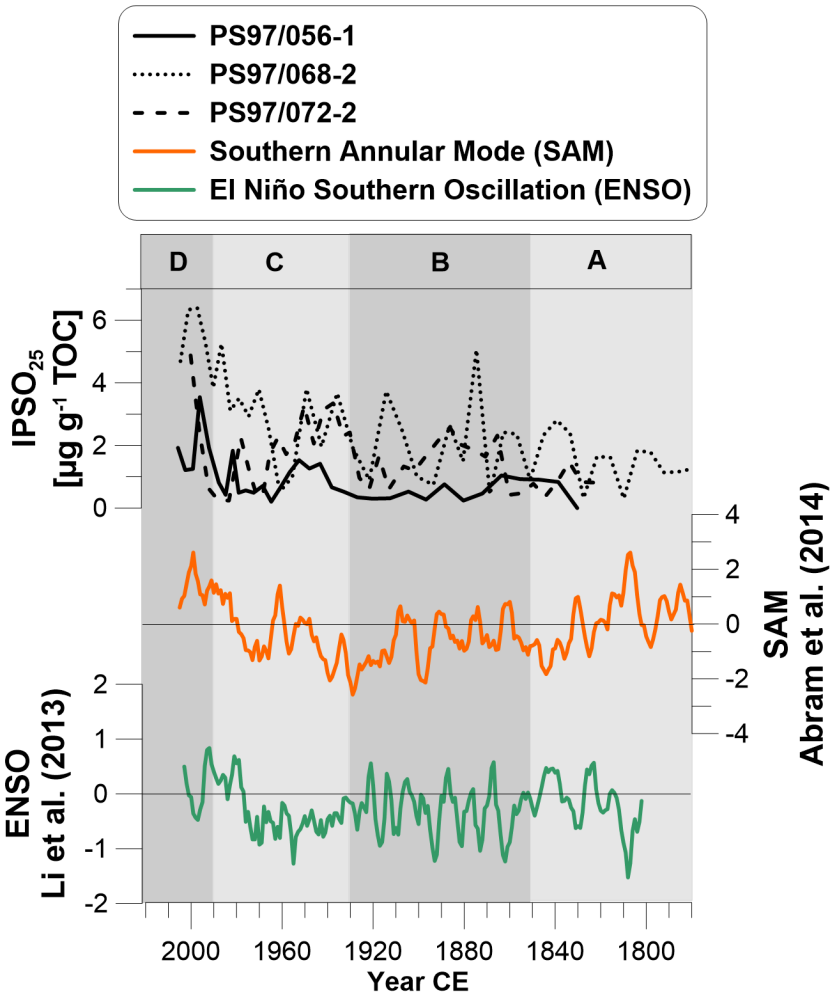

Figure 6.7 Concentrations of biomarker $IPSO_{25}$ in all three sediment cores compared to circulation pattern of the Southern Annular Mode (SAM, 5 year running mean; Abram et al., 2014), and the El Niño Southern Oscillation (ENSO, 5 year running mean; Li et al., 2013). Vertical grey bars denote the stratigraphic units A to D.

6.5 CONCLUSION

In this study we analyzed the spring sea ice biomarker $IPSO_{25}$ and other organic biomarkers as well as diatom assemblages in three sediment cores from the Western Antarctic Peninsula region covering the industrial era and combined them with numerical model data, satellite observations, temperature records and paleo records of atmospheric circulation patterns. We note that the interpretation of the biomarker data for past sea ice estimates in Antarctica is strongly impacted by the origin of water masses and mixing, nutrient input and dynamics of sea ice-related primary

production. Based on sea ice biomarkers and sea ice indices, the 200-year records can be divided into four units:

Unit A Before 1850 CE, the sea ice cover in the WAP was moderate with a low primary productivity and low seasonal sea ice variability influenced by WSW inflow into the Bransfield Strait.

Unit B From 1850 to 1930 CE, low to moderate stable sea ice cover was common at the coastal WAP, while rapid changes in sea ice seasonality were evident at the East Bransfield Basin due to changes in oceanographic pattern and enhanced BSW inflow.

Unit C 1930 CE marked a turning point in sea ice cover with increased sea ice dynamics triggering melting and primary production of both open marine and sea ice species, with periods of high (1940s-1950s) and low sea ice cover (1960s-1970s).

Unit D Since 1990 CE, the anthropogenic warming reversal is evident in subsurface ocean temperatures and low sea ice cover with high seasonal dynamics promoting marine production and causing maximum sea ice indices.

While $IPSO_{25}$ concentrations agree with satellite sea ice data, they seem to contradict with long-term large-scale ice core and model data. We explain this as a result of local coastal influences, high sea ice dynamics and thinner sea ice promoting the production of both sea ice diatoms and open marine phytoplankton affecting the interpretation of $IPSO_{25}$ and the sea ice index $PIPSO_{25}$. When estimating spring sea ice cover, the strong susceptibility of $IPSO_{25}$ to local influences such as water masses, coastal interaction and, e.g. a higher sea ice algae productivity resulting from thinner ice cover need to be taken into account. We hence recommend to consider additional phytoplankton data instead of constructing sea ice estimates on $IPSO_{25}$ and $PIPSO_{25}$ records solely. We do not observe a relation between ocean temperature evolution and retreating sea ice in the 20th century. The examination of ENSO and SAM paleo records reveals that both seem to affect the sea ice regime at the WAP and that SAM in particular could be a main driver for sea ice conditions favoring $IPSO_{25}$ production.

DATA AVAILABILITY

All data will be available at the open access repository www.pangaea.de.

AUTHOR CONTRIBUTIONS

The study was conceived by MV and JM. Data collections and experimental investigations were done by MV together with PC, LR, PM and CBL (diatoms, dating), WG (dating), OE (diatom transfer functions), JM and GM (HBIs, GDGTs), XS and GL (modelling and supplement Figure Appendix 8), CH (satellite sea ice data), and TO (ice cores). MV drafted the manuscript and figures. JM supervised the study. All authors contributed to the interpretation and discussion of the results and the conclusion of this study.

ACKNOWLEDGEMENT

We thank the captain, crew and chief scientist Frank Lamy of RV Polarstern cruise PS97. Denise Diekstall, Jens Hefter, Ingrid Stimac and Ruth Cordelair are thanked for their laboratory support. Simon Belt is acknowledged for providing the 7-HND internal standard for HBI quantification. Financial support was provided through the Helmholtz Research grant VH-NG-1101.

7 PART III: FROM THE LAST GLACIAL MAXIMUM UNTIL TODAY: A MULTIPROXY STUDY ON SEA ICE AND CLIMATE DYNAMICS AT THE WESTERN ANTARCTIC PENINSULA

Maria-Elena Vorrath[1], Juliane Müller[1,2,3], Paola Cárdenas[4], Sebastian Mieruch-Schnülle[1], Oliver Esper[1], Thomas Opel[1], Andrea Vieth-Hillebrand[5], Niko Lahajnar[6], Carina B. Lange[4,7,8,9], Amy Leventer[10], Gesine Mollenhauer[1,2]

[1]Alfred Wegener Institute, Helmholtz Centre for Polar and Marine Research, Bremerhaven, Germany

[2]MARUM – Center for Marine Environmental Sciences, University of Bremen, Germany

[3]Department of Geosciences, University of Bremen, Germany

[4]Centro de Investigación Dinámica de Ecosistemas Marinos de Altas Latitudes (IDEAL), Universidad Austral de Chile, Valdivia, Chile

[5]Helmholtz Research Centre for Geosciences, GFZ, Potsdam, Germany

[6]Universität Hamburg, Institute for Geology, Hamburg, Germany

[7]Centro Oceanográfico COPAS Sur-Austral, Universidad de Concepción, Chile

[8]Departamento de Oceanografía, Universidad de Concepción, Chile

[9]Scripps Institution of Oceanography, La Jolla, CA 92037, USA

[10]Department of Geology, Colgate University, New York, USA

Submission planned in *Quaternary Science Reviews*, August 2020.

Abstract

The reconstruction of past sea ice distribution in Antarctica provides crucial information to evaluate and improve model projections of Antarctic climate. The Western Antarctic Peninsula (WAP) is heavily exposed to a rapid warming and the associated decrease in sea ice cover contradicts the generally increasing trend of Antarctic sea ice. To reveal long-term sea ice conditions at the WAP under different and changing climate conditions we examined a marine sediment core from the eastern basin of the Bransfield Strait covering the last deglacial and the

Holocene. We focused on the specific biomarker lipid $IPSO_{25}$, a highly branched isoprenoid (HBI), from sea ice algae in combination with biomarkers derived from open marine diatom species, i.e. HBI trienes and sterols. Further, we considered the sedimentological and geochemical composition of the sediment, the use of diatom assemblages and glycerol dialkyl glycerol tetraether (GDGTs) as well as independent records such as ice core sea salt sodium aerosol records and large-scale atmospheric circulation reconstructions. Sea salt sodium flux records revealed a positive relationship to our sea ice biomarker $IPSO_{25}$ and the derived sea ice indicator $PIPSO_{25}$, indicating it to be a reliable source of paleo sea ice information. Using biomarker concentrations and sedimentological data we reconstruct a retreat of the floating ice shelf and an opening of the ocean surface at 16.4 ka BP at the core site. During the deglaciation, an extensive sea ice cover weakened due to the warming which is interrupted by the Antarctic Cold Reversal from 13.2 ka to 12.4 ka BP. Both warming and sea ice retreat continued in the early Holocene (12 ka to 9 ka BP) and stabilized in the middle Holocene, characterized by maximum phytoplankton productivity. Between 12 ka and 5 ka BP, sea ice conditions changed from stable sea ice edges to shorter sea ice seasons with high amplitudes. The late Holocene is characterized by unstable sea ice and climatic conditions with a prominent cooling trend towards today. Large-scale atmospheric circulation patterns such as the El Niño Southern Oscillation (ENSO) and the Southern Annular Mode (SAM) were found to govern temperature and sea ice biomarker production at the WAP. Prevailing positive SAM and negative ENSO indices promoted middle Holocene warm conditions with highly variable sea ice conditions, while the opposite pattern supported cold conditions with moderate sea ice cover in the late-Holocene.

7.1 INTRODUCTION

Sea ice has significant impacts on the global climate system as well as the Southern Ocean and Antarctica by controlling albedo, primary production, ocean circulation, the carbon cycle and the physical and chemical properties of the water masses. Sea ice cover limits the atmosphere-ocean exchange of heat and gas, impacting evaporation and precipitation and increases the reflection of solar radiation due to a high albedo (Allison et al., 1982; Butterworth and Miller, 2016; Turner et al., 2017). During spring the melting of sea ice stimulates marine primary production due to the release of nutrients and by promoting ocean stratification and a shallow mixed layer depth (Arrigo et al., 1997; Vernet et al., 2008). Enhanced carbon fixation and high particle fluxes lead to high exports of organic carbon to the ocean floor and an efficient biological pump (Kim et al., 2004; Schofield et al., 2018; Wefer et al., 1988). The nutrient supply is also stimulated via local upwelling induced by to winds along the sea ice edges (Alexander and Niebauer, 1981). Recently, the volatile compound dimethylsulphide – which affects the radiative properties of clouds – was found in thin

Antarctic sea ice and is supposed to be released due to sea ice melting (Trevena and Jones, 2006). During sea ice formation, cold, high-density brines develop and contribute to the formation of intermediate and deep waters (Nicholls et al., 2009). Further, the sinking water mass prevents warm currents to reach the continental slope to melt the base of Antarctic ice shelves with implications on the stabilization of ice shelves and eventually global sea level (Cook et al., 2016; Escutia et al., 2019; Etourneau et al., 2019; Hellmer et al., 2012; Huss and Farinotti, 2014). Since instrumental records are available, fast and profound transformations have been observed globally due to anthropogenic global warming (IPCC, 2018, 2019). Especially the Western Antarctic Peninsula (WAP) experiences a rapid warming of the atmosphere (Vaughan et al., 2003) and the ocean (Cook et al., 2016). This is accompanied by rapidly retreating glaciers and ice shelves (Cook et al., 2016; Rignot et al., 2019) and by significant losses of sea ice cover in the adjacent seas (Parkinson and Cavalieri, 2012).

The deglacial and Holocene climate history at the Antarctic Peninsula (AP) has been extensively studied. The deglaciation, the transition from the Last Glacial Maximum (LGM, btween 25 ka and 19 ka BP, Clark et al., 2009) to the Holocene, is characterized by a rapid warming punctuated with an intermediate, distinct cold event, the so-called Antarctic Cold Reversal (ACR) from 13.2 ka to 12.4 ka BP (EPICA Community Members et al., 2004; Mulvaney et al., 2012; WAIS Divide Project Members et al., 2015). This drastic cooling of both atmosphere and ocean temperature is mainly recorded by stable isotopes in ice cores all over Antarctica (Blunier and Brook, 2001; Domack et al., 2001; Jouzel et al., 1995; Morigi et al., 2003; Stenni et al., 2001). It occurred simultaneously to the Bølling-Allerød warm stage in the North Atlantic, supporting the suggestions of a teleconnection of both hemispheres via the bipolar seesaw pattern (Anderson et al., 2009; Broecker, 1998; Pedro et al., 2016). During the deglaciation, the Antarctic Peninsula Ice Sheet (APIS) retreated rapidly from the outer shelf to its modern configuration in the Middle Holocene with heavy melt water discharge (Bentley et al., 2014). Several syntheses of Holocene climate reflected in marine sediment cores reveal that the timing of environmental change is highly variable at the WAP (Allen et al., 2010; Ingólfsson et al., 2003; Minzoni et al., 2015; Taylor and Sjunneskog, 2002). An overall consensus is the ocean warming during the early and middle Holocene optimum between 12 ka and 4 ka BP, often divided into two phases with short cold interruptions (Taylor and Sjunneskog, 2002). The period from 4 ka BP to today, i.e. the Late Holocene or Neoglacial, shows many different climate patterns around the AP and a consistent climate stratigraphy is not defined. While in some records the Neoglacial is reflected by a constant cooling (Etourneau et al., 2013), other records resolve warmer and colder phases such as the Mediaeval Climate Anomaly or the Little Ice Age (Bentley et al., 2009).

PART III

The relationship of sea ice and oceanic heat distribution is supposed to be related to oceanic circulation patterns and ocean-atmospheric coupling to the El Niño Southern Oscillation (ENSO) and the Southern Annular Mode (SAM) (Liu et al., 2004; Stammerjohn et al., 2008a). Both, ENSO and SAM, are assumed to cause different sea ice trends in the Pacific and Atlantic sector of the Southern Ocean via teleconnections (Stammerjohn et al., 2008b). While such studies have been conducted mainly over the instrumental era for the AP (Clem et al., 2016; Ding et al., 2012; Marshall et al., 2006; Stammerjohn et al., 2008b, 2008a; Yuan, 2004), two paleo studies based on marine sediments show a sensitivity of sea ice to ENSO variability on millennial scales (Barbara et al., 2016; Etourneau et al., 2013). They conclude that high sea ice cover and high sea surface temperatures (SST) are related to a rising number of ENSO events leading to increasing seasonal amplitudes of warm summers and cold winters. The strength and latitudinal position of the Southern Westerly Winds (SWW) is suggested to resemble SAM-like conditions in the Holocene Patagonian glacier history (Moreno et al., 2014; Reynhout et al., 2019) which controls the distribution of water contributions from several sources triggering warm water intrusions, varying SSTs and increased storm activity (Martinson and McKee, 2012; Meredith and King, 2005). At the Palmer Deep, WAP, strong SWWs as well as their southward latitudinal position are associated with a supply of warm water masses due to upwelling of Upper Circumpolar Deep Water (UCDW) (Etourneau et al., 2013; Pike et al., 2013), leading to high SSTs and a sea ice retreat.

Knowledge of past sea ice variability is crucial for modelling of climate feedbacks or the Antarctic ice sheet stability during the transition from the LGM to the Holocene. For periods beyond the satellite era respective data is only based on proxies from marine sediments and ice cores (Bracegirdle et al., 2015, 2019; Escutia et al., 2019) and climate modelling. Model studies, however, often hamper to reproduce seasonal sea ice cycles for both glacial and interglacial periods and often disagree with geological proxies (Roche et al., 2012). From ice cores, sea ice reconstructions for the LGM are based on the precipitation of sea salt sodium and calcite, the snow accumulation and also the deuterium excess (Sinclair et al., 2014; Thomas et al., 2019). Since the evaporation and precipitation of such proxies are affecte by atmospheric circulation these climate archives are sensitive to the highly variable wind direction and meteorological conditions in Antarctica (Thomas et al., 2019). Climate archives from marine sediments may often have a lower temporal resolution than ice cores but their advantage lies in the ability to resolve regional and/or large scale paleoceaongraphic information of sea surface and subsurface ocean temperature, primary productivity and marine ecology, ocean currents and sea ice (Hillaire-Marcel and de Vernal, 2007). Here, the geochemical composition of the sediments, such as ice rafted debris (IRD), and sea ice related diatom assemblages are common (e.g. Gersonde et al., 2005) but since diatom frustules are sensitive to selected dissolution in the ocean (Burckle and Cooke, 1983; Esper and Gersonde,

2014a; Leventer, 1998; Ragueneau et al., 2000) these approaches are limited. New approaches focus on specific organic biomarkers, from highly branched isoprenoids (HBIs), as reliable proxies to distinguish between open marine and sea ice covered environments. The diunsaturated HBI $IPSO_{25}$ (**I**ce **P**roxy for the **S**outhern **O**cean C_{25}; Belt et al., 2016; Massé et al., 2011) has already been applied for Antarctic sea ice reconstructions in several studies (Barbara et al., 2013; Denis et al., 2010; Etourneau et al., 2013). Following the PIP_{25} approach from the Arctic (Müller et al., 2011) $IPSO_{25}$ is combined with HBI trienes and/or sterols to determine the phytoplankton-$IPSO_{25}$ sea ice index, called $PIPSO_{25}$ (Vorrath et al., 2019). Very recently, this semi-quantitative sea ice proxy $PIPSO_{25}$ has already been applied for the first time in paleo sea ice studies (Lamping et al., 2020; Vorrath et al., submitted, see Part II, chapter 6).

Here, we present a marine sediment record covering the transition of regional climate, sea ice and ice shelf dynamics over the last 17 ka BP from the deglaciation to the Holocene at the WAP. Our study is based on a multiproxy approach focusing on the sea ice biomarker $IPSO_{25}$, marine phytoplankton biomarkers (HBI trienes and sterols), and on glycerol dialkyl glycerol tetraether (GDGTs) for subsurface ocean temperatures (SOT). Additional sedimentological data comes from x-ray fluorescence (XRF) measurements while information about the winter sea ice (WSI) concentration and summer sea surface temperature (SSST) is retrieved from diatom assemblages using transfer functions. We compare our findings with several adjacent sediment records for the Holocene, paleo records of ENSO and SAM and ice core sea salt sodium records. By doing so, we reveal the history of ice shelf retreat, Holocene climate and sea ice variability at the WAP and provide further insight into environmental dynamics across the deglaciation and the Holocene.

7.2 Material and Methods

7.2.1 Study Area

The Bransfield Strait is located between the Western Antarctic Peninsula (WAP) and the South Shetland Islands (SSI). Within this area, the Bransfield Basin is characterized by a shallow shelf and deeper parts with water depths exceeding 2000 m (Figure 7.1). The shelf area has been affected by intense ice sheet dynamics during the last glaciation (Canals and Amblas, 2016b; Ingólfsson et al., 2003) leaving ice sheet grounding lines and glacial troughs on the sea floor (Canals et al., 2016; Canals and Amblas, 2016a). The Bransfield Basin is influenced by complex oceanic currents systems which are not fully constrained because three different water masses enter the basin from the east and the west into the basin (Moffat and Meredith, 2018; Sangrà et al., 2011) and their mixing is not well understood yet. The Weddell Sea Water (WSW) enters from the east, flows alongshore the peninsula and fills the basin below 150m surface. The water mass is known to be cold (< 0°C) and relatively salty. The WSW is also observed in greater depths (200-600 m) north

of the SSI and at Elephant Island due to wind driven modulation (Meijers et al., 2016). In the western part of the Bransfield Strait the WSW is supposed to mix with the second water mass, the Bellingshausen Sea Water (BSW) (Collares et al., 2018), which is a branch of the Antarctic Circumpolar Current (ACC). It conveys well-stratified, fresh and warm (> 0°C) surface water (Sangrà et al., 2011). A third water mass originating from the Circumpolar Deep Water (CDW) is present in a depth of 200 m to 550 m (Sangrà et al., 2017). BSW and CDW flow eastward along the SSI, turn around and flow westward at the northern side of the islands (Sangrà et al., 2011). The BSW forms the subsurface Bransfield front with the CDW in depth and the surface Peninsula Front with the WSW, parallel to the Antarctic mainland (Sangrà et al., 2011, 2017). The eddy system at the Peninsula Front is assumed to play a key role for mixing and upwelling of the different water masses (Sangrà et al., 2011; Zhou et al., 2002) while glaciers from the WAP influence coastal surface water due to meltwater discharge (Meredith et al., 2018).

Primary production is mainly driven by mixing of water masses at the fronts (Gonçalves-Araujo et al., 2015), mixed layer depth and upwelling (Sangrà et al., 2011), sea ice dynamics (Vernet et al., 2008) and iron availability (Klunder et al., 2014). High concentrations of chlorophyll and diatoms are distributed north of the Peninsula Front and at the SSI, while lower production and communities of nanoplankton are found between the Peninsula Front and the WAP (Gonçalves-Araujo et al., 2015). Further, changes in coastal primary production are driven by upwelling, iron distribution and the retreat of sea ice cover in spring releasing nutrients and stabilizing the water

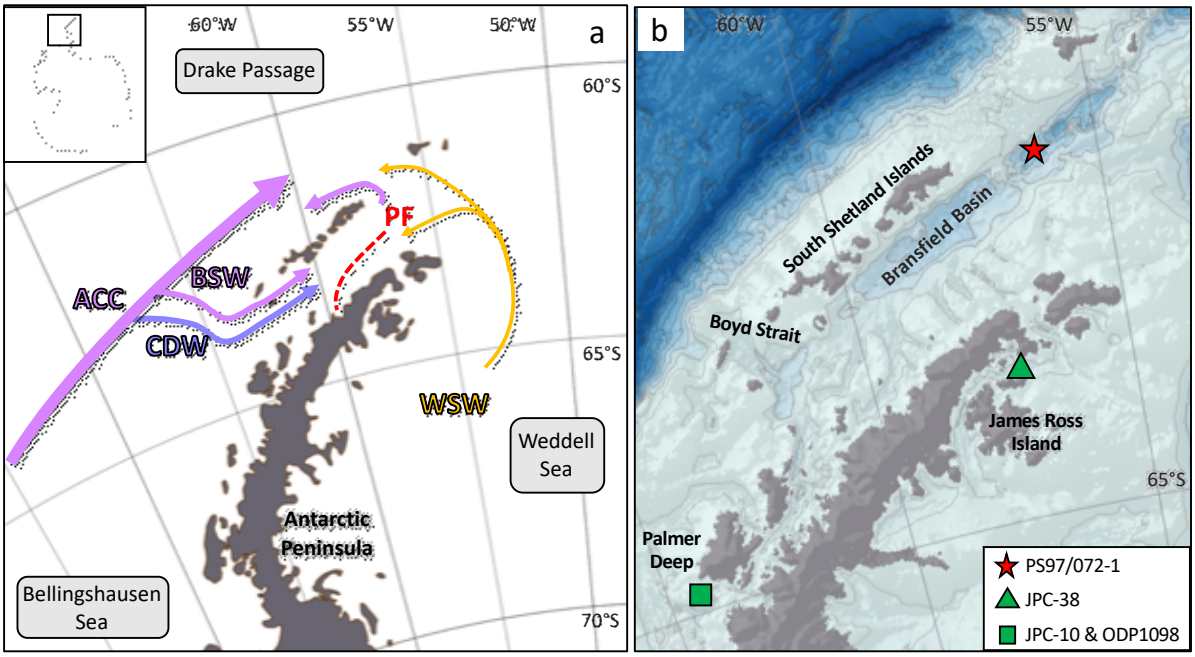

Figure 7.1 a) Overview map with modern oceanography in the study area (modified after Hofmann et al., 1996; Sangrà et al., 2011) with ACC = Antarctic Circumpolar Current, BSW = Bellingshausen Sea Water, CDW = Circumpolar Deep Water, WSW = Weddell Sea Water, and PF = Peninsula Front. B) Bathymetric features in the Bransfield Strait with sediment core and geographic locations mentioned in the text. Maps were generated using QGIS 3.0 (2018) and the bathymetry was taken from GEBCO_14 from 2015.

column in spring (Vernet et al., 2008). A close link between marine primary production at the surface and sediment composition at the ocean floor is reflected in high concentrations of total organic carbon (TOC), pigments, sterols and diatoms, low carbonate values, low C/N and $\delta^{13}C$ values (Cárdenas et al., 2019) and supported by studies confirming high fluxes of sinking particles (Kim et al., 2004; Wefer et al., 1988 and others). Particle flux is highly variable with seasonal peaks appear in late spring, which account for 85% of the total flux (Ducklow et al., 2008). Lithogenically, the sediments consist mainly of terrestrial silt and clay with varying amounts of diatom ooze and sand (Cádiz Hernández, 2019; Lamy, 2016; Wu et al., 2019).

7.2.2 SEDIMENT SAMPLES AND AGE MODEL

The piston core PS97/072-1 (62° 0.39' S, 56° 3.86' W, 1993 m water depth, 1583 cm long) was recovered during the *Polarstern* cruise PS97 in the eastern Bransfield Strait Basin at the WAP (Figure 7.1). The composition of the sediment core is dominated by silt with thin layers of sand, clay, and traces of volcanic ash. Single pebbles are present below 630 cm. Since we found disturbed sediments below 1015 cm we only considered samples from above this level for our analyses. The core sampling was done at the Alfred Wegener Institute (AWI) where the samples were stored frozen in glass vials (for biomarker samples) and at 4° C in plastic bags (for micropaleontology), respectively. The magnetic susceptibility was measured on the whole round core section on board the *Polarstern* with a GEOTEK multi-sensor core logger. The elemental analysis was done with an AVAATECH profiling X-ray fluorescence (XRF) core-scanner at AWI.

The ^{14}C radiocarbon dating for core PS97/072-1 was done on six calcite samples with the mini carbon dating system (MICADAS) at AWI following the method of Wacker et al. (2010). Further, we dated the acid-insoluble organic matter (AIO) of sixteen samples also using the MICADAS and following the procedure of Heroy et al. (2008). Because the core location is in a deep sediment collecting basin close to the Antarctic mainland we considered the influence of terrestrial organic carbon and calculated the relative fraction of marine organic matter (f_{marine}) from $\delta^{13}C$ measurements (see chapter 7.2.3). We used a two end-member mixing model (Thornton and McManus, 1994) based on the endmembers of marine plankton with $\delta^{13}C$ = -23.5‰ (after Fischer, 1991; Mincks et al., 2008) and endmembers from mosses and peat with $\delta^{13}C$ = -28.0‰ (after Bramley-Alves et al., 2016; Royles et al., 2013, 2016) typical for the WAP:

$$f_{marine}\ (\%) = \frac{(\delta^{13}C_{org\ sample} - \delta^{13}C_{org\ terrestrial})}{(\delta^{13}C_{org\ marin} - \delta^{13}C_{org\ terrestrial})}. \quad (1)$$

Afterwards we subtracted the marine radiocarbon reservoir age based on simulation from Butzin et al. (2017) and from each dating result and calibrated the ages with the calibration curve SHCal13 (Hogg et al., 2013) to calendar years before present (cal BP) with Calib 7.1 (Stuiver et al., 2018)

(Table Appendix 16). Based on the identification of specific diatom species, the analysis of bulk parameters and stable carbon isotopes, we suppose that the main source of organic matter in our sediments is marine. However, we assume that our calcareous fossil records and organic matter composition could be biased from the influx of older, reworked sediments. This is supported by the identification of the diatom species *Actinocyclus ingens*, *Rouxia leventerae*, and *Cladogramma sp.* in isolated samples below 540 cm and which are related to marine isotope stage (MIS) 6 (0.14-0.13 Ma), the lower MIS 8 (0.3-0.28 Ma) (Zielinski and Gersonde, 2002), and late MIS 11 (0.38 Ma) (Zielinski et al., 2002). Also, the comparison to adjacent marine sediments and ice cores using e.g. magnetic susceptibility and reconstruced water temperature (Domack et al., 2001; Heroy et al., 2008; WAIS Divide Project Members et al., 2015; Willmott et al., 2006; Xiao et al., 2016a) let us conclude that the ^{14}C ages obtained from deeper samples overestimate the true ages due to the addition of "dead carbon". In consequence, we correlated our age model to that of the West Antarctic Ice Sheet Divide ice core (WAIS Divide Project Members et al., 2015) using prominent features in the TOC content and reconstructed temperature records (see detailed description in Appendix 19). The core top was defined to be of recent age after ^{210}Pb dating on a short core (see Part II, chapter 6.2.2). We applied the bayesian age model *hummingage*, which is developed at AWI and freely available at https://github.com/hummingbird-dev/hummingage. The GitHub repository provides source code for the R programming language and a Jupyter Notebook containing detailed explanations, example data and code for running a full procedure. Additionally, an easy to use web service is provided at https://hummingage.awi.de/ for applying *hummingage* online in the browser without the need to install any software. The web service provides the download of the created figures as PNG or PDF as well as the original and interpolated (1 cm) model output for further analyses as ASCII text files. The age depth model *hummingage* can be an alternative to the widely used Bacon (Blaauw and Christeny, 2011) method. In addition to *hummingage* we also apply Bacon to our data and show the comparison of both approaches in the supplements (see Appendix 19). Based on this approach, the sediment core covers the last 17.2 ka BP with a mean sedimentation rates of 60cm/ka (Figure 7.2, Table Appendix 20).

7.2.3 ORGANIC GEOCHEMICAL ANALYSES PISTON CORER PS97/072-1

For the analyses of several organic compounds and biomarkers the sediments were freeze-dried and homogenized in an agate mortar. Total carbon (C) and nitrogen (N) were analyzed with a CNS analyzer (Elementar Vario EL III, error of standards and duplicates < 5%). TOC was measured on 0.1 g of acidified samples (500 µl HCl) and determined in a carbon-sulphur determinator (CS-800, ELTRA, standard error < 0.6%). The amount of carbonate was calculated with $CaCO_3$ (wt%)

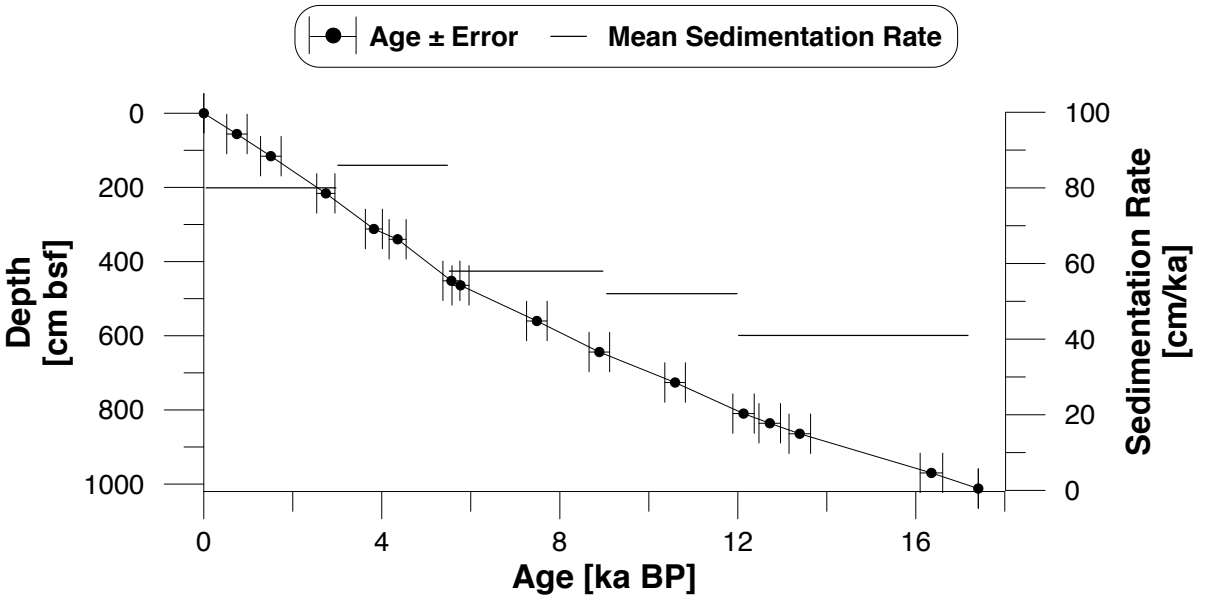

Figure 7.2 Resulting age-depth model with error bars and mean sedimentation rates (cm/ka) from piston core PS97/072-1. All plots were done with Grapher™ 13.

= total carbon – TOC x 8.333. C/N reflects the ratio of TOC against total nitrogen. Biogenic opal was measured at the University of Concepción, Chile, after the methods established by Mortlock and Froehlich (1989) and modified after Müller and Schneider (1993). The analysis was described in details by Rebolledo et al. (2019). The analytical error was ±0.5%.

The examination of HBIs followed the analytical protocol of the international community of researchers conducting HBI sea ice reconstructions (see Belt et al., 2013, 2014; Stein et al., 2012; Vorrath et al., 2019). At first the internal standards 7-hexylnonadecane (7-HND), C_{46}, and 5α-androstan-3β-ol were added to 5 g of sediment. The lipid extraction was done three times with an ultrasonic bath (15 min) and a mixture of CH_2Cl_2:MeOH (v/v 2:1; 6ml) added to the samples. After this, the solvent was centrifugated (2500 rpm for 1 min) and decanted after centrifugation. HBIs, sterols and GDGTs were separated by means of open column chromatography using SiO_2 at the stationary phase. First, the apolar HBIs were eluted with 5 ml hexane, and second, the polar fraction containing sterols and GDGTs was eluted with 5 ml dichlormethane:MeOH (v/v 1:1). The polar fraction was split and one half was further purified by column chromatography with 8 ml ethylacetate:hexane (v/v 20:80) to obtain the sterol fraction, while the other half was kept for GDGT analysis. The analysis of HBIs and sterols was done with an Agilent 7890B gas chromatograph (30 m DB 1MS column, 0.25 mm diameter, 0.250 μm film thickness) coupled to an Agilent 5977B mass spectrometer (MSD, 70 eV constant ionization potential, ion source temperature 230° C). The temperature program for HBIs started with an oven temperature of 60° C which was held for 3 min, ramped to 325° C within 23 min, and was held at 325° C for 16 min. Prior to measurement, the sterols were silylated (200 μl BSTFA; 60° C; 2 hours). Sterols were

analyzed with a different oven temperature program (60° C for 2 min, rise to 150° C within 6 min, rise to 325° C within 56 min 40 sec). HBIs were identified via comparison of their retention times and mass spectra with published mass spectra (Belt et al., 2000) and quantified using the ratio of peak areas of individual HBIs and the 7-HND standard. A sample with known HBI concentrations served as external calibration for HBI diene and trienes to determine the response factors of the HBI molecular ions (*m/z* 346; *m/z* 348) and the fragment ion of 7-HND (*m/z* 266). The quantification is based on the manual peak area integration of the molecular ions of HBIs and the fragment ion m/z 266 of 7-HND. Sterols were identified by comparison of their retention times and mass spectra with reference compounds in the same sequence run (brassicasterol *m/z* 470, dinosterol *m/z* 500, campesterol *m/z* 472, b-sitosterol *m/z* 486, desmosterol *m/z* 456). The error of duplicates was <1.4% for $IPSO_{25}$, <2.6% for HBI trienes, and < 2% for bassicasterol and dinosterol.

GDGTs were analyzed after the extract was dried, re-dissolved in 120 µl hexane:isopropanol (v/v 99:1) and filtered through polytetrafluoroethylene filters (0.45 µm in diameter). The analysis was done with high performance liquid chromatography (HPLC, Agilent 1200 series HPLC system) coupled to a single quadrupole mass spectrometer (MS, Agilent 6120 MSD) via an atmospheric pressure chemical ionization (APCI) interface. The individual GDGTs were separated at 30° C on a Prevail Cyano column (150 mm x 2.1 mm, 3µm). After injection of the sample (20 µl) it passed a 5 min isocratic elution with mobile phase A (hexane/2-propanol/chloroform; 98:1:1, flow rate 0.2 ml/min). The mobile phase B (hexane/2-propanol/chloroform; 89:10:1) was increased to 100% in two steps: a linear increase to 10% over 20 min followed by an increase to 100% within 10 min. During the measurement the column was cleaned after 7 min via backflush (5 min, flow 0.6 ml/min) and re-equilibrated with solvent A (10 min, flow 0.2 ml/min). The conditions of the APCI were a nebulizer pressure of 50 psi, vaporizer temperature and N_2 drying gas temperature 350°C, flow 5 l/min, capillary voltage 4 kV, and corona current 5 µA. The GDGTs were detected by selective ion monitoring (SIM) of ($M+H^+$) ions (dwell time 76 ms). In relation to the internal standard C_{46} (*m/z* 744) the molecular ions *m/z* of GDGTs-I (*m/z* 1300), GDGTs-II (*m/z* 1298), GDGTs-III (*m/z* 1296), and crenarchaeol (*m/z* 1292) were quantified. Also, the branched GDGTs-Ia (*m/z* 1022), GDGTs-IIa (*m/z* 1036), GDGTs-IIIa (*m/z* 1050) were quantified. The hydroxylated GDGTs OH-GDGT-0 (*m/z* 1318), OH-GDGT-1 (*m/z* 1316), and OH-GDGT-2 (*m/z* 1314) were quantified in the scans of their related GDGTs (see Fietz et al., 2013). The standard deviation was 0.01 units of TEX^L_{86}.

Kalanetra et al. (2009) propose that temperatures based on GDGTs reflect near-surface waters and the highest abundance on crenarchaea in Antarctica were found between 50m and 200m water

depth (Kim et al., 2012). We therefore consider our results to reflect subsurface ocean temperatures (SOTs). We calculated TEX^{L}_{86} after Kim et al. (2010) with the m/z 12963 (GDGT-3), m/z 1298 (GDGT-2), m/z 1300 (GDGT-1):

$$TEX^{L}_{86} = \log\left(\frac{[GDGT-2]}{[GDGT-1]+[GDGT-2]+[GDGT-3]}\right) \quad (2)$$

and calibrated with $SOT^{TEX} = 67.5 * TEX^{L}_{86} + 46.9$ (Kim et al., 2010). (3)

For the calculation of temperatures based on hydroxylated GDGTs we followed the approach of Lü et al. (2015)

$$RI-OH' = \frac{[OH-GDGT-1]+2\times[OH-GDGT-2]}{[OH-GDGT-0]+[OH-GDGT-1]+[OH-GDGT-2]} \quad (4)$$

and calibrated it with SOT^{OH} = (RI-OH' - 0.1) / 0.0382. (5)

For inter-comparison with temperature data from other studies we used temperature anomalies for GDGT-based and diatom-based temperatures records that we calculated as anomaly T° = absolute T° – mean T°.

For the branched and isoprenoid tetraether (BIT) index for indicating terrestrial organic matter (Hopmans et al., 2004) we used crenarchaeol (m/z 1292) and the branched GDGTs and calculated it with

$$BIT = \frac{[GDGT-Ia]+[GDGT-IIa]+[GDGT-IIIa]}{[Crenarchaeol]+[GDGT-Ia]+[GDGT-IIa]+[GDGT-IIIa]}. \quad (6)$$

The phytoplankton-$IPSO_{25}$ index ($PIPSO_{25}$) was calculated after Vorrath et al. (2019) with

$$PIPSO_{25} = \frac{IPSO_{25}}{IPSO_{25}+(c\times phytoplankton\ marker)}\ . \quad (7)$$

Brassicasterol, dinosterol and both HBI trienes were considered as phytoplankton biomarkers and the concentration balance factor c (c = mean $IPSO_{25}$ / mean phytoplankton biomarker) was 0.28 for basssicasterol and 0.94 for dinosterol to account for the high offsets from $IPSO_{25}$. Since HBI trienes concentrations were on the same level as $IPSO_{25}$, the c-factor was set to 1 (Vorrath et al., 2019). The different indices were defined using the terms P_ZIPSO_{25} (using the Z-triene), P_EIPSO_{25} (using the E-triene), P_BIPSO_{25} (using bassicasterol), and P_DIPSO_{25} (using dinosterol).

The measurements of stable carbon isotopes of organic $\delta^{13}C$ were done at the University of Hamburg. For this, the samples were acidified three times with 100 µl 1 N HCl and dried on a hotplate. High-temperature combustion was done in an Elementar CHNOS Vario isotope elemental analyser at 950° C and the analysis was conducted with an Elementar IsoPrime 100 isotope ratio mass spectrometer. We calibrated the pure tank CO_2 with the International Atomic Energy Agency reference standards IAEA-CH6 and IAEA-CH7. These, and two other standards (IVA Sediment and Sucrose) acted as internal standards in the measurement. The error of

continuous standard duplicates was < 0.2‰ and <0.06‰ for sample duplicates. $\delta^{13}C$ values are expressed in ‰ against Vienna Pee Dee Belemnite (VPDB). Additional measurement of stable carbon isotopes was done at the Washington State University in cooperation with Universidad Austral de Chile, Valdivia, Chile. The method is described in detail in Cárdenas et al. (2019).

The of stable carbon isotope composition of $IPSO_{25}$ was examined on 8 samples (with minimum 50 ng carbon) with GC-irm-MS at the GFZ Potsdam, Germany. The GC (7890N Agilent) equipped with Ultra1 column (50 m x 0.2 mm diameter, 0.33 μm film thickness) was connected to a DeltaVPlus isotope ratio mass spectrometer through a modified GC-Isolink interface. The sample was separated chromatographically with a temperature program that started with an oven temperature of 80° C, which was held for 3 min, ramped to 250° C with 3° C per min and then ramped to 320° C with 5° C per min and finally reached temperature of 325° C with a ramp of 1°C per min and held for 15 min. The organic substances of the GC effluent stream were oxidised to CO_2 in the combustion furnace held at 940° C on a CuO/Ni/Pt catalyst. Samples were measured in duplicate and the standard deviation was ≤0.5‰. The quality of the isotope measurements was checked regularly by measuring different n-alkane standards with known isotopic composition (provided by Campro Scientific, Germany and Arndt Schimmelmann, Indiana University, USA).

7.2.4 DIATOM ANALYSIS AND TRANSFER FUNCTION

We selected a set of 70 depths across the core for diatom analysis. The procedure was made at the University of Concepción, Chile, and Colgate University, USA. Between 20-120 mg of freeze-dried sediment samples were treated with hydrogen peroxide and sodium pyrophosphate to remove the organic material and clays, respectively. To prepare the permanent slides and promoting an even distribution of settled particles, the treated samples were settled in B-Ker2 settling chambers for six hours (Scherer, 1994; Warnock and Scherer, 2014). Once the samples were dry, the slides were mounted with Nortland mounting medium (refraction index=1.56). The diatom valves were counted per slide using an Axioscop 2 Plus and Olympus BX60 at a magnification of x1000 following the procedure of Schrader and Gersonde (1978). Diatoms were identified to species or species group level and, if applicable, to variety or form level following the taxonomy described by e.g., Gersonde and Zielinsky (2000), Armand and Zielinski (2001), Crosta et al. (2004), Armand et al. (2005), Crosta et al. (2005), Romero et al. (2005), Esper et al. (2010), Esper and Gersonde (2014a, 2014b). We performed two sets of counting, including *Chaetoceros* resting spores and without *Chaetoceros* resting spores. For each count, at least 400 intact diatom valves were counted along random transects on the slides.

For estimation of winter sea ice (WSI) concentrations we applied the transfer function MAT-D274/28/4an which comprises 274 reference samples with 28 diatom taxa/taxa groups and

considers an average of 4 analogues (Esper and Gersonde, 2014a). The analogues refer to surface sediments from the Atlantic, Pacific and western Indian sector of the Southern Ocean. The WSI renders the sea-ice concentrations in a 1° by 1° grid for the September average of the time frame 1981 to 2010 (National Oceanic and Atmospheric Administrations, NOAA; Reynolds et al., 2002, 2007). The threshold of an open ocean to sea ice covered area is set on 15% of sea ice concentration (Zwally et al., 2002) and the average sea ice edge is defined at 40% (Gersonde et al., 2005; Gloersen et al., 1993). The qualitative estimation of sea ice concentration was derived by the abundance pattern of diatom sea-ice indicators (Gersonde and Zielinski, 2000). The estimation of summer sea surface temperature (SSST) came from the transfer function IKM-D336/29/3q comprising 336 reference samples (Pacific, Atlantic and Indian Southern Ocean) with 29 diatom taxa and three factors (Esper and Gersonde, 2014b). The calculations were done with the software R (R Core Team, 2017) using the packages Vegan (Oksanen et al., 2012) and Analogue (Simpson and Oksanen, 2012).

7.2.5 ADDITIONAL DATA

We used a clay/silt ratio from Chilean fjord sediments (Lamy et al., 2010) as a paleo record of SWWs core strength and a sand record from El Junco (Conroy et al., 2008) as an record of ENSO variability. We further considered the sea salt sodium concentration ($ssNa^+$) from the EPICA Dronning Maud Land ice core (EDML, Augustin et al., 2004) and WAIS Divide ice core (WAIS Divide Project Members et al., 2015).

7.3 RESULTS

The biomarker results from piston core PS97/072-1 presented in this study are summarized in Figure 7.3 (additional data in Figure Appendix 21, Tables Appendix 20 and 22). The concentrations of $IPSO_{25}$ range from 0.1 to 31.5 μg g^{-1} TOC, and concentrations above 10 μg g^{-1} TOC only appear from 16.4 ka to 11.9 ka BP. $IPSO_{25}$ is absent before 16.4 ka BP and rises rapidly to maximum values at 15.5 ka BP. Subsequently, concentrations decrease substantiallyuntil 9 ka BP and then remain on a level of average ~4 μg g^{-1} TOC with a slightly decreasing trend and smaller peaks at 6 ka and 2.4 ka BP. Stable carbon isotopes $\delta^{13}C$ of $IPSO_{25}$ vary between -15.1‰ and -19.5‰ supporting its origin from sea ice (Table Appendix 22; Massé et al., 2011; Sinninghe Damsté et al., 2007). Concentrations of HBI trienes are generally lower than $IPSO_{25}$ (Z-trienes 0.1-6.6 μg g^{-1} TOC, Figure 7.3; E-Trienes 0.1-2.5 μg g^{-1} TOC, Figure Appendix 21). They are largely absent until 15.5 ka BP and show high concentrations after 9 ka BP with high fluctuations from 7 ka to 5 ka BP and from 3 ka BP to present. Sterols appear after 15.9 ka BP (brassicasterol 0.3 to 70.5 μg g^{-1} TOC, Figure 7.3; dinosterol 0.1 to 20.4 μg g^{-1} TOC, Figure Appendix 21) with distinct peaks at 7.5 ka BP

and from 4 ka to 3 ka BP and minima at 13 ka, 6 ka and after 2 ka BP. The general trends of both phytoplankton biomarker show higher concentrations after 9 ka BP and lower at 1 ka BP. All $PIPSO_{25}$ sea ice indices range between 0 and 1, where highest values appear in the first half of the record and lowest values between 6.7 ka BP and 5.5 ka BP and around 0.4 ka BP (Figure 7.3). Generally, biomarker concentrations ins samples older than 16.4 ka BP are close to the detection limit or absent. We suggest that they represent artefacts from sediment drift and do not refer to them as indicators of an open marine surface at the core site (Smith et al., 2019).

Ice indicating species such as *Fragilariopsis curta* and *Fragilariopsis cylindrus* (Buffen et al., 2007; Pike et al., 2008) are most abundant before 10.8 ka BP and open marine indicating species like *Thalassiosira lentiginosa* and *Fragilariopsis kerguelensis* (Esper et al., 2010) show high values since 9 ka BP (Figure Appendix 23, Table Appendix 24). The estimations of winter sea ice cover (WSI)

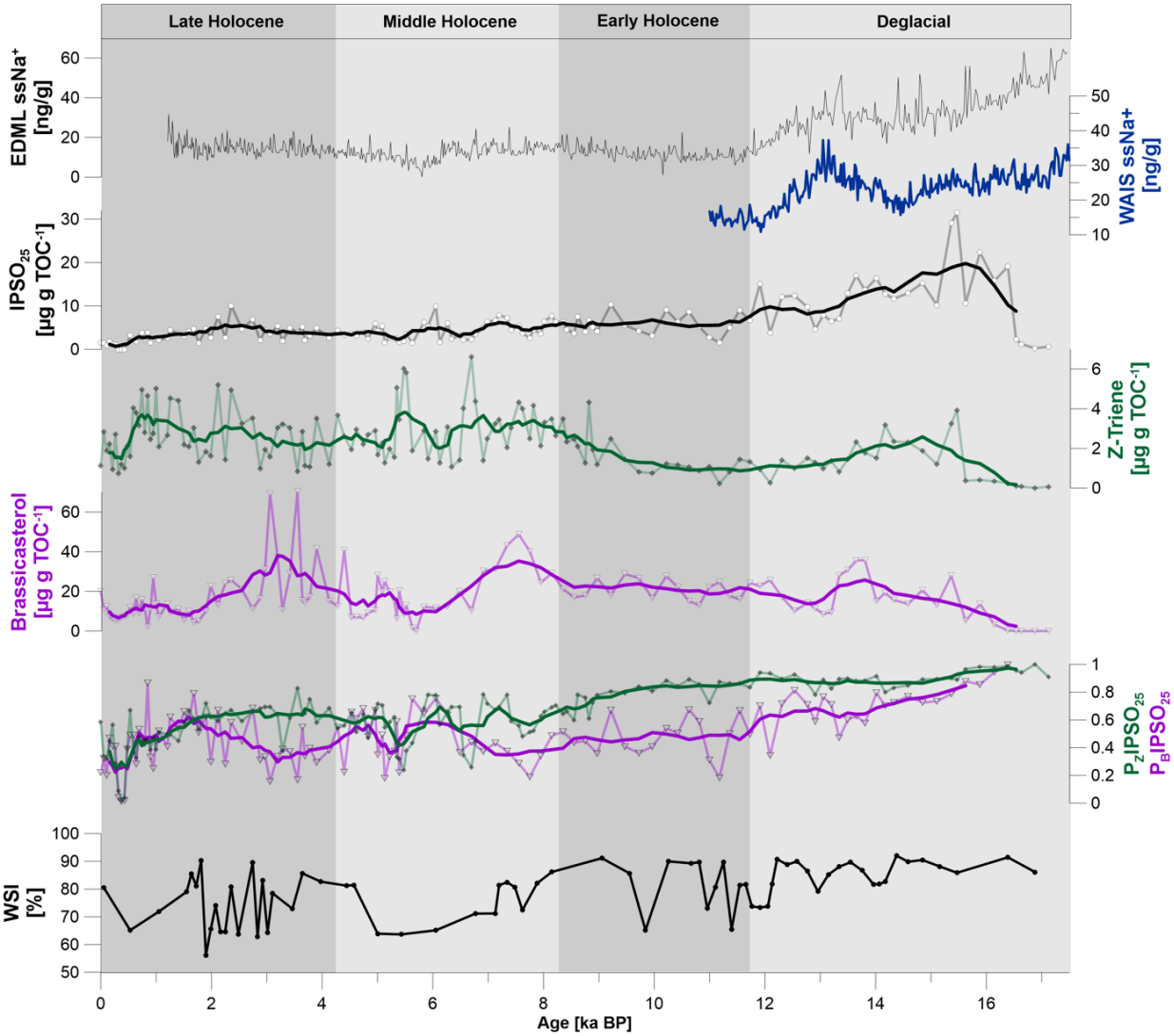

Figure 7.3 Overview of the biomarker composition in comparison with sea salt sodium concentrations from the EDML ice core (EPICA Community Members et al., 2004) and WAIS ice core (WAIS Divide Project Members et al., 2015) (from top to bottom), concentrations of $IPSO_{25}$, HBI Z-triene, brassicasterol and the sea ice indices P_ZIPSO_{25}, P_BIPSO_{25}, and diatom-derived winter sea ice (WSI) (running means based on seven points).

based on diatom assemblages are constantly high between 56-92% with some single minima at 11.4 ka, 9.8 ka, and longer minima between 7 ka and 5 ka and 3 ka and 2 ka BP (Figure 7.3). Estimated summer sea surface temperatures (SSST) range from -2.2°C to 1.6°C with a slightly increasing trend and distinct cold phases around 12 ka, 10.7 ka, 7.5 ka, and 2.7 ka BP (Figure 7.4).

SOT^{TEX} from GDGTs cover a temperature range of 5.4° C (absolute temperatures from -1.4°C to 4.0°C) and show highest values before 10 ka BP with lower temperatures at 12.8 ka, 7.8 ka and 3 ka BP, and warmer phases in between (Figure 7.4). SOT^{OH} exhibit a smaller range of 0.7° C

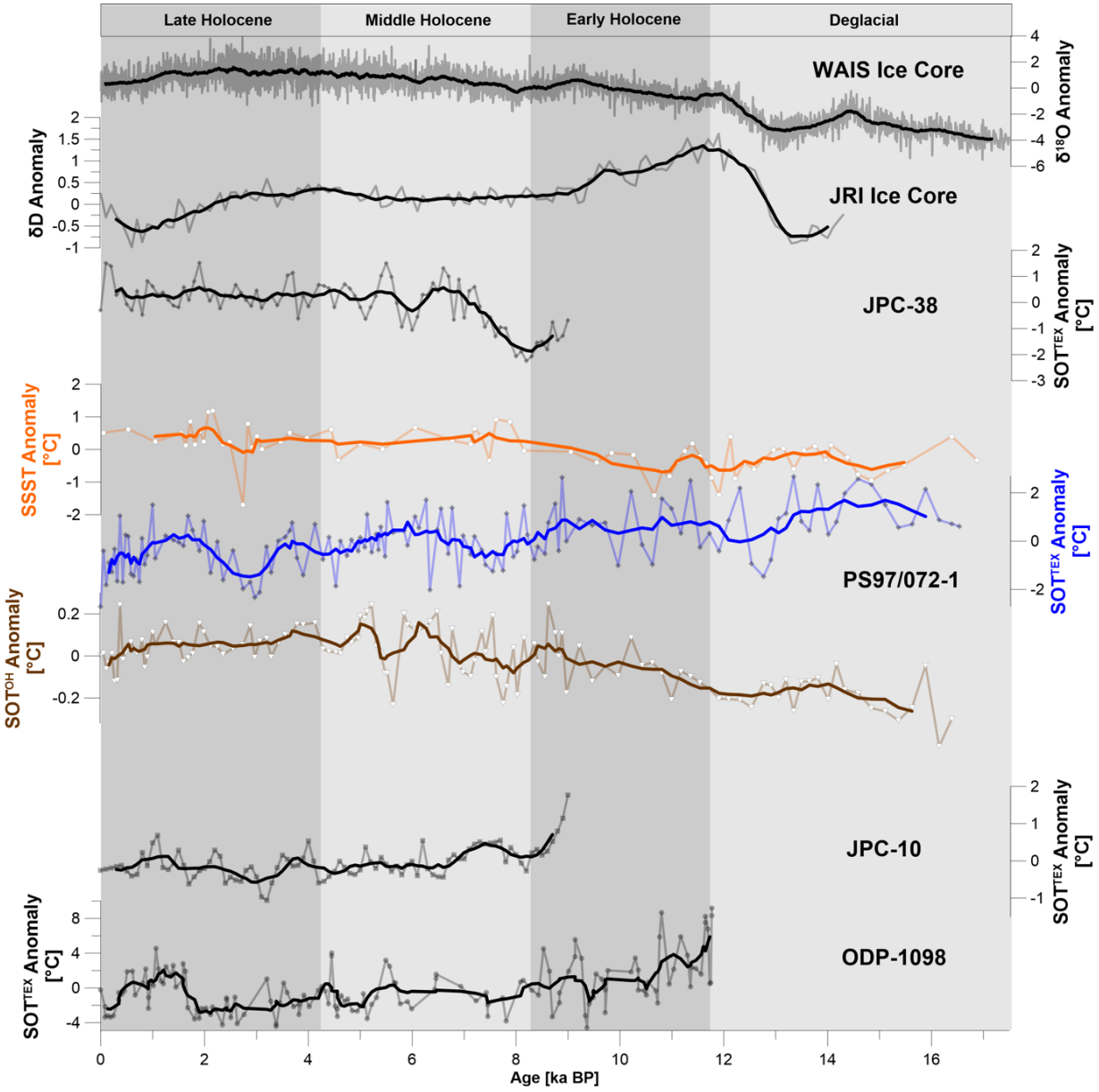

Figure 7.4 Comparison of temperature anomalies at the AP between (from top to bottom) atmospheric temperatures from stable isotope records from the WAIS ice core ($\delta^{18}O$, WAIS Divide Project Members et al., 2015), the James Ross Ice core (δD, Mulvaney et al., 2012) and several marine records: temperature anomalies of subsurface ocean temperatures at the EAP (JPC-38, Etourneau et al., 2019), at the northern WAP from our sediment core PS97/072-1 (diatom derived SSST, SOT^{TEX} and SOT^{OH}) and from two cores at the southern WAP, JPC-10 (Etourneau et al., 2013) and ODP-1098 (Shevenell et al., 2011). Core position can be found in Figure 1. All SOT^{TEX} was calibrated after Kim et al. (2010) (running means based on seven points).

(absolute temperatures -1.9°C to -1.2°C) and display an opposite trend of rising temperatures until 8.6 ka BP and a slight cooling after 5 ka BP (Figure 7.4). In comparison to other temperature records at the WAP, the values of SOT^{TEX} are significantly high and indicate temperatures about +3.9°C during the deglacial time. Also, SOT^{TEX} runs contrary to SOT^{OH} in some parts. We hence treat this record with caution and consider that temperatures from GDGTs and hydroxylated GDGTs might have different sensitivities to environmental conditions (see discussion in Park et al., 2019) and might not reflect absolute but rather relative temperature changes. We therefore only use temperature anomalies for our discussion.

The content of TOC shows a generally rising trend from very low values of 0.1 wt% at 16.8 ka BP to a stable high level of ~0.8 wt% since 11 ka BP with single peaks and lows (Figure Appendix 21, Table Appendix 20). Biogenic opal shows a similar pattern rising from 3.2 wt% at 15.6 ka BP to a maximum of 54.4 wt% at 5.5 ka BP (Figure Appendix 21, Table Appendix 20). All results from stable carbon isotopes of TOC ($\delta^{13}C$ from -22.2 to -25.5‰), the C/N ratio (<8.5) and the BIT

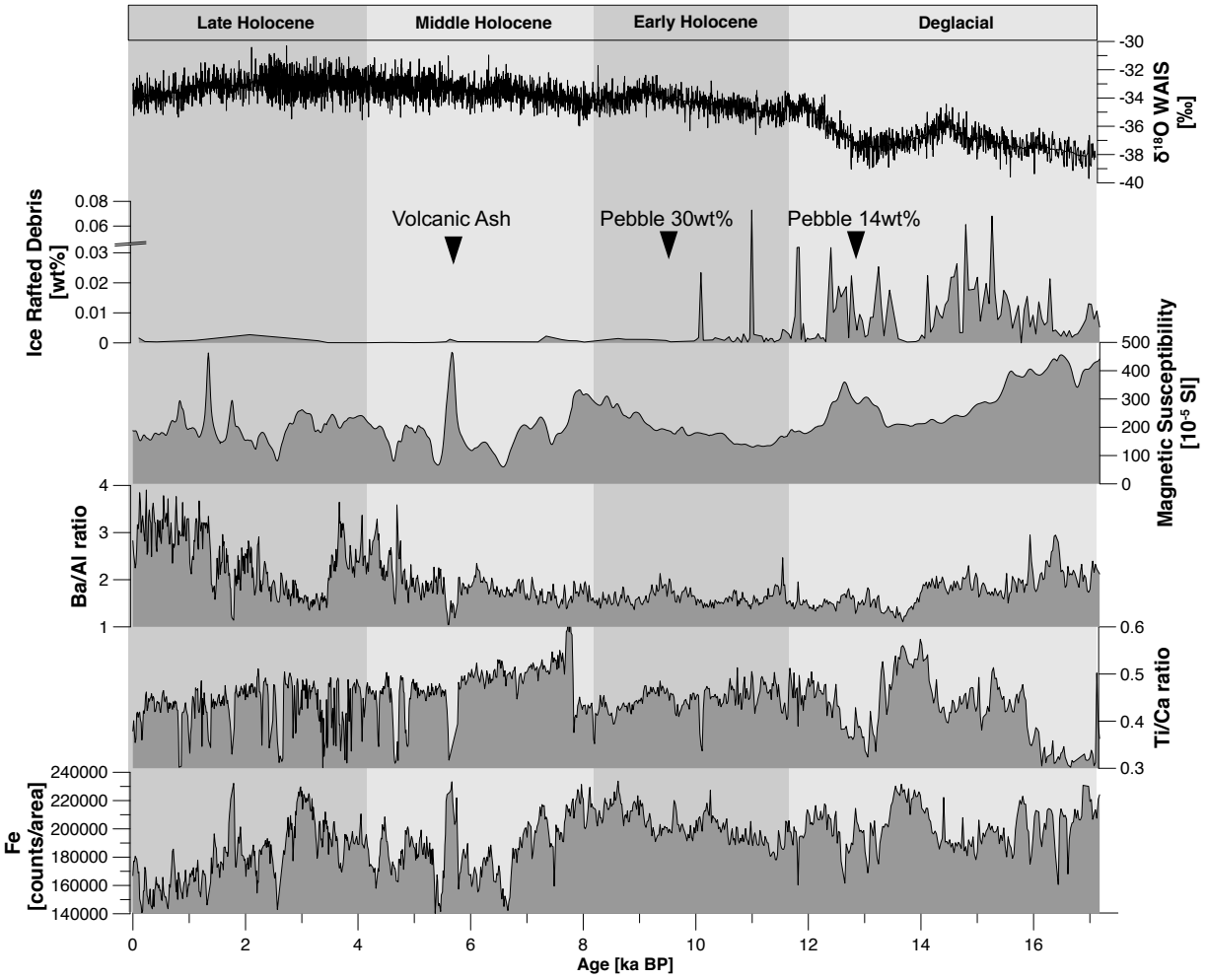

Figure 7.5 Stable isotope records from the WAIS ice core ($\delta^{18}O$, WAIS Divide Project Members et al., 2015) with selected sedimentological data from core PS97/072-1 showing (from top to bottom) ice rafted debris (IRD), magnetic susceptibility, Ba/Al, Ti/Ca and iron (Fe). The appearance of volcanic ash corresponds to a tephra layer found in the western Bransfield Basin at 5.5 ka BP (Heroy et al., 2008).

index (<0.05) point to a predominance of marine organic matter in the sediment core (Hopmans et al., 2004) (Table Appendix 20).

The magnetic susceptibility shows generally higher values before 8 ka BP (Figure 7.5, Table Appendix 25). In this period, IRD and larger single pebbles appear frequently, especially between 16.2 ka and 10 ka BP, with highest amounts from 15.8 ka to 14.6 ka, and 13.6 ka to 12.4 ka BP (Figure 7.5, Table Appendix 25). From the XRF data we selected Fe as an indicator of terrigenous and aeolian dust input (Hepp et al., 2006; Lamy et al., 2004), Ti/Ca for influx of IRD and deglacial melt water discharge (Soulet et al., 2011), and Ba/Al for export production (Hillenbrand et al., 2009) (Figure 7.5, Table Appendix 25). We did not consider Al alone since it may be biased by uptake and accumulation from diatoms (van Bennekom et al., 1989; Moran and Moore, 1992). The counts of Fe are generally higher before 7 ka BP and lower afterwards with several maxima and minima. The ratio of Ti/Ca is lower in the period of 13.2 ka BP and 8.0 ka BP and shows high level counts afterwards with frequently short minima. The ratio of Ba/Al is low until 5.5 ka BP and from 3.5 ka to 2.3 ka BP, while the counts are generally high during the period of 5.5 ka BP to 3.5 ka BP and after 2.3 ka BP. Sedimentation rates are low (38-60cm/ka, mean 48cm/ka) before 5.5 ka BP and thereafter distinctively higher until today (53-93cm/ka, mean 83cm/ka)(Figure 7.2, Table Appendix 20).

7.4 DISCUSSION

7.4.1 EVALUATION OF ORGANIC BIOMARKERS WITH RESPECT TO ATMOSPHERIC SEA SALT DEPOSITIONS

Sea salt sodium aerosols ($ssNa^+$) originate from sea ice formation and sea ice cover around Antarctica (Wolff et al., 2003) and were successfully linked to sea ice reconstructions from marine diatom records (Mezgec et al., 2017). The concentrations of $ssNa^+$ of the EDML ice core are positively related with winter sea ice in the Weddell Sea (Rahaman et al., 2016), while those of the WAIS Divide ice core reflect the sea ice extent in the Ross and Amundsen Sea (WAIS Divide Project Members et al., 2013) and we use both records to evaluate the information on sea ice conditions deduced from biomarkers in core PS97/072-1. Figure 7.3 displays $ssNa^+$ together with $IPSO_{25}$ and both $PIPSO_{25}$ sea ice indices. Together with WSI, all sea ice indicators follow a similar pattern and indicate high sea ice cover before 12 ka BP and lower sea ice cover afterwards. Comparison with $ssNa^+$ from the EDML ice core for the past 17 ka BP reveals a positive correlation with WSI and a weaker correspondence with $IPSO_{25}$ and brassicasterol (Figure Appendix 26). Also, WSI corresponds very well with $IPSO_{25}$, both $PIPSO_{25}$ and correlates negatively with HBI Z-trienes (Figure Appendix 26). Based on this, we suggest that the organic biomarker lipids preserved at site PS97/072-1 and $PIPSO_{25}$ indices as well as WSI approximately reflect sea ice dynamics around the AP. As the correlation between WSI and P_ZIPSO_{25} is highest,

we suggest that P_ZIPSO_{25} seems to be affected by diatom production dynamics in relation to winter sea ice. This is supported by the observation that the HBI Z-triene is more negatively correlated to the presence of sea ice (than brassicasterol concentrations), which may point to a lower tolerance of HBI triene source organisms to sea ice cover. We hence suggest, that the distribution pattern of HBI trienes and sterols in relation to sea ice may have an impact on the significance of the $PIPSO_{25}$ index. In sediment surface studies from Smik et al. (2016) and Vorrath et al. (2019), HBI Z-trienes where found in the marginal sea ice zone and also remote from sea ice edges, while brassicasterol concentrations were highest in areas of stable sea ice edges and/or seasonal sea ice. In general, brassicasterol is found under various ocean conditions due to the numerous source organisms that are adapted to different environments (Volkman, 1986). When HBI Z-triene concentrations are generally higher in sea ice remote areas, P_ZIPSO_{25} might be more sensitive to changes in distal (or less ice covered) ocean areas, while P_BIPSO_{25} seems to better suited to reflect conditions in frequently ice-covered or ice marginal settings.

Temperature estimations and biomarker data reveal a good agreement of low SOT^{OH} and SSST to high $IPSO_{25}$, both $PIPSO_{25}$ and WSI values and also high SOT^{OH} and SSST to high HBI Z-triene concentrations (Figure Appendix 27). For SOT^{TEX} the correlations are inverse (high temperatures correspond to higher sea ice estimations) which let us suppose that SOT^{OH} and SSST may better resolve cold/ice-rich and warm/ice-low conditions (Figure Appendix 27).

7.4.2 UNIT 1: THE DEGLACIATION AND ANTARCTIC COLD REVERSAL FROM 17.2 KA TO 11.7 KA BP

In the oldest part of our sediment record from 17.2 ka until 11.7 ka BP (1012-788 cm below sea floor, bsf) we observe drastic environmental changes indicated by biomarker and sedimentary records. Before 16.4 ka BP the low concentrations of biomarkers, TOC and biogenic opal suggest that open marine and also sea ice associated production was diminished. The high counts of iron and magnetic susceptibility refer to a coarse-grained sediment from terrigenous input and the amount of IRD is low (compared to the time afterwards) as it is described for glacial distal sediments (Smith et al., 2019)(Figure 7.5). Sea ice indices $PIPSO_{25}$ and WSI show the highest values and point towards maximum sea ice cover, while SOT^{OH} show lowest ocean temperatures in the entire record (Figure 7.3 and 7.4). The combination of both nearly absent $IPSO_{25}$ and phytoplankton biomarkers are likely to present a very thick or permanent sea ice cover (Müller et al., 2009). Lamping et al. (2020) explain this kind of biomarker composition with an sea surface covered by an ice shelf prior to the Holocene in the western Amundsen Sea. Since $IPSO_{25}$ concentrations rise steeply and peak at 15.5 ka BP we suggest that the traces of biomarkers before 16.4 ka BP are artefacts from lateral advection and that marine production was absent at the core site due to the lack of an open water surface (Smith et al., 2019). Reconstructions of grounding

lines at the WAP support this as they show that ice shelves advanced to the shelf break in the Bransfield Strait during the LGM (Bentley et al., 2014; Ó Cofaigh et al., 2014) and ice streams delivered sediment input into the Bransfield Basin (Canals et al., 2016). The core site is in a narrow basin, and the shelf breaks are located 15 km away to the north and south, so the basin likely was engulfed by the grounding line of the ice sheet during the LGM. Therefore, it is likely that the (almost complete) absence of biomarker lipids indicates the presence of the floating ice shelf canopy from the Antarctic Peninsula Ice Sheet (APIS) or permanent sea ice before 16.4 ka BP (Figure 7.6). This corresponds well to the ice shelf retreat from the outer shelf of the WAP dated to 17.5 ka BP (Heroy and Anderson, 2007) and is much earlier than the retreat around 14 ka BP at the South Shetland Islands (Milliken et al., 2009) or 13.2 ka at BP Palmer Deep at the southern WAP (Taylor and Sjunneskog, 2002). The break-up of the permanent ice (shelf) cover is reflected by the sudden rise of $IPSO_{25}$ at 16.4 ka BP and a later increase of the sterols (at 15.9 ka BP) and HBI trienes (at 15.5 ka BP) as phytoplankton markers (Figure 7.3). The elemental composition of the sediment shows a rise in the Ti/Ca ratio and IRD referring to high glacial melt water discharge between 16 ka and 15 ka BP (Figure 7.5). A short peak of Ba/Al appears parallel to the onset of $IPSO_{25}$ which may point to an increased export of marine production initiated by high sea ice algae growth (Figure 7.5). The opening of the sea surface and the ice shelf retreat continued under the presence of frequent winter and spring sea ice cover until 13.3 ka BP indicated by high $IPSO_{25}$ and low phytoplankton biomarker concentrations with high values of $PIPSO_{25}$ and WSI (Figure 7.3). Simultaneously a gradual warming is displayed by SOT^{OH} (Figure 7.4). It is noteworthy that TOC and biogenic opal concentrations remained low indicating reduced marine productivity at the sea ice edge, while the export production was elevated. We hence conclude that sea ice cover must have been dominant in this area and suppressed primary production after the ocean opening, while the growth of sea ice algae was favored (Figure 7.6).

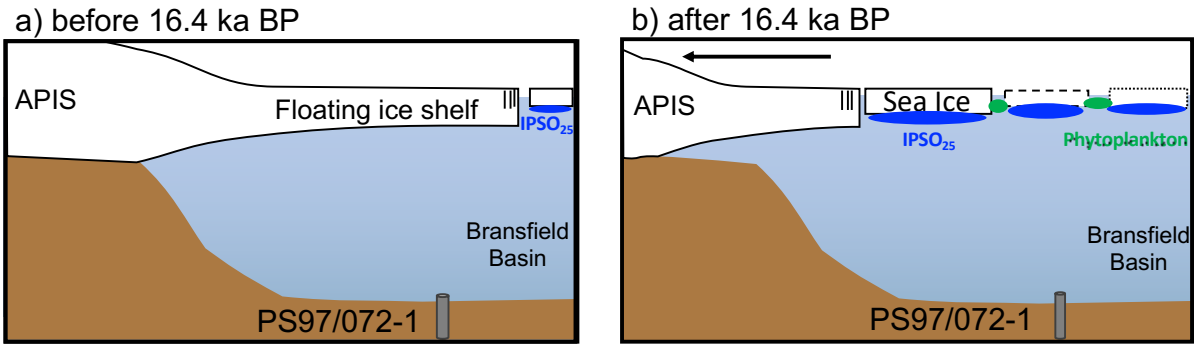

Figure 7.6 Illustration of the sea ice conditions at the core site in the Bransfield Strait with a) a closed ocean surface before 16.4 ka BP by a floating ice shelf and b) the opening of the ocean after 16.4. ka BP by a retreat of the Antarctic Peninsula Ice Sheet (APIS) and the dominance of sea ice cover allowing the production of $IPSO_{25}$ and smaller production of phytoplankton marker at the core site.

While the Antarctic Cold Reversal (ACR) lasts from 14.7 ka to 13 ka BP (Pedro et al., 2016) a delayed Oceanic Cold Reversal occurs 800 a later in the Southern Indian Ocean and is recorded by several ice cores (Stenni et al., 2001). Our sediment record shows a maximum response to a cooling from 13.2 ka to 12.4 ka BP. The onset of the cooling takes place within 100 years, from 13.3 ka to 13.2 ka BP, shown by a steep drop of melt water discharge (Ti/Ca) and terrigenous input indicated by iron, while a decrease in marine production in observed since 14 ka BP (Figure 7.5). Also, the magnetic susceptibility rises suddenly and higher amounts of IRD and single bigger pebbles are recorded. The ACR is reflected in our records between 13.5 ka to 12.4 ka BP – similar to marine and atmospheric records from previous studies (Blunier and Brook, 2001; Jouzel et al., 1995; WAIS Divide Project Members et al., 2015; Xiao et al., 2016b). During this time the ice sheet retreat paused and primary production was diminished by cold temperatures that are only indicated by SOT^{TEX} in our record (Figure 7.4). $IPSO_{25}$ increases during this time and $PIPSO_{25}$ and WSI remain on high levels, revealing high and variable winter and spring sea ice similar to the time directly after the ice shelf retreat around 16.4 ka BP (Figure 7.3). At this time the ice shelf must have been retreated so far that another closing of the sea surface with permanent ice did not occur at the core site despite low temperatures. Right after the ACR the warming trend at the WAP continues, which is also apparent in other records (Denton et al., 2010; Domack et al., 2001; Shevenell et al., 2011; WAIS Divide Project Members et al., 2015; Xiao et al., 2016b). Shorter spring sea ice season are indicated by moderate P_BIPSO_{25} values and a fast continuation of meltwater discharge and IRD delivery is reflected in the elemental records. The warm reversal and sea ice decrease may have been an expression of the inter-hemispheric teleconnections through a global reorganization of atmospheric and ocean circulation that is related to a bipolar seesaw pattern of opposite climate trends between northern and southern hemispheres (Anderson et al., 2009; Broecker, 1998; EPICA Community Members et al., 2006; Pedro et al., 2016). With cooling of the northern hemisphere, a southward shift of the Intertropical Convergence Zone and the southern hemisphere westerlies (Lamy et al., 2007) resulted in intensified wind stress in the Drake Passage (Timmermann et al., 2007) and increased upwelling that may have driven the continued warming and sea ice retreat in Antarctica towards the Holocene (Anderson et al., 2009).

7.4.3 UNIT 2: EARLY HOLOCENE WARM OPTIMUM FROM 11.7 KA TO 8.2 KA BP

Unit 2 covers the Early Holocene from 11.7 ka to 8.2 ka BP (788-604 cm bsf) and is characterized by highly variable, decreasing winter and spring sea ice cover as shown by lower WSI and P_BIPSO_{25} values. A higher primary production is indicated by the constantly rising concentrations of HBI Z-triene and brassicasterol (Figure 7.3) and high contents of biogenic opal (Figure Appendix 21). Rising counts of iron and rising magnetic susceptibility point to an enhanced terrigenous input due

to continued melting of the Antarctic ice sheet, while the increasing distance to the retreating grounding line is reflected in a decrease of IRD in the distal, glacimarine sediments (Evans and Pudsey, 2002) (Figure 7.5). $IPSO_{25}$ concentrations declined to ca. 4 µg g^{-1} TOC and remained at this level until the present; a similar pattern is noted for sea ice related diatoms (Figure 7.3, Figure Appendix 23). An oceanic warming is indicated by SOT^{OH} and SSST, while SOT^{TEX} rather shows fluctuating temperatures without a clear trend (Figure 7.4). We suggest SOT^{TEX} to be more sensitive to short term temperature changes at the sea surface, while SOT^{OH} and SSST are more suitable to indicate long term trends.

Both WSI and P_BIPSO_{25} suggest a highly variable sea ice cover with few distinct sea ice minima at 11.3 ka and 9.8 ka BP, while P_ZIPSO_{25} indicates stable sea ice conditions with an accelerating declining trend (Figure 7.3). We interpret this as a sign of prolonged sea ice seasons with stable sea ice edges during spring and generally short summers with a gradual sea ice decline and warming towards the Middle Holocene (Figure 7.7).

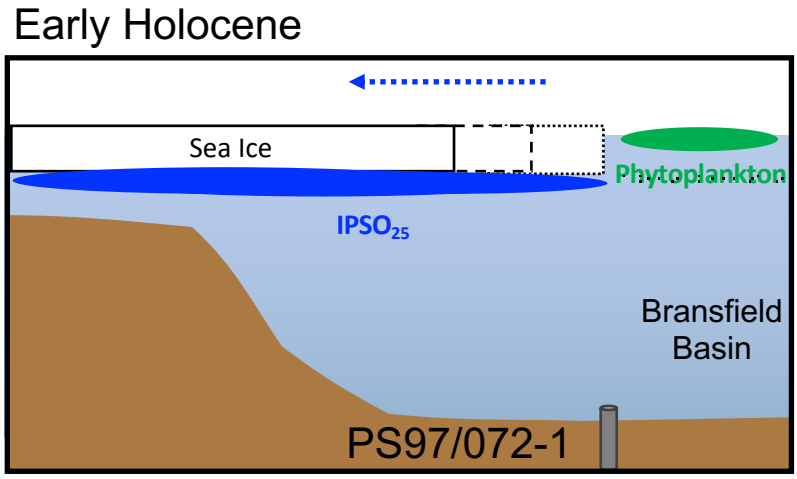

Figure 7.7 Illustration of the stable spring sea ice edge at the core site during the Earl Holocene and the gradual sea ice decline towards the Middle Holocene.

Sea ice minima may have resulted from punctual warming events e.g. at 11.3 ka BP, when SSST and SOT^{TEX} show a short temperature peak (Figure 7.4), and suggest that winter and spring sea ice were significantly diminished at this time. The continuous decrease in P_ZISPO_{25} values may reveal the transition from short to longer ice-diminished summer seasons, while P_BIPSO_{25} implies a decrease of stable spring sea ice edge conditions in response to short term changes in winter sea ice. Between 15 ka and 10 ka BP the ice sheets at the AP retreated almost to their present configuration (Bentley et al., 2014) which may have diminished the impact of melt water on our core site. Hence, sea ice melting may have become the main contributor of nutrients and dominant driver of marine productivity. Therefore, we suggest warm, stratified surface waters with moderate production in summer. This corresponds to suggestions of long sea ice seasons with stable sea ice edges in the western Bransfield Basin (Heroy et al., 2008) but less to other studies suggesting warm and sea ice reduced open marine conditions at the southern WAP (Etourneau et al., 2013; Milliken

et al., 2009). Temperature records from the Palmer Deep sediment core ODP-1098 indicate a distinct cooling during this period, which is opposite to our records (Figure 7.4, Shevenell et al., 2011). In comparison to atmospheric temperature records we see our marine record corresponding to the overall slight warming trend of the remote WAIS Divide ice core but opposite to the James Ross Ice core located close to the core site, which shows a cooling (Figure 7.4). While a paleo sea ice study from the southern WAP (Etourneau et al., 2013) points to warm and sea-ice reduced conditions, a study from the EAP (Barbara et al., 2016) reveals heavy sea ice conditions due to glacial melting during the Early Holocene. From this, we speculate that the climate development on the east and west side of the AP might have been disconnected at this time because the ice sheet on the mainland acted as a barrier between both.

At the end of the Early Holocene rising contents of phytoplankton biomarker lipids and a decline in $IPSO_{25}$ concentrations, $PIPSO_{25}$ values and diatom sea ice species point to an environmental change towards a warm and predominantly sea-ice reduced WAP. Nevertheless, the transition to the Middle Holocene is marked by a short cooling evident in SOT^{TEX} and SOT^{OH} which is also observed in marine sediments at the EAP (JPC-38, Etourneau et al., 2019) and at the WAP (JPC-10, Etourneau et al., 2013; ODP-1098, Shevenell et al., 2011) (Figure 7.4).

7.4.4 UNIT 3: THE MIDDLE HOLOCENE FROM 8.2 KA UNTIL 4.2 KA BP

The Middle Holocene from 8.2 ka to 4.2 ka BP (604-332cm bsf) is a period of significant sea ice retreat at the core site indicated by a decreasing and low P_ZIPSO_{25} and P_BIPSO_{25} values, respectively, as well as reduced WSI (Figure 7.3) and an oceanic warming reflected in GDGT-based SOT^{OH}, interrupted by a cold event around 7.8 ka BP (Figure 7.4). Between 8.2 ka and 5.5 ka BP, moderate sedimentation rates (average 58cm/ka, Figure 7.2), the almost complete absence of IRD and decreasing terrigenous inputs are inferred from decreasing iron counts and a lower magnetic susceptibility (Figure 7.5) and linked to a temporary stabilization of the Antarctic ice sheet (Bentley et al., 2014). The rising content of organic carbon and biogenic opal in the sediment (Figure Appendix 21) as well as the increasing Ba/Al ratio (Figure 7.5) indicate an enhanced paleoproductivity. The concentrations of $IPSO_{25}$ and phytoplankton biomarkers show remarkable changes: while $IPSO_{25}$ concentrations are low and steadily decreasing, concentrations of HBI Z-triene reach highest values throughout the entire record and also brassicasterol concentrations are high and decline towards 6.0 ka BP (Figure 7.3). Together with the declining P_ZIPSO_{25} and WSI this points to a decrease of both winter and spring sea ice and potentially ice-free summers (Figure 7.8). This is in accordance with sea ice studies from the Palmer Deep, WAP, showing reduced seasonal sea ice based on the low abundances of sea ice related diatoms and high ocean temperatures (Etourneau et al., 2013). Since the ice shelf retreated between 10 ka and 5 ka BP from

the Bransfield Strait, it finally opened the passage for ACC surface waters from the west (Bentley et al., 2014; Ó Cofaigh et al., 2014). As a result, we suppose that sea ice conditions at our core site were predominantly influenced by branches of the ACC (the BSW and CDW) and inflow from the Weddell Sea was diminished due to the still grounded ice shelves at the tip of the AP. The influence from the Weddell Sea was weak and opposite sea ice conditions were reconstructed for the east AP where HBI biomarker and diatom assemblages record extended sea ice cover and increased sea ice seasonality (Barbara et al., 2016; Minzoni et al., 2015).

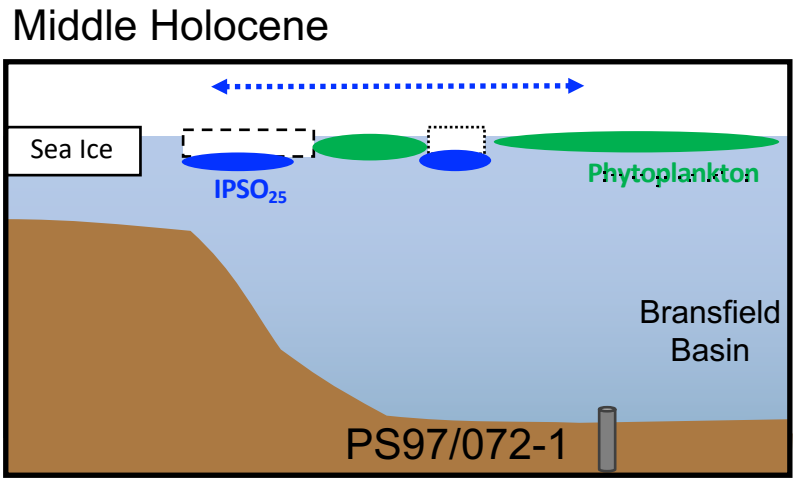

Figure 7.8 Illustration of the retreat of sea ice during the Middle Holocene with fast sea ice advance during short term cold phases.

Around 5.5 ka BP, a short but drastic environmental change is indicated by a peak in the magnetic susceptibility, the appearance of IRD and iron counts and a minimum in the Ti/Ca and Ba/Al ratio. This change might be due to a higher content of volcanic ash which could be linked to a tephra layer in a western Bransfield Basin sediment core at the same time (Heroy et al., 2008). Therefore, the minimum in all sea ice indices and SOT^{OH} might be a result from input from volcanic ash and does not interrupt the trends of sea ice or temperatures indicators (Figure 7.3 and 4).

As the Ti/Ca ratio remains high and Ba/Al rises (Figure 7.5), we speculate that sea ice retreat might have slowed down due to increased sea ice formation in response to freshwater discharge and that the presence of sea ice edges promoted (sea-ice related) diatom blooms. This is supported especially by the rise of brassicasterol reflecting marine productivity in the vicinity of sea ice edges (Figure 7.3). A high seasonal amplitude is expressed in rising winter sea ice, nutrient release by sea ice melting in spring and warm summers with highly stratified water columns, and supports the highest primary production during the Holocene. This is apparent by maximum contents of biogenic opal, TOC and enhanced export production (Figure 7.5, Figure Appendix 21).

Regarding ocean temperatures, we observe a colder period from 8.2 to 7.8 ka BP in SOT^{OH} and SOT^{TEX} with a minimum at 7.8 ka BP. A rapid warm reversal potentially lead to abrupt melt water inputs (Ti/Ca, Figure 7.5) and a steep rise in brassicasterol points to enhanced productivity (Figure 7.3). Simultaneously, a sudden rise of Ti/Ca indicates heavy meltwater discharges and water mass

changes to appear between 7.8 ka and 7.7 ka BP (Figure 7.5). The cooling was also discovered in studies on both east and west AP: at the EAP a remarkable ocean temperature minimum is reconstructed for 8.2 ka BP in near-coastal marine sediment cores around James Ross Island (Barbara et al., 2016) and at the WAP in records at the Palmer Deep in JPC-10 at 8.2 ka BP (Etourneau et al., 2013) and ODP-1098 at 7.8 ka BP (Figure 7.4; Shevenell et al., 2011). Only subtle evidence of cooling from 7.9 ka to 7.5 ka BP is found in several Antarctic ice core records (Figure 7.4; Augustin et al., 2004; Mulvaney et al., 2012; WAIS Divide Project Members et al., 2015). We suggest that local meltwater pulses due to a fast retreat of the ice shelf in the Bransfield Basin (Ó Cofaigh et al., 2014) could explain this cold event. The collapse of the ice shelf of George VI Island at 7.9 ka BP is also supposed to be linked to this event (Shevenell et al., 2011). Also, the cold event might be referred to the global cooling phenomenon at 8.2 ka BP, mainly observed in northern hemisphere records (Morrill and Jacobsen, 2005). It is possibly linked to a slowing of the Atlantic meridional overturning circulation resulting from pulsed melt water inputs associated with the drainage of proglacial lakes from the Laurentide Ice Sheet in North America (Ellison et al., 2006). Since the cold event is found at different ages in marine sediments around the AP (between 8.2 and 7.8 ka BP) it is uncertain if the regional cooling occurred simultaneous or delayed to the northern hemisphere cooling.

Between 7.5 and 4.2 ka BP the stabilized, warm Holocene optimum is evident in our data as also recorded by other sediment records at the AP (Barbara et al., 2016; Etourneau et al., 2013; Heroy et al., 2008; Minzoni et al., 2015; Shevenell et al., 2011), all over West Antarctica (Allen et al., 2010; Taylor and Sjunneskog, 2002) and also in ice core records (Figure 7.4). Temperature records around the AP, from Palmer Deep to the EAP (Figure 7.4), show mostly stable, uniform warm conditions over this period. The absence of IRD refers to a retreat of ice shelves at the AP nearly to their present state (Allen et al., 2010; Ó Cofaigh et al., 2014) (Figure 7.5) and higher sedimentation rates after 5.5 ka BP (mean 86cm/ka) are driven by higher downward particle flux from remarkably high marine productivity (Figure 7.3, Figure Appendix 21).

During the Middle Holocene, we suggest that highly variable environmental conditions promoted open marine productivity during warm phases and diminished it during cold phases (Figure 7.8). In cold phases, the growth of sea ice diatoms was also reduced under thicker sea ice, with less nutrient release from reduced sea ice melting and less abundance of sea ice edge conditions. So, although short-term heavy sea ice increases might have occurred, this is recorded differently by biomarkers compared to slowly changing or stable sea ice conditions as we observed during the deglaciation. High production pulses of open marine biomarkers during warm times may have masked signals from short and heavy sea ice cover. An overprinting of $IPSO_{25}$ and the $PIPSO_{25}$

indices due to short-term changing sea ice conditions was already observed and is an important limiting factor for HBI-based sea ice studies (Part II, chapter 6). However, the overall trend of a Middle Holocene warming and sea ice decrease evident in many records (Barbara et al., 2016; Etourneau et al., 2013; Heroy et al., 2008; Shevenell et al., 2011) is also resolved by our organic biomarker records. Melt water pulses from the AP ice sheet likely promoted open marine diatom growth in higher stratified water columns (Taylor and Sjunneskog, 2002) as we also see in high HBI Z-triene and TOC content.

7.4.5 UNIT 4: LATE HOLOCENE AND NEOGLACIAL FROM 4.2 KA BP UNTIL TODAY

The Late Holocene from 4.2 ka BP until today (332-0 cm bsf) is also often associated with the Neoglacial with advancing glaciers due to large-scale cooling (Bárcena et al., 2006). It is characterized by a general atmospheric cooling recorded in ice cores but also evident in SOT^{TEX} and SOT^{OH} from our sediment core (Figure 7.4). There are two periods of profound cooling in SSST and SOT^{TEX} around 3 ka and in SOT^{TEX} and SOT^{OH} at 0.5 ka BP and a short warming around 2 ka BP (Figure 7.4). However, the temperature patterns in the Late Holocene are very variable and the cooling is linked to persistent, increased sea ice cover present in many records at the AP (Allen et al., 2010; Barbara et al., 2016; Bárcena et al., 1998; Bentley et al., 2009; Etourneau et al., 2013; Shevenell et al., 2011)(Figure 7.4). Since 4.2 ka BP, the content of iron and IRD decreases with lower glacial melt water input and the rising Ba/Al ratio points to higher marine productivity (Figure 7.5). From 3 ka to 1 ka BP, high P_ZIPSO_{25} values contrast low P_BISPO_{25} and WSI values (Figure 7.3). Here, we suggest a sea ice advance with moderate winter sea ice cover with a rapid retreat in spring and ice-reduced, cool summer seasons which diminish marine production at the sea ice edge but promote open marine summer diatom growth causing higher concentrations of HBI Z-triene in the sediment record (Figure 7.9).

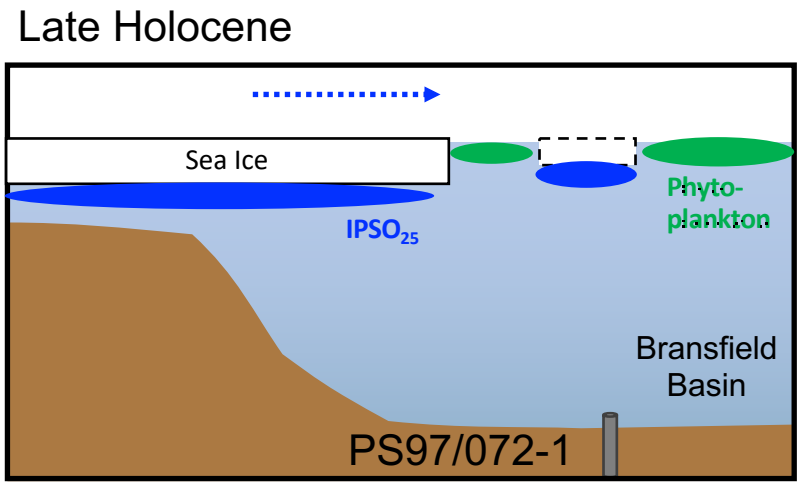

Figure 7.9 Illustration of the Late Holocene sea ice advance and higher production of phytoplankton marker due to open marine summer diatom blooms.

After 1 ka BP, the $PIPSO_{25}$ indices and WSI show highest variabilities and finally point to a significantly decreased sea ice cover at 0.4 ka BP (Figure 7.3) when $IPSO_{25}$ is at the detection limit

during the Little Ice Age (Bentley et al., 2009; Sjunneskog and Taylor, 2002; Taylor and Sjunneskog, 2002). Similar to our observation for the deglacial, the observation of low phytoplankton biomarker and minimum $IPSO_{25}$ concentrations may point to perennial cold conditions and the establishment of thick and/or compacted sea ice limiting the productivity of both phytoplankton and also sea ice diatoms.

An influence of warming due to anthropogenic forcing is not present in our sediment records because ocean warming at this core site was found to be detectable only since 1990 (Part II, chapter 6) and is not resolved in our data.

7.4.6 ATMOSPHERE-OCEAN INTERACTIONS AND GLOBAL CIRCULATION PATTERNS

The large-scale circulation patterns ENSO and SAM influence the transport of heat on both sides of the AP differently (Stammerjohn et al., 2008b). As the core site is located at the tip of the AP, we suggest it to be sensitive to changes in oceanographic current patterns transporting BSW and WSW, both driven by atmospheric pressure cells. Studies for the industrial era suggest that both an El Niño (+ENSO) or a positive SAM (+SAM) lead to cold and ice-rich conditions at the WAP, while La Niña events (-ENSO) or a negative SAM (-SAM) lead to warm and ice-reduced states (Clem et al., 2016; Ding et al., 2012; Marshall et al., 2006; Stammerjohn et al., 2008b, 2008a; Yuan, 2004). A combination of both circulation patterns has been observed to have different and much higher impacts especially during the spring season: when they are "in-phase", that means +ENSO/-SAM, environmental conditions are more likely cold with an extended sea ice. The opposite in-phase pattern, -ENSO/+SAM is referred to warm and ice-reduced conditions (Clem et al., 2016; Marshall et al., 2006; Stammerjohn et al., 2008b; Yuan, 2004). Out-of-phase events (+ENSO/+SAM or -ENSO/-SAM) seem to not have any significant influence (Clem and Fogt, 2013).

The paleo record of ENSO variability (El Junco Sand; Conroy et al., 2008) shows two peaks at 9 ka and 6 ka BP and high fluctuations from 4 ka BP to today (Figure 7.10). This pattern is also observed in other ENSO reconstructions (e.g. Chen et al., 2016; Gomez et al., 2012; Menking and Anderson, 2003). An overall relation of the ENSO variability to our $IPSO_{25}$ or $PIPSO_{25}$ could not be observed. Therefore, it is not clear whether a high or low ENSO variability leads to changes in regional sea ice trends. However, we note that $IPSO_{25}$ concentrations rise coincident with rapid peaks in ENSO variability at 9 ka, 6 ka, and around 2 ka BP. At 2 ka BP, $PIPSO_{25}$ and WSI increase as well. Studies from Etourneau et al. (2013) and Shevenell et al. (2011) suggest a link between high ENSO variability with warm SST (due to upwelling of UCDW) and enhanced sea ice cover from higher seasonal amplitudes at Palmer Deep. Our records point to highly variable sea ice conditions and warm temperatures at 2 ka BP when ENSO variability is strongest. Since there is hardly any

statistical correlation between ENSO and any of our other records during the Holocene, we are not able to identify an impact of ENSO variability on climate conditions at the core site (Figure Appendix 28).

The paleo record of the SWWs (clay/silt ratio from Chilean fjord sediments, Lamy et al., 2010) reflects the strength of the wind belt core in the Pacific Southern Ocean (Figure 7.10). Weak SWWs are associated with the northward expansion of the wind belt, typical for the austral winter, while strong SWWs reflect a contraction and southward shift of the wind belt. In the Early Holocene the strength of SWWs is highest, while it is moderate during the Middle Holocene and weak in the Late Holocene. In our data we find strong positive correlations of SWW strength with both $PIPSO_{25}$ indices, $IPSO_{25}$ concentrations, WSI and SOT^{TEX} (in decending order)(Figure Appendix 28). Strong negative correlations are seen between SWW strength and SOT^{OH}, SSST and HBI Z-triene concentrations. Hence, we suggest a relationship between SWWs, ocean temperature and sea ice conditions, where strong SWWs promote sea ice cover and $IPSO_{25}$ production under a

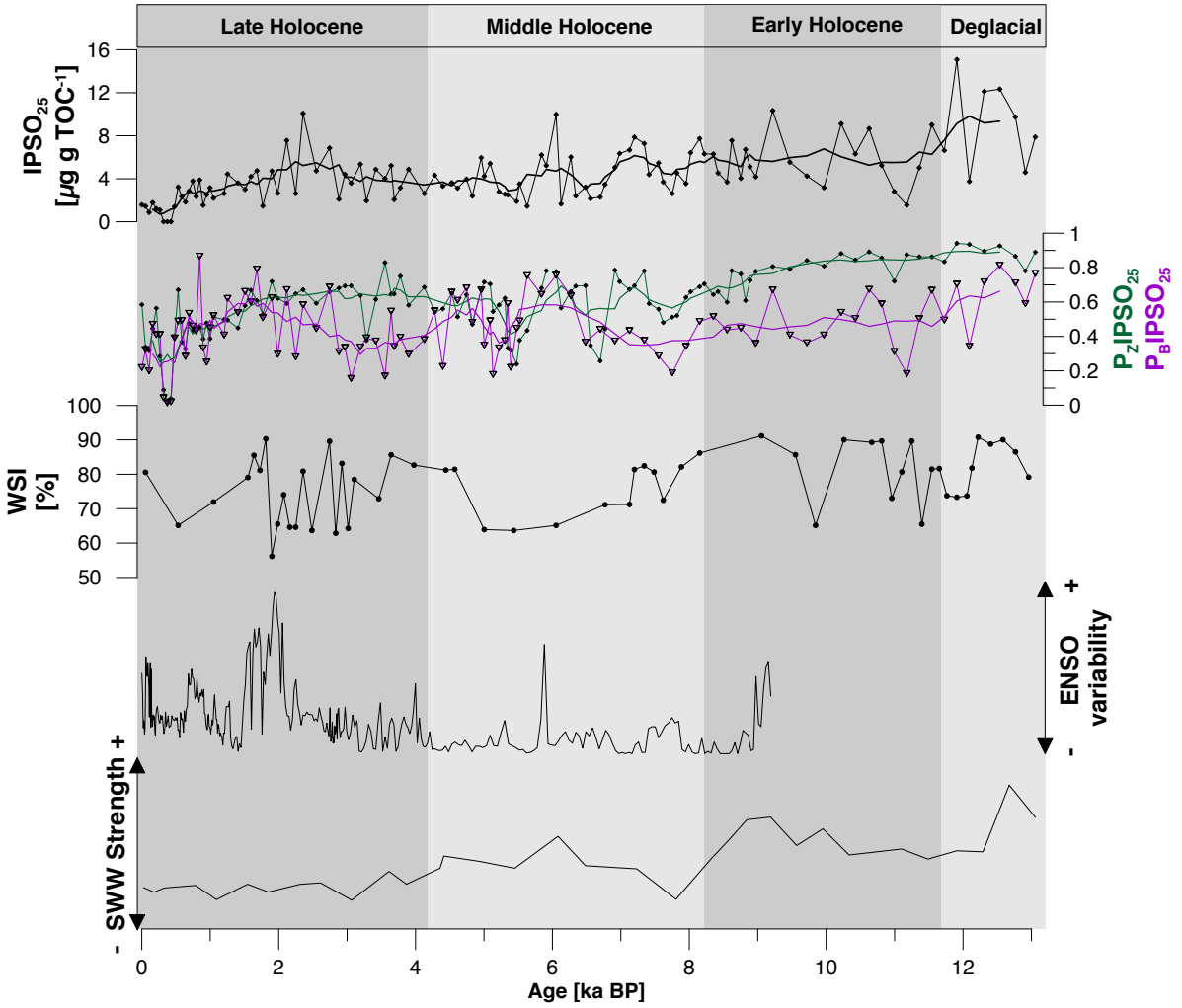

Figure 7.10 The records of (from top to bottom) sea ice biomarker $IPSO_{25}$ concentrations, sea ice indicators P_ZIPSO_{25}, P_BIPSO_{25} and WSI in comparison with records of ENSO variability (El Junco sand, Conroy et al., 2008) and strength of SWWs (derived from the clay/silt ratio from Chilean fjord sediments, Lamy et al., 2010) (running means based on seven points).

colder ocean surface with possibly warmer deep waters. Pike et al. (2013) associated strong SWWs to a peak of glacial discharge at Palmer Deep due to a warmer upper water column from intensified upwelling of UCDW. We suggest that such environmental conditions could have had a positive impact on $IPSO_{25}$ concentrations and $PIPSO_{25}$ and WSI values because a lense of cold, low-dense freshwater at the sea surface could have favoured sea ice formation and sea ice diatom growth (Bintanja et al., 2013).

Since the reconstructed ENSO records account for the variability and not for the positive or negative state of ENSO, we assume that a higher variability includes a higher number of +ENSO events and may be considered as an ENSO indicator. Strong SWWs have been associated with "positive SAM-like" conditions during the Holocene (Moreno et al., 2014; Reynhout et al., 2019). When we combine the atmospheric circulation pattern as described by Stammerjohn et al. (2008b), the in-phase state of -ENSO/+SAM can be assumed before 4.5 ka BP promoting warm and ice-reduced conditions. This state fits well to the observed warmth of Middle Holocene climate reconstructions from our core site and other marine records from the WAP (Etourneau et al., 2013; Heroy et al., 2008; Shevenell et al., 2011) with shorter sea ice seasons due to enhanced heat flux from the ocean (Martinson and McKee, 2012). After 2.5 ka BP, weaker SWWs and a higher ENSO variability might be supposed as +ENSO/-SAM (referring to colder temperatures) and may have dominated and caused a regional Neoglacial cooling and sea ice advance as seen in several paleo records including ours.

We accordingly agree with the suggestion that the SWWs and the concomitant SAM-like conditions could be the dominant driver of ocean heat distribution promoting sea ice cover and growth of $IPSO_{25}$ producing sea ice diatoms in the Early Holocene. A relation of +SAM to sea-ice favouring conditions at the WAP and warmer, sea-ice reduced conditions at the EAP was already stated for the industrial era (Jones et al., 2016). We suggest that weaker SWWs may have reduced the influence of ACC and UCDW upwelling on the WAP shelf and allowed enhanced input of colder WSW from the Weddell Gyre into the Bransfield Strait. This could have supported the Late Holocene cooling and moderate re-advance of sea ice at the core site.

7.5 CONCLUSION

We reconstructed the sea ice and climate development at the northwest AP during the deglaciation, over the Holocene and into the Neoglacial using sediment core PS97/072-1. In this multiproxy study we focused on the biomarker $IPSO_{25}$ as sea ice indicator, on HBI trienes and sterols as indicators for open marine environments and GDGTs for ocean temperature reconstructions. The transfer function approach applied to diatom assemblages was used for winter sea ice and summer sea surface temperature reconstructions. Additional information was derived from

sedimentological records such as IRD and the elemental composition. Our results reveal the deglacial retreat of a floating ice shelf canopy, sea ice retreat during the warm Early and Middle Holocene as well as cooling and sea ice re-advance during the Neoglacial, which is in good agreement with previous climate studies from the AP.

The deglaciation from 17.2 ka to 11.7 ka BP was a highly dynamic period: until 16.4 ka BP the sedimentation of organic proxies was diminished due to a permanent ice cover. With ice shelf retreat, long sea ice seasons established and allowed primary production to evolve during a moderate warming which was interrupted around 13.2 ka BP by the oceanic response to the ACR and renewed sea ice expansion. The ACR terminated with a rebound to warm conditions at 12.4 ka BP along with a retreat in spring sea ice and melt water input from ice sheet melting. The Early Holocene from 11.7 ka to 8.2 ka BP was characterized by continuous warming with warm stratified surface waters in summer and prolonged sea ice cover in winter with stable sea ice edges in spring. In the Middle Holocene from 8.2 ka to 4.2 ka BP the stable warm phase was interrupted by a cooling event at 7.8 ka BP. In general, sea ice seasons were short and sea ice cover significantly reduced, whereas high seasonal amplitudes promoted maximum marine production in long, warm summers and the AP ice sheet retreated nearly to its modern configuration. During the Late Holocene and Neoglacial, respectively, the last 4.2 ka BP experience a cooling with a short warming around 2 ka BP. Phytoplankton biomarkers as well as sea ice proxies ($IPSO_{25}$, $PIPSO_{25}$, WSI) decreased and were lowest during the Little Ice Age which we relate to the establishment of a permantent-like sea ice cover.

While an influence of ENSO variability was not clarified by our data we found that the strength of SWWs have a major impact on sea ice conditions at the WAP. Stronger SWWs and a possible southward shift of the wind belt (SAM-like conditions) are associated with upwelling of warm deep waters and simultaneous promotion of $IPSO_{25}$ production and high sea ice indices due to enhanced melt water input in the Early Holocene. Weaker SWWs in the Late Holocene may have allowed the Neoglacial cooling at the WAP and a restablishment of sea ice cover due to an increased impact from colder WSW.

DATA AVAILABILITY

All data will be available at the open access repository www.pangaea.de.

AUTHOR CONTRIBUTIONS

The study was conceived by MV and JM. Data collections and experimental investigations were done by MV together with PC, CBL and AL (diatoms), OE (diatom transfer function), GM

(GDGTs, dating), AVH ($\delta^{13}C$ $IPSO_{25}$), NL ($\delta^{13}C$ TOC). MV drafted the manuscript and did the visualizations. JM supervised the study and reviewed it together with TO. All authors contributed to the interpretation and discussion of the results and the conclusion of this study.

ACKNOWLEDGEMENT

We thank the captain, crew and chief scientist Frank Lamy of RV Polarstern cruise PS97. Denise Diekstall, Jens Hefter and Ingrid Stimac are thanked for their laboratory support. Simon Belt is acknowledged for providing the 7-HND internal standard for HBI quantification. Financial support was provided through the Helmholtz Research grant VH-NG-1101. Partial support from IDEAL Center grant FONDAP 15150003, Chile, is acknowledged.

8 CONCLUSIONS AND OUTLOOK OF THE THESIS

CONCLUSIONS

The gain in knowledge within the framework of this thesis is the evaluation of $IPSO_{25}$ as a tool for paleo sea ice studies in Antarctica and the Southern Ocean. It is the first employment of $PIPSO_{25}$ - in analogy to the Arctic sea ice index PIP_{25} (Müller et al., 2011) - and its first application in a high-resolution, pre-Holocene paleo record (the study of Collins et al. (2013) dates back to 60 ka BP but has a far lower resolution). This provides robust evidence of its applicability and opens the opportunity for further reconstructions of the sea ice extent, sea ice seasonality and climate conditions to improve climate and sea ice projections.

In **Part I** of the thesis I could demonstrate that the distribution pattern of $IPSO_{25}$ and the application of the semi-quantitative sea ice index $PIPSO_{25}$ bear a high reliability for assessing recent sea ice cover. I found $IPSO_{25}$ in near-coastal surface sediments, an environment where the occurrence of its source species *B. adeliensis* is possible. The spatial distribution of $IPSO_{25}$ is in accordance with sea-ice information from satellite observations and diatom assemblage data. Simultaneously, $IPSO_{25}$ was absent in the open marine and ice-free Drake Passage. Both, $IPSO_{25}$ and the sea ice index $PIPSO_{25}$ hold the potential to reflect sea ice cover in the Bransfield Strait, showing a clear offshore gradient. The distribution of phytoplankton markers indicating open marine conditions showed higher concentrations in permanent ice-free environments in case of HBI trienes and a wide distribution of sterols under several sea ice conditions. I suppose these findings to reflect recent sea ice conditions as they are corresponding well to a similar study in East Antarctica (Smik et al., 2016a). Assessing the suitability of phytoplankton markers for calculation of the sea ice index $PIPSO_{25}$, I found that HBI Z-trienes have an advantage over sterols, since HBI trienes are mainly distributed in areas remote from recent sea ice. I suggest that a $PIPSO_{25}$ index based on HBI trienes may therefore better indicate between sea ice covered and ice-free areas. Recently, a study in the Arctic also showed that PIP_{25} based on HBI trienes is more suitable as a sea ice index (Köseoğlu et al., 2018). Nevertheless, $PIPSO_{25}$ indices based on HBI Z-trienes and brassicasterol corresponded well with sea-ice information from satellite observations and fossil diatom assemblages. However, these findings need to be treated with caution: in contrast to findings of a distribution study from the Arctic (Navarro-Rodriguez et al., 2013), where PIP_{25} matched well with satellite spring sea ice data, the appearance of $IPSO_{25}$ and the sea ice index $PIPSO_{25}$ at the WAP is more likely related to winter sea ice as deduced from satellite observations. It is suggested that this discrepancy is related to the fact that the sediment samples from the WAP cover sea ice biomarker records for roughly 200 years but satellite data only 40 years. Due to the recent decline in sea ice, I supposed that past spring sea ice distribution integrated by marine

sediments show an extent comparable to modern winter sea ice cover. Nevertheless, the good agreement of $PIPSO_{25}$ to winter sea ice estimations from diatom fossil assemblages indicates that this index reflects sea ice cover reasonably well.

In the study of multiple short cores in **Part II** of the thesis I did the first paleo interpretation of the sea ice index $PIPSO_{25}$ and showed that both, $IPSO_{25}$ and $PIPSO_{25}$, are likely influenced mostly by sea ice dynamics. Other regional factors such as ocean mixing, nutrient input, and different water masses play also a role. Another important result is that $IPSO_{25}$ reflects regional sea ice dynamics and characteristics better than the total sea ice cover. In the study I revealed the good agreement of $IPSO_{25}$ with satellite-based sea ice time series during the last 40 years, whereas it contrasts centennial scale ice-core based sea ice reconstructions. Since existing ice core records do not directly reflect sea ice dynamics at the WAP but those of the Amundsen or Bellingshausen Seas (Abram et al., 2010), it is difficult to relate ice core and marine sediment data. However, a comparison of normalized biomarker concentrations of two adjacent sediment cores from the west and east side of the AP (Barbara et al., 2013) underlined the similar sea ice development and seasonality on both sides of the WAP in the 20th century.

I found that $IPSO_{25}$ is more sensitive to high sea ice dynamics, because sea ice fluctuations promote higher marine production due to nutrient release and higher light penetration through thinner sea ice and at the sea ice edge. Therefore, sea ice reconstructions should not be solely based on $IPSO_{25}$ but should consider biomarkers indicating open marine conditions as well as e.g. ocean temperature for a comprehensive sea ice interpretation. The finding of parallel sea ice and open marine biomarker patterns indicates, that in over the last two centuries sea ice dynamics were favourable for both biomarkers. A study by Schofield et al. (2018) at the southern WAP supports this suggestion since they found higher phytoplankton productivity in relation to high sea ice cover. Earlier studies already hypothesized an impact of SAM on sea ice distribution and ocean temperature in recent (Clem et al., 2016; Stammerjohn et al., 2008b) and past times (Barbara et al., 2013; Etourneau et al., 2013; Shevenell et al., 2011). I could show that the production of $IPSO_{25}$ is related to positive SAM modes at the WAP but the exact relationships between both parameters are still unknown.

In **Part III** of the thesis, I applied $IPSO_{25}$ on millennial time scales and showed the robustness of $PIPSO_{25}$ under both slowly and rapidly changing climate conditions between the LGM and today. Using a sediment core from the East Bransfield Basin, I could identify the retreat of the ice shelf at the AP and the opening of the ocean surface around 17.2 ka BP. The retreat of sea ice cover during the deglacial and Early Holocene is clearly indicated by biomarker concentrations and $PIPSO_{25}$ and fits into the Antarctic wide pattern of sea ice retreat reflected by ice core records

(EPICA Community Members et al., 2004; WAIS Divide Project Members et al., 2015). The changing amplitudes of sea ice seasonality could be determined from specific biomarker concentrations as well as from $PIPSO_{25}$ and diatom based WSI and are similar to reconstructions based on a sediment core from the Palmer Deep, WAP (Etourneau et al., 2013). By comparing sea ice biomarkers with reconstructions of ENSO variability and the strength of SWWs, I found indications that especially SWWs have an impact on climate conditions and $IPSO_{25}$ production also on millennial timescales: while an impact of ENSO is hardly distinguishable from our data, we see a clear positive relationship of SWWs strength possibly being a dominant driver of subsurface ocean heat distribution, higher $IPSO_{25}$ concentrations and sea ice cover from enhanced fresh water input under high seasonal sea ice amplitudes.

A result of all three studies is an enhanced understanding of the significance of $IPSO_{25}$ in relation to HBI trienes and sterols. $PIPSO_{25}$ is not linearly connected to sea ice cover because the highest production of $IPSO_{25}$ occurs under thin sea ice and at sea ice margins and not when there is a high and thick sea ice cover. This is supported by findings from Arrigo et al. (2012) and Hancke et al. (2018), who observed a positive effect on phytoplankton blooms due to thinner Arctic sea ice. Therefore, the production of both sea ice and open ocean biomarkers may be promoted equally under certain conditions. In cases of an opposite biomarker pattern, the value of the $PIPSO_{25}$ index can be related to higher or lower sea ice cover, whereas in the case of parallel biomarker patterns, $PIPSO_{25}$ must be handled with caution since the index does not vary and propose a constant level of sea ice cover. Hence, a theoretical concept (Figure 8.1) of an advanced interpretation for past sea ice reconstructions is based on two factors:

1. The absolute concentration of biomarkers during a certain time interval in comparison with the entire record and
2. the interrelation of sea ice and phytoplankton biomarker patterns.

The paleo sea ice studies showed that parallel biomarker patterns are the result of marine production favorable for both biomarker types. In the case of a high sea ice cover with cold, ice-rich summer seasons concentrations of $IPSO_{25}$ are high and those of phytoplankton biomarkers low (Figure 8.1a). With increased seasonal contrasts, the production of phytoplankton marker is also promoted due to enhanced sea ice melt and stable water column conditions promoting phytoplankton growth. As a result, both types of biomarker show a parallel pattern on high concentration levels (Figure 8.1b). During low sea ice cover and warm, long summers, $IPSO_{25}$ concentrations are low and phytoplankton markers are either low due to diminished mixing of the ocean surface and limited nutrient supply (Figure 8.1c). Under conditions of generally low sea ice

cover and a high seasonal amplitude, low $IPSO_{25}$ and high phytoplankton marker concentrations appear in the record (Figure 8.1d).

Another result from this thesis is, that $PIPSO_{25}$ based on HBI trienes more likely reflects sea ice cover in relation to summer conditions because HBI trienes were predominantly distributed in open marine, ice-free areas. In contrast, sterols were found to not have environmental preferences but were higher concentrated in the zone of sea ice edges. So, sterols and sterol-based $PIPSO_{25}$ might therefore be rather indicators for spring sea ice edges as they benefit from sea ice edge-open marine interactions. In summary, $IPSO_{25}$ and $PIPSO_{25}$ are rather indicators of sea ice dynamics and sea ice properties, such as thickness or the velocity of retreat, than of absolute sea ice cover. Also, the differences between WSI and $PIPSO_{25}$ show the gradients between winter and spring sea ice according to the sea ice seasonality.

From the high-resolution records of the second study (Part II) I suggest a positive relationship of $IPSO_{25}$ production to SAM and almost no impact of ENSO. During a positive SAM, the WAP is more likely characterized by warmer ocean temperatures and higher storm frequency (Martinson and McKee, 2012; Meredith and King, 2005). This suggests that warmer temperatures and high seasonal dynamics promote $IPSO_{25}$ production (as indicated in Figure 8.1b) and a high seasonal

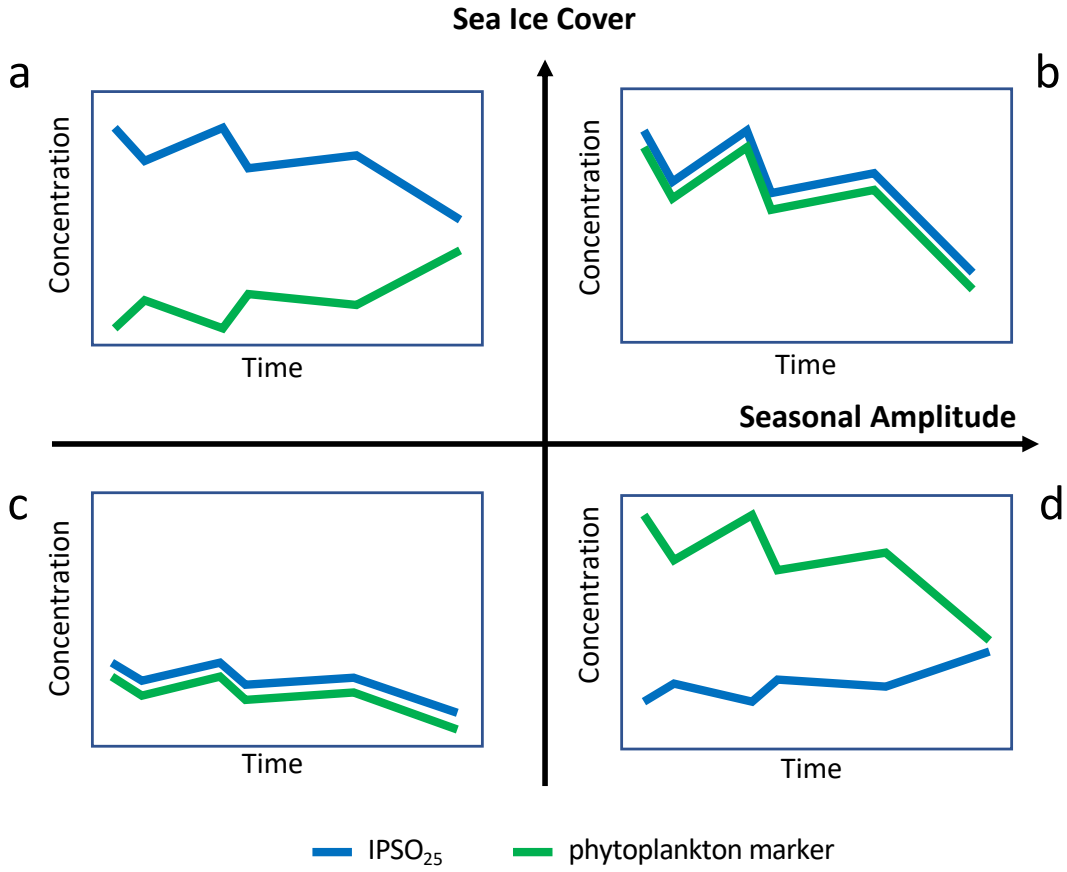

Figure 8.1 The theoretical concept of $IPSO_{25}$ interpretation depending on absolute biomarker concentrations and pattern of both sea ice and phytoplankton biomarker.

amplitude might overprint the signal of sea ice cover indicated by $PIPSO_{25}$. So, for a comprehensive reconstruction of sea ice cover one should always consider an ensemble of other sea ice and climate proxies like phytoplankton marker, diatom assemblages, ice core data (MSA, $ssNa^{+}$), geochemical data or simply the total biomarker concentrations in comparison to the entire record.

OUTLOOK

Within this thesis, I found promising results that $IPSO_{25}$ and $PIPSO_{25}$ may improve paleo sea ice reconstructions in Antarctica. This might contribute to an enhanced capability of climate models for future projections of Antarctic climate and sea ice interrelations. The newly retrieved data is crucial as reference data for future calibration studies at the WAP but also for the Southern Ocean in general. Based on the results of this thesis, I strongly recommend to conduct a comprehensive assessment of biomarkers in surface sediments (e.g. using satellite observations) for every region prior to paleo sea ice studies for an enhanced interpretation of the different biomarkers and derived indices. As shown in this thesis, the $PIPSO_{25}$ index works well with HBI Z-trienes and brassicasterol at the WAP, whereas a $PIPSO_{25}$ based on dinosterol seems to resolve past sea ice better in the Amundsen Sea (Lamping et al., 2020). Additionally, a data base with reference data of evaluated surface sediments, providing information of the regional characteristics, interpretation and application of $PIPSO_{25}$ could be established. Such a data base may eventually obviate the need for such evaluation pre-studies and would allow to focus on paleoenvironmental studies.

In the light of previous paleo sea ice (e.g. Barbara et al., 2016; Etourneau et al., 2013), recent (Clem et al., 2016; Stammerjohn et al., 2008b) and my own studies, sea ice investigations at the WAP should always take into account large-scale atmospheric circulation patterns. A consideration of these circulation patterns could support interpretations of paleo climate and sea ice reconstructions regarding influences from e.g. storms, upwelling of CDW or the "Föhn" effect on the east side of the AP (Klemp and Lilly, 1975). Under progressing global warming, positive SAM is establishing and higher ocean temperatures are observed at the WAP. The warm SSTs and enhanced heat flux from the ocean to the atmosphere are strengthening low pressure cells (and therefore SAM) and may establish a positive feedback at the WAP (Yuan et al., 1999). I therefore assume, that future sea ice will face a high seasonality, disturbance and likely a retreat, which would hereafter reinforce a positive SAM and a strengthening of the SWWs. Due to the strong atmospheric-sea-ice-ocean interactions, modelling of past and future sea ice at the WAP must specifically consider the forcing from ENSO and SAM for significant results.

Overall, the impact of SAM and ENSO on the west, and especially on the east AP is still not resolved well. Recently, a study from Etourneau et al. (2019) found oceanographic patterns to be the main driver of sea ice and ice sheet stability on the east AP. But still, due to sparse data, a

reconstruction of the complex oceanographic and atmospheric interactions and a detailed assessment of ENSO and SAM impacts on sea ice is still not possible for the east AP. To study this, a suite of short and long sediment cores, retrieved on the *Polarstern* cruises PS97 and PS118, are available for temporal and spatial high-resolution sea ice studies. Such a high spatial coverage of the area could be used to develop a detailed conceptual 4D-sea ice model of this region (Figure 8.2) and this data could be integrated in a coupled atmosphere-ocean-model. With such a model, a far more better understanding of sea ice interactions with atmospheric and oceanographic circulation patterns is possible. This would enhance the capability of regional sea ice modelling at the WAP which is often hampered by the unique geographic configuration of the peninsula.

For further sea ice reconstructions, a compilation of existing biomarker data (with comparable stratigraphic units and revised, reliable age models) as aimed by the PAGES C-side working group would gain the benefit the sea ice research community and would make paleo sea ice data more accessible for modelling studies. Further, studies of $IPSO_{25}$ on its source organisms or its pathway

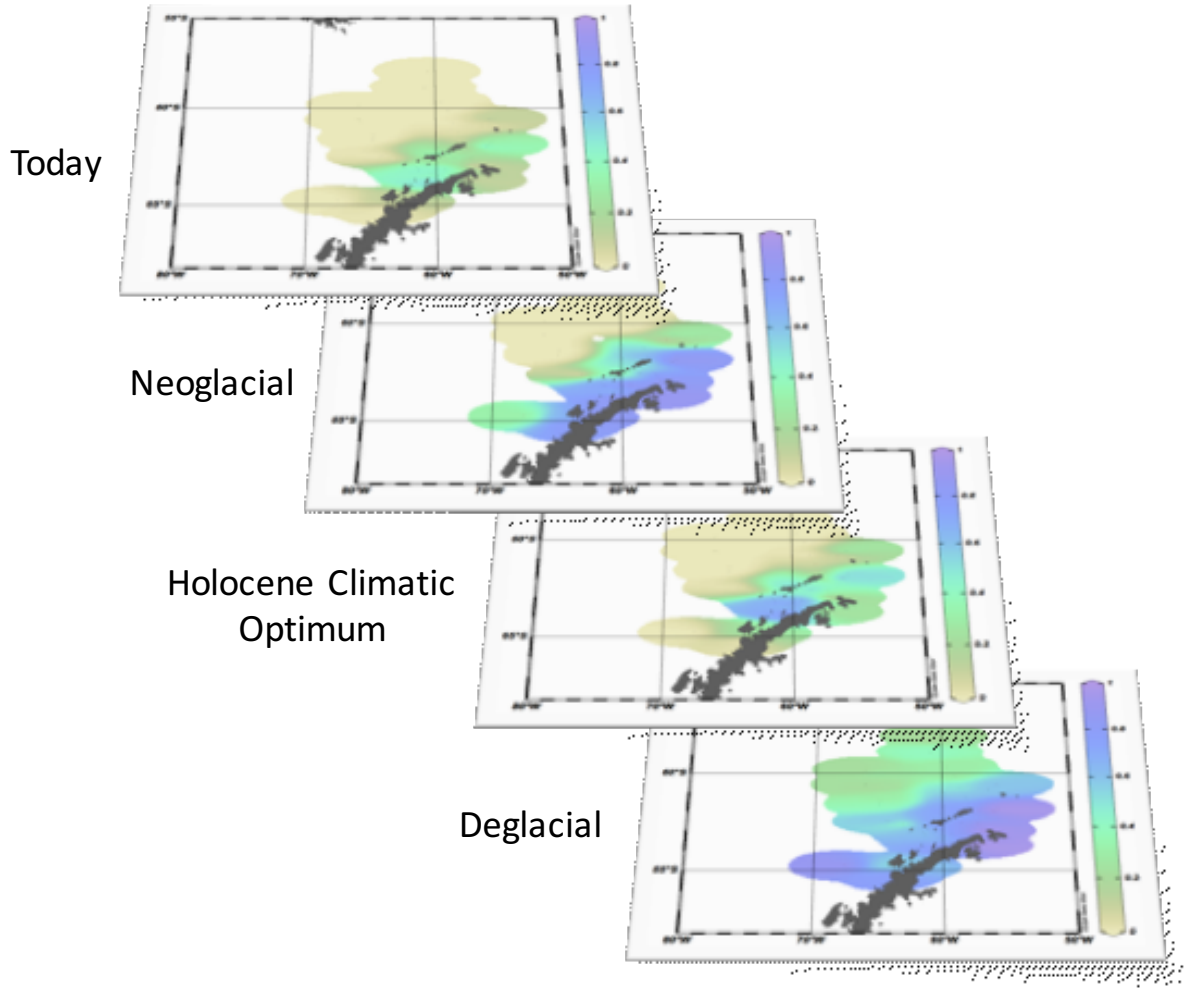

Figure 8.2 Example of a 4D-model based on reconstructed sea ice conditions at the Antarctic Peninsula with the novel tool $IPSO_{25}$ showing the sea ice distribution in different spatial and temporal dimensions. Data could be used from published studies and examination of available sediment cores. Colors and time intervals based on fictional numbers for demonstration.

from the ocean surface into the sediment could enhance a more detailed view on past sea ice using this biomarker.

9 REFERENCES

Abram, N. J., Thomas, E. R., McConnell, J. R., Mulvaney, R., Bracegirdle, T. J., Sime, L. C. and Aristarain, A. J.: Ice core evidence for a 20th century decline of sea ice in the Bellingshausen Sea, Antarctica, J. Geophys. Res., 115(D23), D23101, doi:10.1029/2010JD014644, 2010.

Abram, N. J., Mulvaney, R., Wolff, E. W., Triest, J., Kipfstuhl, S., Trusel, L. D., Vimeux, F., Fleet, L. and Arrowsmith, C.: Acceleration of snow melt in an Antarctic Peninsula ice core during the twentieth century, Nat. Geosci., 6(5), 404–411, doi:10.1038/ngeo1787, 2013.

Abram, N. J., Mulvaney, R., Vimeux, F., Phipps, S. J., Turner, J. and England, M. H.: Evolution of the Southern Annular Mode during the past millennium, Nat. Clim. Chang., 4(7), 564–569, doi:10.1038/nclimate2235, 2014.

Abram, N. J., McGregor, H. V, Tierney, J. E., Evans, M. N., McKay, N. P. and Kaufman, D. S.: Early onset of industrial-era warming across the oceans and continents, Nature, 536(7617), 411–418, doi:10.1038/nature19082, 2016.

Ainley, D. G. and DeMaster, D. P.: The upper trophic levels in polar marine ecosystems, in Polar Oceanography, edited by W. O. J. Smith, pp. 599–630, Academic Press, New York and London., 1990.

Alexander, V. and Niebauer, H. J.: Oceanography of the eastern Bering Sea ice-edge zone in spring, Limn, 26(6), 1111–1125 [online] Available from: http://doi.wiley.com/10.1029/2007RG000250, 1981.

Allen, C. S.: Proxy development: a new facet of morphological diversity in the marine diatom Eucampia antarctica (Castracane) Mangin, J. Micropalaeontology, 33(2), 131–142, doi:10.1144/jmpaleo2013-025, 2014.

Allen, C. S., Oakes-Fretwell, L., Anderson, J. B. and Hodgson, D. A.: A record of Holocene glacial and oceanographic variability in Neny Fjord, Antarctic Peninsula, The Holocene, 20(4), 551–564, doi:10.1177/0959683609356581, 2010.

Allison, I., Tivendale, C. M., Akerman, G. J., Tann, J. M. and Wills, R. H.: Seasonal Variations In The Surface Energy Exchanges Over Antarctic Sea Ice and Coastal Waters, Ann. Glaciol., 3, 12–16, doi:10.3189/S0260305500002445, 1982.

Anderson, R. F., Ali, S., Bradtmiller, L. I., Nielsen, S. H. H., Fleisher, M. Q., Anderson, B. E. and Burckle, L. H.: Wind-driven upwelling in the Southern Ocean and the deglacial rise in atmospheric CO2., Science (80-.)., 323(5920), 1443–1448, doi:10.1126/science.1167441, 2009.

Anon: All About Sea Ice | National Snow and Ice Data Center, [online] Available from: https://nsidc.org/cryosphere/seaice/index.html (Accessed 3 April 2020), n.d.

Appleby, P. G. and Oldfield, F.: The calculation of lead-210 dates assuming a constant rate of supply of unsupported 210Pb to the sediment, CATENA, 5(1), 1–8, doi:10.1016/S0341-8162(78)80002-2, 1978.

Armand, L., Ferry, A. and Leventer, A.: Advances in palaeo sea ice estimation, in Sea Ice, pp. 600–629, John Wiley & Sons, Ltd, Chichester, UK., 2016.

Armand, L. K. and Zielinski, U.: Diatom Species of the genus Rhizosolenia from Southern Ocean sediments: distribution and taxonomic notes, Diatom Res., 16(2), 259–294, doi:10.1080/0269249X.2001.9705520, 2001.

Armand, L. K., Crosta, X., Romero, O. and Pichon, J.-J.: The biogeography of major diatom taxa in Southern Ocean sediments: 1. Sea ice related species, Palaeogeogr. Palaeoclimatol. Palaeoecol., 223(1–2), 93–126, doi:10.1016/J.PALAEO.2005.02.015, 2005.

Arrhenius, S.: Worlds in the making: the evolution of the universe, 1908.

Arrigo, K. R.: Sea Ice Ecosystems, Ann. Rev. Mar. Sci., 6(1), 439–467, doi:10.1146/annurev-marine-010213-135103, 2014.

Arrigo, K. R. and Thomas, D. N.: Large scale importance of sea ice biology in the Southern Ocean, Antarct. Sci., 16(4), 471–486, doi:10.1017/S0954102004002263, 2004.

REFERENCES

Arrigo, K. R., Worthen, D. L., Lizotte, M. P., Dixon, P. and Dieckmann, G. S.: Primary Production in Antarctic Sea Ice, Science (80-.)., 276(5311), 394–397, doi:10.1126/science.276.5311.394, 1997.

Arrigo, K. R., Worthen, D., Schnell, A. and Lizotte, M. P.: Primary production in Southern Ocean waters, J. Geophys. Res. Ocean., 103(C8), 15587–15600, doi:10.1029/98JC00930, 1998.

Arrigo, K. R., Robinson, D. H., Dunbar, R. B., Leventer, A. R. and Lizotte, M. P.: Physical control of chlorophyll a, POC, and TPN distributions in the pack ice of the Ross Sea, Antarctica, J. Geophys. Res. C Ocean., 108(10), 11–14, doi:10.1029/2001jc001138, 2003.

Arrigo, K. R., Perovich, D. K., Pickart, R. S., Brown, Z. W., van Dijken, G. L., Lowry, K. E., Mills, M. M., Palmer, M. A., Balch, W. M., Bahr, F., Bates, N. R., Benitez-Nelson, C., Bowler, B., Brownlee, E., Ehn, J. K., Frey, K. E., Garley, R., Laney, S. R., Lubelczyk, L., Mathis, J., Matsuoka, A., Mitchell, B. G., Moore, G. W. K., Ortega-Retuerta, E., Pal, S., Polashenski, C. M., Reynolds, R. A., Schieber, B., Sosik, H. M., Stephens, M. and Swift, J. H.: Massive Phytoplankton Blooms Under Arctic Sea Ice, Science (80-.)., 336(6087), 1408–1408, doi:10.1126/science.1215065, 2012.

Barbara, L., Crosta, X., Massé, G. and Ther, O.: Deglacial environments in eastern Prydz Bay, East Antarctica, Quat. Sci. Rev., 29(19–20), 2731–2740, doi:10.1016/j.quascirev.2010.06.027, 2010.

Barbara, L., Crosta, X., Schmidt, S. and Massé, G.: Diatoms and biomarkers evidence for major changes in sea ice conditions prior the instrumental period in Antarctic Peninsula, Quat. Sci. Rev., 79, 99–110, doi:10.1016/j.quascirev.2013.07.021, 2013.

Barbara, L., Crosta, X., Leventer, A., Schmidt, S., Etourneau, J., Domack, E. and Massé, G.: Environmental responses of the Northeast Antarctic Peninsula to the Holocene climate variability, Paleoceanography, 31(1), 131–147, doi:10.1002/2015PA002785, 2016.

Bárcena, M. A., Gersonde, R., Ledesma, S., Fabrés, J., Calafat, A. M., Canals, M., Sierro, F. J. and Flores, J. A.: Record of Holocene glacial oscillations in Bransfield Basin as revealed by siliceous microfossil assemblages, Antarct. Sci., 10(03), 269–285, doi:10.1017/S0954102098000364, 1998.

Bárcena, M. Á., Fabrés, J., Isla, E., Flores, J. A., Sierro, F. J., Canals, M. and Palanques, A.: Holocene neoglacial events in the Bransfield Strait (Antarctica). Palaeocenographic and paleoclimatic significance, Sci. Mar., 70(4), 607–619, doi:10.3989/scimar.2006.70n4607, 2006.

Barker, D. H. N., Christeson, G. L., Austin, J. A. and Dalziel, I. W. D.: Backarc basin evolution and cordilleran orogenesis: Insights from new ocean-bottom seismograph refraction profiling in Bransfield Strait, Antarctica, Geology, 31(2), 107, doi:10.1130/0091-7613(2003)031<0107:BBEACO>2.0.CO;2, 2003.

Barnard, A., Wellner, J. S. and Anderson, J. B.: Late Holocene climate change recorded in proxy records from a Bransfield Basin sediment core, Antarctic Peninsula, Polar Res., 33(1), doi:10.3402/polar.v33.17236, 2014.

Belt, S. T.: Source-specific biomarkers as proxies for Arctic and Antarctic sea ice, Org. Geochem., 125, 277–298, doi:10.1016/j.orggeochem.2018.10.002, 2018.

Belt, S. T.: What do IP25 and related biomarkers really reveal about sea ice change?, Quat. Sci. Rev., 204, 216–219, doi:10.1016/j.quascirev.2018.11.025, 2019.

Belt, S. T. and Cabedo-Sanz, P.: Characterisation and isomerisation of mono- and di-unsaturated highly branched isoprenoid (HBI) alkenes: Considerations for palaeoenvironment studies, Org. Geochem., 87, 55–67, doi:10.1016/j.orggeochem.2015.07.003, 2015.

Belt, S. T. and Müller, J.: The Arctic sea ice biomarker IP 25 : a review of current understanding , recommendations for future research and applications in palaeo sea ice reconstructions, Quat. Sci. Rev., 79, 9–25, doi:10.1016/j.quascirev.2012.12.001, 2013.

Belt, S. T., Allard, W. G., Massé, G., Robert, J.-M. and Rowland, S. J.: Highly branched isoprenoids (HBIs): identification of the most common and abundant sedimentary isomers, Geochim. Cosmochim. Acta, 64(22), 3839–3851, doi:10.1016/S0016-7037(00)00464-6, 2000.

Belt, S. T., Mass, G., Rowland, S. J., Poulin, M., Michel, C. and Leblanc, B.: A novel chemical fossil of palaeo sea ice : IP 25, Org. Geochem., 38, 16–27, doi:10.1016/j.orggeochem.2006.09.013, 2007.

Belt, S. T., Brown, T. A., Ringrose, A. E., Cabedo-Sanz, P., Mundy, C. J., Gosselin, M. and Poulin, M.: Quantitative measurement of the sea ice diatom biomarker IP25 and sterols in Arctic sea ice and underlying sediments: Further considerations for palaeo sea ice reconstruction, Org. Geochem., 62, 33–45, doi:10.1016/J.ORGGEOCHEM.2013.07.002, 2013.

REFERENCES

Belt, S. T., Cabedo-Sanz, P., Smik, L., Navarro-Rodriguez, A., Berben, S. M. P., Knies, J. and Husum, K.: Identification of paleo Arctic winter sea ice limits and the marginal ice zone: Optimised biomarker-based reconstructions of late Quaternary Arctic sea ice, Earth Planet. Sci. Lett., 431, 127–139, doi:10.1016/j.epsl.2015.09.020, 2015.

Belt, S. T., Smik, L., Brown, T. A., Kim, J. H., Rowland, S. J., Allen, C. S., Gal, J. K., Shin, K. H., Lee, J. I. and Taylor, K. W. R.: Source identification and distribution reveals the potential of the geochemical Antarctic sea ice proxy IPSO25, Nat. Commun., 7, 1–10, doi:10.1038/ncomms12655, 2016.

Belt, S. T., Brown, T. A., Smik, L., Tatarek, A., Wiktor, J., Stowasser, G., Assmy, P., Allen, C. S. and Husum, K.: Identification of C25 highly branched isoprenoid (HBI) alkenes in diatoms of the genus Rhizosolenia in polar and sub-polar marine phytoplankton, Org. Geochem., 110, 65–72, doi:10.1016/j.orggeochem.2017.05.007, 2017.

Belt, S. T., Brown, T. A., Smik, L., Assmy, P. and Mundy, C. J.: Sterol identification in floating Arctic sea ice algal aggregates and the Antarctic sea ice diatom Berkeleya adeliensis, Org. Geochem., 118, 1–3, doi:10.1016/j.orggeochem.2018.01.008, 2018.

Belt, S. T. T., Brown, T. A. A., Ampel, L., Cabedo-Sanz, P., Fahl, K., Kocis, J. J. J., Massé, G., Navarro-Rodriguez, A., Ruan, J. and Xu, Y.: An inter-laboratory investigation of the Arctic sea ice biomarker proxy IP25 in marine sediments: key outcomes and recommendations, Clim. Past, 10(1), 155–166, doi:10.5194/cp-10-155-2014, 2014.

van Bennekom, A. J., Fred Jansen, J. H., van der Gaast, S. J., van Iperen, J. M. and Pieters, J.: Aluminium-rich opal: an intermediate in the preservation of biogenic silica in the Zaire (Congo) deep-sea fan, Deep Sea Res. Part A, Oceanogr. Res. Pap., 36(2), 173–190, doi:10.1016/0198-0149(89)90132-5, 1989.

Bentley, M. J., Hodgson, D. A., Smith, J. A., Cofaigh, C. Ó., Domack, E. W., Larter, R. D., Roberts, S. J., Brachfeld, S., Leventer, A., Hjort, C., Hillenbrand, C.-D. and Evans, J.: Mechanisms of Holocene palaeoenvironmental change in the Antarctic Peninsula region, The Holocene, 19(1), 51–69, doi:10.1177/0959683608096603, 2009.

Bentley, M. J., Ó Cofaigh, C., Anderson, J. B., Conway, H., Davies, B., Graham, A. G. C., Hillenbrand, C.-D., Hodgson, D. A., Jamieson, S. S. R., Larter, R. D., Mackintosh, A., Smith, J. A., Verleyen, E., Ackert, R. P., Bart, P. J., Berg, S., Brunstein, D., Canals, M., Colhoun, E. A., Crosta, X., Dickens, W. A., Domack, E., Dowdeswell, J. A., Dunbar, R., Ehrmann, W., Evans, J., Favier, V., Fink, D., Fogwill, C. J., Glasser, N. F., Gohl, K., Golledge, N. R., Goodwin, I., Gore, D. B., Greenwood, S. L., Hall, B. L., Hall, K., Hedding, D. W., Hein, A. S., Hocking, E. P., Jakobsson, M., Johnson, J. S., Jomelli, V., Jones, R. S., Klages, J. P., Kristoffersen, Y., Kuhn, G., Leventer, A., Licht, K., Lilly, K., Lindow, J., Livingstone, S. J., Massé, G., McGlone, M. S., McKay, R. M., Melles, M., Miura, H., Mulvaney, R., Nel, W., Nitsche, F. O., O'Brien, P. E., Post, A. L., Roberts, S. J., Saunders, K. M., Selkirk, P. M., Simms, A. R., Spiegel, C., Stolldorf, T. D., Sugden, D. E., van der Putten, N., van Ommen, T., Verfaillie, D., Vyverman, W., Wagner, B., White, D. A., Witus, A. E. and Zwartz, D.: A community-based geological reconstruction of Antarctic Ice Sheet deglaciation since the Last Glacial Maximum, Quat. Sci. Rev., 100(August), 1–9, doi:10.1016/j.quascirev.2014.06.025, 2014.

Berben, S. M. P., Husum, K., Cabedo-Sanz, P. and Belt, S. T.: Holocene sub-centennial evolution of Atlantic water inflow and sea ice distribution in the western Barents Sea, Clim. Past, 10(1), 181–198, doi:10.5194/cp-10-181-2014, 2014.

Berger, A. L.: Long-Term Variations of Daily Insolation and Quaternary Climate Changes, J. Atmos. Sci., 35, 2362–2367, 1978.

Berger, W. H. and Wefer, G.: Export production: seasonality and intermittency, and paleoceanographic implications, Glob. Planet. Change, 3(3), 245–254, doi:10.1016/0921-8181(90)90020-D, 1990.

Bevington, P. R., Robinson, D. K. and Bunce, G.: Data Reduction and Error Analysis for the Physical Sciences, 2nd Edition, American Association of Physics Teachers., 1993.

Bintanja, R., Van Oldenborgh, G. J., Drijfhout, S. S., Wouters, B. and Katsman, C. A.: Important role for ocean warming and increased ice-shelf melt in Antarctic sea-ice expansion, Nat. Geosci., 6(5), 376–379, doi:10.1038/ngeo1767, 2013.

Blaauw, M.: Methods and code for 'classical' age-modelling of radiocarbon sequences, Quat. Geochronol., 5(5), 512–518, doi:10.1016/J.QUAGEO.2010.01.002, 2010.

Blaauw, M. and Christeny, J. A.: Flexible paleoclimate age-depth models using an autoregressive gamma

process, Bayesian Anal., 6(3), 457–474, doi:10.1214/11-BA618, 2011.

Blunier, T. and Brook, E. J.: Timing of millennial-scale climate change in antarctica and greenland during the last glacial period, Science (80-.)., 291(5501), 109–112, doi:10.1126/science.291.5501.109, 2001.

Boon, J. J., Rijpstra, W. I. C., De Lange, F., De Leeuw, J. W., Yoshioka, M. and Shimizu, Y.: Black Sea sterol-A molecular fossil for dinoflagellate blooms [8], Nature, 277(5692), 125–127, doi:10.1038/277125a0, 1979.

Bracegirdle, T. J., Stephenson, D. B., Turner, J. and Phillips, T.: The importance of sea ice area biases in 21st century multimodel projections of Antarctic temperature and precipitation, Geophys. Res. Lett., 42(24), 10,810-832,839, doi:10.1002/2015GL067055, 2015.

Bracegirdle, T. J., Colleoni, F., Abram, N. J., Bertler, N. A. N., Dixon, D. A., England, M., Favier, V., Fogwill, C. J., Fyfe, J. C., Goodwin, I., Goosse, H., Hobbs, W., Jones, J. M., Keller, E. D., Khan, A. L., Phipps, S. J., Raphael, M. N., Russell, J., Sime, L., Thomas, E. R., van den Broeke, M. R. and Wainer, I.: Back to the Future: Using Long-Term Observational and Paleo-Proxy Reconstructions to Improve Model Projections of Antarctic Climate, Geosciences, 9(6), 255, doi:10.3390/geosciences9060255, 2019.

Bramley-Alves, J., Wanek, W. and Robinson, S. A.: Moss δ 13 C: Implications for subantarctic palaeohydrological reconstructions, Palaeogeogr. Palaeoclimatol. Palaeoecol., 453, 20–29, doi:10.1016/j.palaeo.2016.03.028, 2016.

Brault, M. and Simoneit, B. R. T.: Steroid and triterpenoid distributions in bransfield strait sediments: Hydrothermally-enhanced diagenetic transformations, Org. Geochem., 13(4–6), 697–705, doi:10.1016/0146-6380(88)90091-5, 1988.

Broecker, W. S.: Paleocean circulation during the Last Deglaciation: A bipolar seesaw?, Paleoceanography, 13(2), 119–121, doi:10.1029/97PA03707, 1998.

Brown, T. A. and Belt, S. T.: Novel tri- and tetra-unsaturated highly branched isoprenoid (HBI) alkenes from the marine diatom Pleurosigma intermedium, Org. Geochem., 91, 120–122, doi:10.1016/j.orggeochem.2015.11.008, 2016.

Buffen, A., Leventer, A., Rubin, A. and Hutchins, T.: Diatom assemblages in surface sediments of the northwestern Weddell Sea, Antarctic Peninsula, Mar. Micropaleontol., 62(1), 7–30, doi:10.1016/J.MARMICRO.2006.07.002, 2007.

Burckle, L. H. and Cooke, D. W.: Late Pleistocene Eucampia antarctica Abundance Stratigraphy in the Atlantic Sector of the Southern Ocean, Micropaleontology, 29(1), 6, doi:10.2307/1485648, 1983.

Butterworth, B. J. and Miller, S. D.: Air-sea exchange of carbon dioxide in the Southern Ocean and Antarctic marginal ice zone, Geophys. Res. Lett., 43(13), 7223–7230, doi:10.1002/2016GL069581, 2016.

Butzin, M., Köhler, P. and Lohmann, G.: Marine radiocarbon reservoir age simulations for the past 50,000 years, Geophys. Res. Lett., 44(16), 8473–8480, doi:10.1002/2017GL074688, 2017.

Cabedo-Sanz, P., Belt, S. T., Knies, J. and Husum, K.: Identification of contrasting seasonal sea ice conditions during the Younger Dryas, Quat. Sci. Rev., 79, 74–86, doi:10.1016/j.quascirev.2012.10.028, 2013.

Cabedo-Sanz, P., Smik, L. and Belt, S. T.: On the stability of various highly branched isoprenoid (HBI) lipids in stored sediments and sediment extracts, Org. Geochem., 97, 74–77, doi:10.1016/J.ORGGEOCHEM.2016.04.010, 2016.

Cádiz Hernández, A.: Evidencia de cambios en la productividad marina a partir de testigos sedimentarios recuperados en Bahía Fildes (Maxwell Bay) y Costa de Palmer, Península Antártica durante los últimos ~ 1000 años, Universidad de Valparaíso., 2019.

Campagne, P., Crosta, X., Houssais, M. N., Swingedouw, D., Schmidt, S., Martin, A., Devred, E., Capo, S., Marieu, V., Closset, I. and Massé, G.: Glacial ice and atmospheric forcing on the Mertz Glacier Polynya over the past 250 years, Nat. Commun., 6(1), 1–9, doi:10.1038/ncomms7642, 2015.

Campagne, P., Crosta, X., Schmidt, S., Noëlle Houssais, M., Ther, O. and Massé, G.: Sedimentary response to sea ice and atmospheric variability over the instrumental period off Adélie Land, East Antarctica, Biogeosciences, 13(14), 4205–4218, doi:10.5194/bg-13-4205-2016, 2016.

Canals, M. and Amblas, D.: Seafloor kettle holes in Orleans Trough, Bransfield Basin, Antarctic Peninsula, Geol. Soc. London, Mem., 46(1), 313–314, doi:10.1144/M46.16, 2016a.

Canals, M. and Amblas, D.: The bundle: a mega-scale glacial landform left by an ice stream, Western Bransfield Basin, Geol. Soc. London, Mem., 46(1), 177–178, doi:10.1144/M46.157, 2016b.

REFERENCES

Canals, M., Amblas, D. and Casamor, J. L.: Cross-shelf troughs in Central Bransfield Basin, Antarctic Peninsula, Geol. Soc. London, Mem., 46(1), 171–172, doi:10.1144/M46.138, 2016.

Cárdenas, P., Lange, C. B., Vernet, M., Esper, O., Srain, B., Vorrath, M.-E. M.-E., Ehrhardt, S., Müller, J., Kuhn, G., Arz, H. W. H. W. H. W., Lembke-Jene, L., Lamy, F. and Paola Cárdenas, Carina B. Lange, Maria Vernet, Oliver Esper, Benjamin Srain, Maria-Elena Vorrath, Sophie Ehrhardt, Juliane Müller, Gerhard Kuhn, Helge W.Arz, Lester Lembke-Jene, F. L.: Biogeochemical proxies and diatoms in surface sediments across the Drake Passage reflect oceanic domains and frontal systems in the region, Prog. Oceanogr., 174, 72–88, doi:10.1016/j.pocean.2018.10.004, 2019.

Cavalieri, D. J., Parkinson, C. L., Gloersen, P. and Zwally, H. J.: Sea Ice Concentrations from Nimbus-7 SMMR and DMSP SSM/I-SSMIS Passive Microwave Data, Version 1, Boulder, Color. USA, doi:10.5067/8GQ8LZQVL0VL, 1996.

Cefarelli, A. O., Ferrario, M. E., Almandoz, G. O., Atencio, A. G., Akselman, R. and Vernet, M.: Diversity of the diatom genus Fragilariopsis in the Argentine Sea and Antarctic waters: morphology, distribution and abundance, Polar Biol., 33(11), 1463–1484, doi:10.1007/s00300-010-0794-z, 2010.

Chen, S., Hoffmann, S. S., Lund, D. C., Cobb, K. M., Emile-Geay, J. and Adkins, J. F.: A high-resolution speleothem record of western equatorial Pacific rainfall: Implications for Holocene ENSO evolution, Earth Planet. Sci. Lett., 442, 61–71, doi:10.1016/j.epsl.2016.02.050, 2016.

Cheng, L., Abraham, J., Zhu, J., Trenberth, K. E., Fasullo, J., Boyer, T., Locarnini, R., Zhang, B., Yu, F., Wan, L., Chen, X., Song, X., Liu, Y. and Mann, M. E.: Record-Setting Ocean Warmth Continued in 2019, Adv. Atmos. Sci., 37(2), 137–142, doi:10.1007/s00376-020-9283-7, 2020.

Clark, P. U., Dyke, A. S., Shakun, J. D., Carlson, A. E., Clark, J., Wohlfarth, B., Mitrovica, J. X., Hostetler, S. W. and McCabe, A. M.: The Last Glacial Maximum, Science (80-.)., 325(5941), 710–714, doi:10.1126/science.1172873, 2009.

Clem, K. R. and Fogt, R. L.: Varying roles of ENSO and SAM on the Antarctic Peninsula climate in austral spring, J. Geophys. Res. Atmos., 118(20), 11,411-481,492, doi:10.1002/jgrd.50860, 2013.

Clem, K. R., Renwick, J. A., McGregor, J. and Fogt, R. L.: The relative influence of ENSO and SAM on Antarctic Peninsula climate, J. Geophys. Res. Atmos., 121(16), 9324–9341, doi:10.1002/2016JD025305, 2016.

Collares, L. L., Mata, M. M., Kerr, R., Arigony-Neto, J. and Barbat, M. M.: Iceberg drift and ocean circulation in the northwestern Weddell Sea, Antarctica, Deep Sea Res. Part II Top. Stud. Oceanogr., 149(January 2019), 10–24, doi:10.1016/j.dsr2.2018.02.014, 2018.

Collins, L. G., Allen, C. S., Pike, J., Hodgson, D. A., Weckström, K. and Massé, G.: Evaluating highly branched isoprenoid (HBI) biomarkers as a novel Antarctic sea-ice proxy in deep ocean glacial age sediments, Quat. Sci. Rev., 79, 87–98, doi:10.1016/j.quascirev.2013.02.004, 2013.

Conroy, J. L., Overpeck, J. T., Cole, J. E., Shanahan, T. M. and Steinitz-Kannan, M.: Holocene changes in eastern tropical Pacific climate inferred from a Galápagos lake sediment record, Quat. Sci. Rev., 27(11–12), 1166–1180, doi:10.1016/j.quascirev.2008.02.015, 2008.

Cook, A. J., Fox, A. J., Vaughan, D. G. and Ferrigno, J. G.: Retreating glacier fronts on the Antarctic Peninsula over the past half-century, Science (80-.)., 308(5721), 541–544, doi:10.1126/science.1104235, 2005.

Cook, A. J., Holland, P. R., Meredith, M. P., Murray, T., Luckman, A. and Vaughan, D. G.: Ocean forcing of glacier retreat in the western Antarctic Peninsula, Science (80-.)., 353(6296), 283–286, doi:10.1126/science.aae0017, 2016.

Cripps, G. C. and Clarke, A.: Seasonal variation in the biochemical composition of particulate material collected by sediment traps at Signy Island, Antarctica, Polar Biol., 20(6), 414–423, doi:10.1007/s003000050323, 1998.

Criscitiello, A. S., Das, S. B., Evans, M. J., Frey, K. E., Conway, H., Joughin, I., Medley, B. and Steig, E. J.: Ice sheet record of recent sea-ice behavior and polynya variability in the Amundsen Sea, West Antarctica, J. Geophys. Res. Ocean., 118(1), 118–130, doi:10.1029/2012JC008077, 2013.

Crosta, X.: Antarctic Sea Ice History, Late Quaternary, in Encyclopedia of Paleoclimatology and Ancient Environments, edited by V. Gornitz, p. 1047, New York., 2009.

Crosta, X., Pichon, J.-J. and Burckle, L. H.: Application of modern analog technique to marine Antarctic diatoms: Reconstruction of maximum sea-ice extent at the Last Glacial Maximum, Paleoceanography, 13(3),

284–297, doi:10.1029/98PA00339, 1998.

Crosta, X., Sturm, A., Armand, L. and Pichon, J.-J.: Late Quaternary sea ice history in the Indian sector of the Southern Ocean as recorded by diatom assemblages, Mar. Micropaleontol., 50(3–4), 209–223, doi:10.1016/S0377-8398(03)00072-0, 2004.

Crosta, X., Romero, O., Armand, L. K. and Pichon, J. J.: The biogeography of major diatom taxa in Southern Ocean sediments: 2. Open ocean related species, Palaeogeogr. Palaeoclimatol. Palaeoecol., 223(1–2), 66–92, doi:10.1016/j.palaeo.2005.03.028, 2005.

Damsté, J. S. S., Muyzer, G., Abbas, B., Rampen, S. W., Massé, G., Allard, W. G., Belt, S. T., Robert, J. M., Rowland, S. J., Moldowan, J. M., Barbanti, S. M., Fago, F. J., Denisevich, P., Dahl, J., Trindade, L. A. F. and Schouten, S.: The Rise of the Rhizosolenid Diatoms, Science (80-.)., 304(5670), 584–587, doi:10.1126/science.1096806, 2004.

Danilov, S., Sidorenko, D., Wang, Q. and Jung, T.: The Finite-volumE Sea ice–Ocean Model (FESOM2), Geosci. Model Dev., 10(2), 765–789, doi:10.5194/gmd-10-765-2017, 2017.

DeConto, R. M., Pollard, D., Wilson, P. A., Pälike, H., Lear, C. H. and Pagani, M.: Thresholds for Cenozoic bipolar glaciation, Nature, 455(7213), 652–656, doi:10.1038/nature07337, 2008.

DeLaRocha, C. L. and Passow, U.: Factors influencing the sinking of POC and the efficiency of the biological carbon pump, Deep Sea Res. Part II Top. Stud. Oceanogr., 54(5–7), 639–658, doi:10.1016/j.dsr2.2007.01.004, 2007.

Denis, D., Crosta, X., Barbara, L., Massé, G., Renssen, H., Ther, O. and Giraudeau, J.: Sea ice and wind variability during the Holocene in East Antarctica: insight on middle–high latitude coupling, Quat. Sci. Rev., 29(27–28), 3709–3719, doi:10.1016/J.QUASCIREV.2010.08.007, 2010.

Denton, G. H., Anderson, R. F., Toggweiler, J. R., Edwards, R. L., Schaefer, J. M. and Putnam, A. E.: The Last Glacial Termination, Science (80-.)., 328(5986), 1652–1656, doi:10.1126/science.1184119, 2010.

Ding, Q., Steig, E. J., Battisti, D. S. and Wallace, J. M.: Influence of the tropics on the southern annular mode, J. Clim., 25(18), 6330–6348, doi:10.1175/JCLI-D-11-00523.1, 2012.

Domack, E., Leventer, A., Dunbar, R., Taylor, F., Brachfeld, S. and Sjunneskogs, C.: Chronology of the Palmer Deep site, Antarctic Peninsula: a Holocene palaeoenvironmental reference for the circum-Antarctic, The Holocene, 11(1), 1–9, doi:10.1191/095968301673881493, 2001.

Ducklow, H. W., Baker, K., Martinson, D. G., Quetin, L. B., Ross, R. M., Smith, R. C., Stammerjohn, S. E., Vernet, M. and Fraser, W.: Marine pelagic ecosystems: The West Antarctic Peninsula, Philos. Trans. R. Soc. B Biol. Sci., 362(1477), 67–94, doi:10.1098/rstb.2006.1955, 2007.

Ducklow, H. W., Erickson, M., Kelly, J., Montes-Hugo, M., Ribic, C. A., Smith, R. C., Stammerjohn, S. E. and Karl, D. M.: Particle export from the upper ocean over the continental shelf of the west Antarctic Peninsula: A long-term record, 1992–2007, Deep Sea Res. Part II Top. Stud. Oceanogr., 55(18–19), 2118–2131, doi:10.1016/j.dsr2.2008.04.028, 2008.

Eayrs, C., Holland, D., Francis, D., Wagner, T., Kumar, R. and Li, X.: Understanding the Seasonal Cycle of Antarctic Sea Ice Extent in the Context of Longer-Term Variability, Rev. Geophys., 57(3), 1037–1064, doi:10.1029/2018RG000631, 2019.

Eglinton, T. I. and Eglinton, G.: Molecular proxies for paleoclimatology, Earth Planet. Sci. Lett., 275(1–2), 1–16, doi:10.1016/j.epsl.2008.07.012, 2008.

Ellison, C. R. W. W. C. R. W., Chapman, M. R. and Hall, I. R.: Surface and deep ocean interactions during the cold climate event 8200 years ago, Science (80-.)., 312(5782), 1929–1932, doi:10.1126/science.1127213, 2006.

EPICA Community Members, Augustin, L., Barbante, C., Barnes, P. R. F., Barnola, J. M., Bigler, M., Castellano, E., Cattani, O., Chappellaz, J., Dahl-Jensen, D., Delmonte, B., Dreyfus, G., Durand, G., Falourd, S., Fischer, H., Flückiger, J., Hansson, M. E., Huybrechts, P., Jugie, G., Johnsen, S. J., Jouzel, J., Kaufmann, P., Kipfstuhl, J., Lambert, F., Lipenkov, V. Y., Littot, G. C., Longinelli, A., Lorrain, R., Maggi, V., Masson-Delmotte, V., Miller, H., Mulvaney, R., Oerlemans, J., Oerter, H., Orombelli, G., Parrenin, F., Peel, D. A., Petit, J. R., Raynaud, D., Ritz, C., Ruth, U., Schwander, J., Siegenthaler, U., Souchez, R., Stauffer, B., Steffensen, J. P., Stenni, B., Stocker, T. F., Tabacco, I. E., Udisti, R., van de Wal, R. S. W., van den Broeke, M., Weiss, J., Wilhelms, F., Winther, J. G., Wolff, E. W. and Zucchelli, M.: Eight glacial cycles from an Antarctic ice core, Nature, 429(6992), 623–628, doi:10.1038/nature02599, 2004.

REFERENCES

EPICA Community Members, Augustin, L., Barbante, C., Barnes, P. R. F., Barnola, J. M., Bigler, M., Castellano, E., Cattani, O., Chappellaz, J., Dahl-Jensen, D., Delmonte, B., Dreyfus, G., Durand, G., Falourd, S., Fischer, H., Flückiger, J., Hansson, M. E., Huybrechts, P., Jugie, G., Johnsen, S. J., Jouzel, J., Kaufmann, P., Kipfstuhl, J., Lambert, F., Lipenkov, V. Y., Littot, G. C., Longinelli, A., Lorrain, R., Maggi, V., Masson-Delmotte, V., Miller, H., Mulvaney, R., Oerlemans, J., Oerter, H., Orombelli, G., Parrenin, F., Peel, D. A., Petit, J. R., Raynaud, D., Ritz, C., Ruth, U., Schwander, J., Siegenthaler, U., Souchez, R., Stauffer, B., Steffensen, J. P., Stenni, B., Stocker, T. F., Tabacco, I. E., Udisti, R., van de Wal, R. S. W., van den Broeke, M., Weiss, J., Wilhelms, F., Winther, J. G., Wolff, E. W. and Zucchelli, M.: One-to-one coupling of glacial climate variability in Greenland and Antarctica, Nature, 444(7116), 195–198, doi:10.1038/nature05301, 2006.

Escutia, C., DeConto, R., Dunbar, R., De Santis, L., Shevenell, A. and Nash, T.: Keeping an Eye on Antarctic Ice Sheet Stability, Oceanography, 32(1), 32–46, doi:10.5670/oceanog.2019.117, 2019.

Esper, O. and Gersonde, R.: New tools for the reconstruction of Pleistocene Antarctic sea ice, Palaeogeogr. Palaeoclimatol. Palaeoecol., 399, 260–283, doi:10.1016/J.PALAEO.2014.01.019, 2014a.

Esper, O. and Gersonde, R.: Quaternary surface water temperature estimations: New diatom transfer functions for the Southern Ocean, Palaeogeogr. Palaeoclimatol. Palaeoecol., 414, 1–19, doi:10.1016/J.PALAEO.2014.08.008, 2014b.

Esper, O., Gersonde, R. and Kadagies, N.: Diatom distribution in southeastern Pacific surface sediments and their relationship to modern environmental variables, Palaeogeogr. Palaeoclimatol. Palaeoecol., 287(1–4), 1–27, 2010.

Etourneau, J., Collins, L. G., Willmott, V., Kim, J. H., Barbara, L., Leventer, A., Schouten, S., Sinninghe Damsté, J. S., Bianchini, A., Klein, V., Crosta, X. and Massé, G.: Holocene climate variations in the western Antarctic Peninsula: Evidence for sea ice extent predominantly controlled by changes in insolation and ENSO variability, Clim. Past, 9(4), 1431–1446, doi:10.5194/cp-9-1431-2013, 2013.

Etourneau, J., Sgubin, G., Crosta, X., Swingedouw, D., Willmott, V., Barbara, L., Houssais, M. N., Schouten, S., Damsté, J. S. S., Goosse, H., Escutia, C., Crespin, J., Massé, G. and Kim, J. H.: Ocean temperature impact on ice shelf extent in the eastern Antarctic Peninsula, Nat. Commun., 10(1), 8–15, doi:10.1038/s41467-018-08195-6, 2019.

Evans, J. and Pudsey, C. J.: Sedimentation associated with Antarctic Peninsula ice shelves: implications for palaeoenvironmental reconstructions of glacimarine sediments, J. Geol. Soc. London., 159(3), 233–237, doi:10.1144/0016-764901-125, 2002.

Fahl, K. and Stein, R.: Modern seasonal variability and deglacial/Holocene change of central Arctic Ocean sea-ice cover: New insights from biomarker proxy records, Earth Planet. Sci. Lett., 351–352, 123–133, doi:10.1016/j.epsl.2012.07.009, 2012.

Falkowski, P. G., Barber, R. T. and Smetacek, V. S.: Biogeochemical Controls and Feedbacks on Ocean Primary Production, Science (80-.)., 281(5374), 200–206, doi:10.1126/science.281.5374.200, 1998.

Fietz, S., Huguet, C., Rueda, G., Hambach, B. and Rosell-Melé, A.: Hydroxylated isoprenoidal GDGTs in the Nordic Seas, Mar. Chem., 152, 1–10, doi:10.1016/j.marchem.2013.02.007, 2013.

Fischer, G.: Stable carbon isotope ratios of plankton carbon and sinking organic matter from the Atlantic sector of the Southern Ocean, Mar. Chem., 35(1–4), 581–596, doi:10.1016/S0304-4203(09)90044-5, 1991.

FitzGerald, D. M., Fenster, M. S., Argow, B. A. and Buynevich, I. V: Coastal Impacts Due to Sea-Level Rise, Annu. Rev. Earth Planet. Sci., 36(1), 601–647, doi:10.1146/annurev.earth.35.031306.140139, 2008.

Flores, H., van Franeker, J. A., Siegel, V., Haraldsson, M., Strass, V., Meesters, E. H., Bathmann, U. and Wolff, W. J.: The association of Antarctic krill Euphausia superba with the under-ice habitat, PLoS One, 7(2), doi:10.1371/journal.pone.0031775, 2012.

Flynn, W. W.: The determination of low levels of polonium-210 in environmental materials, Anal. Chim. Acta, 43(C), 221–227, doi:10.1016/S0003-2670(00)89210-7, 1968.

Foster, A. F. M., Curran, M. A. J., Smith, B. T., Van Ommen, T. D. and Morgan, V. I.: Covariation of Sea ice and methanesulphonic acid in Wilhelm II Land, East Antarctica, Ann. Glaciol., 44, 429–432, doi:10.3189/172756406781811394, 2006.

Fryxell, G. A. and Prasad, A. K. S. K.: Eucampia antarctica var. recta (Mangin) stat. nov. (Biddulphiaceae, Bacillariophyceae): life stages at the Weddell Sea ice edge, Phycologia, 29(1), 27–38, doi:10.2216/i0031-8884-29-1-27.1, 1990.

Fütterer, D. K.: Die Expedition ANTARKTIS-VI mit FS Polarstern 1987/1988 (The Expedition ANTARKTIS-VI of RV Polarstern in 1987/88), Alfred-Wegener-Institut für Polar- und Meeresforschung, Bremerhaven., 1988.

Garrison, D. L.: Antarctic Sea Ice Biota, Am. Zool., 31(1), 17–34, doi:10.1093/icb/31.1.17, 1991.

Gersonde, R. and Zielinski, U.: The reconstruction of late Quaternary Antarctic sea-ice distribution — the use of diatoms as a proxy for sea-ice, Palaeogeogr. Palaeoclimatol. Palaeoecol., 162, 263–286, doi:10.1016/S0031-0182(00)00131-0, 2000.

Gersonde, R., Crosta, X., Abelmann, A. and Armand, L.: Sea-surface temperature and sea ice distribution of the Southern Ocean at the EPILOG Last Glacial Maximum—a circum-Antarctic view based on siliceous microfossil records, Quat. Sci. Rev., 24(7–9), 869–896, doi:10.1016/J.QUASCIREV.2004.07.015, 2005.

Gibson, J. A. E., Trull, T., Nichols, P. D., Summons, R. E. and McMinn, A.: Sedimentation of 13C-rich organic matter from Antarctic sea-ice algae: A potential indicator of past sea-ice extent, Geology, 27(4), 331–334, doi:10.1130/0091-7613(1999)027<0331:socrom>2.3.co;2, 1999.

Gladu, P. K., Patterson, G. W., Wikfors, G. H., Chitwood, D. J. and Lusby, W. R.: The occurrence of brassicasterol and epibrassicasterol in the chromophycota, Comp. Biochem. Physiol. Part B Comp. Biochem., 97(3), 491–494, doi:10.1016/0305-0491(90)90149-N, 1990.

Gloersen, P., Campbell, W. J., Cavalieri, D. J., Comiso, J. C., Parkinson, C. L. and Zwally, H. J.: Arctic and antarctic sea ice, 1978, Ann. Glaciol., 17, 149–154, 1993.

Goad, L. J., Holz, G. G. and Beach, D. H.: Identification of (24S)-24-methylcholesta-5,22-dien-3$β$-ol as the major sterol of a marine cryptophyte and a marine prymnesiophyte, Phytochemistry, 22(2), 475–476, doi:10.1016/0031-9422(83)83028-3, 1983.

Gomez, B., Carter, L., Orpin, A. R., Cobb, K. M., Page, M. J., Trustrum, N. A. and Palmer, A. S.: ENSO/SAM interactions during the middle and late Holocene, The Holocene, 22(1), 23–30, doi:10.1177/0959683611405241, 2012.

Gonçalves-Araujo, R., de Souza, M. S., Tavano, V. M. and Garcia, C. A. E.: Influence of oceanographic features on spatial and interannual variability of phytoplankton in the Bransfield Strait, Antarctica, J. Mar. Syst., 142, 1–15, doi:10.1016/J.JMARSYS.2014.09.007, 2015.

Goodwin, B. P., Mosley-Thompson, E., Wilson, A. B., Porter, S. E. and Sierra-Hernandez, M. R.: Accumulation Variability in the Antarctic Peninsula: The Role of Large-Scale Atmospheric Oscillations and Their Interactions, J. Clim., 29(7), 2579–2596, doi:10.1175/JCLI-D-15-0354.1, 2016.

Gough, A. J., Mahoney, A. R., Langhorne, P. J., Williams, M. J. M., Robinson, N. J. and Haskell, T. G.: Signatures of supercooling: McMurdo Sound platelet ice, J. Glaciol., 58(207), 38–50, doi:10.3189/2012jog10j218, 2012.

Haase, K. M., Beier, C., Fretzdorff, S., Smellie, J. L. and Garbe-Schönberg, D.: Magmatic evolution of the South Shetland Islands, Antarctica, and implications for continental crust formation, Contrib. to Mineral. Petrol., 163(6), 1103–1119, doi:10.1007/s00410-012-0719-7, 2012.

Hamm, C. E., Merkel, R., Springer, O., Jurkojc, P., Maiert, C., Prechtelt, K. and Smetacek, V.: Architecture and material properties of diatom shells provide effective mechanical protection, Nature, 421(6925), 841–843, doi:10.1038/nature01416, 2003.

Hancke, K., Lund-Hansen, L. C., Lamare, M. L., Højlund Pedersen, S., King, M. D., Andersen, P. and Sorrell, B. K.: Extreme Low Light Requirement for Algae Growth Underneath Sea Ice: A Case Study From Station Nord, NE Greenland, J. Geophys. Res. Ocean., 123(2), 985–1000, doi:10.1002/2017JC013263, 2018.

Hasle, G. R. and Syvertsen, E. E.: Marine diatoms, in Identifying Marine Diatoms and Dinoflagellates, edited by C. R. Tomas, pp. 5–385, Academic Press Limited, London., 1996.

Hellmer, H. H., Kauker, F., Timmermann, R., Determann, J. and Rae, J.: Twenty-first-century warming of a large Antarctic ice-shelf cavity by a redirected coastal current, Nature, 485(7397), 225–228, doi:10.1038/nature11064, 2012.

Hellmer, H. H., Jacobs, S. S. and Jenkins, A.: Oceanic Erosion of a Floating Antarctic Glacier in the Amundsen Sea, in Ocean, Ice, and Atmosphere: Interactions at the Antarctic Continental Margin, Volume 75, edited by S. S. Jacobs and R. F. Weiss, pp. 83–99, American Geophysical Union (AGU)., 2013.

Hepp, D. A., Mörz, T. and Grützner, J.: Pliocene glacial cyclicity in a deep-sea sediment drift (Antarctic

Peninsula Pacific Margin), in Palaeogeography, Palaeoclimatology, Palaeoecology, vol. 231, pp. 181–198, Elsevier., 2006.

Heroy, D. C. and Anderson, J. B.: Radiocarbon constraints on Antarctic Peninsula Ice Sheet retreat following the Last Glacial Maximum (LGM), Quat. Sci. Rev., 26(25–28), 3286–3297, doi:10.1016/j.quascirev.2007.07.012, 2007.

Heroy, D. C., Sjunneskog, C. and Anderson, J. B.: Holocene climate change in the Bransfield Basin, Antarctic Peninsula: evidence from sediment and diatom analysis, Antarct. Sci., 20(01), 69–87, doi:10.1017/S0954102007000788, 2008.

Hillaire-Marcel, C. and de Vernal, A.: Proxies in Late Cenozoic Paleoceanography, edited by C. Hillaire-Marcel and A. de Vernal, Elsevier, Amsterdam. [online] Available from: https://linkinghub.elsevier.com/retrieve/pii/S1572548007010056 (Accessed 5 May 2020), 2007.

Hillenbrand, C.-D., Kuhn, G. and Frederichs, T.: Record of a Mid-Pleistocene depositional anomaly in West Antarctic continental margin sediments: an indicator for ice-sheet collapse?, Quat. Sci. Rev., 28(13–14), 1147–1159, doi:10.1016/j.quascirev.2008.12.010, 2009.

Hillenbrand, C. D., Smith, J. A., Hodell, D. A., Greaves, M., Poole, C. R., Kender, S., Williams, M., Andersen, T. J., Jernas, P. E., Elderfield, H., Klages, J. P., Roberts, S. J., Gohl, K., Larter, R. D. and Kuhn, G.: West Antarctic Ice Sheet retreat driven by Holocene warm water incursions, Nature, 547(7661), 43–48, doi:10.1038/nature22995, 2017.

Hobbs, W. R., Massom, R., Stammerjohn, S., Reid, P., Williams, G. and Meier, W.: A review of recent changes in Southern Ocean sea ice , their drivers and forcings, Glob. Planet. Change, 143, 228–250, doi:10.1016/j.gloplacha.2016.06.008, 2016.

Hofmann, E. E., Klinck, J. M., Lascara, C. M. and Smith, D. A.: Water mass distribution and circulation west of the Antarctic Peninsula and including Bransfield Strait, in Foundations for Ecological Research West of the Antarctic Peninsula, edited by R. M. Ross, E. E. Hofmann, and L. B. Quetin, pp. 61–80, American Geophysical Union (AGU), Washington, D. C., 1996.

Hogg, A. G., Hua, Q., Blackwell, P. G., Niu, M., Buck, C. E., Guilderson, T. P., Heaton, T. J., Palmer, J. G., Reimer, P. J., Reimer, R. W., Turney, C. S. M. and Zimmerman, S. R. H.: SHCal13 Southern Hemisphere Calibration, 0–50,000 Years cal BP, Radiocarbon, 55(4), 1889–1903, doi:10.2458/azu_js_rc.55.16783, 2013.

Holland, P. R.: The seasonality of Antarctic sea ice trends, Geophys. Res. Lett., 41(12), 4230–4237, doi:10.1002/2014GL060172, 2014.

Hopmans, E. C., Weijers, J. W. H., Schefuß, E., Herfort, L., Sinninghe Damsté, J. S. and Schouten, S.: Variability in the Benguela Current upwelling system over the past 70,000 years, Earth Planet. Sci. Lett., 224(1–2), 107–116, doi:10.1016/j.epsl.2004.05.012, 2004.

Hoppmann, M., Nicolaus, M., Paul, S., Hunkeler, P. A., Heinemann, G., Willmes, S., Timmermann, R., Boebel, O., Schmidt, T., Kühnel, M., König-Langlo, G. and Gerdes, R.: Ice platelets below weddell sea landfast sea ice, Ann. Glaciol., 56(69), 175–190, doi:10.3189/2015AoG69A678, 2015.

Huss, M. and Farinotti, D.: A high-resolution bedrock map for the Antarctic Peninsula, Cryosph., 8(4), 1261–1273, doi:10.5194/tc-8-1261-2014, 2014.

Ingólfsson, Ó., Hjort, C. and Humlum, O.: Glacial and Climate History of the Antarctic Peninsula since the Last Glacial Maximum, Arctic, Antarct. Alp. Res., 35(2), 175–186, doi:10.1657/1523-0430(2003)035[0175:GACHOT]2.0.CO;2, 2003.

IPCC: Summary for Policymakers, in Global Warming of 1.5°C. An IPCC Special Report on the impacts of global warming of 1.5°C above pre-industrial levels and related global greenhouse gas emission pathways, in the context of strengthening the global response to the threat of climate change, edited by V. Masson-Delmotte, P. Zhai, H.-O. Pörtner, D. Roberts, J. Skea, P. R. Shukla, A. Pirani, W. Moufouma-Okia, C. Péan, R. Pidcock, S. Connors, J. B. R. Matthews, Y. Chen, X. Zhou, M. I. Gomis, E. Lonnoy, T. Maycock, M. Tignor, and T. Waterfield, p. 24. [online] Available from: https://www.ipcc.ch/site/assets/uploads/sites/2/2019/05/SR15_SPM_version_report_LR.pdf, 2018.

IPCC: Summary for Policymakers, in IPCC Special Report on the Ocean and Cryosphere in a Changing Climate, edited by H. O. Pörtner, D. C. Roberts, V. Masson-Delmotte, P. Zhai, M. Tignor, E. Poloczanska, K. Mintebeck, M. Nicolai, A. Okem, J. Petzold, B. Rama, and N. Weyer, p. 42. [online] Available from: https://report.ipcc.ch/srocc/pdf/SROCC_SPM_Approved.pdf, 2019.

Johns, L., Wraige, E. J., Belt, S. T., Lewis, C. A., Massé, G., Robert, J. M. and Rowland, S. J.: Identification

of a C25 highly branched isoprenoid (HBI) diene in Antarctic sediments, Antarctic sea-ice diatoms and cultured diatoms, Org. Geochem., 30(11), 1471–1475, doi:10.1016/S0146-6380(99)00112-6, 1999.

Jones, J. M., Gille, S. T., Goosse, H., Abram, N. J., Canziani, P. O., Charman, D. J., Clem, K. R., Crosta, X., de Lavergne, C., Eisenman, I., England, M. H., Fogt, R. L., Frankcombe, L. M., Marshall, G. J., Masson-Delmotte, V., Morrison, A. K., Orsi, A. J., Raphael, M. N., Renwick, J. A., Schneider, D. P., Simpkins, G. R., Steig, E. J., Stenni, B., Swingedouw, D. and Vance, T. R.: Assessing recent trends in high-latitude Southern Hemisphere surface climate, Nat. Clim. Chang., 6(10), 917–926, doi:10.1038/nclimate3103, 2016.

Jouzel, J., Lorius, C., Petit, J. R., Genthon, C., Barkov, N. I., Kotlyakov, V. M. and Petrov, V. M.: Vostok ice core: A continuous isotope temperature record over the last climatic cycle (160,000 years), Nature, 329(6138), 403–408, doi:10.1038/329403a0, 1987.

Jouzel, J., Vaikmae, R., Petit, J. R., Martin, M., Duclos, Y., Stievenard, M., Lorius, C., Toots, M., Mélières, M. A., Burckle, L. H., Barkov, N. I. and Kotlyakov, V. M.: The two-step shape and timing of the last deglaciation in Antarctica, Clim. Dyn., 11(3), 151–161, doi:10.1007/BF00223498, 1995.

Kalanetra, K. M., Bano, N. and Hollibaugh, J. T.: Ammonia-oxidizing Archaea in the Arctic Ocean and Antarctic coastal waters, Environ. Microbiol., 11(9), 2434–2445, doi:10.1111/j.1462-2920.2009.01974.x, 2009.

Kanazawa, A., Yoshioka, M. and Teshima, S.-I.: The occurrence of brassicasterol in the diatoms, Cyclotella nana and Nitzschia closterium, Bull. Japanese Soc. Sci. Fish., 37, 889–903, 1971.

Kennett, J. P.: Cenozoic evolution of Antarctic glaciation, the circum-Antarctic Ocean, and their impact on global paleoceanography, J. Geophys. Res., 82(27), 3843–3860, doi:10.1029/JC082i027p03843, 1977.

Kim, D., Kim, D. Y., Kim, Y. J., Kang, Y. C. and Shim, J.: Downward fluxes of biogenic material in Bransfield Strait, Antarctica, Antarct. Sci., 16(3), 227–237, doi:10.1017/S0954102004002032, 2004.

Kim, D. Y., Kim, D. Y., Park, J. S. and Kim, Y. J.: Interannual variation of particle fluxes in the eastern Bransfield Strait, Antarctica: A response to the sea ice distribution, Deep. Res. Part I Oceanogr. Res. Pap., 52(11), 2140–2155, doi:10.1016/j.dsr.2005.06.008, 2005.

Kim, J.-H., van der Meer, J., Schouten, S., Helmke, P., Willmott, V., Sangiorgi, F., Koç, N., Hopmans, E. C. and Damsté, J. S. S.: New indices and calibrations derived from the distribution of crenarchaeal isoprenoid tetraether lipids: Implications for past sea surface temperature reconstructions, Geochim. Cosmochim. Acta, 74(16), 4639–4654, doi:10.1016/j.gca.2010.05.027, 2010.

Kim, J.-H., Crosta, X., Willmott, V., Renssen, H., Bonnin, J., Helmke, P., Schouten, S. and Sinninghe Damsté, J. S.: Holocene subsurface temperature variability in the eastern Antarctic continental margin, Geophys. Res. Lett., 39(6), doi:10.1029/2012GL051157, 2012.

Kim, Y. S. and Orsi, A. H.: On the Variability of Antarctic Circumpolar Current Fronts Inferred from 1992–2011 Altimetry*, J. Phys. Oceanogr., 44(12), 3054–3071, doi:10.1175/jpo-d-13-0217.1, 2014.

King, J.: A resolution of the Antarctic paradox, Nature, 505(7484), 491–492, doi:10.1038/505491a, 2014.

King, J. C. and Harangozo, S. A.: Climate change in the western Antarctic Peninsula since 1945: observations and possible causes, Ann. Glaciol., 27, 571–575, doi:10.3189/1998AoG27-1-571-575, 1998.

Klemp, J. B. and Lilly, D. R.: The Dynamics of Wave-Induced Downslope Winds, J. Atmos. Sci., 32(2), 320–339, doi:10.1175/1520-0469(1975)032<0320:TDOWID>2.0.CO;2, 1975.

Klinck, J. M.: Heat and salt changes on the continental shelf west of the Antarctic Peninsula between January 1993 and January 1994, J. Geophys. Res. C Ocean., 103(3334), 7617–7636, doi:10.1029/98jc00369, 1998.

Klunder, M. B., Laan, P., De Baar, H. J. W., Middag, R., Neven, I. and Van Ooijen, J.: Dissolved Fe across the Weddell Sea and Drake Passage: impact of DFe on nutrient uptake, Biogeosciences, 11(3), 651–669, doi:10.5194/bg-11-651-2014, 2014.

Köhler, P., Nehrbass-Ahles, C., Schmitt, J., Stocker, T. F. and Fischer, H.: A 156 kyr smoothed history of the atmospheric greenhouse gases CO2, CH4, and N2O and their radiative forcing, Earth Syst. Sci. Data, 9(1), 363–387, doi:10.5194/essd-9-363-2017, 2017.

Kolling, H. M., Stein, R., Fahl, K., Perner, K. and Moros, M.: Short-term variability in late Holocene sea ice cover on the East Greenland Shelf and its driving mechanisms, Palaeogeogr. Palaeoclimatol. Palaeoecol., 485, 336–350, doi:10.1016/j.palaeo.2017.06.024, 2017.

Köseoğlu, D., Belt, S. T., Smik, L., Yao, H., Panieri, G. and Knies, J.: Complementary biomarker-based methods for characterising Arctic sea ice conditions: A case study comparison between multivariate analysis

and the PIP25 index, Geochim. Cosmochim. Acta, 222, 406–420, doi:10.1016/j.gca.2017.11.001, 2018.

Kunz, M., King, M. A., Mills, J. P., Miller, P. E., Fox, A. J., Vaughan, D. G. and Marsh, S. H.: Multi-decadal glacier surface lowering in the Antarctic Peninsula, Geophys. Res. Lett., 39(19), n/a--n/a, doi:10.1029/2012GL052823, 2012.

Lamping, N., Müller, J., Esper, O., Hillenbrand, C., Smith, J. A. and Kuhn, G.: Highly branched isoprenoids reveal onset of deglaciation followed by dynamic sea-ice conditions in the western Amundsen Sea, Antarctica, Quat. Sci. Rev., 228, 106103, doi:10.1016/j.quascirev.2019.106103, 2020.

Lamy, F.: The expedition PS97 of the research vessel POLARSTERN to the Drake Passage in 2016, Reports Polar Mar. Res., 7'01, 1–571, doi:10.2312/BzPM_0702_2016, 2016.

Lamy, F., Kaiser, J., Ninnemann, U., Hebbeln, D., Arz, H. W. and Stoner, J.: Antarctic timing of surface water changes off Chile and Patagonian ice sheet response, Science (80-.)., 304(5679), 1959–1962, doi:10.1126/science.1097863, 2004.

Lamy, F., Kaiser, J., Arz, H. W., Hebbeln, D., Ninnemann, U., Timm, O., Timmermann, A. and Toggweiler, J. R.: Modulation of the bipolar seesaw in the Southeast Pacific during Termination 1, Earth Planet. Sci. Lett., 259(3–4), 400–413, doi:10.1016/j.epsl.2007.04.040, 2007.

Lamy, F., Kilian, R., Arz, H. W., Francois, J.-P., Kaiser, J., Prange, M. and Steinke, T.: Holocene changes in the position and intensity of the southern westerly wind belt, Nat. Geosci., 3(10), 695–699, doi:10.1038/ngeo959, 2010.

Lenton, T. M., Held, H., Kriegler, E., Hall, J. W., Lucht, W., Rahmstorf, S. and Schellnhuber, H. J.: Tipping elements in the Earth's climate system, Proc. Natl. Acad. Sci., 105(6), 1786–1793, doi:10.1073/pnas.0705414105, 2008.

Leventer, A.: The fate of Antarctic "sea ice diatoms" and their use as paleoenvironmental indicators, in Antarctic Research Series, edited by M. P. Lizotte and K. R. Arrigo, pp. 121–137, American Geophysical Union (AGU)., 1998.

Li, J., Xie, S.-P., Cook, E. R., Morales, M. S., Christie, D. A., Johnson, N. C., Chen, F., D'Arrigo, R., Fowler, A. M., Gou, X. and Fang, K.: El Niño modulations over the past seven centuries, Nat. Clim. Chang., 3(9), 822–826, doi:10.1038/nclimate1936, 2013.

Liu, J., Curry, J. A. and Martinson, D. G.: Interpretation of recent Antarctic sea ice variability, Geophys. Res. Lett., 31(2), 2000–2003, doi:10.1029/2003GL018732, 2004.

Livermore, R., Nankivell, A., Eagles, G. and Morris, P.: Paleogene opening of Drake Passage, Earth Planet. Sci. Lett., 236(1–2), 459–470, doi:10.1016/j.epsl.2005.03.027, 2005.

Lizotte, M. P.: The Contributions of Sea Ice Algae to Antarctic Marine Primary Production, Am. Zool., 41(1), 57–73, doi:10.1093/icb/41.1.57, 2001.

Lorenz, S. J. and Lohmann, G.: Acceleration technique for Milankovitch type forcing in a coupled atmosphere-ocean circulation model: Method and application for the Holocene, Clim. Dyn., 23(7–8), 727–743, doi:10.1007/s00382-004-0469-y, 2004.

Lü, X., Liu, X. L., Elling, F. J., Yang, H., Xie, S., Song, J., Li, X., Yuan, H., Li, N. and Hinrichs, K. U.: Hydroxylated isoprenoid GDGTs in Chinese coastal seas and their potential as a paleotemperature proxy for mid-to-low latitude marginal seas, Org. Geochem., 89–90, 31–43, doi:10.1016/j.orggeochem.2015.10.004, 2015.

Marcq, S. and Weiss, J.: Influence of sea ice lead-width distribution on turbulent heat transfer between the ocean and the atmosphere, Cryosphere, 6(1), 143–156, doi:10.5194/tc-6-143-2012, 2012.

Marshall, G. J., Orr, A., van Lipzig, N. P. M. and King, J. C.: The Impact of a Changing Southern Hemisphere Annular Mode on Antarctic Peninsula Summer Temperatures, J. Clim., 19(20), 5388–5404, doi:10.1175/JCLI3844.1, 2006.

Martinson, D. G. and McKee, D. C.: Transport of warm Upper Circumpolar Deep Water onto the western Antarctic Peninsula continental shelf, Ocean Sci., 8(4), 433–442, doi:10.5194/os-8-433-2012, 2012.

Massé, G., Belt, S. T., Crosta, X., Schmidt, S., Snape, I., Thomas, D. N. and Rowland, S. J.: Highly branched isoprenoids as proxies for variable sea ice conditions in the Southern Ocean, Antarct. Sci., 23(05), 487–498, doi:10.1017/S0954102011000381, 2011.

Matsumoto, G. I., Matsumoto, E., Sasaki, K. and Watanuki, K.: Geochemical features of organic matter in sediment cores from Lutzow-Holm Bay, Antarctica, in Organic Matter, Productivity, Accumluation and

Preservation in Recent and Ancient Sediments, edited by J. K. Whelan and J. W. Farrington, pp. 142–175, Columbia University Press, New York., 1992.

Meijers, A. J. S., Meredith, M. P., Abrahamsen, E. P., Morales Maqueda, M. A., Jones, D. C. and Naveira Garabato, A. C.: Wind-driven export of Weddell Sea slope water, J. Geophys. Res. Ocean., 121(10), 7530–7546, doi:10.1002/2016JC011757, 2016.

Meinshausen, M., Smith, S. J., Calvin, K., Daniel, J. S., Kainuma, M. L. T., Lamarque, J.-F., Matsumoto, K., Montzka, S. A., Raper, S. C. B., Riahi, K., Thomson, A., Velders, G. J. M. and van Vuuren, D. P. P. P.: The RCP greenhouse gas concentrations and their extensions from 1765 to 2300, Clim. Change, 109(1–2), 213–241, doi:10.1007/s10584-011-0156-z, 2011.

Melnikov, I. A.: Recent sea ice ecosystem in the Arctic Ocean: a review, in Influence of Climate Change on the Changing Arctic and Sub-Arctic Conditions, pp. 57–71, Springer Netherlands., 2009.

Mendes, C. R. B., Tavano, V. M., Leal, M. C., de Souza, M. S., Brotas, V. and Garcia, C. A. E.: Shifts in the dominance between diatoms and cryptophytes during three late summers in the Bransfield Strait (Antarctic Peninsula), Polar Biol., 36(4), 537–547, doi:10.1007/s00300-012-1282-4, 2013.

Menking, K. M. and Anderson, R. Y.: Contributions of La Niña and El Niño to middle Holocene drought and late Holocene moisture in the American Southwest, Geology, 31(11), 937–940, doi:10.1130/G19807.1, 2003.

Meredith, M., Sommerkorn, M., Cassotta, S., Derksen, C., Ekaykin, A., Hollowed, A., Kofinas, G., Mackintosh, A., Melbourne-Thomas, J., Muelbert, M. M. C., Ottersen, G., Pritchard, H. and Schuu, E. A. G.: Polar Regions, in IPCC Special Report on the Ocean and Cryosphere in a Changing Climate, edited by H.-O. Pörtner, D. C. Roberts, V. Masson-Delmotte, P. Zhai, M. Tignor, E. Poloczanska, K. Mintenbeck, A. Alegría, M. Nicolai, A. Okem, J. Petzold, B. Rama, N. M. Weyer, and 20, pp. 203–320., 2019.

Meredith, M. P. and King, J. C.: Rapid climate change in the ocean west of the Antarctic Peninsula during the second half of the 20th century, Geophys. Res. Lett., 32(19), 1–5, doi:10.1029/2005GL024042, 2005.

Meredith, M. P., Falk, U., Bers, A. V., Mackensen, A., Schloss, I. R., Barlett, E. R., Jerosch, K., Busso, A. S. and Abele, D.: Anatomy of a glacial meltwater discharge event in an Antarctic cove, Philos. Trans. R. Soc. A Math. Phys. Eng. Sci., 376(2122), doi:10.1098/rsta.2017.0163, 2018.

Mezgec, K., Stenni, B., Crosta, X., Masson-Delmotte, V., Baroni, C., Braida, M., Ciardini, V., Colizza, E., Melis, R., Salvatore, M. C., Severi, M., Scarchilli, C., Traversi, R., Udisti, R. and Frezzotti, M.: Holocene sea ice variability driven by wind and polynya efficiency in the Ross Sea, Nat. Commun., 8(1), doi:10.1038/s41467-017-01455-x, 2017.

Milliken, K. T., Anderson, J. B., Wellner, J. S., Bohaty, S. M. and Manley, P. L.: High-resolution Holocene climate record from Maxwell Bay, South Shetland Islands, Antarctica, Geol. Soc. Am. Bull., 121(11–12), 1711–1725, doi:10.1130/B26478.1, 2009.

Mincks, S. L., Smith, C. R., Jeffreys, R. M. and Sumida, P. Y. G.: Trophic structure on the West Antarctic Peninsula shelf: Detritivory and benthic inertia revealed by $δ$13C and $δ$15N analysis, Deep Sea Res. Part II Top. Stud. Oceanogr., 55(22–23), 2502–2514, doi:10.1016/j.dsr2.2008.06.009, 2008.

Minzoni, R. T., Anderson, J. B., Fernandez, R. and Wellner, J. S.: Marine record of Holocene climate, ocean, and cryosphere interactions: Herbert Sound, James Ross Island, Antarctica, Quat. Sci. Rev., 129, 239–259, doi:10.1016/j.quascirev.2015.09.009, 2015.

Moffat, C. and Meredith, M.: Shelf-ocean exchange and hydrography west of the Antarctic Peninsula: A review, Philos. Trans. R. Soc. A Math. Phys. Eng. Sci., 376(2122), doi:10.1098/rsta.2017.0164, 2018.

Moore, J. K. and Abbott, M. R.: Surface chlorophyll concentrations in relation to the Antarctic Polar Front: Seasonal and spatial patterns from satellite observations, J. Mar. Syst., 37(1–3), 69–86, doi:10.1016/S0924-7963(02)00196-3, 2002.

Moran, S. B. and Moore, R. M.: Kinetics of the removal of dissolved aluminum by diatoms in seawater: A comparison with thorium, Geochim. Cosmochim. Acta, 56(9), 3365–3374, doi:10.1016/0016-7037(92)90384-U, 1992.

Moreno, P. I., Vilanova, I., Villa-Martínez, R., Garreaud, R. D., Rojas, M. and De Pol-Holz, R.: Southern Annular Mode-like changes in southwestern Patagonia at centennial timescales over the last three millennia, Nat. Commun., 5(1), 4375, doi:10.1038/ncomms5375, 2014.

Morigi, C., Capotondi, L., Giglio, F., Langone, L., Brilli, M., Turi, B. and Ravaioli, M.: A possible record of the Younger Dryas event in deep-sea sediments of the Southern Ocean (Pacific sector), in Palaeogeography,

Palaeoclimatology, Palaeoecology, vol. 198, pp. 265–278, Elsevier B.V., 2003.

Morrill, C. and Jacobsen, R. M.: How widespread were climate anomalies 8200 years ago?, Geophys. Res. Lett., 32(19), doi:10.1029/2005GL023536, 2005.

Morrison, A. K., England, M. H. and Hogg, A. M.: Response of Southern Ocean Convection and Abyssal Overturning to Surface Buoyancy Perturbations, J. Clim., 28(10), 4263–4278, doi:10.1175/JCLI-D-14-00110.1, 2015.

Mortlock, R. A. and Froelich, P. N.: A simple method for the rapid determination of biogenic opal in pelagic marine sediments, Deep Sea Res. Part A, Oceanogr. Res. Pap., 36(9), 1415–1426, doi:10.1016/0198-0149(89)90092-7, 1989.

Müller, J. and Stein, R.: High-resolution record of late glacial and deglacial sea ice changes in Fram Strait corroborates ice–ocean interactions during abrupt climate shifts, Earth Planet. Sci. Lett., 403, 446–455, doi:10.1016/j.epsl.2014.07.016, 2014.

Müller, J., Massé, G., Stein, R. and Belt, S. T. T.: Variability of sea-ice conditions in the Fram Strait over the past 30,000 years, Nat. Geosci., 2(11), 772–776, doi:10.1038/ngeo665, 2009.

Müller, J., Wagner, A., Fahl, K., Stein, R., Prange, M. and Lohmann, G.: Towards quantitative sea ice reconstructions in the northern North Atlantic: A combined biomarker and numerical modelling approach, Earth Planet. Sci. Lett., 306(3–4), 137–148, doi:10.1016/J.EPSL.2011.04.011, 2011.

Müller, J., Werner, K., Stein, R., Fahl, K., Moros, M. and Jansen, E.: Holocene cooling culminates in sea ice oscillations in Fram Strait, Quat. Sci. Rev., 47, 1–14, doi:10.1016/j.quascirev.2012.04.024, 2012.

Müller, P. J. and Schneider, R.: An automated leaching method for the determination of opal in sediments and particulate matter, Deep. Res. Part I, 40(3), 425–444, doi:https://doi.org/10.1016/0967-0637(93)90140-X, 1993.

Mulvaney, R., Abram, N. J., Hindmarsh, R. C. A., Arrowsmith, C., Fleet, L., Triest, J., Sime, L. C., Alemany, O. and Foord, S.: Recent Antarctic Peninsula warming relative to Holocene climate and ice-shelf history, Nature, 489(7414), 141–144, doi:10.1038/nature11391, 2012.

Navarro-Rodriguez, A., Belt, S. T., Knies, J. and Brown, T. A.: Mapping recent sea ice conditions in the Barents Sea using the proxy biomarker IP25: implications for palaeo sea ice reconstructions, Quat. Sci. Rev., 79, 26–39, doi:10.1016/J.QUASCIREV.2012.11.025, 2013.

Nicholls, K. W., Østerhus, S., Makinson, K., Gammelsrød, T. and Fahrbach, E.: Ice-ocean processes over the continental shelf of the southern Weddell Sea, Antarctica: A review, Rev. Geophys., 47(3), RG3003, doi:10.1029/2007RG000250, 2009.

Nichols, D. S., Nichols, P. D. and Sullivan, C. W.: Fatty acid, sterol and hydrocarbon composition of Antarctic sea ice diatom communities during the spring bloom in McMurdo Sound, Antarct. Sci., 5(3), 271–278, doi:10.1017/S0954102093000367, 1993.

Nichols, P. D., Volkman, J. K., Palmisano, A. C., Smith, G. A. and White, D. C.: Occurrence of an Isoprenoid C25 diunsaturated alkene and high neutral lipid content in Antarctic Sea-Ice Diatom communities, J. Phycol., 24, 90–96, 1988.

Nichols, P. D., Palmisano, A. C., Rayner, M. S., Smith, G. A. and White, D. C.: Changes in the lipid composition of Antarctic sea-ice diatom communities during a spring bloom: an indication of community physiological status, Antarct. Sci., 1(2), 133–140, doi:10.1017/S0954102089000209, 1989.

Nicol, S., Worby, A. and Leaper, R.: Changes in the Antarctic sea ice ecosystem: potential effects on krill and baleen whales, Mar. Freshw. Res., 59(5), 361, doi:10.1071/MF07161, 2008.

Ó Cofaigh, C., Davies, B. J., Livingstone, S. J., Smith, J. A., Johnson, J. S., Hocking, E. P., Hodgson, D. A., Anderson, J. B., Bentley, M. J., Canals, M., Domack, E., Dowdeswell, J. A., Evans, J., Glasser, N. F., Hillenbrand, C.-D., Larter, R. D., Roberts, S. J. and Simms, A. R.: Reconstruction of ice-sheet changes in the Antarctic Peninsula since the Last Glacial Maximum, Quat. Sci. Rev., 100, 87–110, doi:10.1016/j.quascirev.2014.06.023, 2014.

Oksanen, J., Blanchet, F. G., Kindt, R., Legendre, P., Minchin, P. R., O´Hara, R. B., Simpson, G. L., Solymos, P., Stevens, M. H. H. and Wagner, H.: Vegan: Community Ecology Package (R Package Version 2.0-3), 2012.

Oppenheimer, M., Glavovic, B., Hinkel, J., van de Wal, R., Magnan, A. K., Abd-Elgawad, A., Cai, R., Cifuentes-Jara, M., DeConto, R. M., Ghosh, T., Hay, J., Isla, F., Marzeion, B., Meyssignac, B. and Sebesvari,

Z.: Sea Level Rise and Implications for Low Lying Islands, Coasts and Communities., in IPCC Special Report on the Ocean and Cryosphere in a Changing Climate, vol. 355, edited by H.-O. Pörtner, D. C. Roberts, V. Masson-Delmotte, P. Zhai, M. Tignor, E. Poloczanska, K. Mintenbeck, A. Alegría, M. Nicolai, A. Okem, J. Petzold, B. Rama, and N. M. Weyer, pp. 321–446., 2019.

Orsi, A. H., Whitworth, T. and Nowlin, W. D.: On the meridional extent and fronts of the Antarctic Circumpolar Current, Deep. Res. Part I, 42(5), 641–673, doi:10.1016/0967-0637(95)00021-W, 1995.

Orsi, A. H., Smethie, W. M. and Bullister, J. L.: On the total input of Antarctic waters to the deep ocean: A preliminary estimate from chlorofluorocarbon measurements, J. Geophys. Res., 107, 31--, doi:10.1029/2001JC000976, 2002.

Otto-Bliesner, B. L., Braconnot, P., Harrison, S. P., Lunt, D. J., Abe-Ouchi, A., Albani, S., Bartlein, P. J., Capron, E., Carlson, A. E., Dutton, A., Fischer, H., Goelzer, H., Govin, A., Haywood, A., Joos, F., LeGrande, A. N., Lipscomb, W. H., Lohmann, G., Mahowald, N., Nehrbass-Ahles, C., Pausata, F. S. R., Peterschmitt, J.-Y. Y., Phipps, S. J., Renssen, H. and Zhang, Q.: The PMIP4 contribution to CMIP6 - Part 2: Two interglacials, scientific objective and experimental design for Holocene and Last Interglacial simulations, Geosci. Model Dev., 10(11), 3979–4003, doi:10.5194/gmd-10-3979-2017, 2017.

Pachauri, R. K., Mayer, L., Intergovernmental Panel on Climate Change, V. R., Broome, J., Cramer, W., Christ, R., Church, J. A., Clarke, L., Dahe, Q. D., Dasqupta, P., Dubash, N. K., Edenhofer, O., Elgizouli, I., Field, C. B., Forster, P., Friedlingstein, P., Fuglestvedt, J., Gomez-Echeverri, L., Hallegatte, S., Hegerl, G., Howden, M., Jiang, K., Cisneros, B. J., Kattsov, V., Lee, H., Mach, K. J., Marotzke, J., Mastrandrea, M. D., Meyer, L., Minx, J., Mulugetta, Y., O'Brien, K., Oppenheimer, M., Pereira, J. J., Pichs-Madruga, R., Plattner, G.-K., Pörtner, H.-O., Power, S. B., Preston, B., Ravindranath, N. H., Reisinger, A., Riahi, K., Rusticucci, M., Scholes, R., Seyboth, K., Sokona, Y., Stavins, R., Stocker, T. F., Tschakert, P., van Vuuren, D. and van Ypersele, J.-P.: Climate change 2014 : synthesis report, IPCC. [online] Available from: https://research-repository.uwa.edu.au/en/publications/climate-change-2014-synthesis-report-contribution-of-working-grou, 2014.

Park, E., Hefter, J., Fischer, G., Iversen, M. H., Ramondenc, S., Nöthig, E.-M. and Mollenhauer, G.: Seasonality of archaeal lipid flux and GDGT-based thermometry in sinking particles of high-latitude oceans: Fram Strait (79° N) and Antarctic Polar Front (50° S), Biogeosciences, 16(11), 2247–2268, doi:10.5194/bg-16-2247-2019, 2019.

Parkinson, C. L.: Trends in the length of the Southern Ocean sea-ice season, 1979-99, Ann. Glaciol., 34(1), 435–440, doi:10.3189/172756402781817482, 2002.

Parkinson, C. L.: A 40-y record reveals gradual Antarctic sea ice increases followed by decreases at rates far exceeding the rates seen in the Arctic, Proc. Natl. Acad. Sci., 116(29), 14414–14423, doi:10.1073/pnas.1906556116, 2019.

Parkinson, C. L. and Cavalieri, D. J.: Antarctic sea ice variability and trends, 1979–2010, Cryosph., 6, 871–880, doi:10.5194/tc-6-871-2012, 2012.

Pearson, P. N. and Palmer, M. R.: Atmospheric carbon dioxide concentrations over the past 60 million years, Nature, 406(6797), 695–699, doi:10.1038/35021000, 2000.

Pedro, J. B., Bostock, H. C., Bitz, C. M., He, F., Vandergoes, M. J., Steig, E. J., Chase, B. M., Krause, C. E., Rasmussen, S. O., Markle, B. R. and Cortese, G.: The spatial extent and dynamics of the Antarctic Cold Reversal, Nat. Geosci., 9(1), 51–55, doi:10.1038/ngeo2580, 2016.

Peterson, B. G., Carl, P., Boudt, K., Bennett, R., Ulrich, J., Zivot, E., Cornilly, D., Hung, E., Lestel, M., Balkissoon, K., Wuertz, D., Christidis, A. A., Martin, R. D., Zhou, Z. "Zenith" and Shea, J. M.: Econometric tools for performance and risk analysis, , 240 [online] Available from: https://github.com/braverock/PerformanceAnalytics, 2020.

Petrich, C. and Eicken, H.: Overview of sea ice growth and properties, in Sea Ice: Third Edition, pp. 1–41, Wiley Blackwell., 2016.

Pike, J., Allen, C. S., Leventer, A., Stickley, C. E. and Pudsey, C. J.: Comparison of contemporary and fossil diatom assemblages from the western Antarctic Peninsula shelf, Mar. Micropaleontol., 67(3–4), 274–287, doi:10.1016/J.MARMICRO.2008.02.001, 2008.

Pike, J., Swann, G. E. A., Leng, M. J. and Snelling, A. M.: Glacial discharge along the west Antarctic Peninsula during the Holocene, Nat. Geosci., 6(3), 199–202, doi:10.1038/ngeo1703, 2013.

Pisias, N. G. and Mix, A. C.: Aliasing of the geologic record and the search for long-period Milankovitch

cycles, Paleoceanography, 3(5), 613–619, doi:10.1029/PA003i005p00613, 1988.

Porter, S. E., Parkinson, C. L. and Mosley-Thompson, E.: Bellingshausen Sea ice extent recorded in an Antarctic Peninsula ice core, J. Geophys. Res. Atmos., 121(23), 13,813-886,900, doi:10.1002/2016JD025626, 2016.

QGIS Development Team: QGIS Geographic Information System, [online] Available from: http://qgis.osgeo.org, 2018.

R Core Team: R: a Language and Environment for Statistical Computing, R Foundation for Statistical computing, Vienna., 2017.

Raddatz, T. J., Reick, C. H., Knorr, W., Kattge, J., Roeckner, E., Schnur, R., Schnitzler, K. G., Wetzel, P. and Jungclaus, J.: Will the tropical land biosphere dominate the climate-carbon cycle feedback during the twenty-first century?, Clim. Dyn., 29(6), 565–574, doi:10.1007/s00382-007-0247-8, 2007.

Ragueneau, O., Tréguer, P., Leynaert, A., Anderson, R. . F., Brzezinski, M. . A., DeMaster, D. . J., Dugdale, R. . C., Dymond, J., Fischer, G., François, R., Heinze, C., Maier-Reimer, E., Martin-Jézéquel, V., Nelson, D. . M. and Quéguiner, B.: A review of the Si cycle in the modern ocean: recent progress and missing gaps in the application of biogenic opal as a paleoproductivity proxy, Glob. Planet. Change, 26(4), 317–365, doi:10.1016/S0921-8181(00)00052-7, 2000.

Rahaman, W., Thamban, M. and Laluraj, C. M.: Twentieth-century sea ice variability in the Weddell Sea and its effect on moisture transport: Evidence from a coastal East Antarctic ice core record, The Holocene, 26(3), 338–349, doi:10.1177/0959683615609749, 2016.

Rahaman, W., Chatterjee, S., Ejaz, T. and Thamban, M.: Increased influence of ENSO on Antarctic temperature since the Industrial Era, Sci. Rep., 9(1), 6006, doi:10.1038/s41598-019-42499-x, 2019.

Rebolledo, L., Bertrand, S., Lange, C. B., Tapia, F. J., Quiroga, E., Troch, M., Silva, N., Cárdenas, P. and Pantoja, S.: Compositional and biogeochemical variations of sediments across the terrestrial-marine continuum of the Baker-Martínez fjord system (Chile, 48°S), Prog. Oceanogr., 174, 89–104, doi:10.1016/j.pocean.2018.12.004, 2019.

Reimer, P. J., Bard, E., Bayliss, A., Beck, J. W., Blackwell, P. G., Ramsey, C. B., Buck, C. E., Cheng, H., Edwards, R. L., Friedrich, M., Grootes, P. M., Guilderson, T. P., Haflidason, H., Hajdas, I., Hatté, C., Heaton, T. J., Hoffmann, D. L., Hogg, A. G., Hughen, K. A., Kaiser, K. F., Kromer, B., Manning, S. W., Niu, M., Reimer, R. W., Richards, D. A., Scott, E. M., Southon, J. R., Staff, R. A., Turney, C. S. M. and van der Plicht, J.: IntCal13 and Marine13 Radiocarbon Age Calibration Curves 0–50,000 Years cal BP, Radiocarbon, 55(4), 1869–1887, doi:10.2458/azu_js_rc.55.16947, 2013.

Reynhout, S. A., Sagredo, E. A., Kaplan, M. R., Aravena, J. C., Martini, M. A., Moreno, P. I., Rojas, M., Schwartz, R. and Schaefer, J. M.: Holocene glacier fluctuations in Patagonia are modulated by summer insolation intensity and paced by Southern Annular Mode-like variability, Quat. Sci. Rev., 220, 178–187, doi:10.1016/j.quascirev.2019.05.029, 2019.

Reynolds, R. W., Rayner, N. A., Smith, T. M., Stokes, D. C., Wang, W., Reynolds, R. W., Rayner, N. A., Smith, T. M., Stokes, D. C. and Wang, W.: An Improved In Situ and Satellite SST Analysis for Climate, J. Clim., 15(13), 1609–1625, doi:10.1175/1520-0442(2002)015<1609:AIISAS>2.0.CO;2, 2002.

Reynolds, R. W., Smith, T. M., Liu, C., Chelton, D. B., Casey, K. S., Schlax, M. G., Reynolds, R. W., Smith, T. M., Liu, C., Chelton, D. B., Casey, K. S. and Schlax, M. G.: Daily High-Resolution-Blended Analyses for Sea Surface Temperature, J. Clim., 20(22), 5473–5496, doi:10.1175/2007JCLI1824.1, 2007.

Rhodes, R. H., Bertler, N. A. N., Baker, J. A., Sneed, S. B., Oerter, H. and Arrigo, K. R.: Sea ice variability and primary productivity in the Ross Sea, Antarctica, from methylsulphonate snow record, Geophys. Res. Lett., 36(10), L10704, doi:10.1029/2009GL037311, 2009.

Riaux-Gobin, C. and Poulin, M.: Possible symbiosis of Berkeleya adeliensis Medlin, Synedropsis fragilis (Manguin) Hasle et al. and Nitzschia lecointei Van Heurck (bacillariophyta) associated with land-fast ice in Adélie Land, Antarctica, Diatom Res., 19(2), 265–274, doi:10.1080/0269249X.2004.9705874, 2004.

Riaux-Gobin, C., Poulin, M., Prodon, R. and Treguer, P.: Land-fast ice microalgal and phytoplanktonic communities (Adélie Land, Antarctica) in relation to environmental factors during ice break-up, Antarct. Sci., 15(3), 353–364, doi:10.1017/S0954102003001378, 2003.

Rignot, E., Mouginot, J., Scheuchl, B., van den Broeke, M., van Wessem, M. J. and Morlighem, M.: Four decades of Antarctic Ice Sheet mass balance from 1979–2017, Proc. Natl. Acad. Sci., 116(4), 1095–1103, doi:10.1073/pnas.1812883116, 2019.

Rintoul, S. R.: Rapid freshening of Antarctic Bottom Water formed in the Indian and Pacific oceans, Geophys. Res. Lett., 34(6), doi:10.1029/2006GL028550, 2007.

Roche, D. M., Crosta, X. and Renssen, H.: Evaluating Southern Ocean sea-ice for the Last Glacial Maximum and pre-industrial climates: PMIP-2 models and data evidence, Quat. Sci. Rev., 56, 99–106, doi:10.1016/j.quascirev.2012.09.020, 2012.

Romero, O. E., Armand, L. K., Crosta, X. and Pichon, J. J.: The biogeography of major diatom taxa in Southern Ocean surface sediments: 3. Tropical/Subtropical species, Palaeogeogr. Palaeoclimatol. Palaeoecol., 223(1–2), 49–65, doi:10.1016/j.palaeo.2005.03.027, 2005.

Rontani, J.-F., Belt, S. T., Vaultier, F., Brown, T. A. and Massé, G.: Autoxidative and Photooxidative Reactivity of Highly Branched Isoprenoid (HBI) Alkenes, Lipids, 49(5), 481–494, doi:10.1007/s11745-014-3891-x, 2014.

Rontani, J.-F., Aubert, C. and Belt, S. T.: Electron ionization mass spectrometry fragmentation and multiple reaction monitoring quantification of bacterial metabolites of the sea ice biomarker proxy IP_{25} in Arctic sediments, Rapid Commun. Mass Spectrom., 32(10), 775–783, doi:10.1002/rcm.8101, 2018a.

Rontani, J., Smik, L. and Belt, S. T.: Autoxidation of the sea ice biomarker proxy IPSO25 in the near-surface oxic layers of Arctic and Antarctic sediments, Org. Geochem., 129, 63–76, doi:10.1016/J.ORGGEOCHEM.2019.02.002, 2019a.

Rontani, J. F., Belt, S. T., Vaultier, F. and Brown, T. A.: Visible light induced photo-oxidation of highly branched isoprenoid (HBI) alkenes: Significant dependence on the number and nature of double bonds, Org. Geochem., 42(7), 812–822, doi:10.1016/j.orggeochem.2011.04.013, 2011.

Rontani, J. F., Charriere, B., Petit, M., Vaultier, F., Heipieper, H. J., Link, H., Chaillou, G. and Sempéré, R.: Degradation state of organic matter in surface sediments from the Southern Beaufort Sea: A lipid approach, Biogeosciences, 9(9), 3513–3530, doi:10.5194/bg-9-3513-2012, 2012.

Rontani, J. F., Belt, S. T. and Amiraux, R.: Biotic and abiotic degradation of the sea ice diatom biomarker IP25 and selected algal sterols in near-surface Arctic sediments, Org. Geochem., 118, 73–88, doi:10.1016/j.orggeochem.2018.01.003, 2018b.

Rontani, J. F., Smik, L., Belt, S. T., Vaultier, F., Armbrecht, L., Leventer, A. and Armand, L. K.: Abiotic degradation of highly branched isoprenoid alkenes and other lipids in the water column off East Antarctica, Mar. Chem., 210, 34–47, doi:10.1016/j.marchem.2019.02.004, 2019b.

Rothwell, R. G. and Croudace, I. w.: Twenty Years of XRF Core Scanning Marine Sediments: What Do Geochemical Proxies Tell Us?, pp. 25–102, Springer, Dordrecht., 2015.

Royles, J., Amesbury, M. J., Convey, P., Griffiths, H., Hodgson, D. A., Leng, M. J. and Charman, D. J.: Plants and Soil Microbes Respond to Recent Warming on the Antarctic Peninsula, Curr. Biol., 23(17), 1702–1706, doi:10.1016/j.cub.2013.07.011, 2013.

Royles, J., Amesbury, M. J., Roland, T. P., Jones, G. D., Convey, P., Griffiths, H., Hodgson, D. A. and Charman, D. J.: Moss stable isotopes (carbon-13, oxygen-18) and testate amoebae reflect environmental inputs and microclimate along a latitudinal gradient on the Antarctic Peninsula, Oecologia, 181(3), 931–945, doi:10.1007/s00442-016-3608-3, 2016.

Sanchez-Cabeza, J.-A., Ruiz-Fernández, A. C., Ontiveros-Cuadras, J. F., Pérez Bernal, L. H. and Olid, C.: Monte Carlo uncertainty calculation of 210Pb chronologies and accumulation rates of sediments and peat bogs, Quat. Geochronol., 23, 80–93, doi:10.1016/J.QUAGEO.2014.06.002, 2014.

Sanchez, N., Reiss, C. S., Holm-Hansen, O., Hewes, C. D., Bizsel, K. C. and Ardelan, M. V: Weddell-Scotia Confluence Effect on the Iron Distribution in Waters Surrounding the South Shetland (Antarctic Peninsula) and South Orkney (Scotia Sea) Islands During the Austral Summer in 2007 and 2008, Front. Mar. Sci., 6(December), 1–16, doi:10.3389/fmars.2019.00771, 2019.

Sangrà, P., Gordo, C., Hernández-Arencibia, M., Marrero-Díaz, A., Rodríguez-Santana, A., Stegner, A., Martínez-Marrero, A., Pelegrí, J. L. and Pichon, T.: The Bransfield current system, Deep Sea Res. Part I Oceanogr. Res. Pap., 58(4), 390–402, doi:10.1016/J.DSR.2011.01.011, 2011.

Sangrà, P., Stegner, A., Hernández-Arencibia, M., Marrero-Díaz, Á., Salinas, C., Aguiar-González, B., Henríquez-Pastene, C. and Mouriño-Carballido, B.: The Bransfield Gravity Current, Deep. Res. Part I Oceanogr. Res. Pap., 119(November 2016), 1–15, doi:10.1016/j.dsr.2016.11.003, 2017.

Scher, H. D. and Martin, E. E.: Timing and Climatic Consequences of the Opening of Drake Passage, Science (80-.)., 312(5772), 428–430, doi:10.1126/science.1120044, 2006.

Scherer, R. P.: A new method for the determination of absolute abundance of diatoms and other silt-sized sedimentary particles, J. Paleolimnol., 12(2), 171–179, doi:10.1007/BF00678093, 1994.

Schlitzer, R.: Ocean Data View. Version 4.7.10, [online] Available from: http://odv.awi.de, 2017.

Schlosser, E., Haumann, F. A. and Raphael, M. N.: Atmospheric influences on the anomalous 2016 Antarctic sea ice decay, Cryosph., 12(3), 1103–1119, doi:10.5194/tc-12-1103-2018, 2018.

Schmidt, K., Brown, T., Belt, S., Ireland, L., Taylor, K. W. R., Thorpe, S., Ward, P. and Atkinson, A.: Do pelagic grazers benefit from sea ice? Insights from the Antarctic sea ice proxy IPSO25, Biogeosciences, 15(7), 1987–2006, doi:10.5194/bg-15-1987-2018, 2018.

Schofield, O., Brown, M., Kohut, J., Nardelli, S., Saba, G., Waite, N. and Ducklow, H.: Changes in the upper ocean mixed layer and phytoplankton productivity along the West Antarctic Peninsula, Philos. Trans. R. Soc. A Math. Phys. Eng. Sci., 376(2122), doi:10.1098/rsta.2017.0173, 2018.

Schrader, H. and Gersonde, R.: Diatoms and silicoflagellates, in Micropaleontological Methods and Techniques - An Excercise on an Eight Meter Section of the Lower Pliocene of Capo Rossello, Sicily, Utrecht Micropaleontological Bulletins, vol. 17, edited by W. J. Zachariasse, W. R. Riedel, A. Sanfilippo, R. R. Schmidt, M. J. Brolsma, H. J. Schrader, R. Gersonde, M. M. Drooger, and J. A. Broekman, pp. 129–176., 1978.

Schwarz, G.: Estimating the Dimension of a Model, Ann. Stat., 6(2), 461–464, doi:10.1214/AOS/1176344136, 1978.

Shevenell, A. E., Ingalls, A. E., Domack, E. W. and Kelly, C.: Holocene Southern Ocean surface temperature variability west of the Antarctic Peninsula, Nature, 470(7333), 250–254, doi:10.1038/nature09751, 2011.

Shi, X. and Lohmann, G.: Simulated response of the mid-Holocene Atlantic meridional overturning circulation in ECHAM6-FESOM/MPIOM, J. Geophys. Res. Ocean., 121(8), 6444–6469, doi:10.1002/2015JC011584, 2016.

Shi, X., Lohmann, G., Sidorenko, D. and Yang, H.: Early-Holocene simulations using different forcings and resolutions in AWI-ESM, The Holocene, 095968362090863, doi:10.1177/0959683620908634, 2020.

Sidorenko, D., Goessling, H. F., Koldunov, N. V, Scholz, P., Danilov, S., Barbi, D., Cabos, W., Gurses, O., Harig, S., Hinrichs, C., Juricke, S., Lohmann, G., Losch, M., Mu, L., Rackow, T., Rakowsky, N., Sein, D., Semmler, T., Shi, X., Stepanek, C., Streffing, J., Wang, Q., Wekerle, C., Yang, H. and Jung, T.: Evaluation of FESOM2.0 coupled to ECHAM6.3: Pre-industrial and HighResMIP simulations, J. Adv. Model. Earth Syst., 2019MS001696, doi:10.1029/2019MS001696, 2019.

Siegert, M., Atkinson, A., Banwell, A., Brandon, M., Convey, P., Davies, B., Downie, R., Edwards, T., Hubbard, B., Marshall, G., Rogelj, J., Rumble, J., Stroeve, J. and Vaughan, D.: The Antarctic Peninsula Under a 1.5°C Global Warming Scenario, Front. Environ. Sci., 7(JUN), 1–7, doi:10.3389/fenvs.2019.00102, 2019.

Simpson, G. L. and Oksanen, J.: Analogue: Analogue Matching and Modern Analogue Technique Transfer Function Models. R Package Version 0.8-2, 2012.

Sinclair, K. E., Bertler, N. A. N., Bowen, M. M. and Arrigo, K. R.: Twentieth century sea-ice trends in the Ross Sea from a high-resolution, coastal ice-core record, Geophys. Res. Lett., 41(10), 3510–3516, doi:10.1002/2014GL059821, 2014.

Sinninghe Damsté, J. S. S., Rijpstra, W. I. C. I. C., Coolen, M. J. L. J. L., Schouten, S. and Volkman, J. K. K.: Rapid sulfurisation of highly branched isoprenoid (HBI) alkenes in sulfidic Holocene sediments from Ellis Fjord, Antarctica, Org. Geochem., 38(1), 128–139, doi:10.1016/j.orggeochem.2006.08.003, 2007.

Sivia, D. S. and Skilling, J.: Data analysis : a Bayesian tutorial., Oxford University Press., 2006.

Sjunneskog, C. and Taylor, F.: Postglacial marine diatom record of the Palmer Deep, Antarctic Peninsula (ODP Leg 178, Site 1098) 1. Total diatom abundance, Paleoceanography, 17(3), PAL 4--1--PAL 4--8, doi:10.1029/2000PA000563, 2002.

Smetacek, V., Scharek, R., Gordon, L. I., Eicken, H., Fahrbach, E., Rohardt, G. and Moore, S.: Early spring phytoplankton blooms in ice platelet layers of the southern Weddell Sea, Antarctica, Deep Sea Res. Part A, Oceanogr. Res. Pap., 39(2), 153–168, doi:10.1016/0198-0149(92)90102-Y, 1992.

Smik, L.: Development of biomarker-based proxies for paleo sea-ice reconstructions, University of Plymouth., 2016.

Smik, L., Belt, S. T., Lieser, J. L., Armand, L. K. and Leventer, A.: Distributions of highly branched

isoprenoid alkenes and other algal lipids in surface waters from East Antarctica: Further insights for biomarker-based paleo sea-ice reconstruction, Org. Geochem., 95, 71–80, doi:10.1016/J.ORGGEOCHEM.2016.02.011, 2016a.

Smik, L., Cabedo-Sanz, P. and Belt, S. T.: Semi-quantitative estimates of paleo Arctic sea ice concentration based on source-specific highly branched isoprenoid alkenes: A further development of the PIP 25 index, Org. Geochem., 92, 63–69, doi:10.1016/j.orggeochem.2015.12.007, 2016b.

Smith, J. A., Graham, A. G. C., Post, A. L., Hillenbrand, C.-D., Bart, P. J. and Powell, R. D.: The marine geological imprint of Antarctic ice shelves, Nat. Commun., 10(1), 5635, doi:10.1038/s41467-019-13496-5, 2019.

Soulet, G., Ménot, G., Garreta, V., Rostek, F., Zaragosi, S., Lericolais, G. and Bard, E.: Black Sea "Lake" reservoir age evolution since the Last Glacial - Hydrologic and climatic implications, Earth Planet. Sci. Lett., 308(1–2), 245–258, doi:10.1016/j.epsl.2011.06.002, 2011.

Stammerjohn, S. E., Martinson, D. G., Smith, R. C. and Iannuzzi, R. A.: Sea ice in the western Antarctic Peninsula region: Spatio-temporal variability from ecological and climate change perspectives, Deep. Res. Part II Top. Stud. Oceanogr., 55(18–19), 2041–2058, doi:10.1016/j.dsr2.2008.04.026, 2008a.

Stammerjohn, S. E., Martinson, D. G., Smith, R. C., Yuan, X. and Rind, D.: Trends in Antarctic annual sea ice retreat and advance and their relation to El Niño–Southern Oscillation and Southern Annular Mode variability, J. Geophys. Res., 113(C3), C03S90, doi:10.1029/2007JC004269, 2008b.

Stastna, V.: Spatio-temporal changes in surface air temperature in the region of the northern Antarctic Peninsula and south Shetland islands during 1950–2003, Polar Sci., 4(1), 18–33, doi:10.1016/j.polar.2010.02.001, 2010.

Stein, R., Fahl, K. and Müller, J.: Proxy Reconstruction of Cenozoic Arctic Ocean Sea-Ice History: from IRD to IP25, Polarforschung, 82(1), 37–71, 2012.

Stein, R., Fahl, K., Gierz, P., Niessen, F. and Lohmann, G.: Arctic Ocean sea ice cover during the penultimate glacial and the last interglacial, Nat. Commun., 8(1), 373, doi:10.1038/s41467-017-00552-1, 2017.

Stenni, B., Masson-Delmotte, V., Johnsen, S., Jouzel, J., Longinelli, A., Monnin, E., Röthlisberger, R. and Selmo, E.: An Oceanic Cold Reversal During the Last Deglaciation, Science (80-.)., 293(5537), 2074–2077, doi:10.1126/science.1059702, 2001.

Stevens, B., Giorgetta, M., Esch, M., Mauritsen, T., Crueger, T., Rast, S., Salzmann, M., Schmidt, H., Bader, J., Block, K., Brokopf, R., Fast, I., Kinne, S., Kornblueh, L., Lohmann, U., Pincus, R., Reichler, T. and Roeckner, E.: Atmospheric component of the MPI-M Earth System Model: ECHAM6, J. Adv. Model. Earth Syst., 5(2), 146–172, doi:10.1002/jame.20015, 2013.

Stroeve, J. C., Jenouvrier, S., Campbell, G. G., Barbraud, C. and Delord, K.: Mapping and assessing variability in the Antarctic marginal ice zone, pack ice and coastal polynyas in two sea ice algorithms with implications on breeding success of snow petrels, Cryosph., 10(4), 1823–1843, doi:10.5194/tc-10-1823-2016, 2016.

Stuiver, M., Reimer, P. J. and Reimer, R. W.: Calib 7.1, [online] Available from: http://calib.org, 2018.

Taylor, F. and Sjunneskog, C.: Postglacial marine diatom record of the Palmer Deep, Antarctic Peninsula (ODP Leg 178, Site 1098) 2. Diatom assemblages, Paleoceanography, 17(3), PAL 2--1--PAL 2--12, doi:10.1029/2000PA000564, 2002.

Taylor, F., Whitehead, J. and Domack, E.: Holocene paleoclimate change in the Antarctic Peninsula: Evidence from the diatom, sedimentary and geochemical record, Mar. Micropaleontol., 41(1–2), 25–43, doi:10.1016/S0377-8398(00)00049-9, 2001.

Thomas, Allen, Etourneau, King, Severi, Winton, Mueller, Crosta and Peck: Antarctic Sea Ice Proxies from Marine and Ice Core Archives Suitable for Reconstructing Sea Ice over the past 2000 Years, Geosciences, 9(12), 506, doi:10.3390/geosciences9120506, 2019.

Thomas, D. and Dieckmann, G.: Biogeochemistry of Antarctic Sea Ice, in Oceanography and Marine Biology: an Annual review, edited by R. N. Gibson, M. Barnes, and R. J. A. Atkinson, pp. 143–169, Taylor & Francis, London., 2002.

Thomas, D. N.: Sea Ice, edited by D. N. Thomas, John Wiley & Sons, Ltd, Chichester, UK., 2017.

Thomas, E. R. and Abram, N. J.: Ice core reconstruction of sea ice change in the Amundsen-Ross Seas since

1702 A.D., Geophys. Res. Lett., 43(10), 5309–5317, doi:10.1002/2016GL068130, 2016.

Thomas, E. R. and Bracegirdle, T. J.: Precipitation pathways for five new ice core sites in Ellsworth Land, West Antarctica, Clim. Dyn., 44(7–8), 2067–2078, doi:10.1007/s00382-014-2213-6, 2015.

Thompson, A. F.: The atmospheric ocean: eddies and jets in the Antarctic Circumpolar Current, Philos. Trans. R. Soc. A Math. Phys. Eng. Sci., 366(1885), 4529–4541, doi:10.1098/rsta.2008.0196, 2008.

Thompson, A. F., Heywood, K. J., Thorpe, S. E., Renner, A. H. H. and Trasviña, A.: Surface Circulation at the Tip of the Antarctic Peninsula from Drifters, J. Phys. Oceanogr., 39(1), 3–26, doi:10.1175/2008JPO3995.1, 2009.

Thornton, S. F. and McManus, J.: Application of Organic Carbon and Nitrogen Stable Isotope and C/N Ratios as Source Indicators of Organic Matter Provenance in Estuarine Systems: Evidence from the Tay Estuary, Scotland, Estuar. Coast. Shelf Sci., 38(3), 219–233, doi:10.1006/ecss.1994.1015, 1994.

Timmermann, A., Okumura, Y., An, S.-I., Clement, A., Dong, B., Guilyardi, E., Hu, A., Jungclaus, J. H., Renold, M., Stocker, T. F., Stouffer, R. J., Sutton, R., Xie, S.-P. and Yin, J.: The Influence of a Weakening of the Atlantic Meridional Overturning Circulation on ENSO, J. Clim., 20(19), 4899–4919, doi:10.1175/JCLI4283.1, 2007.

Tortell, P. D., Mills, M. M., Payne, C. D., Maldonado, M. T., Chierici, M., Fransson, A., Alderkamp, A. C. and Arrigo, K. R.: Inorganic C utilization and C isotope fractionation by pelagic and sea ice algal assemblages along the Antarctic continental shelf, Mar. Ecol. Prog. Ser., 483, 47–66, doi:10.3354/meps10279, 2013.

Trachsel, M. and Telford, R. J.: All age–depth models are wrong, but are getting better, The Holocene, 27(6), 860–869, doi:10.1177/0959683616675939, 2017.

Trevena, A. J. and Jones, G. B.: Dimethylsulphide and dimethylsulphoniopropionate in Antarctic sea ice and their release during sea ice melting, Mar. Chem., 98(2–4), 210–222, doi:10.1016/j.marchem.2005.09.005, 2006.

Turner, J., Orr, A., Gudmundsson, G. H., Jenkins, A., Bingham, R. G., Hillenbrand, C.-D. and Bracegirdle, T. J.: Atmosphere-ocean-ice interactions in the Amundsen Sea Embayment, West Antarctica, Rev. Geophys., 55(1), 235–276, doi:10.1002/2016RG000532, 2017.

Turner, J., Marshall, G. J., Clem, K., Colwell, S., Phillips, T. and Lu, H.: Antarctic temperature variability and change from station data, Int. J. Climatol., (June), joc.6378, doi:10.1002/joc.6378, 2019.

Vaughan, D. G., Marshall, G. J., Connolley, W. M., Parkinson, C., Mulvaney, R., Hodgson, D. A., King, J. C., Pudsey, C. J. and Turner, J.: Recent Rapid Regional Climate Warming on the Antarctic Peninsula, Clim. Change, 60(3), 243–274, doi:10.1023/A:1026021217991, 2003.

Venkatesan, M. I.: Organic geochemistry of marine sediments in Antarctic region: Marine lipids in McMurdo Sound, Org. Geochem., 12(I), 13–27, 1988.

De Vernal, A., Gersonde, R., Goosse, H., Seidenkrantz, M. S. and Wolff, E. W.: Sea ice in the paleoclimate system: The challenge of reconstructing sea ice from proxies - an introduction, Quat. Sci. Rev., 79, 1–8, doi:10.1016/j.quascirev.2013.08.009, 2013.

Vernet, M., Martinson, D., Iannuzzi, R., Stammerjohn, S., Kozlowski, W., Sines, K., Smith, R. and Garibotti, I.: Primary production within the sea-ice zone west of the Antarctic Peninsula: I—Sea ice, summer mixed layer, and irradiance, Deep Sea Res. Part II Top. Stud. Oceanogr., 55(18–19), 2068–2085, doi:10.1016/j.dsr2.2008.05.021, 2008.

Volkman, J. K.: A review of sterol markers for marine and terrigenous organic matter, Org. Geochem., 9(2), 83–99, doi:10.1016/0146-6380(86)90089-6, 1986.

Volkman, J. K.: Sterols in microorganisms, Appl. Microbiol. Biotechnol., 60(5), 495–506, doi:10.1007/s00253-002-1172-8, 2003.

Volkman, J. K.: Lipid markers for marine organic matter, in Marine Organic Matter, edited by J. K. Volkman, pp. 27–70, Springer-Verlag, Berlin, Heidelberg., 2006.

Vorrath, M.-E., Müller, J., Esper, O., Mollenhauer, G., Haas, C., Schefuß, E. and Fahl, K.: Highly branched isoprenoids for Southern Ocean sea ice reconstructions: a pilot study from the Western Antarctic Peninsula, Biogeosciences, 16(15), 2961–2981, doi:10.5194/bg-16-2961-2019, 2019.

Wacker, L., Bonani, G., Friedrich, M., Hajdas, I., Kromer, B., Němec, M., Ruff, M., Suter, M., Synal, H.-A. and Vockenhuber, C.: MICADAS: Routine and High-Precision Radiocarbon Dating, Radiocarbon, 52(02), 252–262, doi:10.1017/S0033822200045288, 2010.

WAIS Divide Project Members, Fudge, T. J., Steig, E. J., Markle, B. R., Schoenemann, S. W., Ding, Q., Taylor, K. C., McConnell, J. R., Brook, E. J., Sowers, T., White, J. W. C., Alley, R. B., Cheng, H., Clow, G. D., Cole-Dai, J., Conway, H., Cuffey, K. M., Edwards, J. S., Lawrence Edwards, R., Edwards, R., Fegyveresi, J. M., Ferris, D., Fitzpatrick, J. J., Johnson, J., Hargreaves, G., Lee, J. E., Maselli, O. J., Mason, W., McGwire, K. C., Mitchell, L. E., Mortensen, N., Neff, P., Orsi, A. J., Popp, T. J., Schauer, A. J., Severinghaus, J. P., Sigl, M., Spencer, M. K., Vaughn, B. H., Voigt, D. E., Waddington, E. D., Wang, X. and Wong, G. J.: Onset of deglacial warming in West Antarctica driven by local orbital forcing, Nature, 500(7463), 440–444, doi:10.1038/nature12376, 2013.

WAIS Divide Project Members, Buizert, C., Adrian, B., Ahn, J., Albert, M., Alley, R. B., Baggenstos, D., Bauska, T. K., Bay, R. C., Bencivengo, B. B., Bentley, C. R., Brook, E. J., Chellman, N. J., Clow, G. D., Cole-Dai, J., Conway, H., Cravens, E., Cuffey, K. M., Dunbar, N. W., Edwards, J. S., Fegyveresi, J. M., Ferris, D. G., Fitzpatrick, J. J., Fudge, T. J., Gibson, C. J., Gkinis, V., Goetz, J. J., Gregory, S., Hargreaves, G. M., Iverson, N., Johnson, J. A., Jones, T. R., Kalk, M. L., Kippenhan, M. J., Koffman, B. G., Kreutz, K., Kuhl, T. W., Lebar, D. A., Lee, J. E., Marcott, S. A., Markle, B. R., Maselli, O. J., McConnell, J. R., McGwire, K. C., Mitchell, L. E., Mortensen, N. B., Neff, P. D., Nishiizumi, K., Nunn, R. M., Orsi, A. J., Pasteris, D. R., Pedro, J. B., Pettit, E. C., Price, P. B., Priscu, J. C., Rhodes, R. H., Rosen, J. L., Schauer, A. J., Schoenemann, S. W., Sendelbach, P. J., Severinghaus, J. P., Shturmakov, A. J., Sigl, M., Slawny, K. R., Souney, J. M., Sowers, T. A., Spencer, M. K., Steig, E. J., Taylor, K. C., Twickler, M. S., Vaughn, B. H., Voigt, D. E., Waddington, E. D., Welten, K. C., Wendricks, A. W., White, J. W. C., Winstrup, M., Wong, G. J. and Woodruff, T. E.: Precise interpolar phasing of abrupt climate change during the last ice age, Nature, 520(7549), 661–665, doi:10.1038/nature14401, 2015.

Warnock, J. P. and Scherer, R. P.: A revised method for determining the absolute abundance of diatoms, J. Paleolimnol., 53(1), 157–163, doi:10.1007/s10933-014-9808-0, 2014.

Wefer, G., Fischer, G., Füetterer, D. and Gersonde, R.: Seasonal particle flux in the Bransfield Strait, Antartica, Deep Sea Res. Part A. Oceanogr. Res. Pap., 35(6), 891–898, doi:10.1016/0198-0149(88)90066-0, 1988.

Williams, G., Maksym, T., Wilkinson, J., Kunz, C., Murphy, C., Kimball, P. and Singh, H.: Thick and deformed Antarctic sea ice mapped with autonomous underwater vehicles, Nat. Geosci., 8(1), 61–67, doi:10.1038/ngeo2299, 2015.

Willmott, V., Domack, E. W., Canals, M. and Brachfeld, S.: A high resolution relative paleointensity record from the Gerlache-Boyd paleo-ice stream region, northern Antarctic Peninsula, Quat. Res., 66(1), 1–11, doi:10.1016/j.yqres.2006.01.006, 2006.

Wolff, E. W., Rankin, A. M. and Röthlisberger, R.: An ice core indicator of Antarctic sea ice production?, Geophys. Res. Lett., 30(22), 2–5, doi:10.1029/2003GL018454, 2003.

Wolff, E. W., Fischer, H., Fundel, F., Ruth, U., Twarloh, B., Littot, G. C., Mulvaney, R., Röthlisberger, R., de Angelis, M., Boutron, C. F., Hansson, M., Jonsell, U., Hutterli, M. A., Lambert, F., Kaufmann, P., Stauffer, B., Stocker, T. F., Steffensen, J. P., Bigler, M., Siggaard-Andersen, M. L., Udisti, R., Becagli, S., Castellano, E., Severi, M., Wagenbach, D., Barbante, C., Gabrielli, P. and Gaspari, V.: Southern Ocean sea-ice extent, productivity and iron flux over the past eight glacial cycles, Nature, 440(7083), 491–496, doi:10.1038/nature04614, 2006.

Wollenburg, J. E., Katlein, C., Nehrke, G., Nöthig, E.-M., Matthiessen, J., Wolf- Gladrow, D. A., Nikolopoulos, A., Gázquez-Sanchez, F., Rossmann, L., Assmy, P., Babin, M., Bruyant, F., Beaulieu, M., Dybwad, C. and Peeken, I.: Ballasting by cryogenic gypsum enhances carbon export in a Phaeocystis under-ice bloom, Sci. Rep., 8(1), 7703, doi:10.1038/s41598-018-26016-0, 2018.

World Economic Forum: The Global Risks Report 2020. [online] Available from: http://wef.ch/risks2019, 2020.

Wu, S., Kuhn, G., Diekmann, B., Lembke-Jene, L., Tiedemann, R., Zheng, X., Ehrhardt, S., Arz, H. W. and Lamy, F.: Surface sediment characteristics related to provenance and ocean circulation in the Drake Passage sector of the Southern Ocean, Deep Sea Res. Part I Oceanogr. Res. Pap., 154, 103135, doi:10.1016/j.dsr.2019.103135, 2019.

Xiao, C., Dou, T., Sneed, S. B., Li, R. and Allison, I.: An ice-core record of Antarctic sea-ice extent in the southern Indian Ocean for the past 300 years, Ann. Glaciol., 56(69), 451–455, doi:10.3189/2015AoG69A719, 2015a.

Xiao, W., Frederichs, T., Gersonde, R., Kuhn, G., Esper, O. and Zhang, X.: Constraining the dating of late

Quaternary marine sediment records from the Scotia Sea (Southern Ocean), Quat. Geochronol., 31, 97–118, doi:10.1016/j.quageo.2015.11.003, 2016a.

Xiao, W., Esper, O. and Gersonde, R.: Last Glacial - Holocene climate variability in the Atlantic sector of the Southern Ocean, Quat. Sci. Rev., 135, 115–137, doi:10.1016/j.quascirev.2016.01.023, 2016b.

Xiao, X., Fahl, K. and Stein, R.: Biomarker distributions in surface sediments from the Kara and Laptev seas (Arctic Ocean): indicators for organic-carbon sources and sea-ice coverage, Quat. Sci. Rev., 79, 40–52, doi:10.1016/j.quascirev.2012.11.028, 2013.

Xiao, X., Fahl, K., Müller, J. and Stein, R.: Sea-ice distribution in the modern Arctic Ocean: Biomarker records from trans-Arctic Ocean surface sediments, Geochim. Cosmochim. Acta, 155, 16–29, doi:10.1016/J.GCA.2015.01.029, 2015b.

Yuan, X.: ENSO-related impacts on Antarctic sea ice: a synthesis of phenomenon and mechanisms, Antarct. Sci., 16(4), 415–425, doi:10.1017/S0954102004002238, 2004.

Yuan, X., Martinson, D. G. and Liu, W. T.: Effect of air-sea-ice interaction on winter 1996 Southern Ocean subpolar storm distribution, J. Geophys. Res. Atmos., 104(D2), 1991–2007, doi:10.1029/98JD02719, 1999.

Zhou, M., Niiler, P. P. and Hu, J. H.: Surface currents in the Bransfield and Gerlache Straits, Antarctica, Deep. Res. Part I Oceanogr. Res. Pap., 49(2), 267–280, doi:10.1016/S0967-0637(01)00062-0, 2002.

Zielinski, U. and Gersonde, R.: Diatom distribution in Southern Ocean surface sediments (Atlantic sector): Implications for paleoenvironmental reconstructions, Palaeogeogr. Palaeoclimatol. Palaeoecol., 129(3–4), 213–250, doi:10.1016/S0031-0182(96)00130-7, 1997.

Zielinski, U. and Gersonde, R.: Plio–Pleistocene diatom biostratigraphy from ODP Leg 177, Atlantic sector of the Southern Ocean, Mar. Micropaleontol., 45(3–4), 225–268, doi:10.1016/S0377-8398(02)00031-2, 2002.

Zielinski, U., Gersonde, R., Sieger, R. and Fütterer, D.: Quaternary surface water temperature estimations: Calibration of a diatom transfer function for the Southern Ocean, Paleoceanography, 13(4), 365–383, doi:10.1029/98PA01320, 1998.

Zielinski, U., Bianchi, C., Gersonde, R. and Kunz-Pirrung, M.: Last occurrence datums of the diatoms Rouxia leventerae and Rouxia constricta: indicators for marine isotope stages 6 and 8 in Southern Ocean sediments, Mar. Micropaleontol., 46(1–2), 127–137, doi:10.1016/S0377-8398(02)00042-7, 2002.

Zwally, H. J., Comiso, J. C., Parkinson, C. L., Cavalieri, D. J. and Gloersen, P.: Variability of Antarctic sea ice 1979–1998, J. Geophys. Res., 107(C5), 3041, doi:10.1029/2000JC000733, 2002.

10 APPENDIX

IMPORTANT NOTE: ALL APPENDICES (TABLES, FIGURES, DESCRIPTIONS) ARE PROVIDED ON THE USB-STICK ENCLOSED TO THIS THESIS IN THE FOLDER "APPENDICES". ONLY FIGURES AND DESCRIPTIONS ARE SHOWN IN THE PRINTED VERSION OF THE THESIS.

Appendix 1 Coordinates of sample stations with water depth, concentrations of $IPSO_{25}$, HBI Z- and E-trienes, brassicasterol, and dinosterol normalized to TOC; $\delta^{13}C$ values for $IPSO_{25}$; and values of sea ice indices $PIPSO_{25}$ based on the HBI Z- and E-trienes, brassicasterol, and dinosterol. Concentrations below the detection limit are expressed as 0. The $PIPSO_{25}$ could not be calculated where $IPSO_{25}$ and the phytoplankton marker is absent (blank fields).
→ The data is accessible on the ***USB-stick*** enclosed to this thesis, folder „Appendices", file "Appendix_01".

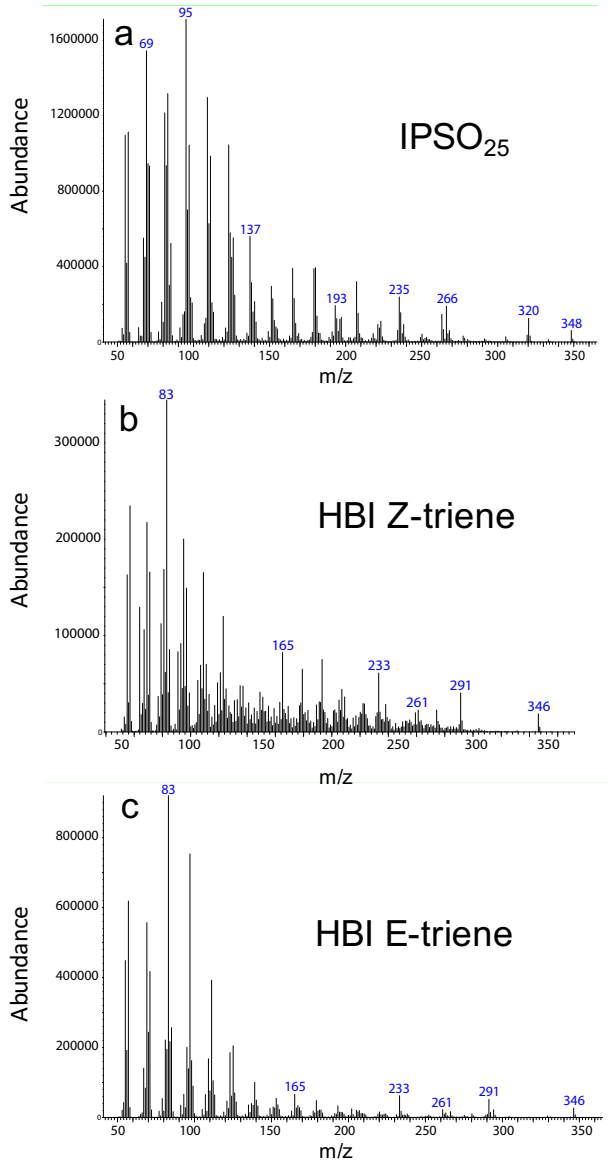

Appendix 2 Examples of mass spectra of $IPSO_{25}$ (m/z 348), HBI Z-triene and E-triene (both m/z 346) obtained from surface sediments in the study area.

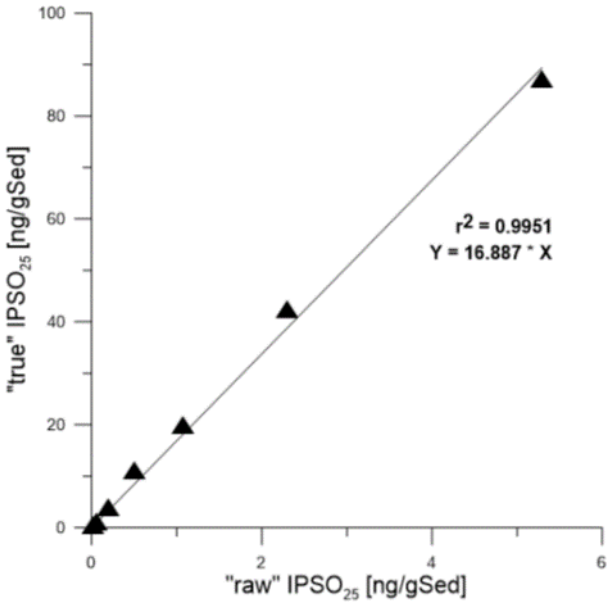

Appendix 3 Example calibration curve for the quantification of $IPSO_{25}$. Different (true) $IPSO_{25}$ concentrations determined via gas chromatography-flame ionization are plotted against (raw) $IPSO_{25}$ concentrations determined via gas chromatography-mass spectrometry using selected ion monitoring (m/z 348). The instrumental response factor is obtained from the regression line.

Appendix 4 Seasonal sea ice concentrations from satellite observations for spring, summer, autumn and winter, with standard deviations.
→ The data is accessible on the ***USB-stick*** enclosed to this thesis, folder „Appendices“, file “Appendix_04”.

Appendix 5 Estimations of winter sea ice (WSI) derived from diatom species and the distribution of main diatom species in each sample.
→ The data is accessible on the ***USB-stick*** enclosed to this thesis, folder „Appendices“, file “Appendix_05”.

Appendix 6 Excess ^{210}Pb activity from the sediment cores with depth in dpm (disintegration per minute) per gram with error bars (1 σ).

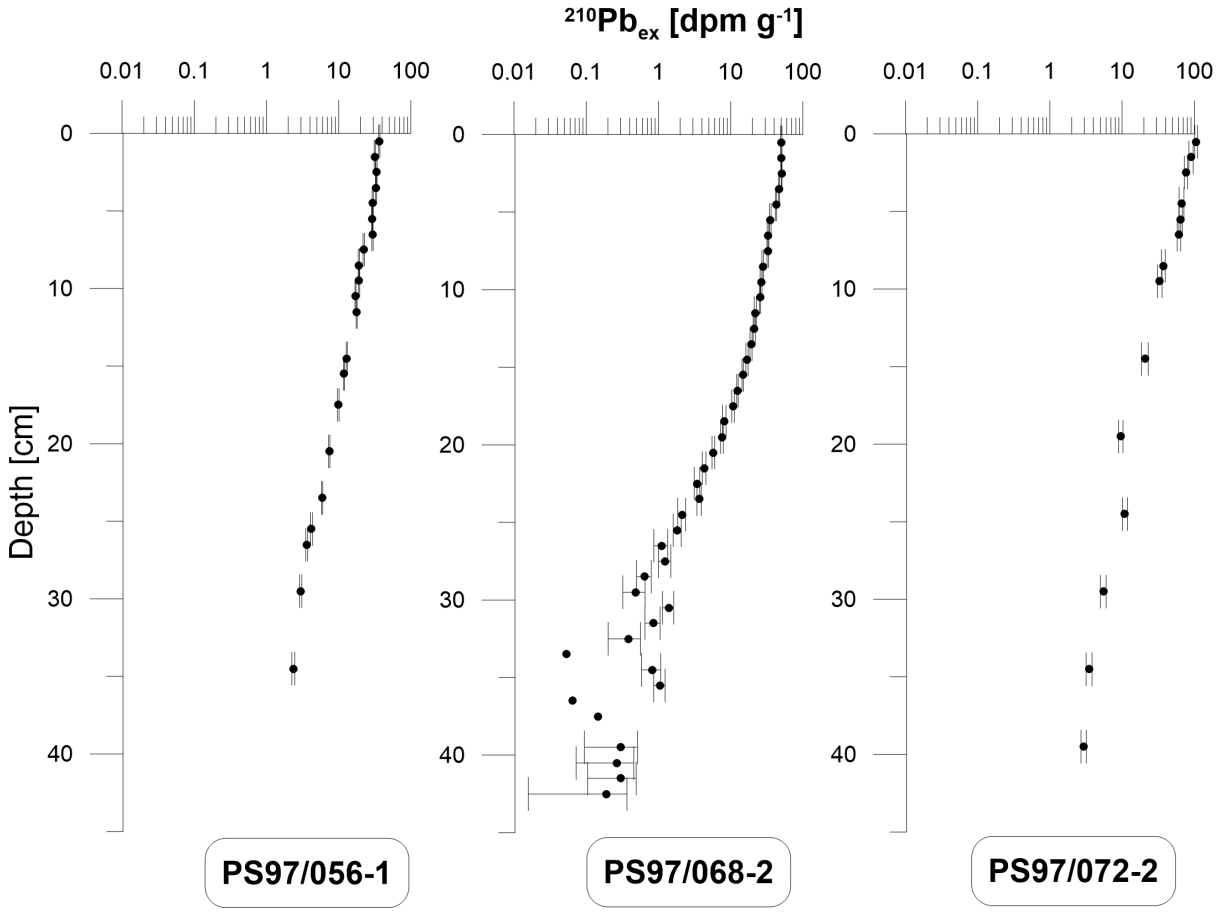

Appendix 7 C-factors for calculation of different $PIPSO_{25}$ based on brassicasterol and dinosterol. The c-factor is defined as mean $IPSO_{25}$/mean phytoplankton marker (Müller et al., 2011).

	Brassicasterol	Dinosterol
PS97/056-1	0.005	0.009
PS97/068-2	0.101	0.168
PS97/072-2	0.018	0.017

Appendix 8 The resolution of the ocean model in AWI-ESM2.

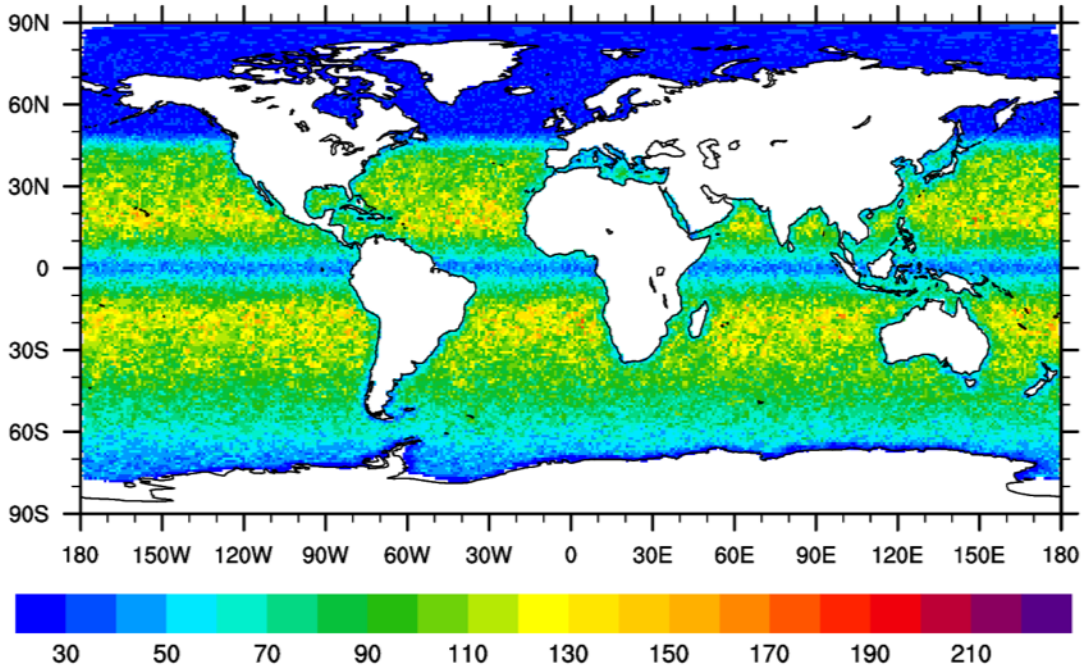

Appendix 9 Table of bulk parameters and organic biomarkers of core PS97/056-1 including ^{210}Pbex, calendar years CE, sedimentation rate, total organic carbon (TOC), C/N ratio, BIT index, and concentrations of $IPSO_{25}$, HBI Z- and E-trienes normalized to TOC. The $PIPSO_{25}$ could not be calculated where $IPSO_{25}$ and the phytoplankton marker not detected (n.d.). Further, sterols and sterol-based $PIPSO_{25}$, GDGT-derived ocean temperatures SOT^{TEX} and SOT^{OH} and diatom derived winter sea ice cover (MAT-WSI 4an) and summer surface temperature (SSST) are listed as well as diatom counts. Sterols of the first 13 cm were lost during the laboratory preparation (sample loss = s.l.). Calendar years before 1880 are extrapolated.
→ The data is accessible on the ***USB-stick*** enclosed to this thesis, folder „Appendices“, file “Appendix_09”.

Appendix 10 Table of bulk parameters and organic biomarkers of core PS97/068-2 including ^{210}Pbex, calendar years CE, sedimentation rate, total organic carbon (TOC), C/N ratio, BIT index, and concentrations of $IPSO_{25}$, HBI Z- and E-trienes normalized to TOC. Further, sterols and sterol-based $PIPSO_{25}$, GDGT-derived ocean temperatures SOT^{TEX} and SOT^{OH} and diatom derived winter sea ice cover (MAT-WSI 4an) and summer surface temperature (SSST) are listed as well as diatom counts. Calendar years before 1880 are extrapolated.
→ The data is accessible on the ***USB-stick*** enclosed to this thesis, folder „Appendices“, file “Appendix_10”.

Appendix 11 Table of bulk parameters and organic biomarkers of core PS97/072-2 including ^{210}Pbex, calendar years CE, sedimentation rate, total organic carbon (TOC), C/N ratio, BIT index, and concentrations of $IPSO_{25}$, HBI Z- and E-trienes normalized to TOC. The $PIPSO_{25}$ could not be calculated where $IPSO_{25}$ and the phytoplankton marker not detected (n.d.). Further, sterols and sterol-based $PIPSO_{25}$, GDGT-derived ocean temperatures SOT^{TEX} and SOT^{OH}. Sterols of the first 16 cm were lost during the laboratory preparation (sample loss = s.l.). Calendar years before 1880 are extrapolated.
→ The data is accessible on the ***USB-stick*** enclosed to this thesis, folder „Appendices“, file “Appendix_11”.

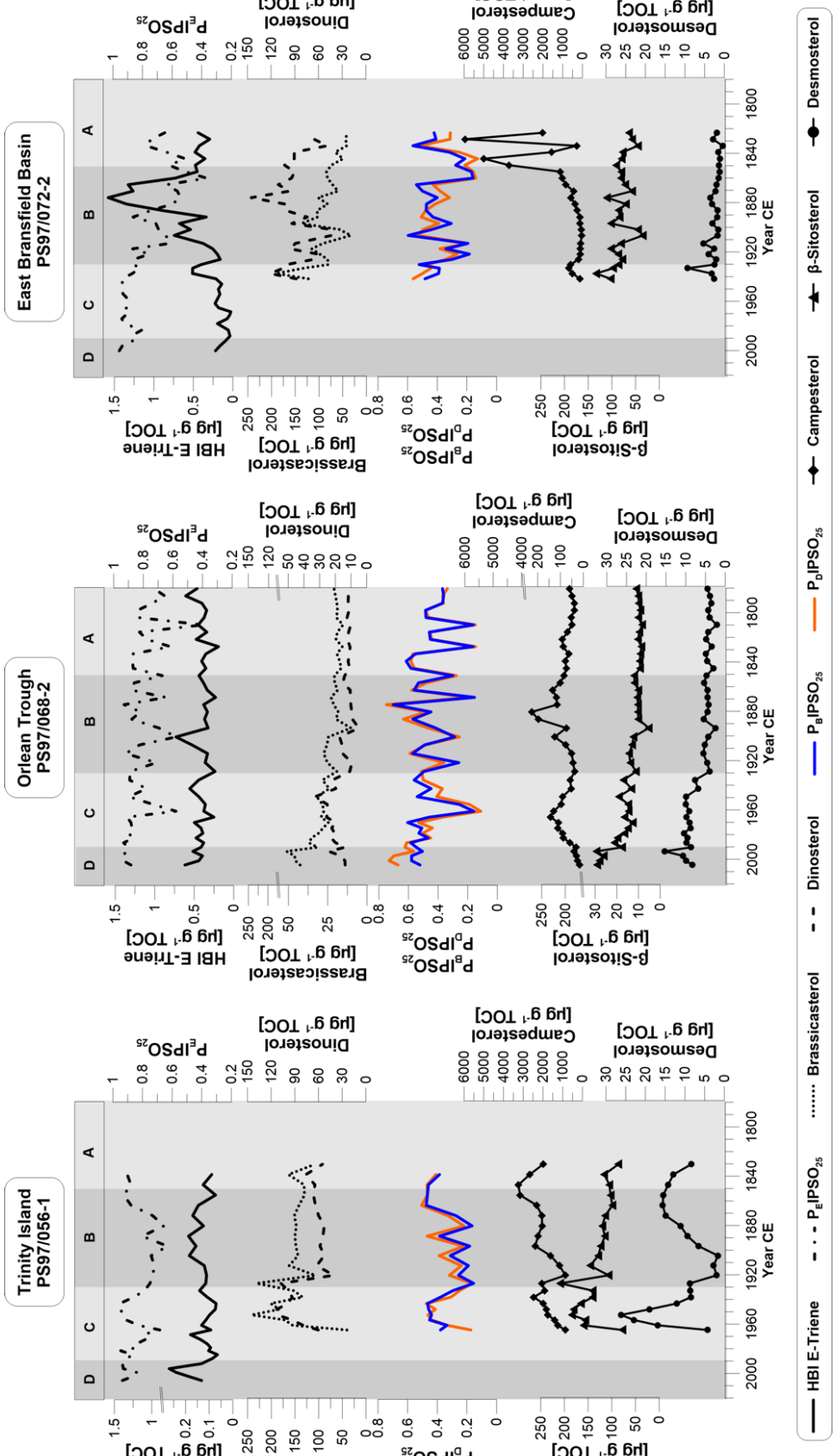

Appendix 12 Additional analytical biomarker results from all three core sites including (from top to bottom) HBI E-triene, the sea ice index P_EIPSO_{25}, brassicasterol and dinosterol (Kanazawa et al., 1971; Volkman, 2003) with their according sea ice indices P_BIPSO_{25} and P_DIPSO_{25}, respectively. The terrestrial biomarkers campesterol and ß-sitosterol (Volkman, 1986) were not used for sea ice estimations. Desmosterol is suspected to be related to sea ice (Cárdenas et al., 2019) but was not considered in our discussion as well. Vertical grey bars denote the stratigraphic units A to D.

Appendix 13 Table of TOC and diatom-derived winter sea ice cover (MAT-WSI 4an) and summer sea surface temperatures (SSST) and diatom counts of trigger core PS97/072-1. The age model is based on a correlation with TOC content of core PS97/072-2.
→ The data is accessible on the ***USB-stick*** enclosed to this thesis, folder „Appendices", file "Appendix_13".

Appendix 14 Table of modelled spring sea ice cover (mSSIC), spring sea ice thickness (mSSIT), subsurface ocena temperature (mSOT), sea surface temperatures (mSST) and the latitudinal spring sea ice edge between 50°W and 70°W.
→ The data is accessible on the ***USB-stick*** enclosed to this thesis, folder „Appendices", file "Appendix_14".

Appendix 15 The normalized biomarker $IPSO_{25}$ and HBI Z-triene from eastern AP (MTC38A) and western AP (MTC18A) (Barbara et al., 2013) compared to biomarker records from this study. High biomarker concentrations are evident in all records since 1930, or later, pointing to a shift towards an environment with dynamic sea ice seasons supporting higher primary production. Vertical grey bars denote the stratigraphic units A to D.

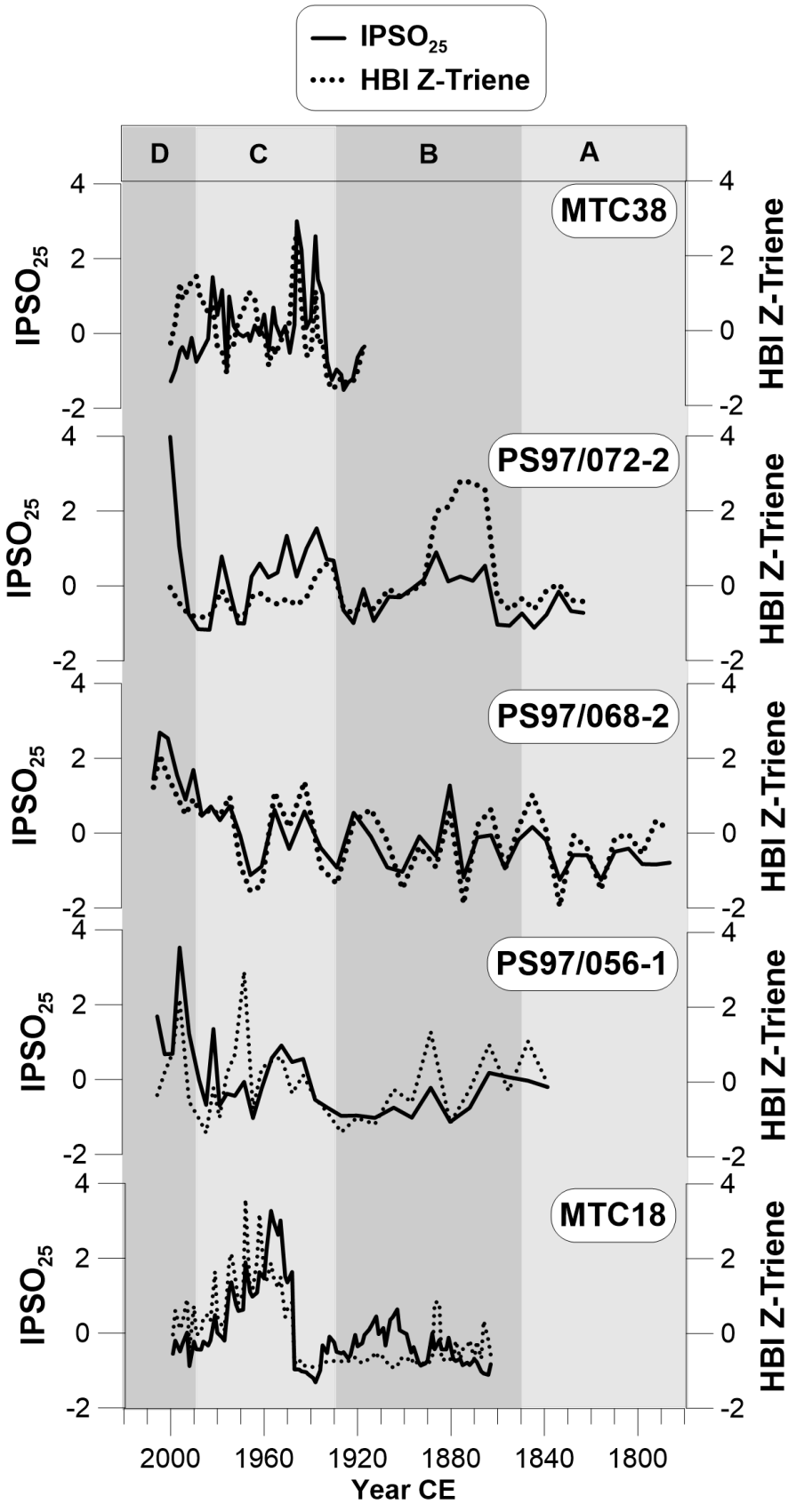

Appendix 16 Seasonal sea ice concentrations from satellite observations for spring and winter at the three core sites PS97/056-1, PS97/068-2 and PS97/072-2.
→ The data is accessible on the ***USB-stick*** enclosed to this thesis, folder „Appendices“, file “Appendix_16”.

Appendix 17 Additional numerical model data from spring sea ice thickness (mSSIT, 10 year running mean) and surface air temperature (mSAT, 10 year running mean) from all three core sites. Vertical grey bars denote the stratigraphic units A to D.

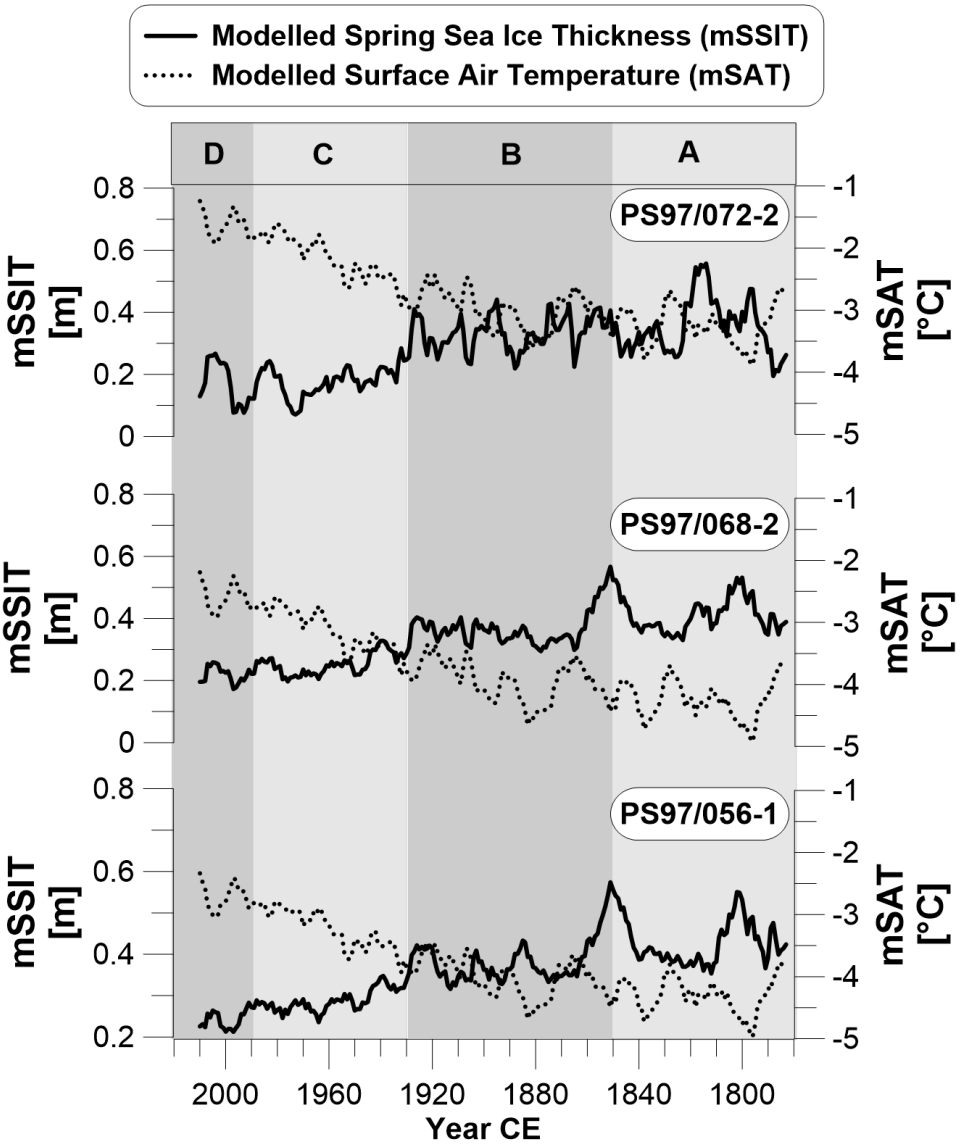

Appendix 18 Data from ^{14}C radiocarbon dating on calcareous and acid insoluble organic matter from piston core PS97/072-1. The sample marked this * remains from the trigger core PS97/072-1 at 70 cm which corresponds to 56 cm sample depth in the piston core.
→ The data is accessible on the ***USB-stick*** enclosed to this thesis, folder „Appendices“, file “Appendix_18”.

Appendix 19 Detailed description of the age model tuning on piston core PS97/072-1. Continues on next page.

We experienced that our ^{14}C radiocarbon dating on calcite and acid-insoluble organic matter did not cover with adjacent sediment core age models and tuned our age model manually via tie-points. For this we compared our results of total organic carbon (TOC) and GDGT-based subsurface ocean temperatures (SOT^{TEX} and SOT^{OH}) with stable isotope $\delta^{18}O$ records of the West Antarctic Ice Sheet Divide ice core (WAIS Divide Project Members et al., 2015) and brought prominent features in accordance (Figure S1).

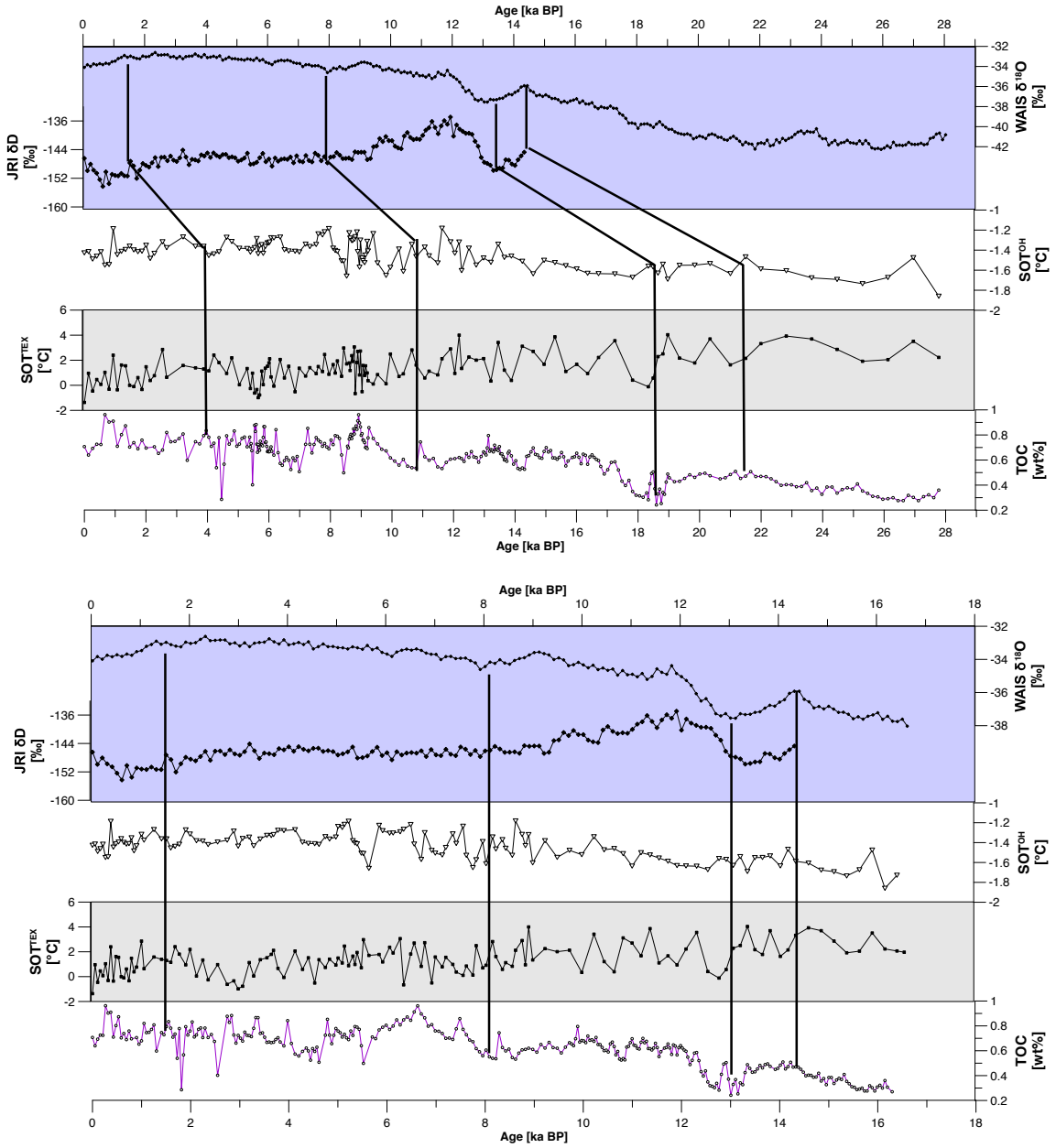

Figure S1: We compare our analyses results (TOC, SOT^{TEX} and SOT^{OH}) with $\delta^{18}O$ records from the WAIS (WAIS Divide Project Members et al., 2015) and James Ross Island ice core (Mulvaney et al., 2012) (violett box) to adjust our age model (above). Below is the corrected age model.

Appendix 19 continued

With these corrected ages (Table Appendix 18) we applied the age models hummingage (https://hummingage.awi.de/) and Bacon shown in Figure S2.

In its current version, *hummingage* requires Gaussian errors of the input age data, which is a fair assumption on our already calibrated data. Basically *hummingage* applies a multi-segment linear regression on the accumulation rate of the sediment data. The decision on the optimal number of segments is made with the objective support of the BIC (Bayesian Informatino Criterion, Schwarz, 1978). The BIC implements the concept of *Ockhams's Razor* (Sivia and Skilling, 2006), which suggest to choose the hypothesis requiring the fewest assumptions among competing hypotheses describing a phenomenon (equally) well. Practically the BIC is an optimal compromise between minimizing the fit residuals and dividing the data into not more segments as needed. For our data it turned out that we even do not need any segments at all.

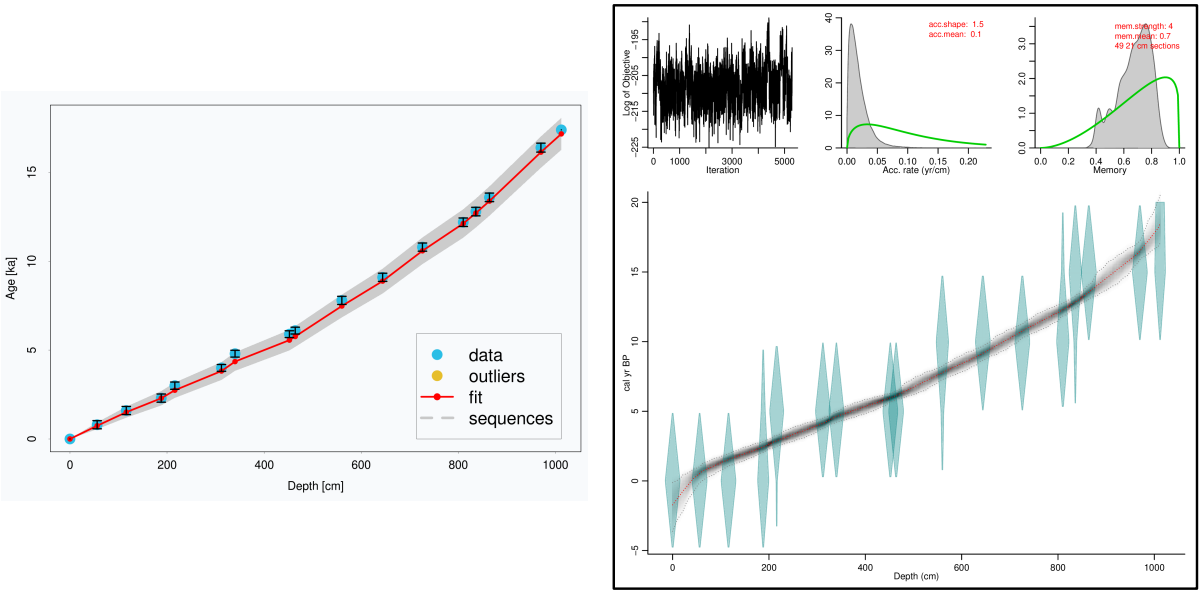

Figure S2: Comparison of the age models conducted with hummingage (left) and Bacon (right.)

Following the linear regression on the accumulation rate *hummingage* applies a Bayesian tuning to find a best fitting curve by interpreting the regression as prior probability and ask for the posterior probability of this regression given the observed data. Following a Gaussian assumption it turned out that the best fitting curve is the weighted average of the regression line and the original data, whereas the weights are given by the regression error and the individual data errors. Details at https://github.com/hummingbird-dev/hummingage.

Because of the novelty of the *hummingage* method we also apply the widely used *Bacon* method to our data (Figure S2, right). Since our data have been already calibrated we disabled the calibration function in *Bacon* (cc=0). *Bacon* also divides the original data into segments and for our data it only suggests roughly to use segments between 10 and 102 segments. Following, it is the subjective decision of the scientist, how many segments to choose until the curve "looks good". One guideline to choose the best number of segments is to assure that the MCMC algorithm used by *Bacon* (Figure S2, right figure, top left panel) mixes well and

Appendix 19 continued

finally we decided to use 49 segments. Lower numbers of segments show bad MCMC mixing and higher numbers of segments introduce unrealistic curvatures.

As can be seen from Figure S2, both the *hummingage* model and the *Bacon* model yield very similar results, especially also the errors are quite similar. This is an important point, because according to Trachsel et al. (2017) the strength of the Bayesian age depth models, in comparison with the standard methods, is a better representation of the errors and thus a more reliable estimation of the age depth relation. Thus, in our case, with the pre-calibrated data, *hummingage* is a real alternative, is easy to use online, and provides similar results to the sophisticated *Bacon* model. Finally, we decided to use the interpolated (1 cm) model output from *hummingage* for our analysis.

Appendix 20 The bulk parameter of piston core PS97/072-1 including core depth, cal. Age BP, sedimentation rate, total organic carbon, biogenic opal, C/N ratio, $\delta^{13}C$ from both the University of Concepción and University of Hamburg and the BIT index.
→ The data is accessible on the ***USB-stick*** enclosed to this thesis, folder „Appendices“, file "Appendix_20".

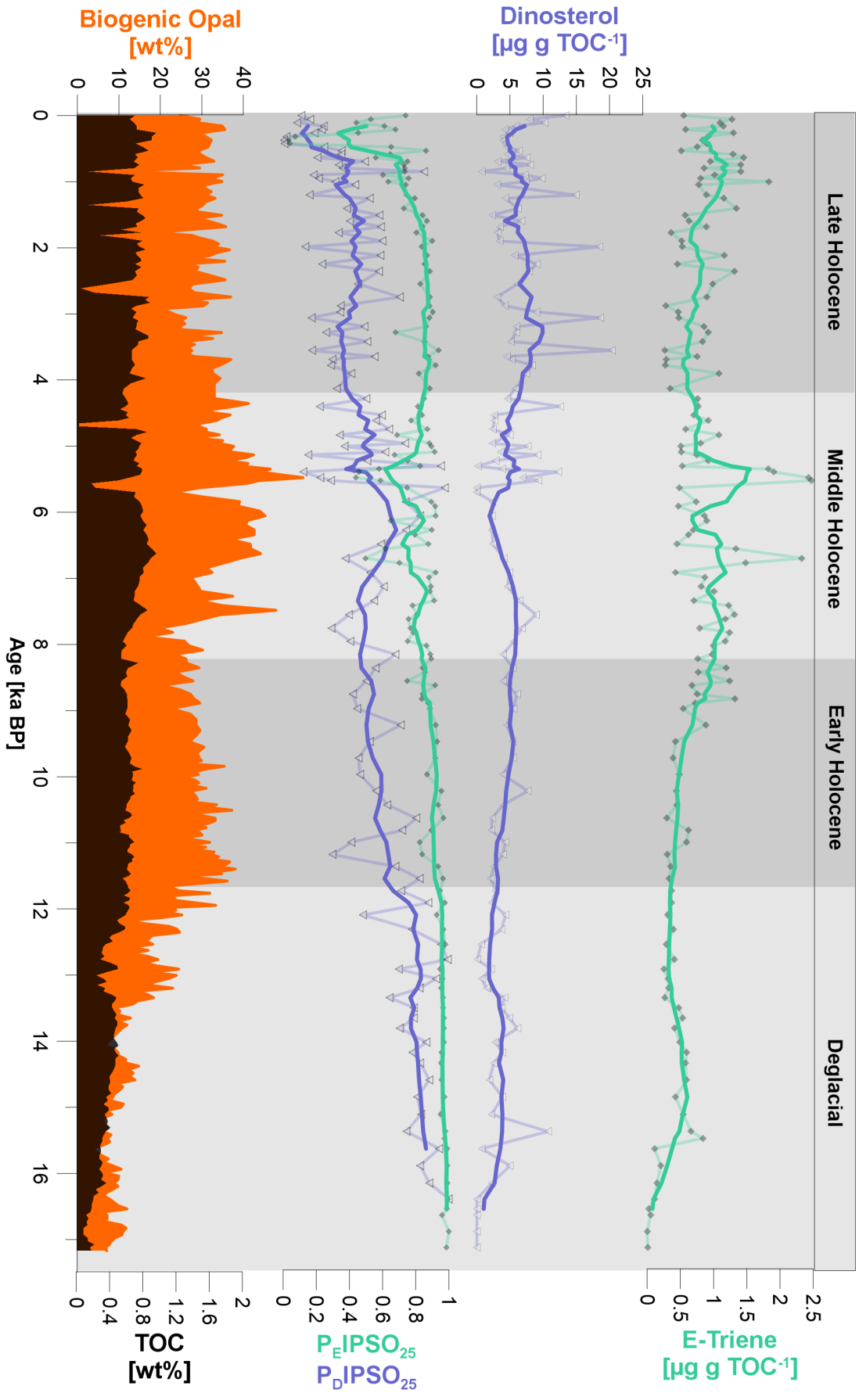

Appendix 21 Additional analytical biomarker results of HBI E-triene, P_EIPSO_{25}, dinosterol, P_DIPSO_{25}, and bulk parameter of TOC and biogenic opal (data see Table Appendix 22) (running means based on seven points).

Appendix 22 Biomarker data of piston core PS97/072-1 including core depth, cal. Age BP, $IPSO_{25}$, HBI Z- and E-trienes, brassicasterol, dinosterol, campesterol, β-sitosterol, desmosterol, the sea ice indices P_ZIPSO_{25},
P_EIPSO_{25}, P_BIPSO_{25}, P_DIPSO_{25}, and WSI, $\delta^{13}C$ of $IPSO_{25}$, and temperature estimations SOT^{TEX}, SOT^{OH}, and SSST.
→ The data is accessible on the ***USB-stick*** enclosed to this thesis, folder „Appendices“, file "Appendix_22".

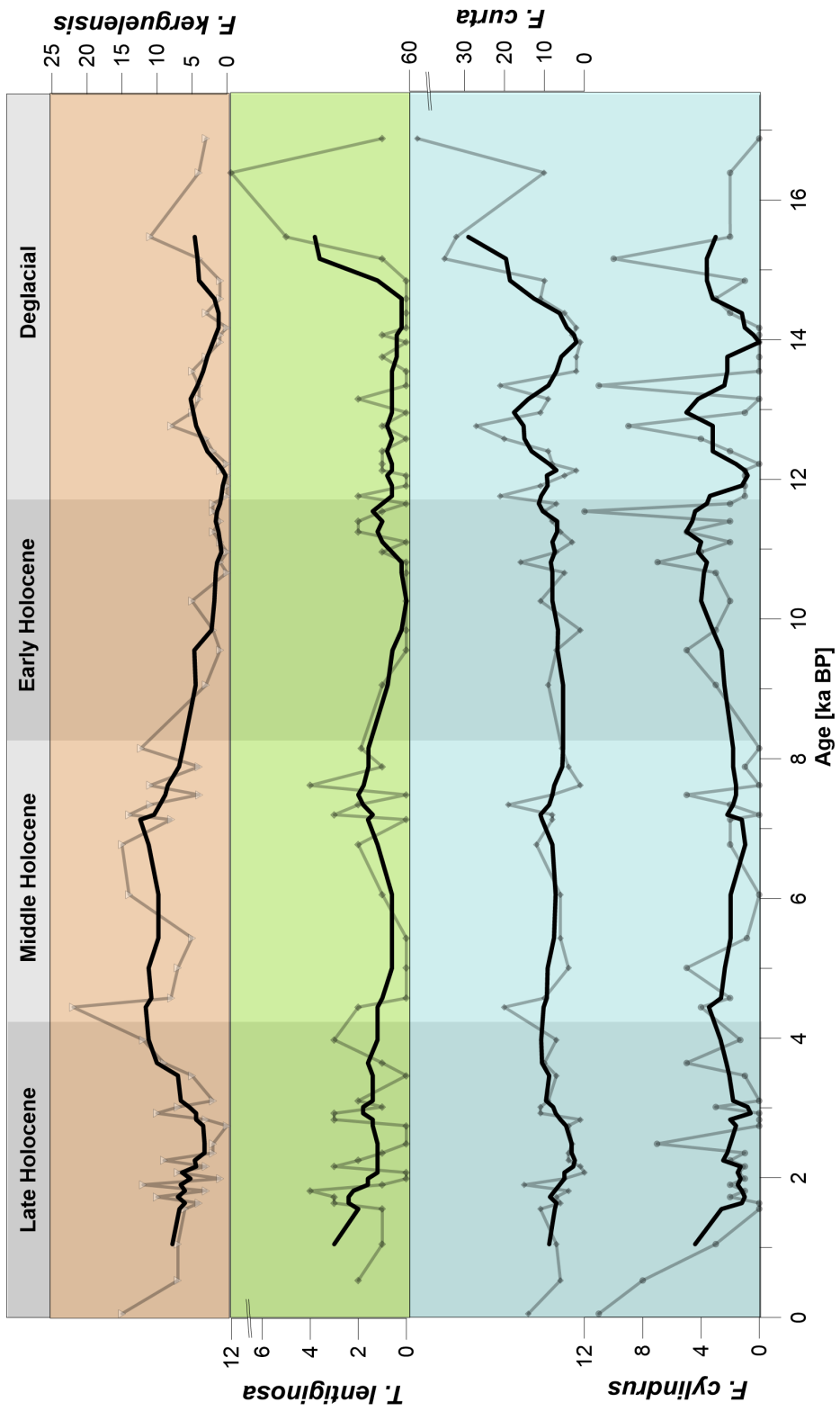

Appendix 23 The selected counts of diatom species indicative for an open, warm ocean (F. kerguelensis, orange box), for an open, cold ocean (T. lentiginosa, green box) and the sea ice edge (F. cylindrus and F. curta, blue box) (running means based on five points).

Appendix 24 Diatom counts per sample of the piston core PS97/072-1.
→ The data is accessible on the ***USB-stick*** enclosed to this thesis, folder „Appendices“, file “Appendix_24”.

Appendix 25 Magnetic susceptibility, ice rafted debris and counts of iron, titan, calcite, barium and aluminium of the sediment of piston core PS97/72-1.
→ The data is accessible on the USB-stick enclosed to this thesis, folder „Appendices“, file “Appendix_25”.

Appendix 26 Pearson´s correlation matrix of sea salt sodium concentrations ($ssNa^+$) with the organic biomarkers $IPSO_{25}$, HBI Z-triene, brassicasterol and sea ice indices P_ZIPSO_{25}, P_BIPSO_{25}, and WSI. All data is resampled on a 10-year interval. Scatter plots with a positive/negative correlation are marked with green/red fields when correlations are relatively strong (-0.3 < r > 0.3) and with a green/red frame when correlations are weaker (-0.15 < r > 0.15). Each significance level is associated to a symbol (p-values are 0.001 = “***”; 0.01 = “**”; 0.05 = “*”; 0.1 = “.”; 0/1 = “ “). All matrices were done with the software R (R Core Team, 2017) and the package PerformanceAnalytics (Peterson et al., 2020).

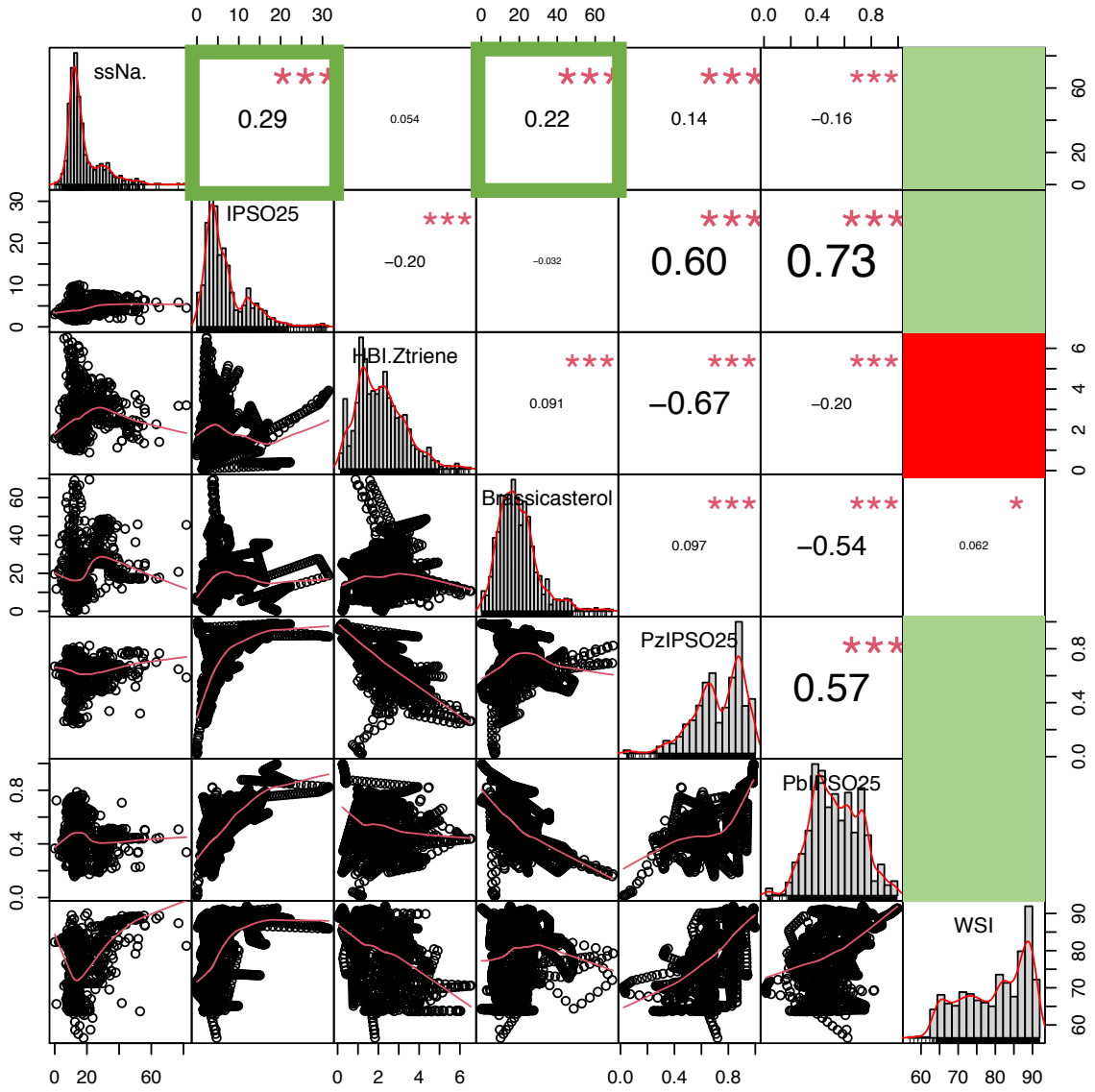

Appendix 27 Pearson´s correlation matrix of temperatures SOT^{TEX}, SOT^{OH} and SSST with the organic biomarkers $IPSO_{25}$, HBI Z-triene, brassicasterol and sea ice indices P_ZIPSO_{25}, P_BIPSO_{25}, and WSI. All data is resampled on a 10-year interval. Scatter plots with a positive/negative correlation are marked with green/red fields when correlations are relatively strong (-0.3 < r > 0.3) and with a green/red frame when correlations are weaker (-0.15 < r > 0.15). Each significance level is associated to a symbol (p-values are 0.001 = "***"; 0.01 = "**"; 0.05 = "*"; 0.1 = "."; 0/1 = " "). All matrices were done with the software R (R Core Team, 2017) and the package PerformanceAnalytics (Peterson et al., 2020).

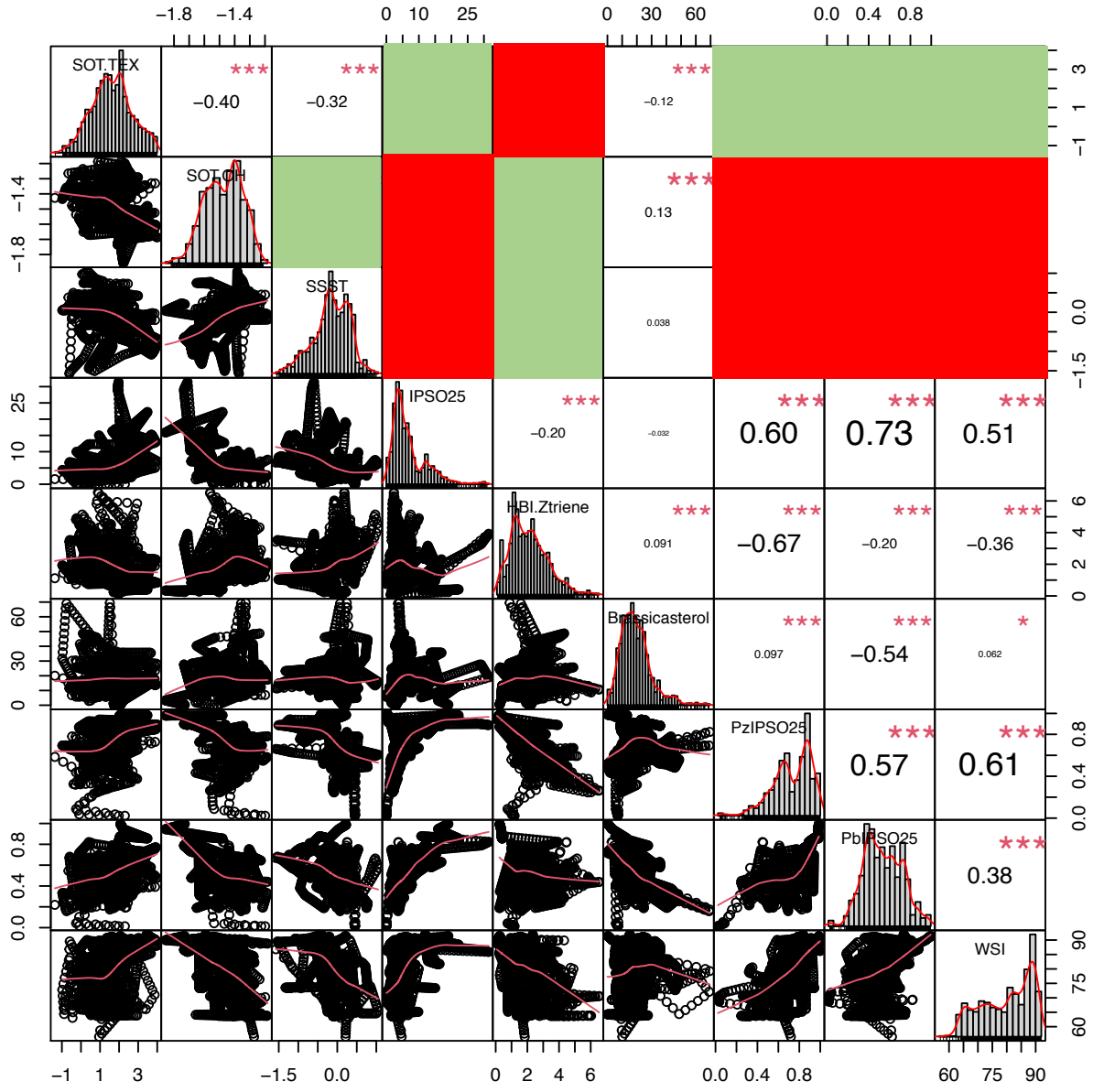

Appendix 28 Pearson´s correlation matrix of ENSO variability (Conroy et al., 2008) and SWW strength (Lamy et al., 2010) with temperature records (SOT^{TEX}, SOT^{OH} and SSST), organic biomarkers ($IPSO_{25}$, HBI Z-triene, brassicasterol) and sea ice indices (P_ZIPSO_{25}, P_BIPSO_{25}, WSI). All data is resampled on a 10-year interval. Scatter plots with a positive/negative correlation are marked with green/red fields when correlations are relatively strong (-0.3 < r > 0.3) and with a green/red frame when correlations are weaker (-0.15 < r > 0.15). Each significance level is associated to a symbol (p-values are 0.001 = "***"; 0.01 = "**"; 0.05 = "*"; 0.1 = "."; 0/1 = " "). All matrices were done with the software R (R Core Team, 2017) and the package PerformanceAnalytics (Peterson et al., 2020).